Modified oligonucleotides for triple helix studies and for the obtention of structures with biomedical and technological interest

Margarita Alvira Torre

Tesis Doctoral

Modified oligonucleotides for triple helix studies and for the obtention of structures with biomedical and technological interest

Margarita Alvira Torre

Departamento de Química Orgánica
Facultad de Química
Universidad de Barcelona
2010

Memoria presentada por

Margarita Alvira Torre

para optar al grado de Doctor Europeo por la Universidad de Barcelona

Departamento de Química Orgánica

Programa de doctorado de Química Orgánica

Bienio 2005-2007

Dirigida y revisada por: Dr. Ramon Eritja Casadellà

Tutora: Dra. Anna Grandas Sagarra

Barcelona, Septiembre de 2010

A mis padres y mi hermana

A mis abuelos

A Alejandro

Acknowledgements

En primer lugar quiero agradecer al Dr. Ramon Eritja, por aceptarme en su grupo y dirigir mi tesis doctoral, por la confianza depositada, la ayuda prestada, la motivación inculcada y sus sabios consejos. Voy a estar siempre agradecida.

También a Anna Grandas, por aceptar ser mi tutora de tesis y estar ahí siempre que la he necesitado.

El haber disfrutado tanto durante mi etapa predoctoral se lo debo en gran parte a las personas con las que he tenido la suerte de trabajar durante estos últimos años: Marta (aunque coincidimos poco tiempo lo pasé muy bien), Sandra (¡suerte con las patentes!), Roger (que máster tan diver..) Anna (contigo he compartido toda mi etapa de tesis, desde que empecé. Mil gracias siempre por tu ayuda y tus consejos), Clara (estoy deseando ver a tu baby..), Brendan (por enseñarnos tantas "nano"cosas), Alejandra (ché, animo con los geles boludos), Rubén (la alegría del laboratorio, siempre son una sonrisa-y una risa tambien. De hecho la estoy oyendo mientras escribo esta página), Montse (una "crack" de la orgánica, ¡espero que sigas publicando tanto! echaré de menos las 'meriendetas'), Carme (por fin te podré hacer el seminario, jeje), Álvaro (por tantas charlas existenciales a horas intempestivas), Santi (el rey de los siRNAs y el delivery), María (la benjamina del labo..), Sonia (¡ánimo con los TTF!), Stefi (¡¡eres parte de este grupo!! y siempre tendrás una familia en Barcelona). Y no me quiero dejar a los compañeros del CSIC, Antonio, Raul, Jose Antonio, Jaume, Miquel Pons, con quienes compartí esos buenos ratos a la hora de la comida el primer año de mi tesis en el CSIC.

Durante mi tesis doctoral he realizado dos estancias breves en el extranjero, durante las cuales he aprendido muchísimo, tanto a nivel profesional como personal. Quiero agradecer al Dr. Morten Grøtli y su grupo, por acogerme en su laboratorio y hacer que mi estancia en Suecia fuera tan agradable, tack så mycket! Al Dr. David Schiffrin por dejarme investigar en su laboratorio y abrirme las puertas al mundo de la electroquímica. Gracias también a la gente del departamento y de su grupo, especialmente a Jose y Laura, por su ayuda con las voltametrías y porque hicieron de mi experiencia en Liverpool un recuerdo inolvidable.

Al Dr. Carlos González, por su ayuda con los experimentos de RMN con los quadruplexes, y a todo su grupo, por las atenciones brindadas durante mi corta estancia en Madrid. Quiero agradecer especialmente a la Dra. Irene Pinto y al Dr. Douglas V. Laurents su ayuda con los experimentos de dicroísmo circular. A la Dra. Irene Fernández y la Dra. Marta Vilaseca, de la Universidad de Barcelona, por su ayuda con la espectrometría de masas en los servicios científico-técnicos, especialmente en la primera parte de mi tesis.

Quiero agradecer también al Ministerio de Educación y Ciencia (ahora MICINN), por la concesión de una beca predoctoral dentro del programa de ayuda

para la Formación de Personal Investigador (Programa FPI), sin la que este trabajo no se hubiera podido realizar.

Por último, me gustaría dar mi más sincero agradecimiento a mi familia, a quienes les dedico este trabajo. A mis padres (¿como podría agradeceros todo lo que hacéis por mí?), mi hermana, mis abuelitos, a Marian, a la ita, a mis tíos, a mis primos. Gracias a todos por ser como sois. ¡Os quiero mucho!

Y sobre todo a Alejandro, mi marido, por ser siempre un apoyo incondicional y por recorrer juntos este camino tan bonito que es la vida.

INDEX

CHAPTER 3: "Synthesis of Oligonucleotides Carrying 5'–5' Linkages Using Copper–Catalyzed Cycloaddition Reactions"

CHAPTER 4: "Oligonucleotides Conjugates Carrying Cu(II) Complexes: Synthesis and Electrochemical Study"

CHAPTER 5: "Synthesis of a Novel DNA Structure Able to Form Stable Monomolecular Quadruplexes. Effect of 8-amino-guanine Substitutions"

CHAPTER 6: "Experimental Section"

CHAPTER 7: "Conclusions"

8. APPENDIX

Abstract

Oligonucleotides are short fragments of DNA composed of a low number of nucleotides (typically between 10-100nt) which are of great interest because their applications in molecular biology, biomedicine and nanotechnology. As a result of their ability to base pairing, oligonucleotides can be used as primers, hybridization probes in biosensors, agents for controlling gene expression, structural material in nanotechnology or as substrates for a variety of biochemical and biophysical studies. Chemical modification of oligonucleotides as well as conjugation to different functional molecules allows for modulation of both therapeutical and biotechnological properties.

This thesis is focused in the nucleic acid chemistry field and the main objective is the synthesis of modified oligonucleotides for obtaining structures with therapeutical and/or biotechnological interest.

Oligonucleotides capable to form structures other than the canonical DNA double helix have received considerable attention in the last years. The ability of triplex forming oligonucleotides (TFOs) to bind specifically to certain duplex DNA regions provides a strategy for site-directed modification of genomic DNA. Besides, G-quadruplexes are four-stranded DNA structures stabilized by stacking of guanine tetrads which have been found in telomeres and some promoters and play a role in regulation of transcription and translation. In addition, they are also interesting for nanotechnological devices.

In this context, the first part of the research work was addressed to synthesize parallel stranded oligonucleotide clamps carrying LNA (locked nucleic acid) residues and study the stability of the triplex formed with DNA and RNA target sequences by melting experiments.

Secondly, a novel strategy to obtain parallel clamps using the non-templated chemical ligation of two oligonucleotides by 5'-5' linkages was developed. For this purpose, several protocols for introduce azido and alkyne moieties in the 5'-end of different sequences were developed so that the modified DNA strands could form a parallel hairpin after their chemical ligation by click chemistry. Cu (I)-catalyzed azide-alkyne cycloaddition reaction was also used to synthesize novel unnatural aminoacids during a FPI predoctoral short-term staying in the Medicinal Chemistry Department at Göteborg University.

Then, a system composed of four DNA strands whose 5' ends are covalently attached was designed to form a monomolecular parallel G-quadruplex. This novel molecule was used to study the effects of some nucleobase modifications in quadruplex structure. The effect of 8-amino-guanine substitutions in quadruplex stability was studied by NMR and CD thermal denaturation experiments.

Finally, modified oligonucleotides for nanotechnology applications were prepared. Synthesis of oligonucleotide conjugates carrying Cu(II) complexes to construct arrays of electrochemical oscillators was performed. Initial electrochemical characterization of the conjugates was carried out during a FPI predoctoral short-term staying, in the Centre for Nanoscale Science at the University of Liverpool.

Resumen

Los oligonucleótidos son fragmentos cortos de DNA que están compuestos por un número relativamente pequeño de nucleótidos (normalmente entre 10 y 100) y tienen un enorme interés por sus aplicaciones en biología molecular, biomedicina y nanotecnología. Como resultado de su habilidad para hibridarse con cadenas complementarias los oligonucleótidos son usados como cebadores (*primers*) en reacciones de amplificación, sondas de hibridación en biosensores, agentes de control de la expresión génica, material estructural para nanotecnología o como base para una gran variedad de estudios bioquímicos y biofísicos. La modificación química de los oligonucleótidos así como su conjugación con diferentes moléculas funcionales permite modular sus propiedades terapéuticas y biotecnológicas.

Esta tesis se enmarca en el campo de la química de los ácidos nucleicos y el principal objetivo es la síntesis de oligonucleótidos modificados para la obtención de estructuras con interés terapéutico y/o biotecnológico.

Los oligonucleótidos capaces de formar estructuras diferentes a la doble hélice canónica de ADN han recibido una atención considerable en los últimos años. La habilidad de los oligonucleótidos formadores de triples hélices (OFT) para unirse específicamente a ciertas regiones de un dúplex de ADN proporciona una estrategia para modificar el ADN en una región determinada del genoma. Por otro lado, los G-quadruplexes son estructuras de DNA de cuatro cadenas formadas por el apilamiento de tétradas de guaninas. Dichas estructuras han sido observadas en los telómeros y en las secuencias promotoras de algunos genes y parecen desempeñar un importante papel en la regulación de la transcripción y la traducción. Además presentan también propiedades interesantes para el uso en dispositivos nanotecnológicos.

En este contexto, la primera parte del trabajo de investigación consistió en sintetizar horquillas de cadenas de ADN paralelas modificadas con ácidos nucleicos bloqueados o LNA (*locked nucleic acids*) y estudiar la estabilidad de las triples hélices formadas con sus secuencias diana (de ADN y ARN) mediante ensayos de desnaturalización térmica.

En segundo lugar, se desarrolló una estrategia para obtener horquillas paralelas de ADN consistente en la unión química de dos oligonucleótidos por sus extremos 5' sin usar ninguna cadena "molde" (*template*). Con este propósito se desarrollaron diversos protocolos para introducir el grupo azida y alquino en el extremo 5' de diferentes secuencias de tal manera que estas cadenas de ADN modificadas pudieran formar una horquilla paralela después de su unión mediante química "click" (*click chemistry*). Además, la cicloadición 1,3-dipolar entre azidas y alquinos catalizada por Cu(I) se utilizó también para sintetizar aminoácidos no naturales durante una estancia breve FPI en el departamento de Química Medicinal de la Universidad de Göteborg.

Posteriormente, se diseñó un sistema compuesto por cuatro cadenas de ADN con sus extremos 5' unidos covalentemente capaces de formar un quadruplex paralelo monomolecular. Esta nueva molécula se ha empleado para estudiar los efectos de alguna nucleobase modificada en la estructura del quadruplex. El efecto de sustituciones de 8-amino-guaninas en la estabilidad de los quadruplexes se estudió por RMN y dicroísmo circular.

Finalmente, se prepararon oligonucleótidos modificados para aplicaciones en nanotecnología. Se sintetizaron conjugados de oligonucleótidos con complejos de cobre (II), propuestos para construir osciladores electroquímicos. Su caracterización electroquímica inicial se llevo a cabo durante una estancia breve FPI en el Centro para la Ciencia a Nanoescala de la Universidad de Liverpool.

List of abbreviations:

A: adenine
ABPP: activity based protein profiling
ACN: acetonitrile
Ac_2O: acetic anhydride
AcOEt: ethyl acetate
AEC: anion exchange chromatography
AFM: atomic force microscopy
AIDS: acquired immune deficiency syndrome
AP: alkaline phosphatase
ATP: adenosine triphosphate
Boc : tert-Butyloxycarbonyl
bp: base pair
C: cytosine
CA: diammonium hydrogen citrate
calc.: calculated
CD: circular dichroism
C.E: counter electrode
CM :ChemMatrix support
CPG: controlled pore glass
CPMV: Cowpea mosaic virus
CPP: cell penetrating peptide
CuAAC: Cu(I) catalyzed azide-alkyne cycloaddition
CV: cyclic voltammetry
DCM: dichloromethane
DIPEA: N,N-Diisopropylethylamine
DMAP: 4-Dimethylaminopyridine
DMF: dimethylformamide
DMSO: dimethyl sulfoxide
DMT: dimethoxytrityl
DNA: deoxyribonucleic acid
DPV: differential pulse voltammetry
dsDNA (RNA) : double-stranded DNA (RNA)
DTNP: 2,2'-Dithiobis-(5-nitropyridine)
EDC: 1-ethyl-3-(3-dimethylaminopropyl) carbodiimide
EDTA: ethylenediaminetetraacetic acid
equiv. (or eq.): equivalents
ESI-MS: electrospray ionization mass spectrometry
EtOH: ethanol
FAM: fluorescein amidite
FAB-MS: Fast Atom Bombardment Mass Spectrometry
Fmoc: 9-fluorenylmethyloxycarbonyl

FRET: Förster resonance energy transfer
G: guanine
GBA: glycosidic bond angles
HIV: human immunodeficiency virus
HIF: Hypoxia-inducible factor
hnRNP: heteronuclear ribonucleoprotein
HPA: 3-Hydroxypicolinic acid
HPLC: high performance liquid chromatography
HRMS: high-resolution mass spectrometry
IR: infrared
LB: leucomethylene blue
LNA: locked nucleic acid
LSV: linear sweep voltammetry
MALDI-TOF: Matrix-assisted laser desorption/ionization- Time-of-Flight
MCE: mercaptoethanol
MCH: mercaptohexanol
MeOH: methanol
MMT: monomethoxytrityl
mRNA: messenger RNA
MB: methylene blue
min: minutes
MW: Molecular weight
n-BuLi: n-butyllithium
NEt_3: triethylamine
NHE: normal hydrogen electrode
NHS: N-hydro-succinimide
NMR: nuclear magnetic resonance
NP: nanoparticle
Nt: nucleotide
ODN: oligonucleotide
OmpC: outer membrane porin protein C
o.n: overnight
PAGE: polyacrylamide gel electrophoresis
PBS: phosphate buffer saline
PIDA : phenyliodonium diacetate
PNA: peptide nucleic acid
PS: polystyrene
pyr: pyrene
RDE: rotating disk electrode
R.E: reference electrode
RISC: RNA-induced silencing complex

RNA: ribonucleic acid
RNAi: interference RNA
RP-HPLC: reversed phase HPLC
r.t: room temperature
SAM: self-assembled monolayer
SCE: saturated calomel electrode
SHE: standard hydrogen electrode
siRNA: small interfering RNA
ssDNA (RNA): single-stranded DNA (RNA)
SVDP: snake venom phosphodiesterase
T: thymidine
TA: thioctic acid
TAE: Tris/acetic acid/EDTA
TBA: thrombin binding aptamer
TBAHP: tetrabutylammonium hexafluorophosphate
TBE: Tris/Borate/EDTA
TBTA: Tris-[(1-benzyl-1H-1,2,3-triazol-4-yl)methyl]amine
tBuOH: tert-butanol
TCA: trichloroacetic acid
TCEP: tris(2-carboxyethyl)phosphine
TEAAc: Triethylammonium acetate

TFA : trifluoroacetic
TfN_3: triflic azide
TFO: triplex forming oligonucleotide
Tf_2O: triflic anhydride
TGS: target-guided synthesis
THAP: 2,4,6-trihydroxyacetophenone monohydride
THF: tetrahydrofuran
thr: threoninol
TLC:thin layer chromatography
Tm: melting temperature
tRNA: transfer RNA
U : uridine
UTR: untranslated regions
UV: ultraviolet
VEGF: Vascular endothelial growth factor
W.E: working electrode
WC: Watson-Crick

CHAPTER 1

Introduction

1.1. DNA: structure and function

Deoxyribonucleic acid (DNA) is the biomolecule responsible for storage, transmission and translation of genetic information and is often compared to a code since it contains the instructions to construct the components of all living organisms. The DNA segments that carry this genetic information are called genes, but other DNA sequences have structural purposes, or are involved in regulating the use of this genetic information.

Chemically, DNA is a polymer consisting in two strands held together in the shape of a helix (Figure 1.1.A) made from repeating units called nucleotides, each of which contains a sugar/phosphate backbone and a nitrogenated base (Figure 1.1.B). The sugars in DNA are 2-deoxyriboses and are joined together by phosphate groups that form phosphodiester bonds between the third and fifth carbon atoms of adjacent sugar rings. The four nitrogenated bases found in DNA are adenine (A), cytosine (C), guanine (G) and thymine (T) and the DNA double helix is stabilized by hydrogen bonds between these bases. Each type of base on one strand forms bonds with just one type of base on the other strand. Thus, adenine forms hydrogen bonds with thymine and guanine with cytosine. (Figure 1.1.C). This complementary base pairing is critical for all the functions of DNA in living organisms. It is the sequence of these four nucleobases which encodes the genetic information.
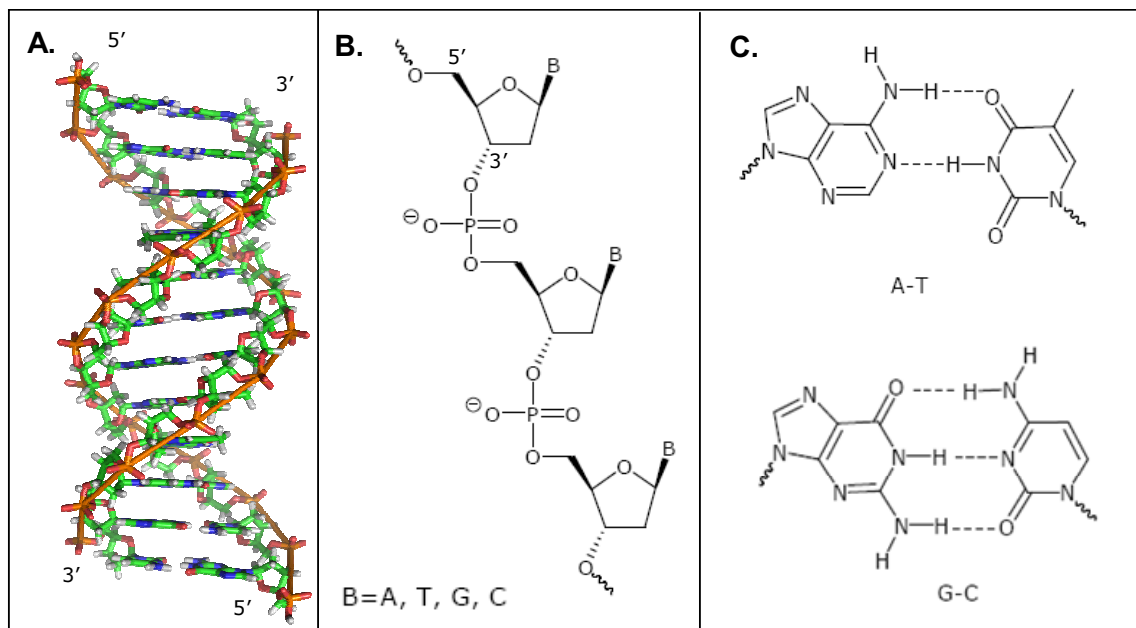
Figure 1.1. A) B-DNA duplex. B) Chemical structure of the backbone of a DNA strand. C) Watson-Crick hydrogen bonds between A-T and C-G.

The sequence of bases is copied into messenger RNA (mRNA) by RNA polymerase in a process called transcription. This mRNA is then decoded by a ribosome that reads its sequence and translates it into proteins. This process is called translation and is determined by a set of rules known as genetic code, which

defines a correspondence between tri-nucleotide sequence of mRNA (codons) and amino acids carried by transfer RNA (tRNA).

One major difference between DNA and RNA (ribonucleic acid) is the sugar, with the 2'-deoxyribose in DNA being replaced by the alternative pentose sugar ribose in RNA, and uracil, a base that pairs with adenine and replaces thymine during DNA transcription.

In a DNA double helix the direction of the nucleotides in one strand is opposite to their direction in the other strand: the strands are antiparallel. The asymmetric ends of DNA strands are known as 5' and 3' ends, with the 5' end having a terminal phosphate group and the 3' end a terminal hydroxyl group.

Three different forms of duplex have been observed (figure 1.2), the most common in functional organisms being the B-form. In this helix, spaces between strands are unequally sized and are known as major and minor groove. Both are targets for DNA-binding drugs. A-form occurs under non-physiological conditions in partially dehydrated samples of DNA (e.g., those employed in crystallographic experiments) while in living cells is adopted in hybrid pairings of DNA and RNA strands, as well as in some enzyme-DNA complexes [1,2]. The A-DNA form is a wider right-handed spiral, with a shallow, wide minor groove and a narrower, deeper major groove than the B-DNA.

Intriguingly, the first resolved DNA crystal presented a left-handed double helix, in contrast to A- and B-form, and was named Z-DNA due to the zig-zag arrangement of its backbone [3] The major and minor grooves, unlike A- and B-DNA, show little difference in width. Z-DNA is believed to be formed transiently and provide torsional strain relief during negative supercoiling generated in transcription processes [4]. In addition other biological roles have been suggested after the discovery that certain classes of proteins bound to Z-DNA with high affinity and great specificity [5-8].

A comparison between the different conformations of a DNA double helix is shown below.
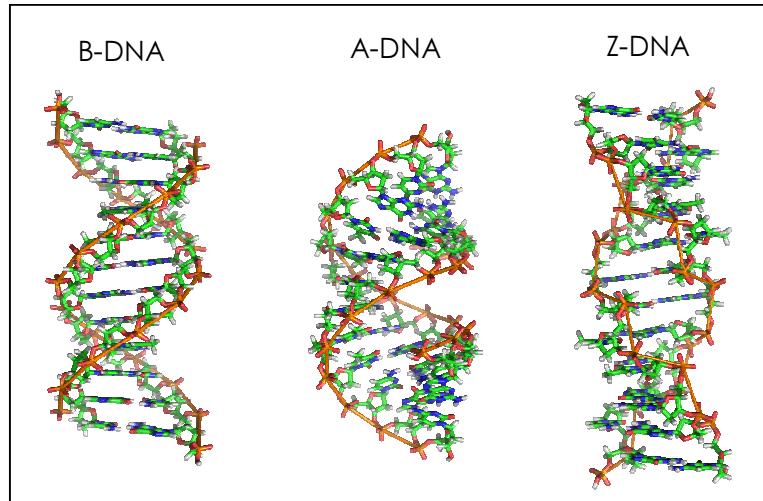
Figure 1.2. Different conformations of a DNA duplex.

The remarkable conformational flexibility of nucleic acids allows for the formation of a great variety of structures besides the double helix such as triplex, G-quadruplex or i-motifs (Figure 1.3).
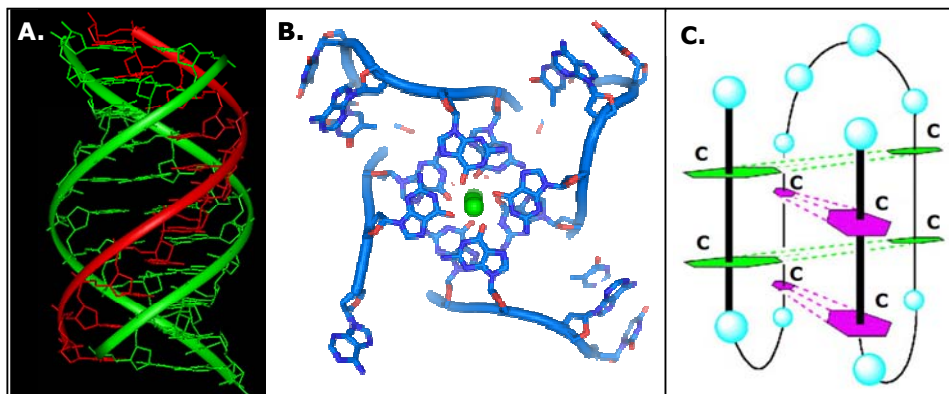
Figure 1.3. Non canonical DNA structures. A) Triple helix. B) Quadruplex. C) i-motif.

In a DNA triplex, the triplex-forming oligonucleotide binds to a polypurine-polypyrimidine region of dsDNA in the major groove through specific hydrogen bonds (Figure 1.3.A).

G-rich and C-rich DNA strands can form unusual structures. The G-rich strand can adopt a four stranded G-quadruplex structure [9] involving planar G-quartets (Figure 1.3.B) while the C-rich strand can form the so-called i-motif (Figure 1.3.C) with intercalated C:C+ base pairs [10].

These DNA structures have received considerable attention in the last years for their biological relevance. The ability of triplex forming oligonucleotides (TFOs) to bind specifically to certain duplex DNA regions provides a strategy for site-directed modification of genomic DNA. On the other hand quadruplexes have been found in telomeres and some promoters and play a role in regulation of

3

transcription and translation. They are also interesting for nanotechnological devices. The description of these structures and properties will be described in more detail in different chapters in this thesis together with a study of modified oligonucleotides capable of forming triplex and quadruplex structures.

1.2. Oligonucleotides and their applications

Oligonucleotides (ODNs) are short fragments of DNA composed of a low number of nucleotides (typically between 10-100nt) which hybridize like their larger relatives and are valuable models to investigate the physical and biological properties of DNA that would be intractable otherwise.

The development of automated synthetic procedures for the obtention of oligonucleotides has triggered the extensive use of these molecules in a high variety of applications ranging from molecular biology to biomedicine and nanotechnology. As a result of their ability to base pairing, oligonucleotides are used as primers, hybridization probes in biosensors, agents for controlling gene expression, structural material in nanodevices or as substrates for a variety of biochemical and biophysical studies.

1.2.1. Oligonucleotides as therapeutic agents

When a cell uses the information in a gene, the DNA sequence is copied into a complementary RNA sequence (transcription) known as messenger RNA or mRNA. This mRNA is then used to make a matching protein sequence in a process called translation.

There are different strategies to modulate the gene expression with oligonucleotides depending on the therapeutic target (Figure 1.4). In the **antigene** strategy oligonucleotides bind to DNA forming a triple helix, thus blocking transcription to mRNA. When the target is the mRNA, the strategy is known as **antisense**. In this case, formation of the oligonucleotide-mRNA complex inhibits translation to proteins. Another possibility to interfere with translation is the use of **ribozymes**, oligonucleotides that bind specifically to mRNA causing its degradation. There are also oligonucleotides called **aptamers** that can bind very specifically to proteins (in a similar way as antibodies do) and modify their activity.

A particularly interesting case is the **RNA interference** (RNAi), a system within living cells that helps to control which genes are active and how active they are. Small interference RNA (siRNA) are 21-23 bp short RNA duplexes that are incorporated into the RNA-induced silencing complex (RISC), which targets messenger RNA, cleaves it and prevents translation. The selective and robust effect of RNAi on gene expression makes it a valuable research tool, both in cell culture and in living organisms because synthetic dsRNA introduced into cells can induce suppression of specific genes of interest.

Figure 1.4 shows a schematic representation of the different therapeutic approaches based on oligonucleotides.
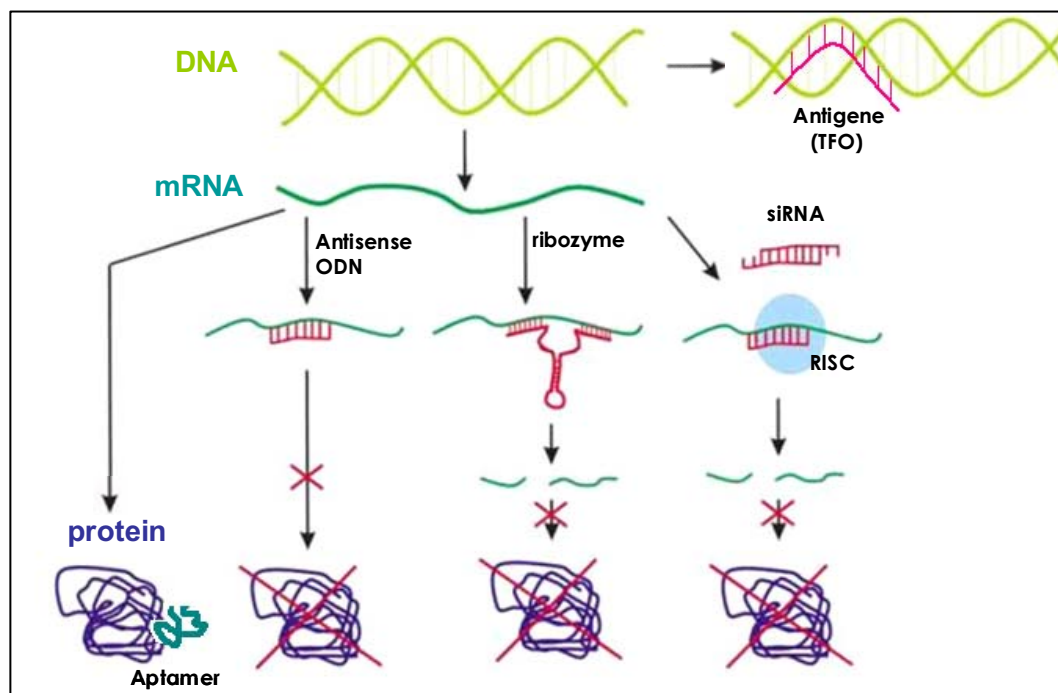
Figure 1.4. Scheme of the different oligonucleotides-based therapeutic strategies.

Although only two DNA-based pharmaceuticals have been approved by regulatory agencies (e.g. Vitravene, an antisense ODN formulation developed by ISIS Pharmaceuticals for the treatment of cytomegalovirus retinitis and Macugen, an ophthalmological anti-VEGF aptamer by Pfizer/ Eyetech Pharmaceuticals), numerous candidates are in advanced stages of human clinical trials and are extremely promising drugs for therapy for a wide range of diseases including cancer [11,12], AIDS [13], diabetes [14,15] or cardiovascular disorders [16].

Limited successes in the development of DNA-based drugs can be attributed to their poor cellular uptake and biological stability with the consequent unpredictable pharmacokinetics. Simultaneous advances in chemical synthesis and derivatization strategies to generate modified oligonucleotides with enhanced delivery, targeting and biostability properties have yielded promising results for clinical applications. Furthermore, recent developments in human genomics, transcriptomics, and proteomics will provide an additional impetus for the advancement of DNA-based therapeutics by supplying novel targets for drug design, screening, and selection.

1.2.2. Oligonucleotides as tools in DNA-templated synthesis

The hybridization properties of DNA can be exploited to direct chemical reactions in a sequence-specific manner. In 2001, Liu and co-workers showed that complementary DNA oligonucleotides can be used to assist certain synthetic reactions, which do not efficiently take place in solution at low concentration [17]. The scheme of figure 1.5 shows the basis of a DNA-templated synthesis, where a DNA duplex is used to accelerate the reaction between chemical moieties displayed at the extremities of the two DNA strands.
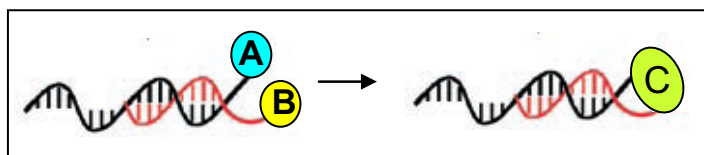
Scheme 1.5. Depiction of a DNA-templated synthesis approach. **A** and **B** substrates are linked to complementary oligonucleotides to yield the **C** product in a DNA-templated fashion.

The close proximity conferred by the DNA hybridization drastically increases the effective molarity of the reaction reagents attached to the oligonucleotides, enabling the desired reaction to occur even at concentrations which are several orders of magnitude lower than those needed for the corresponding conventional organic reaction.

This approach is useful in those reactions that cannot easily be performed by conventional synthetic methods, such as heterocoupling reactions between substrates that preferentially homocouple. These unique features of effective-molarity-controlled reactivity may expand the accessibility and structural diversity of libraries of synthetic small molecules and heteropolymers beyond what is possible with current approaches.

1.2.3. Oligonucleotides as useful tools in nanotechnology

DNA is a unique material for nanotechnology since it is possible to use base sequences to encode instructions for assembly in a predetermined fashion at the nanometer scale. The unique molecular recognition properties of DNA can be used to create self-assembling DNA complexes with useful properties. Thus, DNA has been used for the creation of two-dimensional periodic lattices as well as three-dimensional structures in the shapes of polyhedra [18-20].

Figure 1.6.A. shows a model composed of nine DNA sequences programmed to combine into a specific pattern. The single stranded overhangs located at the ends of double helical domains (known as "sticky ends") allow self-assembling into a highly ordered periodic two-dimensional DNA nanogrid, as can be seen in the AFM image of figure 1.6.B.

A number of three-dimensional molecules have been made of DNA duplexes tracing the edges of a polyhedron, e.g. an octahedron [21] or a cube [22], with a DNA junction at each vertex. In figure 1.6.C a model of a DNA tetrahedron described by Goodman et al. [23-25] is shown. Each edge of the tetrahedron is a 20 base pair DNA duplex, and each vertex is a three-arm junction.

A few years ago a method named "DNA origami" was developed by Rothemund to create two and three dimensional shapes by DNA folding [19]. The process involves the folding of a long single strand of viral DNA aided by multiple shorter strands in various places, resulting in various shapes including a smiling face like the one presented in figure 1.6.D.
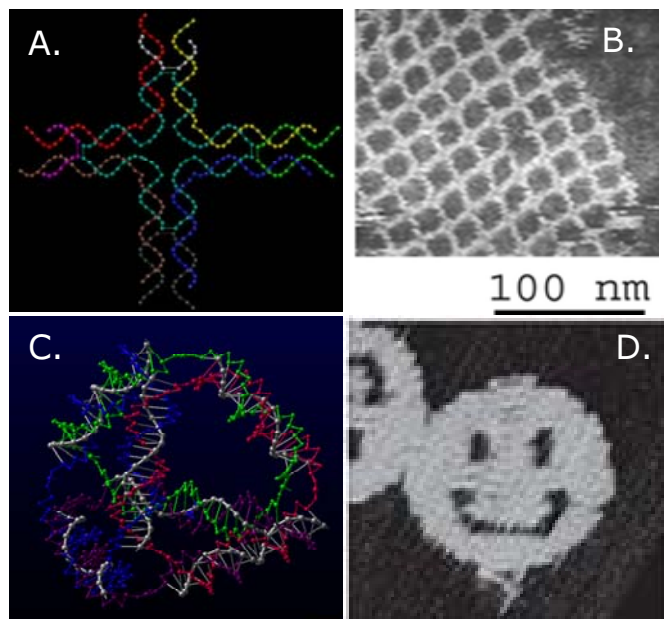
Figure 1.6. A) Model of a DNA tile used to make a two-dimensional periodic lattice. B) Atomic force microscopy (AFM) image of a 2D DNA nanogrid. Extracted from reference [26]. C) DNA tetrahedron described by Goodman *et al.* [23]. D) AFM image of a DNA origami. Extracted from reference [19].

Through the conjugation of synthetic oligonucleotides of predetermined sequences with different materials (e.g. nanoparticles, streptavidine...), the exact spatial positioning of these latter can be designed, which is leading towards fabrication of electronic nanodevices or biosensors [27] (Figure 1.7.A.). In addition the controlled metallization of oligonucleotide strands [28-31] provides also an important step toward the assembly of functional nanocircuits (Figure 1.7.B).
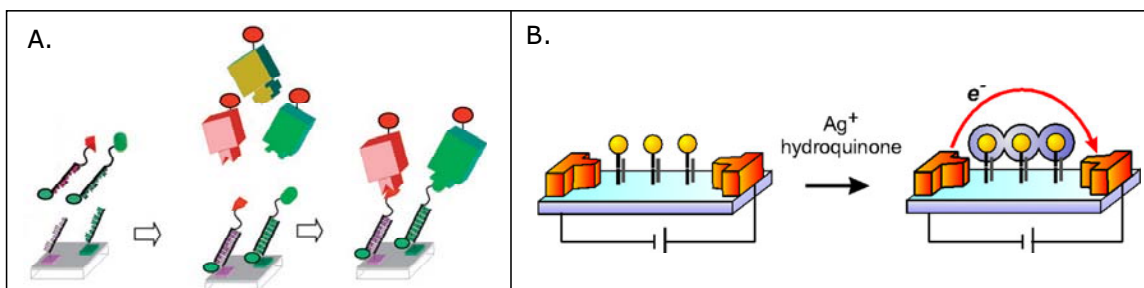
Figure 1.7. A) Schematic representation of the design of biomolecules microarrays using a DNA-anchoring platform [27]. B) Scheme for resistive detection of nanoparticle-labelled DNA microelectrode arrays [31].

For example, a DNA array detection method has been reported by Mirkin *et al.* in which the binding of oligonucleotides functionalized with gold nanoparticles leads to conductivity changes associated with target-probe binding events [31].

1.2.4. Oligonucleotides and chemical modifications

Chemical modifications have been extensively used to improve outstanding problems which limit the use of oligonucleotides as therapeutic agents, such as serum stability or nuclease resistance, bioavailability and cell uptake, specificity, affinity, biodistribution and cell targeting.

Figure 1.8 shows a representation of the different positions in the oligonucleotides structure where modifications can be introduced.
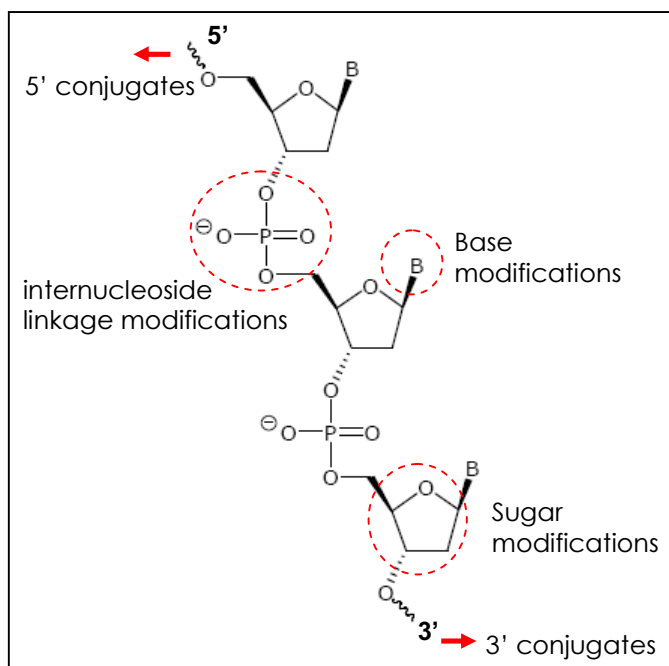
Figure 1.8. Different positions where modifications can be introduced in an oligonucleotide: backbone, sugar and nucleobases as well as derivatization or conjugation at the 3' or 5'.

8

- Backbone modifications

Among the first modifications made to oligonucleotides were alterations of the phosphodiester backbone to stabilize these molecules towards enzymatic degradation and improve their cell membrane permeability.

Modifications such as phosphorothioates [32,33] or phosphoramidates [34] were conceived in order to change electrostatic properties of the negative phosphate backbone of natural DNA. Phosphonoacetate and thiophosphonoacetate were explored by Caruthers and co-workers [35,36] and showed very high nuclease resistance when incubated with snake venom phosphodiesterase or DNase I.

More drastic changes such as the complete replacement of the phosphodiester linkage is also common such as amide [37], guanidine [38], methylthiourea [39] or acetal linkages [40].

- Sugar-phosphodiester backbone modifications

An important class of modified oligonucleotides is one in which the sugar–phosphodiester backbone has been replaced entirely, such is the case of peptide nucleic acids (PNAs) introduced firstly by Nielsen in 1991 [41] and extensively reviewed in the literature [42-44]. PNA's backbone is composed of repeating N-(2-aminoethyl)-glycine units linked by peptide bonds and since it contains no charged phosphate groups, its hybridization with complementary DNA strand is stronger than between DNA/DNA strands of a natural duplex due to the lack of electrostatic repulsion. This increased target affinity compared to unmodified oligonucleotides can be of great help for applications based on sequence-specific detection of DNA/RNA including diagnostics, forensic science, in vivo imaging and biodistribution.

For example work carried out by Spoto *et al.* used PNA capture probes to lower detection limits and increase sensitivity in a surface plasmon resonance sandwich DNA hybridization assay [45].

In addition PNAs are not easily recognized by either nucleases or proteases, which makes them resistant to enzyme degradation and useful for in vivo applications.

- Sugar modifications

Modifications in the sugar moiety of oligonucleotides have also been developed. One of the most notable examples is the locked nucleic acids (LNA) described in 1998 by Wengel and colleagues [46,47]. LNA nucleotides contain a methylene bridge that connects the 2'-oxygen of ribose with the 4'-carbon and their insertion into DNA or RNA strands increase the strength of base-stacking interaction [48,49].This exceptional hybridization affinity toward complementary DNA/RNA has

been exploited in antisense therapy [50,51]. In next chapter, the effect of these modifications on the stability of triple helices will be addressed.

Morpholino derivatives have also been examined as antisense agents and triplex forming agents by different authors [52-54]. In these oligonucleotide analogs the deoxyribose rings are replaced with six-membered morpholino rings commonly linked through phosphorodiamidate groups although other linkages between morpholino units have been developed as is the case of morpholinoamidine [55] or oxalyl diamide morpholino analogs [56].

Substituents in the 2' position of pentose sugar have been extensively used, especially in siRNAs [57,58], to increase their resistance to endonucleases and serum stability and enhance mRNA targeting efficiency. Some examples of these modifications are 2'-O-Methyl (2'-OMe), 2'-O-Methoxyethyl (2'-MOE), 2'-fluoro (2'-F) or 2'-amino (2'-NH_2).

Replacement of the 4'-oxygen of nucleosides by other atoms such as 4'-thio [59] or 4'-selenonucleotide [60] has also been established.

- Nucleobase modifications

Modifications to the nucleobases have been explored to increase the stability of duplexes and triple helices.

Some examples include 5-methylcytosine [61], 8-oxoadenine [62], 8-aminopurines [63,64], 5-halopyrimidines [65], 5-propynylpyrimidines [66,67], 7-deaza-purines [68,69], 7-deaza-xanthine [70], isoguanine [71], etc. A high number of nucleobase modifications have been extensively reviewed in the literature [57,72,73].

- Oligonucleotide derivatives and conjugates

The conjugation of oligonucleotides to different functional molecules is a valuable tool that allows for modulation of both therapeutical and biotechnological properties. Such conjugate groups confer a variety of important properties, these include fluorescent emission to allow sensitive detection [74], altered hydrophobicity or bioaffinity [75], enhanced cellular uptake [76], resistance towards degradation [77], novel electrochemical properties [78] and the ability to coordinate metal ions [79], to mention just a few.

Examples to overcome problems associated with delivery and localization of oligonucleotides in cells include conjugation and/or binding to cholesterol [75], liposomes [80], lipoplexes [81], lipids [76], poly(ethylene glycol) [82], nanoparticles [83], antibodies [84], peptides [85], aptamers [86] or dendrimers [87].

Recently, considerable attention has been paid to cellular transfection of antisense oligonucleotides with a high diversity of nanoparticles (NPs). Among the most polular choice for NP material is gold due to its high affinity for thiolated oligonucleotides [88,89] but other NPs have been developed such as nanosized bioceramic nanoparticles coated with cationic polymers [90].

A common strategy to enhance ability of oligonucleotides to target and accumulate within desired cells is the conjugation to cell surface receptors. Thus, some studies have reported receptor-mediated cell internalization of oligonucleotides based on molecular recognition processes. For example, McNamara *et al*. observed gene silencing specifically in prostate cancer cells expressing the prostate-specific membrane antigen in their surface using siRNAs conjugated to an aptamer against this receptor [91].

Dendrimers are also used to deliver ODNs into cells. These molecules are highly branched, typically symmetric around a core, and often adopt a spherical three-dimensional morphology. Their physical characteristics include encapsulation ability and make these macromolecules good candidates as ODN delivery vehicles [87,92,93].

Other molecules that have shown promise in transfection of ODNs are cell-penetrating peptides (CPPs), such as HIV Tat47–57, transportan, Antp43–58 and oligoarginines, which have been recently reviewed [85,94,95]. Their cationic nature has been suggested to promote ODNs transfection through cellular endocytosis-mediated uptake.

Another field where conjugation of ODNs plays a relevant role is nano and biotechnology. DNA-based biosensors rely on highly specific recognition events (hybridization) to detect target analytes. In a classical DNA-based sensor an immobilized ssDNA sequence act as the probe to detect specific DNA sequence. This DNA probe can be either chemically or enzymatically labeled with radioactive material [96], fluorescent compounds [74], nanoparticles [97] or ligands such as biotin [98], to facilitate the triggering of a detectable signal. In other cases DNA act simply as an anchoring platform, as mentioned before (Figure 1.7), in which cases ODNs are conjugated to molecules able to recognize a desired target [27].

1.3. Objectives

This thesis is focused on nucleic acid chemistry. The main objective is the synthesis of modified oligonucleotides for triple helix studies and for obtaining structures with therapeutical and/or biotechnological interest.

The second chapter covers the study of triplex-stabilizing properties of chemically modified oligonucleotide hairpins. The synthesis of parallel stranded duplexes carrying LNA residues is described and the stability of the triplex formed with their DNA and RNA target sequences are analyzed by melting experiments.

The third chapter focuses in the development of a novel strategy based on click chemistry for the obtention of such structures. For this purpose, azido and alkyne moieties are introduced in the 5'-end of different homopurine and homopyrimidine sequences so that the modified DNA strands could form a parallel hairpin after their chemical ligation by click chemistry.

As mentioned before, conjugation of oligonucleotides with different functional molecules allows modulation of some of their properties. In the fourth chapter derivatization of oligonucleotides with molecules that are able to coordinate copper ions and the study of their electrochemical properties is addressed.

Finally, the last chapter includes the study of quadruplex-forming sequences modified with 8-aminoguanine substitutions. A molecule composed of four oligonucleotide strands whose 5' ends are covalently attached is employed as a system to study the effect of these nucleobase modifications in quadruplex structure and stability.

1.4. References

[1]. Wahl, M., and Sundaralingam, M. (1997) Crystal structures of A-DNA duplexes. *Biopolymers* 44, 45–63.

[2]. Lu, X.J., Shakked, Z., and Olson, W.K. (2000) A-form conformational motifs in ligand-bound DNA structures. *J. Mol. Biol*. 300, 819–840.

[3]. Wang, A.H.J., Quigley, G.J., Kolpak, F.J., Crawford, J.L., van Boom J.H., Van der Marel, G., and Rich, A. (1979) Molecular structure of a left-handed double helical DNA fragment at atomic resolution". *Nature* 282, 680–686.

[4]. Rich, A., and Zhang, S. (2003) Timeline: Z-DNA: the long road to biological function. *Nat. Rev. Genet*. 4, 566–572.

[5]. Nordheim, A., Tesser, P., Azorin, F., Kwon, Y. H., Möller, A., and Rich, A. (1982) Isolation of Drosophila Proteins that Bind Selectively to Left-Handed Z-DNA. *Proc. Natl. Acad. Sci. USA. 79*, 7729-7733.

[6]. Kim, Y. G., Lowenhaupt, K., Schwartz, T. and Rich, A. (1999) The interaction between Z-DNA and the Zab domain of dsRNA adenosine deaminase characterized using fusion nucleases. *J. Biol. Chem*. 274, 19081–19086.

[7]. Oh, D., Kim, Y., and Rich, A. (2002) Z-DNA-binding proteins can act as potent effectors of gene expression in vivo. *Proc. Natl. Acad. Sci. U.S.A*. 99, 16666–16671.

[8]. Kim, Y.G., Lowenhaupt, K., Oh, D.B., Kim, K.K., and Rich, A. (2004) Evidence that vaccinia virulence factor E3L binds to Z-DNA in vivo: Implications for development of a therapy for poxvirus infection. *Proc. Natl. Acad. Sci. USA* 101, 1514–1518.

[9]. Williamson, J.R., Raghuraman, M.K., and Cech, T.R. (1989). Monovalent cation induced structure of telomeric DNA: the G-quartet model. *Cell* 59, 871-680.

[10]. Gehring, K., Leroy, J.L. and Guéron, M. (1993) A tetrameric structure with protonated cytosine-cytosine base pairs. *Nature* 363, 561-565.

[11]. Olie, R. A., Simoes-Wust, A. P., Baumann, B., Leech, S. H., Fabbro, D., Stahel, R. A., and Zangemeister-Wittke, U. (2000) A Novel Antisense Oligonucleotide Targeting Survivin Expression Induces Apoptosis and Sensitizes Lung Cancer Cells to Chemotherapy. *Cancer Res. 60*, 2805-2809.

[12]. Matsubara, H., Takeuchi, T., Nishikawa, E., Yanagisawa, K., Hayashita, Y., Ebi, H., Yamada, H., Suzuki, M., Nagino, M., Nimura, Y., Osada, H., and Takahashi, T. (2007) Apoptosis Induction by Antisense Oligonucleotides Against miR-17-5p and miR-20a in Lung Cancers Overexpressing miR-17-92. *Oncogene. 26*, 6099-6105.

[13]. Agrawal, S., and Tang, J. Y. (1992) GEM 91--an Antisense Oligonucleotide Phosphorothioate as a Therapeutic Agent for AIDS. *Antisense Res. Dev. 2*, 261-266.

[14]. Sloop, K. W., Cao, J. X., Siesky, A. M., Zhang, H. Y., Bodenmiller, D. M., Cox, A. L., Jacobs, S. J., Moyers, J. S., Owens, R. A., Showalter, A. D., Brenner, M. B., Raap, A., Gromada, J., Berridge, B. R., Monteith, D. K. B., Porksen, N., McKay, R. A., Monia, B. P., Bhanot, S., Watts, L. M., and Michael, M. D. (2004) Hepatic and Glucagon-Like Peptide-1-Mediated Reversal of Diabetes by Glucagon Receptor Antisense Oligonucleotide Inhibitors. *J. Clin. Invest. 113*, 1571-1581.

[15]. Zinker, B. A., Rondinone, C. M., Trevillyan, J. M., Gum, R. J., Clampit, J. E., Waring, J. F., Xie, N., Wilcox, D., Jacobson, P., Frost, L., Kroeger, P. E., Reilly, R. M., Koterski, S., Opgenorth, T. J., Ulrich, R. G., Crosby, S., Butler, M., Murray, S. F., McKay, R. A., Bhanot, S., Monia, B. P., and Jirousek, M. R. (2002) PTP1B Antisense Oligonucleotide Lowers PTP1B Protein, Normalizes Blood Glucose, and Improves Insulin Sensitivity in Diabetic Mice. *Proc. Natl. Acad. Sci. USA. 99*, 11357-11362.

[16]. Pollman, M. J., Hall, J. L., Mann, M. J., Zhang, L., and Gibbons, G. H. (1998) Inhibition of Neointimal Cell Bcl-x Expression Induces Apoptosis and Regression of Vascular Disease. *Nat. Med. 4*, 222-227.

[17]. Gartner, Z. J., and Liu, D. R. (2001) The Generality of DNA-Templated Synthesis as a Basis for Evolving Non-Natural Small Molecules. *J. Am. Chem. Soc. 123*, 6961-6963.

[18]. Winfree, E., Liu, F., Wenzler, L. A., and Seeman, N. C. (1998) Design and self-assembly of two-dimensional DNA crystals. *Nature* 394, 539 – 544.

[19]. Rothemund, P. W. K. (2006) Folding DNA to Create Nanoscale Shapes and Patterns. *Nature. 440*, 297-302.

[20]. He, Y., Ye, T., Su, M., Zhang, C., Ribbe, A. E., Jiang, W., and Mao, C. (2008) Hierarchical Self-Assembly of DNA into Symmetric Supramolecular Polyhedra. *Nature. 452*, 198-201.

[21]. Zhang, Y., and Seeman, N. C. (1994) The construction of a DNA truncated octahedron. *J. Am. Chem. Soc*. 116, 1661–1669.

[22]. Chen, J. H., and Seeman, N. C. (1991) Synthesis from DNA of a molecule with the connectivity of a cube. *Nature* 350, 631–633.

[23]. Goodman, R. P., Berry, R. M., and Turberfield, A. J. (2004) The Single-Step Synthesis of a DNA Tetrahedron. *Chem. Commun*. 12, 1372 – 1373.

[24]. Goodman, R. P., Schaap, I. A. T., Tardin, C. F., Erben, C. M., Berry, R. M., Schmidt, C. F., and Turberfield, A. J. (2005) Rapid Chiral Assembly of Rigid DNA Building Blocks for Molecular Nanofabrication. *Science. 310*, 1661-1665.

[25]. Goodman, R. P., Heilemann, M., Doose, S., Erben, C. M., Kapanidis, A. N., and Turberfield, A. J. (2008) Reconfigurable, Braced, Three-Dimensional DNA Nanostructures. *Nat Nano. 3*, 93-96.

[26]. Strong, M. (2004) Protein Nanomachines. *PLoS Biol. 2*, e73.

[27]. Chevolot, Y., Bouillon, C., Vidal, S., Morvan, F., Meyer, A., Cloarec, J-P., Jochum, A., Praly, J-P., Vasseur, J-J., and Souteyrand, E. (2007) DNA-Based Carbohydrate Biochips: A Platform for Surface Glyco-Engineering. *Angew. Chem. Int. Ed*n. *119*, 2450-2454.

[28]. Braun, E., Eichen, Y., Sivan, U., and Ben-Yoseph, G. (1998) DNA-templated assembly and electrode attachment of a conducting silver wire. *Nature* 391, 775–778.

[29] Richter, J., Seidel, R., Kirsch, R., Mertig, M., Pompe, W., Plaschke, J. and Schackert, H. K. (2000) Nanoscale palladium metallization of DNA. *Adv. Mater*. 12, 507-510.

[30] Monson, C. F., and Woolley, A. T. (2003) DNA-Templated Construction Of Copper Nanowires. *Nano Lett*. 3, 359–363.

[31]. Park, S-J., Taton, T.A. and Mirkin, C.A. (2002) Array-Based Electrical Detection of DNA with Nanoparticle Probes. *Science* 295, 1503–1506.

[32]. Eckstein, F. (1985) Nucleoside phosphorothioates, *Annu. Rev. Biochem*. 54, 367-402.

[33]. Vu, H., Hirschbein, B.L. (1991) Internucleotide Phosphite Sulfurization With Tetraethylthiuram Disulfide. Phosphorothioate Oligonucleotide Synthesis Via Phosphoramidite Chemistry, *Tetrahedron Lett*. 32, 3005-3008.

[34]. Gryaznov, S.M. (1999) Oligonucleotide N3' → P5' Phosphoramidates As Potential Therapeutic Agents. *Biochim. Biophys. Acta*, 1489, 131-140.

[35]. Dellinger, D. J., Sheehan, D. M., Christensen, N. K., Lindberg, J. G., and Caruthers, M. H. (2003) Solid-Phase Chemical Synthesis of Phosphonoacetate and Thiophosphonoacetate Oligodeoxynucleotides. *J. Am. Chem. Soc. 125*, 940-950.

[36]. Sheehan, D., Lunstad, B., Yamada, C. M., Stell, B. G., Caruthers, M. H., and Dellinger, D. J. (2003) Biochemical Properties of Phosphonoacetate and Thiophosphonoacetate Oligodeoxyribonucleotides. *Nucl. Acids Res. 31*, 4109-4118.

[37]. Lebreton, J., De Mesmaeker, A., Waldner, A., Fritsch, V., Wolf, R.M., and Freier, S.M. (1993) Synthesis Of Thymidine Dimer Derivalives Containing An Amide Linkage And Their Incorporation Into Oligodeoxyribonucleotides. *Tetrahedron Lett*. 34, 6383-6386.

[38]. Vandendriessche, F., Van Aerschot, A., Voortmans, M., Janssen, G., Busson, R., Van Overbeke, A., Van den Bossche, W., Hoogmartens, J., and Herdewijn, P. (1993) Synthesis, Enzymatic Stability And Base-Pairing Properties Of Oligothymidylates Containing Thymidine Dimmers With Different N-Substituted Guanidine Linkages. *J. Chem. Soc., Perkin Trans. 1*, 1567-1575.

[39]. Arya, D. P., and Bruice, T. C. (1998) Replacement of the Negative Phosphodiester Linkages of DNA by Positive S-Methylthiourea Linkers: A Novel Approach to Putative Antisense Agents. *J. Am. Chem. Soc. 120*, 6619-6620.

[40]. Matteucci, M.D. (1990) Deoxyoligonucleotide Analogs Based On Formacetal Linkages. *Tetrahedron Lett*. 31, 2385-2388.

[41]. Nielsen, P., Egholm, M., Berg, R., and Buchardt, O. (1991) Sequence-Selective Recognition of DNA by Strand Displacement with a Thymine-Substituted Polyamide. *Science. 254*, 1497-1500.

[42]. Wojciechowski, F., and Hudson, R. H. E. (2007) Nucleobase Modifications in Peptide Nucleic Acids. *Curr. Top. Med. Chem*. 7, 667-679.

[43]. Pensato, S., Saviano, M., and Romanelli, A. (2007) New Peptide Nucleic Acid Analogues: Synthesis and Applications. *Expert Opin Biol Ther. 7*, 1219-1232.

[44]. Sahu, N., Shilakari, G., Nayak, A., and Kohli, D. V. (2008) Peptide Nucleic Acids: A Novel Approach. *Curr. Chem. Biol.* 2, 110-121.

[45]. R. D'Agata, R. Corradini, R., Grasso, G., Marchelli, R., and Spoto, G. (2008) Ultrasensitive Detection of DNA by PNA and Nanoparticle-Enhanced Surface Plasmon Resonance Imaging. *ChemBioChem* 9, 2067-2070.

[46]. Koshkin, A. A., Rajwanshi, V. K., and Wengel, J. (1998) Novel Convenient Syntheses of LNA [2.2.1]Bicyclo Nucleosides. *Tetrahedron Lett. 39*, 4381-4384.

[47]. Koshkin, A. A., Singh, S. K., Nielsen, P., Rajwanshi, V. K., Kumar, R., Meldgaard, M., Olsen, C. E., and Wengel, J. (1998) LNA (Locked Nucleic Acids): Synthesis of the Adenine, Cytosine, Guanine, 5-Methylcytosine, Thymine and Uracil Bicyclonucleoside Monomers, Oligomerisation, and Unprecedented Nucleic Acid Recognition. *Tetrahedron. 54*, 3607-3630.

[48]. Petersen, M., Nielsen, C. B., Nielsen, K. E., Jensen, G. A., Bondensgaard, K., Singh, S. K., Rajwanshi, V. K., Koshkin, A. A., Dahl, B. M., Wengel, J., and Jacobsen, J.P. (2000) The Conformations of Locked Nucleic Acids (LNA). *J. Mol. Recognit.* 13, 44-53.

[49]. McTigue, P. M., Peterson, R. J., and Kahn, J. D. (2004) Sequence-Dependent Thermodynamic Parameters for Locked Nucleic Acid (LNA)-DNA Duplex Formation. *Biochemistry.* 43, 5388-5405.

[50]. Wahlestedt, C., Salmi, P., Good, L., Kela, J., Johnsson, T., Hökfelt, T., Broberger, C., Porreca, F., Lai, J., Ren, K., Ossipov, M., Koshkin, A., Jakobsen, N., Skouv, J., Oerum, H., Jacobsen, M. H., and Wengel, J. (2000) Potent and Nontoxic Antisense Oligonucleotides Containing Locked Nucleic Acids. *Proc. Natl. Acad. Sci. USA.* 97, 5633-5638.

[51]. Fluiter, K., ten Asbroek, A. L., de Wissel, M. B., Jakobs, M. E., Wissenbach, M., Olsson, H., Olsen, O., Oerum, H., and Baas, F. (2003) In Vivo Tumor Growth Inhibition And Biodistribution Studies Of Locked Nucleic Acid (LNA) Antisense Oligonucleotides. *Nucleic Acids Res.* 31, 953-962.

[52]. Summerton, J. (1999) Morpholino Antisense Oligomers: The Case For An Rnase H-Independent Structural Type. *Biochim. Biophys. Acta*, 1489, 141-158

[53]. Lacroix, L., Arimondo, P. B., Takasugi, M., Hélène, C., and Mergny, J. (2000) Pyrimidine Morpholino Oligonucleotides Form a Stable Triple Helix in the Absence of Magnesium Ions. *Biochem. Biophys. Res. Commun. 270*, 363-369.

[54]. Torigoe, H., Kawahashi, K., and Tamura, Y. (2003) Promotion of Triplex Formation by Morpholino Modification: Thermodynamic and Kinetic Studies. *NUCLEIC ACIDS SYMP SER (OXF) 3*, 157-158.

[55]. Pérez-Rentero, S., Alguacil, J., and Robles, J. (2009) Novel Oligonucleotide Analogues Containing a Morpholinoamidine Unit. *Tetrahedron*. 65, 1171-1179.

[56]. Abramova, T. V., Kassakin, M. F., Lomzov, A. A., Pyshnyi, D. V., and Silnikov, V. N. (2007) New Oligonucleotide Analogues Based on Morpholine Subunits Joined by Oxalyl Diamide Tether. *Bioorg. Chem. 35*, 258-275.

[57]. Manoharan, M. (2004) RNA Interference and Chemically Modified Small Interfering RNAs. *Curr. Opin. Chem. Biol.* 8, 570-579.

[58]. Bumcrot, D., Manoharan, M., Koteliansky, V., and Sah, D. W. Y. (2006) RNAi Therapeutics: A Potential New Class of Pharmaceutical Drugs. *Nat Chem Biol. 2*, 711-719.

[59]. Jones, G., Lesnik, E., Owens, S., Risen, L., and Walker, R. (1996) Investigation of some Properties of Oligodeoxynucleotides Containing 4'- Thio-2'-Deoxynucleotides: Duplex Hybridization and Nuclease Sensitivity. *Nucl. Acids Res. 24*, 4117-4122.

[60]. Watts, J. K., Johnston, B. D., Jayakanthan, K., Wahba, A. S., Pinto, B. M., and Damha, M. J. (2008) Synthesis and Biophysical Characterization of Oligonucleotides Containing a 4'-Selenonucleotide. *J. Am. Chem. Soc. 130*, 8578-8579.

[61]. Ferrer, E., Shevchenko, A., and Eritja, R. (2000) Synthesis And Hybridization Properties Of DNA-PNA Chimeras Carrying 5-Bromouracil And 5-Methylcytosine. *Bioorg. Med. Chem*. 8, 291-297

[62]. Jetter, M. C., and Hobbs, F. W. (1993) 7,8-Dihydro-8-Oxoadenine as a Replacement for Cytosine in the Third Strand of Triple Helixes. Triplex Formation without Hypochromicity. *Biochemistry 32*, 3249-3254.

[63]. Aviñó, A., Morales, J. C., Frieden, M., de la Torre, B. G., García, R. G., Cubero, E., Luque, F. J., Orozco, M., Azorín, F., and Eritja, R. (2001) Parallel-Stranded Hairpins Containing 8-Aminopurines. Novel Efficient Probes for Triple-Helix Formation. *Bioorg. Med. Chem. Lett. 11*, 1761-1763.

[64]. Aviño, A., Frieden, M., Morales, J. C., Garcia de la Torre, B., Guimil Garcia, R., Azorin, F., Gelpi, J. L., Orozco, M., Gonzalez, C., and Eritja, R. (2002) Properties of Triple Helices Formed by Parallel-Stranded Hairpins Containing 8-Aminopurines. *Nucl. Acids Res. 30*, 2609-2619.

[65]. Ferrer, E., Wiersma, M., Kazimierczak, B., Müller, C. W., and Eritja, R. (1997) Preparation and Properties of Oligodeoxynucleotides Containing 5-Iodouracil and 5-Bromo- and 5-Iodocytosine. *Bioconjug. Chem. 8*, 757-761.

[66]. Shen, L., Siwkowski, A., Wancewicz, E. V., Lesnik, E., Butler, M., Witchell, D., Vasquez, G., Ross, B., Acevedo, O., Inamati, G., Sasmor, H., Manoharan, M., and Monia, B. P. (2003) Evaluation of C-5 Propynyl Pyrimidine-Containing Oligonucleotides in Vitro and in Vivo. *Antisense Nucleic A. 13*, 129-142.

[67]. Wagner, R., Matteucci, M., Lewis, J., Gutierrez, A., Moulds, C., and Froehler, B. (1993) Antisense Gene Inhibition by Oligonucleotides Containing C-5 Propyne Pyrimidines. *Science. 260*, 1510-1513.

[68]. Grein, T., Lampe, S., Mersmann, K., Rosemeyer, H., Thomas, H., and Seela, F. (1994) 3-Deaza- and 7-Deazapurines: Duplex Stability of Oligonucleotides Containing Modified Adenine Or Guanine Bases. *Bioorg. Med. Chem. Lett. 4*, 971-976.

[69]. Schneider, K., and Chait, B. T. (1995) Increased Stability of Nucleic Acids Containing 7-Deaza-Guanosine and 7-Deaza-Adenosine may Enable Rapid DNA Sequencing by Matrix-Assisted Laser Desorption Mass Spectrometry. *Nucl. Acids Res. 23*, 1570-1575.

[70]. Milligan, J. F., Krawazyk, S. H., Wadwani, S., and Matteucci, M. D. (1993) An Anti-Parallel Triple Helix Motif with Oligodeoxynucleotidescontaining 2'-Deoxyguanosine and 7-Deaza-2'-Deoxy Xanthosine. *Nucl. Acids Res. 21*, 327-333.

[71]. Seela, F., and Shaikh, K. I. (2006) PH-Independent Triplex Formation: Hairpin DNA Containing Isoguanine Or 9-Deaza-9-Propynylguanine in Place of Protonated Cytosine. *Org. Biomol. Chem. 4*, 3993–4004.

[72]. Verma, S., and Eckstein, F. (1998) Modified Oligonucleotides: Synthesis and Strategy for Users. *Annu. Rev. Biochem. 67*, 99-134.

[73]. Robles, J., Grandas, A., Pedroso, E., Luque, F. J., Eritja, R., and Orozco, M. (2002) Nucleic Acid Triple Helices: Stability Effects of Nucleobase Modifications. *Curr. Org. Chem. 6*, 1333-1368.

[74]. Fang X., Liu,X., Schuster,S. and Tan,W. (1999) Designing a Novel Molecular Beacon for Surface-Immobilized DNA Hybridization Studies. *J. Am. Chem. Soc.*, 121, 2921–2922.

[75]. Soutschek, J., Akinc, A., Bramlage, B., Charisse, K., Constien, R., Donoghue, M., Elbashir, S., Geick, A., Hadwiger, P., Harborth, J., John, M., Kesavan, V., Lavine, G., Pandey, R. K., Racie, T., Rajeev, K. G., Rohl, I., Toudjarska, I., Wang, G., Wuschko, S., Bumcrot, D., Koteliansky, V., Limmer, S., Manoharan, M., and Vornlocher, H. (2004) Therapeutic Silencing of an Endogenous Gene by Systemic Administration of Modified siRNAs. *Nature. 432*, 173-178.

[76]. Zelphati, O., and Szoka, F. C. (1996) Intracellular Distribution and Mechanism of Delivery of Oligonucleotides Mediated by Cationic Lipids. *Pharm. Res. 13*, 1367-1372.

[77]. Svinarchuk, F. P., Konevetz, D. A., Pliasunova, O. A., Pokrovsky, A. G., and Vlassov, V. V. (1993) Inhibition of HIV Proliferation in MT-4 Cells by Antisense Oligonucleotide Conjugated to Lipophilic Groups. *Biochimie. 75*, 49-54.

[78]. Ihara, T., Maruo, Y., Takenaka, S., and Takagi, M. (1996) Ferrocene-Oligonucleotide Conjugates for Electrochemical Probing of DNA. *Nucl. Acids Res. 24*, 4273-4280.

[79]. Civitello, E. R., Leniek, R. G., Hossler, K. A., Haebe, K., and Stearns, D. M. (2001) Synthesis of Peptide-Oligonucleotide Conjugates for Chromium Coordination. *Bioconjug. Chem. 12*, 459-463.

[80]. Zelphati, O., and Szoka Jr, F.C. (1997) Cationic Liposomes As An Oligonucleotide Carrier: Mechanism Of Action, *J. of Liposome Res. 7*, 31-49.

[81]. Bartsch, M., Weeke-Klimp, A. H., Hoenselaar, E. P. D., Stuart, M. C. A., Meijer, D. K. F., Scherphof, G. L., and Kamps, J. A. A. M. (2004) Stabilized Lipid Coated Lipoplexes for the Delivery of Antisense Oligonucleotides to Liver Endothelial Cells *in Vitro* and *in Vivo. J. Drug Target. 12*. 613 - 621

[82]. Rapozzi, V., Cogoi, S., Spessotto, P., Risso, A., Bonora, G.M., Quadrifoglio F., and Xodo, L.E. (2002) Antigene Effect In K562 Cells Of A PEG-Conjugated Triplex-Forming Oligonucleotide Targeted To The *bcr/abl* Oncogene. *Biochemistry* 41, 502–510.

[83]. Rosi, N. L., Giljohann, D. A., Thaxton, C. S., Lytton-Jean, A. K. R., Han, M. S., and Mirkin, C. A. (2006) Oligonucleotide-Modified Gold Nanoparticles for Intracellular Gene Regulation. *Science. 312*, 1027-1030.

[84]. Song, E., Zhu, P., Lee, S., Chowdhury, D., Kussman, S., Dykxhoorn, D. M., Feng, Y., Palliser, D., Weiner, D. B., Shankar, P., Marasco, W. A., and Lieberman, J. (2005) Antibody Mediated in Vivo Delivery of Small Interfering RNAs Via Cell-Surface Receptors. *Nat Biotech. 23*, 709-717.

[85] Richard, J. P., Melikov, K., Vives, E., Ramos, C., Verbeure, B., Gait, M. J., Chernomordik, L. V., and Lebleu, B. (2003) Cell-Penetrating Peptides. *J. Biol. Chem. 278*, 585-590.

[86]. Chu, T. C., Twu, K. Y., Ellington, A. D., and Levy, M. (2006) Aptamer Mediated siRNA Delivery. *Nucl. Acids Res. 34*, e73.

[87]. Yoo, H., Sazani, P., and Juliano, R. L. (1999) PAMAM Dendrimers as Delivery Agents for Antisense Oligonucleotides. *Pharm. Res. 16*, 1799-1804.

[88]. Mirkin, C. A., Letsinger, R. L., Mucic, R. C., and Storhoff, J. J. (1996) A DNA-Based Method For Rationally Assembling Nanoparticles Into Macroscopic Materials. *Nature* 382, 607–609.

[89]. Li, Z., Jin, R. C., Mirkin, C. A., and Letsinger, R. L. (2002) Multiple Thiol-Anchor Capped DNA-Gold Nanoparticle Conjugates. *Nucleic Acids Res*. 30, 1558–1562.

[90]. Tan, K., Cheang, P., Ho, I. A. W., Lam, P. Y. P., and Hui, K. M. (2007) Nanosized Bioceramic Particles could Function as Efficient Gene Delivery Vehicles with Target Specificity for the Spleen. *Gene Ther.* 14, 828-835.

[91]. McNamara, J. O., Andrechek, E. R., Wang, Y., Viles, K. D., Rempel, R. E., Gilboa, E., Sullenger, B. A., and Giangrande, P. H. (2006) Cell Type-Specific Delivery of siRNAs with Aptamer-siRNA Chimeras. *Nat Biotech. 24*, 1005-1015.

[92]. Hussain, M., Shchepinov, M., Sohail, M., Benter, I. F., Hollins, A. J., Southern, E. M., and Akhtar, S. (2004) A Novel Anionic Dendrimer for Improved Cellular Delivery of Antisense Oligonucleotides. *J. Controlled Release.* 99, 139-155.

[93]. Patil, M. L., Zhang, M., Betigeri, S., Taratula, O., He, H., and Minko, T. (2008) Surface-Modified and Internally Cationic Polyamidoamine Dendrimers for Efficient siRNA Delivery. *Bioconjug. Chem.* 19, 1396-1403.

[94]. Vivès, E., Schmidt, J., and Pèlegrin, A. (2008) Cell-Penetrating And Cell-Targeting Peptides In Drug Delivery. *Biochim. Biophys. Acta*, 1786, 126-138.

[95]. Veldhoen, S. Laufer, S. D. Restle, T. (2008) Recent Developments in Peptide-Based Nucleic Acid Delivery. *Int. J. Mol. Sci.* 9, 1276–1320.

[96]. Wagner, S., Eisenhut, M., Eritja, R., and Oberdorfer, F. (1997) Synthesis of Copper-64 and Technetium-99M Labeled Oligonucleotides with Macrocyclic Ligands. *Nucleos. Nucleot. 16*, 1789-1792.

[97]. Storhoff, J. J., Elghanian, R., Mucic, R. C., Mirkin, C. A., and Letsinger, R. L. (1998) One-Pot Colorimetric Differentiation of Polynucleotides with Single Base Imperfections using Gold Nanoparticle Probes. *J. Am. Chem. Soc. 120*, 1959-1964.

[98]. Jordan, C. E., Frutos, A. G., Thiel, A. J., and Corn, R. M. (1997) Surface Plasmon Resonance Imaging Measurements of DNA Hybridization Adsorption and Streptavidin/DNA Multilayer Formation at Chemically Modified Gold Surfaces. *Anal. Chem.* 69, 4939-4947.

CHAPTER 2

**Triplex-Stabilizing Properties of Parallel Clamps
Carrying LNA Derivatives**

2.1. DNA triplexes

The formation of triple-stranded DNA was demonstrated by Rich and coworkers in 1957 from biophysical experiments on synthetic oligonucleotides in which 2:1 mixtures of poly(U) and poly(A) were found to form a specific three-stranded structure [1,2]. Interest in these structures increased dramatically in the late 1980s with the realization of the potential use of triplex-forming oligonucleotides (TFOs) as antigene agents [3-5] and tools in biomolecular research [6-9].

In a classical DNA triplex, the triplex-forming oligonucleotide binds to a polypurine-polypyrimidine region of dsDNA in the major groove through specific hydrogen bonds. Depending on the orientation and base composition of this third strand, triplexes are classified as parallel or antiparallel.

Homopyrimidine TFOs bind parallel to the duplex purine strand via Hoogsteen hydrogen bonds to form T·AT and C$^+$·GC triplets (Figure 2.1.A), whereas purine-rich TFOs bind in an antiparallel orientation by reverse Hoogsteen bonding and form G·GC, A·AT and T·AT triplets (Figure 2.1.B).
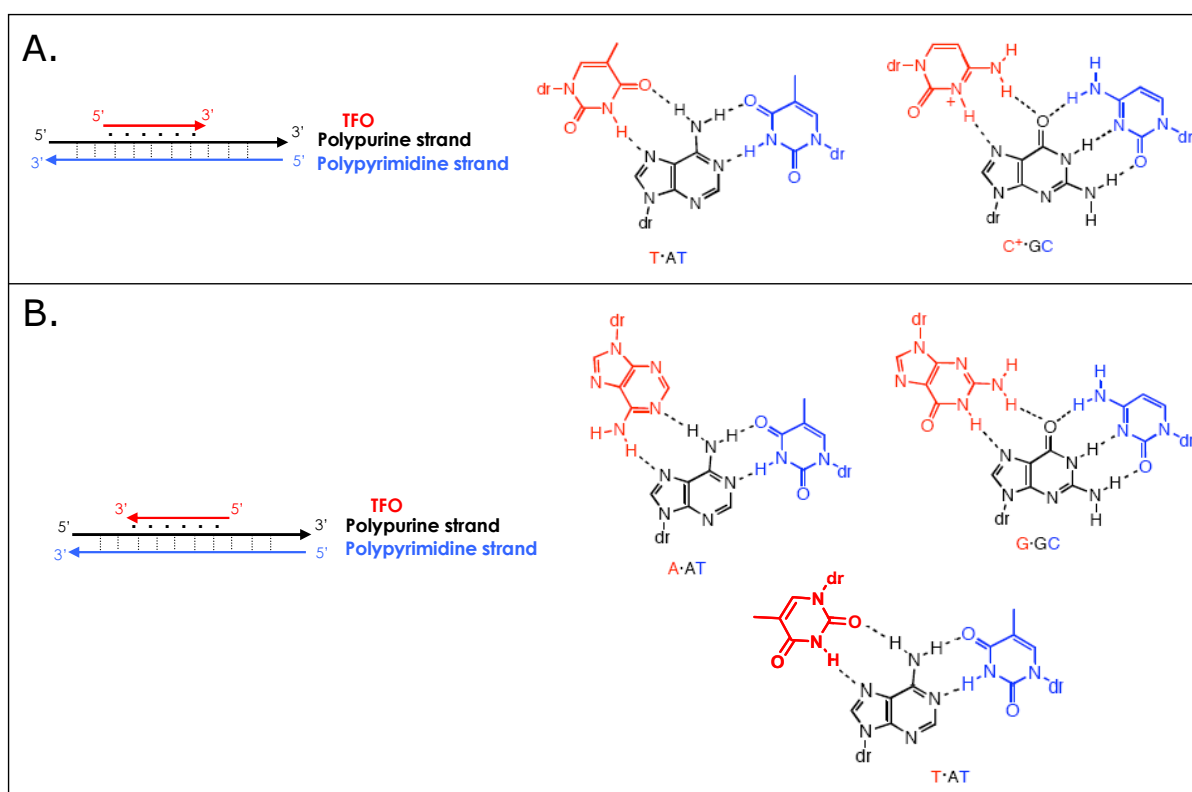
Figure 2.1. A) Chemical structures of parallel triplets T·AT and C$^+$·GC. B) Chemical structures of antiparallel triplets A·AT, G·GC and T·AT.

Formation of parallel triplexes requires conditions of low pH, necessary for protonation of cytosines at N3 to form proper Hoogsteen bonding in $C^+ \cdot GC$ triplets. Because of this limitation, pyrimidine TFOs do not usually bind DNA duplex at physiological pH without further modification. Both triplex motifs are strongly stabilised by the presence of divalent metal cations, which are able to screen the charge repulsions between the negatively charged phosphodiester backbones.

2.2. Oligonucleotide hairpins and triplex

Triplexes are usually formed by adding a TFO to a WC duplex DNA. In addition to this conventional way of forming triplex, there is an alternative approach based on the use of oligonucleotide parallel clamps. In this molecules TFO and homopolypurine WC strand are covalently attached by 3'-3' or 5'-5' internucleotide junctions (loop) and the WC polypyrimidine strand is added (Figure 2.2). These hairpins can bind to pyrimidine ssDNA or RNA sequences with greater affinity and sequence selectivity than those seen for linear ODNs, largely because of the entropic benefit. In addition, the use of parallel clamps decreases the susceptibility of oligonucleotides to degradation by cellular nucleases [10-12].
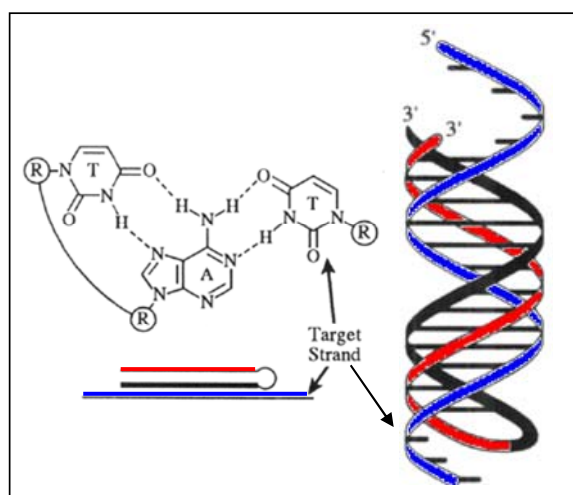
Figure 2.2. Covalent attachment of purine and pyrimidine strands trough a loop forms a parallel hairpin duplex that targets pyrimidine single strand.

2.3. Triplex modifications

Both TFO and hairpin oligonucleotides need to meet certain requirements if one wants to overcome problems inherent to all oligonucleotide-based therapies such as delivery, cellular uptake and stability. Other challenges in using triplex DNA as a tool in molecular genetics include the need for cytosine protonation in the pyrimidine motif, the susceptibility of G-rich oligonucleotides to form intermolecular

complexes in the purine motif or the charge repulsion between the third strand phosphates and those of the duplex target.

Therefore, a large effort has been made to modify oligonucleotides in order to overcome these limitations and enhance triple helix stability. Thus, chemical modifications have been incorporated in the bases (e.g. 5-methylcytosine [13], deoxyuridine [14], 5-propynyl deoxyuridine [15-17]), in the backbone (phosphoramidates [18,19], phosphorothioates [20], guanidinium [21], peptide nucleic acid [22],...) or in the sugar (morpholino [23], 2'-O-methylribose [24,25], 2'-O-aminoethylribose [26], LNA [27-30], ...). Moreover, some compounds have been attached to DNA triple helices to modulate their stability such as intercalators [31] or minor groove binders [32]. The use of modified oligonucleotides for triplex formation has been exhaustively reviewed [33, 34]. In Figure 2.3. some examples of these modifications are depicted.
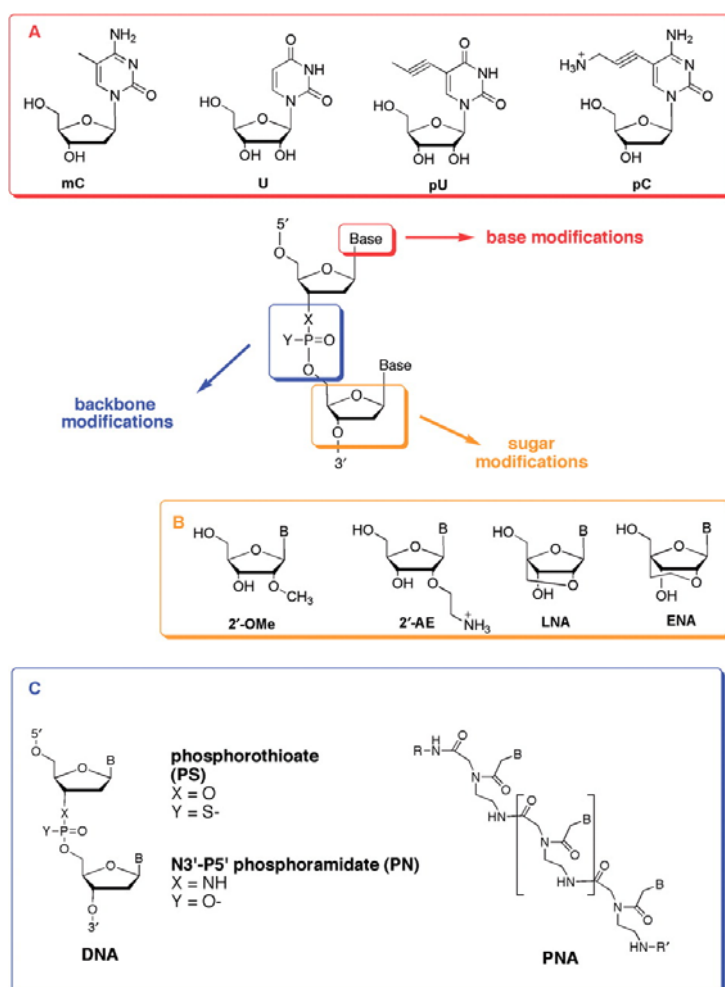
Figure 2.3. Examples of chemical modifications introduced in TFOs. (A) Base modifications; (B) sugar modifications and (C) backbone modifications (extracted from reference [33])

As hairpins used in this work contain LNA modified nucleotides, the relevance of these modifications and their previous applications in triplex will be explained in detail in the next section.

2.3.1. LNA

In 1998, novel conformationally restricted nucleotide analogues known as locked nucleic acid (LNA) were described [27-29]. LNA nucleotides contain a methylene bridge that connects the 2'-oxygen of ribose with the 4'-carbon. This bridge results in a locked 3'-endo conformation (Figure 2.4), reducing the flexibility of the ribose and increasing the local organization of the phosphate backbone. This pre-organization is believed to increase the strength of base-stacking interaction [35, 36]. Several studies demonstrate that LNAs have greater affinity for complementary DNA and RNA sequences [37-42].
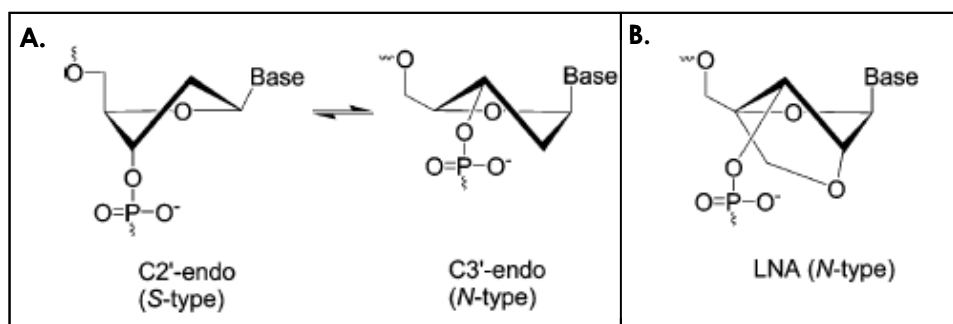
Figure 2.4. A) The C2'-*endo*-C3'-*endo* sugar ring equilibrium present in nucleic acids. B) The molecular structure of locked nucleic acid (LNA), which shows the locked C3'-*endo* sugar conformation.

This exceptionally high hybridization affinity toward complementary DNA/RNA can be exploited in antisense therapy to target highly structured RNAs that are usually inaccessible to the conventional unmodified DNA oligonucleotides. The antisense efficacy of LNA-modified oligonucleotides has been successfully employed in cancer therapy [43-48]; for inhibiting replication of hepatitis and HIV mRNA [49-52]; for understanding molecular mechanisms of various biological processes [53] and as RNA capture probes for in situ detection of mRNA [54, 55].

The hybridization properties of LNA containing oligonucleotides have been evaluated in different sequence context. The triplex-forming properties of oligonucleotides containing LNA have been reported elsewhere [30, 56-59]. Except Petersen and colleagues, who studied an intramolecular dsDNA:LNA triplex [57], the remaining authors focused on adding a homopyrimidine LNA-modified TFO to an existing WC duplex. In these studies the partial incorporation of LNA residues in TFOs has been shown to enhance significantly triple helix formation.

2.4. Objectives

The aim of this work is studying the triplex-stabilizing properties of parallel clamps carrying LNA substitutions at the Hoogsteen strand. In our experiments the homopyrimidine LNA-containing Hoogsteen strand and the natural homopurine WC strand are covalently attached by 5'-5' internucleotide junctions, and the WC pyrimidine strand is the target sequence.

In the present chapter the synthesis of parallel stranded duplexes carrying LNA residues at the Hoogsteen strand is described. The binding properties of these clamps to their polypirimidine DNA and RNA target sequences are carefully analyzed by melting experiments and compared with affinity presented by unmodified hairpins.

2.5. Design of the sequences

Oligonucleotide sequences are based on a triplex characterized previously by Xodo *et al*. [60, 61], which had also been studied in our group in the context of 8-aminopurines substitutions [62-65]. Here, the polypyrimidine Hoogsteen strand was linked to the Watson-Crick (WC) polypurine strand (Figure 2.5). Clamps are formed by two strands of eleven bases connected by 5'-5' through a tetrathymidine loop.
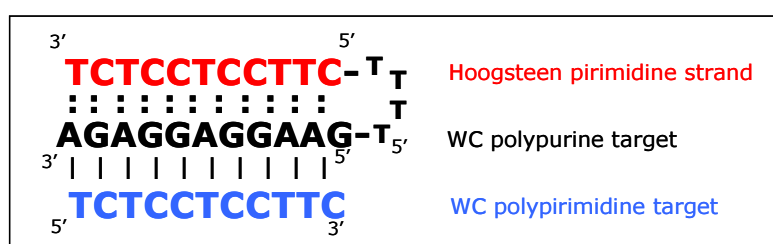
Figure 2.5. Structure of the triplex studied.

The oligonucleotides used in this study are listed in Table 2.6.

Name	Sequence
WC-11mer	$^{5'}$TCTCCTCCTTC$^{3'}$
WC-11mer/2'-OMe	$^{5'}$UCUCCUCCUUC$^{3'}$
B22	$^{3'}$AGAGGAGGAAG$^{5'}$-$^{5'}$-TTTT-CTTCCTCCTCT$^{3'}$
B22-T	$^{3'}$AGAGGAGGAAG$^{5'}$-$^{5'}$-TTTT-CT**t**CC**t**CC**t**CT$^{3'}$
B22-C	$^{3'}$AGAGGAGGAAG$^{5'}$-$^{5'}$-TTTT-CTT**c**CT**c**CT**c**T$^{3'}$
B22-CT	$^{3'}$AGAGGAGGAAG$^{5'}$-$^{5'}$-TTTT-C**t**T**c**C**t**C**c**T**c**T$^{3'}$

Table 2.6. Oligonucleotide sequences used in this study. Lower bold case letters **t** and **c** are LNA thymidine and LNA 5'-methylcytosine respectively. Underlined upper case letters U and C are 2'-O-methyl-RNA derivatives.

Clamp B22 is a control sequence that contains only the natural bases without modifications. Clamp B22-T contains three LNA thymidine nucleotides and B22-C contains three 5'-Me-C-LNA bases. In addition, a clamp bearing two T-LNA and three 5'-Me-C-LNA was prepared (B22-CT) to test whether the stabilizing properties of the two modifications are additive.

To study the effect of the sugar type of the target on triplex stability, the polypyrimidine target strand was synthesized with either DNA or 2'-O-methyl-RNA backbone. A 2'-O-methyl-RNA strand was used as a nuclease-stable model for a natural RNA target.

2.6. Synthesis of oligonucleotides

Oligonucleotide synthesis has been carried out using the phosphite triester approach [66, 67]. In this methodology the oligonucleotide chain is synthesized in the 3' to 5' direction by a stepwise addition of nucleotide residues to the 5'-terminus of the growing chain until the desired sequence is assembled. Each addition is referred to as synthetic cycle which consists of four main steps, as it is shown in the figure 2.7.
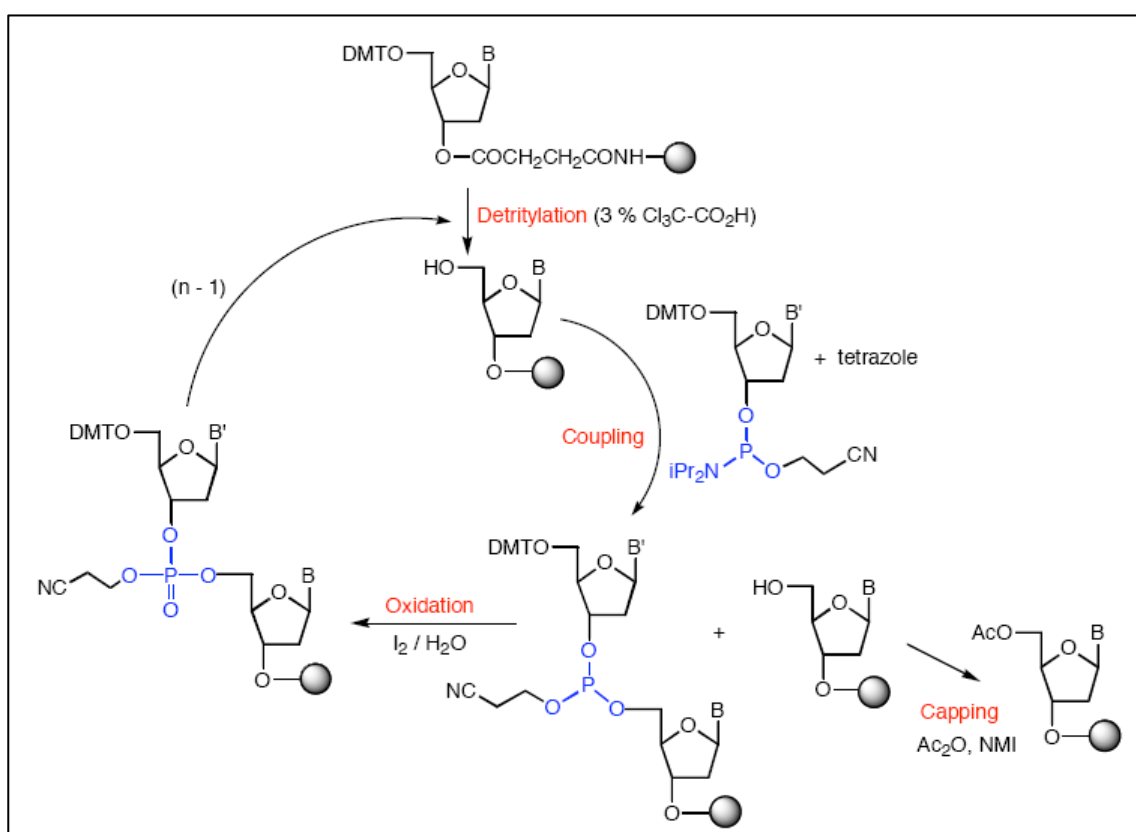
Figure 2.7. Synthetic cycle used in oligonucleotide synthesis.

In each cycle nucleotides residues are incorporated using nucleoside phosphoramidites as building blocks. These molecules consist of a (2-O-cyanoethyl)

(N,N-diisopropyl) phosphoramidite group attached to the 3'-hydroxy group of a nucleoside that has its reactive exocyclic amine and primary hydroxy groups protected. In the first step 5'-hydroxy group is deprotected (detritylation). Then, the desired phosphoramidite is activated by a tetrazole catalyst and brought in contact with the solid support functionalized with a 5'-unprotected nucleoside (either the first nucleoside or the growing chain). In this step, the 5'-hydroxy group reacts with the activated phosphoramidite moiety of the incoming building block to form a phosphite triester linkage. The 5'-hydroxyl groups that remain unreacted need to be blocked (capping) from further chain elongation to prevent formation of oligonucleotides with internal base deletions. The last step is oxidization of the phosphite triester into a stable phosphate triester bond.

For the preparation of a parallel-stranded oligonucleotide (hairpin) at least one of the strands must be synthesized in the 5' to 3' direction so standard oligonucleotide synthesis can not be employed. As alternative, reverse phosphoramidites have to be used as building blocks. These molecules differ from the standard phosphoramidites in that the phosphite group is attached to the 5' end and the DMT is protecting the 3'-hydroxyl group (figure 2.8.B).

The parallel clamps used in this work were prepared in three steps. First, the pyrimidine part was synthesized with the appropriate C, T, LNA-T and LNA 5-methyl-C phosphoramidites (figure 2.8.A). Second, four additional thymidine standard phosphoramidites were added until the point of 5'-5' attachment. This tetranucleotide loop was used to connect the two strands. From there onward, synthesis was continued using reversed G and A phosphoramidite monomers (figure 2.8.B).
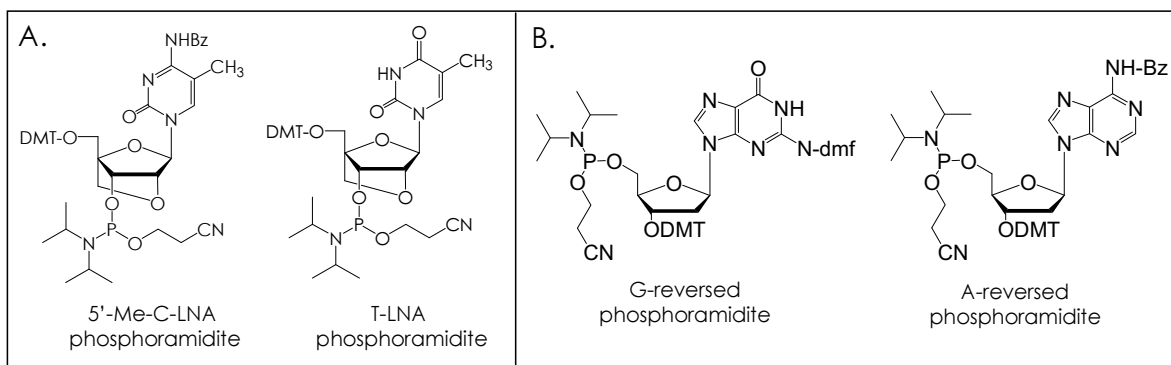
Figure 2.8. A) Phosphoramidites used in this work for the introduction of LNA residues in parallel clamps. B) Reversed phosphoramidites used for the synthesis of the second part of the hairpins in the 5' to 3' direction.

Upon completion of the chain assembly, the oligonucleotides were deprotected and cleaved from the support by aqueous ammonia treatment. Oligonucleotides were synthesized without performing final detritylation to facilitate reverse-phase HPLC purification. All purified products (DMT ON protocol) presented a major peak (figure 2.9), which was collected.
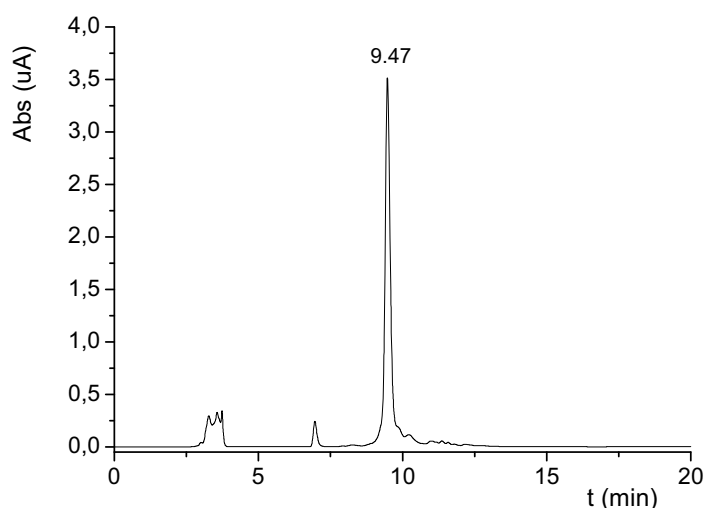
Figure 2.9. HPLC profile of the DMT-protected B22-CT sequence. Gradient: 15→ 80% B in 20 min (A: 5% ACN in 0.1 M TEAAc pH 6.5; B: 70% ACN in 0.1 M TEAAc pH 6.5)

Finally oligonucleotides were detritylated, desalted by NAP-10, quantified by measuring the absorbance at 260nm and analyzed by MALDI-TOF. Masses of the synthesized oligonucleotides measured by MALDI-TOF and their expected MW values are listed in Table 2.10.

Oligonucleotide	Found MW	Theoretical MW
WC-11mer	3194	3194
WC-11mer/ 2'-OMe	3453	3454
B22	7950	7952
B22-T	8028	8036
B22-C	8072	8078
B22-CT	8122	8134

Table 2.10. MW of the oligonucleotides used in this study obtained by MALDI-TOF.

2.7. Thermal denaturation studies

2.7.1. Evaluation of triplex stability by thermal melting curves

The stability of a triplex is often measured by thermal denaturation experiments. Heating a solution of a structured nucleic acid leads to a change on its structure (denaturation) that it is usually reflected by a change on the absorbance of the solution. These changes in the absorbance allow the determination of DNA or RNA secondary structure stability.

Thermal denaturation curves can be obtained using UV spectrophotometry by recording absorbance at 260 nm as a function of temperature. In this way, the stability of DNA and RNA triplexes has been the focus of a number of studies [68-

75]. A typical UV-absorbance melting curve of parallel triplex is shown in figure 2.11.
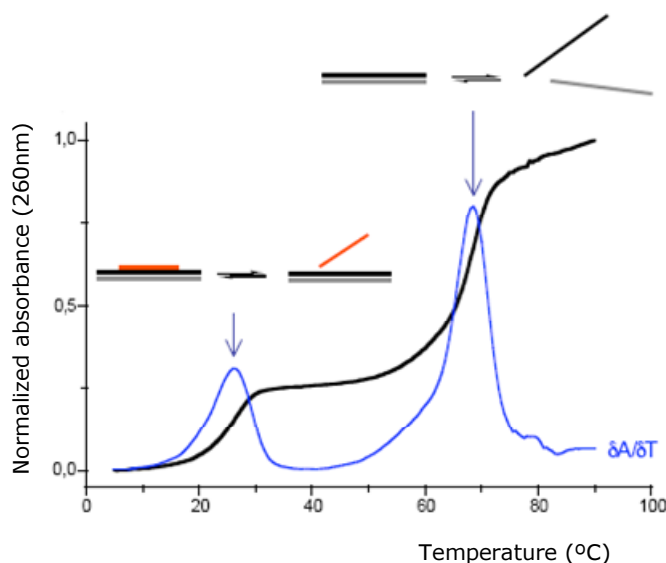
Figure 2.11. Black line: Classic thermal denaturation profile of a parallel triplex shows two transitions. Blue line: First derivative of the absorbance signal.

Usually, these structures have two transitions in their melting profiles: triplex to duplex and duplex to single strands. However these transitions overlap in some cases and are not easily distinguished. When the Hoogsteen strand and one WC strand are covalently linked by a loop, just one single transition is observed corresponding to triplex denaturation to random coil.

The midpoint of each transition is defined as melting temperature or T_m and its value gives an idea of the stability of the structure so that the higher T_m the higher stability. This parameter can be determined as the maximum of the first derivative of the absorbance signal (blue line in figure 2.11). T_m of triplexes will depend on the oligonucleotide strands (length, composition and modifications) and the solution conditions (pH, salt concentration).

Besides 260 nm, denaturation of some structures should be followed at other wavelengths, e.g. 295 nm, as in the case in which protonation/deprotonation of cytosine is involved in structure stability. Thus, melting profiles of our triplexes are recorded also at 295 nm, as it will be explained in the next sections.

2.7.2. Thermal stability of the Hoogsteen parallel duplexes

First, samples were dissolved in 0.1 M sodium phosphate/citric acid buffer containing 1 M NaCl and different pH values, ranging from 5.0 to 7.0. The solutions were heated to 90°C, allowed to cool slowly to room temperature, and stored at 4°C until UV was measured.

Thermal melting curves of 4 μM solutions of clamps (B22, B22-T, B22-C and B22-CT) alone, in the absence of the polypyrimidine target, were recorded at 260 and 295 nm at a heating rate of 1ºC/min (Figure 2.12).

	260 nm	295 nm
pH 6.5		No transition observed
pH 7		No transition observed
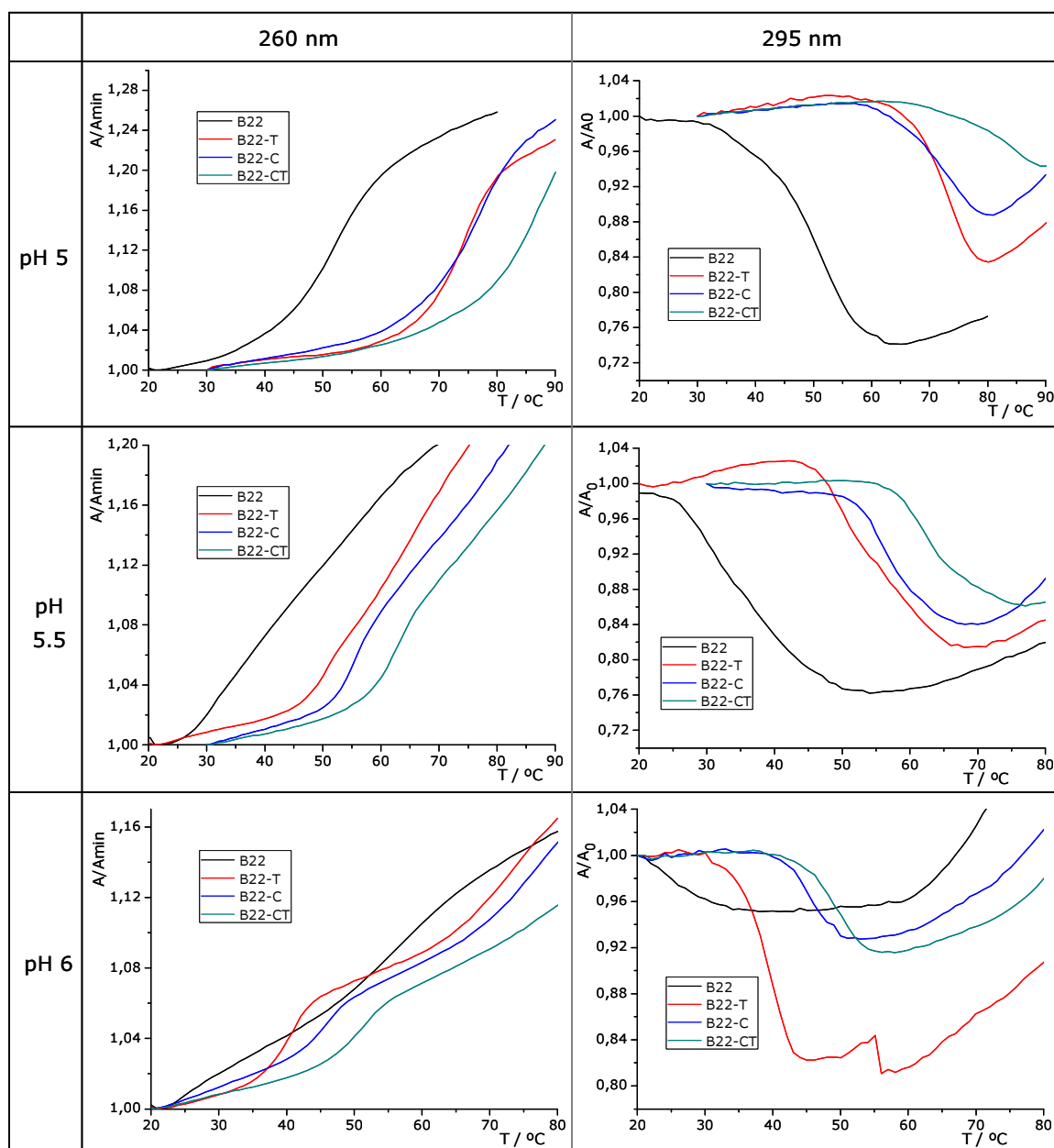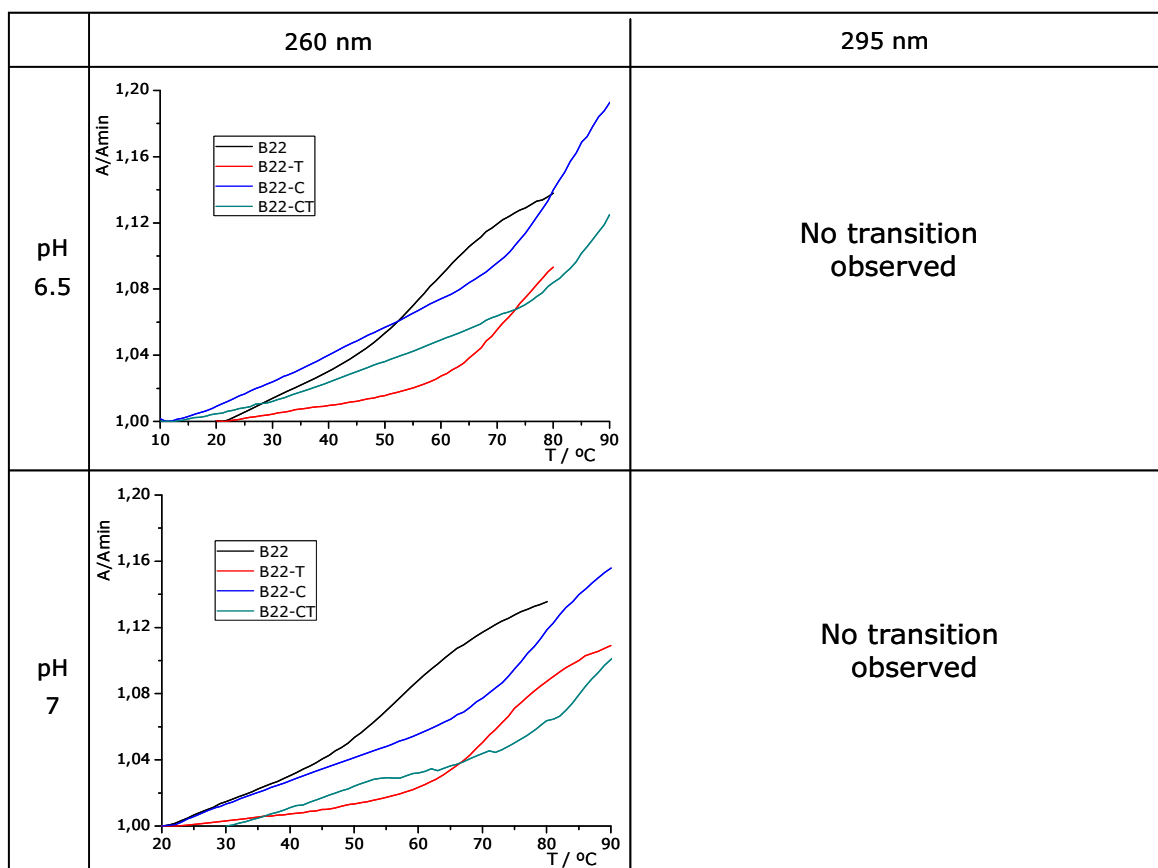
Figure 2.12. Melting curves of B22 and derivatives alone, without target.

Depending on the pH we observed two different transitions. At pH 5 we observed a transition with 15% hyperchromicity (increase in absorbance) at 260 nm that decreased in intensity at higher pH. This transition was assigned to the denaturation of the parallel duplex, as described previously [64, 76-78]. To confirm that this transition corresponds to the denaturation of the Hoogsteen parallel duplex to a random coil, all the melting curves were also recorded at 295 nm.

It has been established that the change of absorbance at 295 nm indicates the formation of a nucleic-acid structure that requires protonation / deprotonation of cytosines [79]. As 295 nm corresponds to a negative peak of the differential spectrum between protonated and non-protonated cytosines, the melting profile recorded at 295 is expected to be inverted. Accordingly, when buffer of low pH are used a melting curve with hypochromicity (decrease in absorbance) is obtained, as expected for a parallel duplex.

At pH above 6, a new transition appears at higher temperatures. We suggest that above this pH the structure rearranges and short intermolecular antiparallel duplexes can be formed with the central part of the oligonucleotides (like a 7mer duplex between -AGGAGGA- and -TCCTCCT-) in the way shown in figure 2.13.

TC**TCCTCCT**TCTTTTGAAGGAGGAGA
| | | | | | | |
TCTCCTCCTTCTTTTGA**AGGAGGA**GA

Figure 2.13. Proposed model for the rearrangement of the parallel clamps to form short intermolecular WC duplex.

This effect is mainly observed in clamps carrying LNA modifications, probably because LNA can enhance hybridization of complementary sequences. These transitions are only observed at 260 nm. The absence of hyperchromism or hypochromism at 295 nm seems to be a general phenomenon for many WC duplex transitions. Thus, the fact of no transitions are observed at 295 nm indicates the presence of an antiparallel Watson-Crick duplex.

Table 2.14 shows the collection of all T_m values obtained from clamps thermal melting curves. The first value corresponds to the first transition and is only observed at low pH. The second one corresponds to the second transition and is only observed above pH 6.

clamp	pH 5.0	pH 5.5	pH 6.0	pH 6.5	pH 7.0
B22	52/--	--/--	--/55	--/55	--/56
B22-T	74/--	52/--	40/--	--/75	--/70
B22-C	76/--	54/--	45/--	--/77	--/75
B22-CT	>90/--	64/--	51/--	--/80	--/80

Table 2.14. Melting temperatures (^{o}C) of transitions observed with B22 and derivatives alone, without target.

The melting temperatures for clamps carrying the LNA were much higher than those for the unmodified sequence. At pH 5.0 the increase in melting temperature is 24 ^{o}C for B22-C and 22 ^{o}C for B22-T. The B22-CT clamp, with the highest LNA content, is the most stable especially at pH 5 (more than 40 ^{o}C difference). These results show that LNA modifications in the polypyrimidine strand enhance the stability of parallel duplexes, and therefore the stability of Hoogsteen base pairs.

2.7.3. Thermal stability of triplexes formed by parallel clamps and their DNA polypyrimidine target strand

For this study, solutions of equimolar amounts of hairpins with the target Watson–Crick pyrimidine strand were mixed in the corresponding melting buffer with a final duplex concentration of 2 μM. As in the case of hairpins, the melting curves for the triplexes were recorded at both 260 and 295 nm to ensure that changes corresponded to triplex-to-random-coil transition.

Thermal melting curves of triplexes formed by the different hairpins and the DNA strand target WC-11mer are shown in figure 2.15.
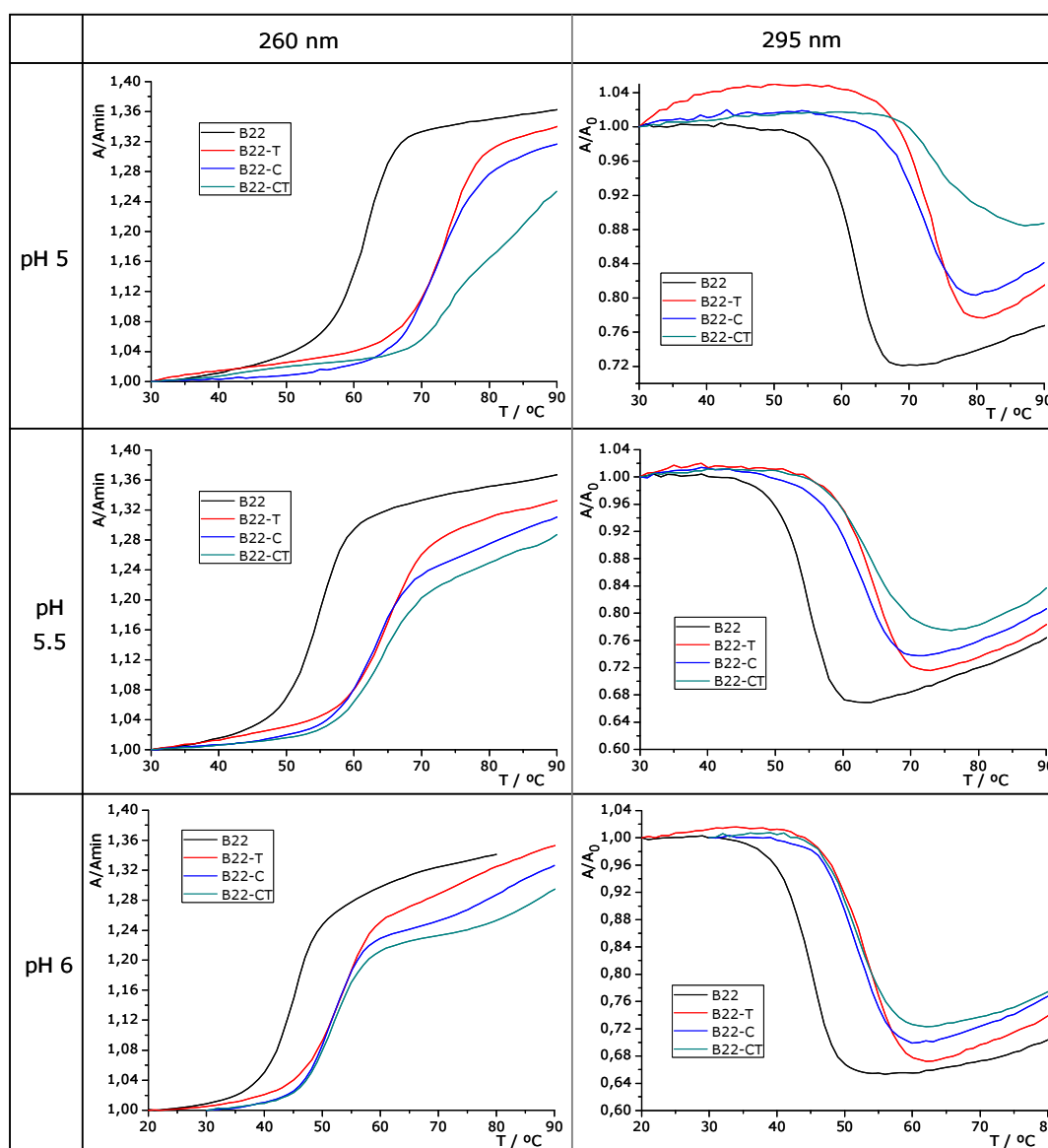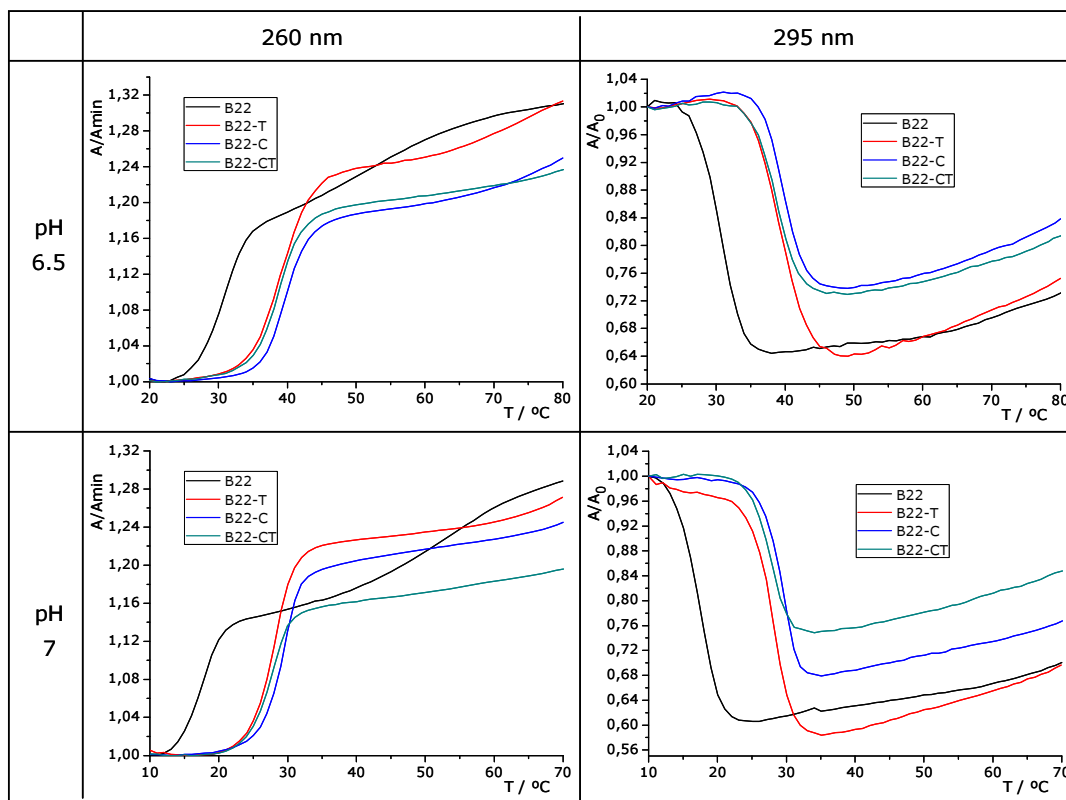
Figure 2.15. Melting curves of triplex formed by B22 and derivatives with the DNA target WC-11mer. One single transition is observed at 260 nm (hyperchromic) and 295 nm (hypochromic).

Although the stability of all these triplexes decreased when the pH was raised (caused by a destabilization of Hoogsteen bond due to a lower proportion of C^+) the transition was still observed at pH 7.

In all cases the resulting triplexes showed single, cooperative melting transitions (sigmoidal curves) with a pH dependent hyperchromicity, ranging from 15% to 30% when pH decreases from pH 7.0 to pH 5.0. This single transition was observed at both 260 and 295 nm throughout the pH range studied, indicating that the Hoogsteen and WC hydrogen-bonded strands dissociate simultaneously and that the change of absorbance in the melting profile is due to triplex-to-random-coil transition as described for clamps carrying 8-aminopurines [64,76,77].

The T_m values obtained in these triplex melting curves are shown in table 2.16. In all cases the triplexes formed by LNA-containing hairpins showed higher T_m values than the unmodified triplexes. The increase in T_m is presented in parentheses next to the T_m data for each pH value. All T_m are calculated with the curves recorded at 260 nm.

clamp	pH 5.0	pH 5.5	pH 6.0	pH 6.5	pH 7.0
B22	62	55	45	31	18
B22-T	74 (+12)	65 (+10)	53 (+8)	39 (+8)	28 (+10)
B22-C	73 (+11)	63 (+8)	52 (+7)	40 (+9)	29 (+11)
B22-CT	79 (+17)	64 (+9)	52 (+7)	39 (+8)	28 (+10)

Table 2.16. Melting temperatures (ºC) for the triplexes formed by B22 and derivatives with the DNA target WC-11mer. Values in parenthesis indicate the ΔT_m relative to unmodified triplexes.

B22T and B22C hairpins stabilized the triplex to a similar extent with an increase in Tm of 8-12ºC relative to the unmodified triplex. For B22-CT, differences in parallel duplex stability relative to B22-C and B22-T disappeared when the triplex was formed, except for pH 5, where B22-CT still showed a significant increase in T_m.

2.7.4. Thermal stability of triplexes formed by parallel clamps and their RNA polypyrimidine target strand

RNA or DNA backbone composition is reported to have dramatic effects on triple helix stability [80,81]. To study such effects, a target RNA polypyrimidine strand was synthesized. A 2'-O-methyl-RNA strand was used as a nuclease-stable model for a natural RNA target.

Melting curves of triplexes formed by hairpins and this 2'-O-methyl-RNA target and the corresponding T_m values are shown in figure 2.17 and table 2.18 respectively.
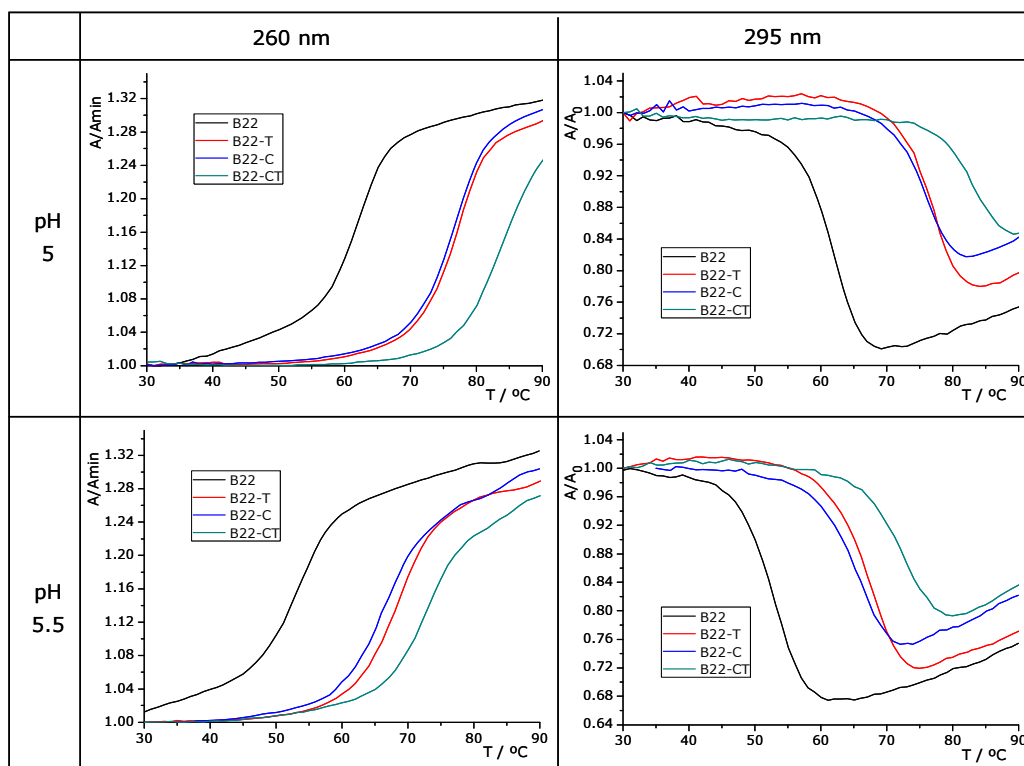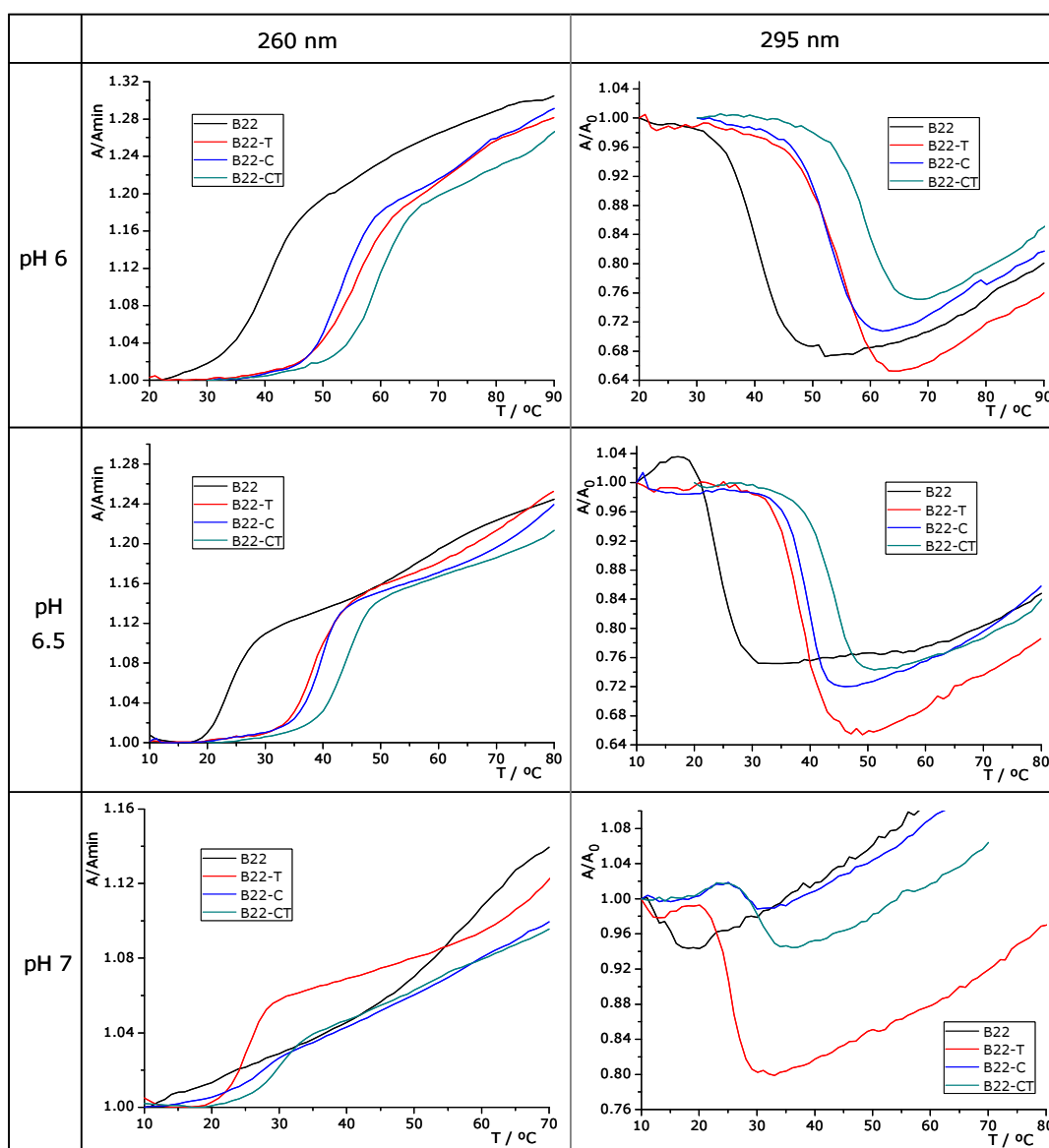
Figure 2.17. Melting curves of triplex formed by B22 and derivatives with the RNA target WC-11mer/2'-OMe. One single transition is observed at 260 nm (hyperchromic) and 295 nm (hypochromic).

clamp	pH 5.0	pH 5.5	pH 6.0	pH 6.5	pH 7.0
B22	62	53	41	24	n.d.
B22-T	77 (+15)	68 (+15)	56 (+15)	39 (+8)	25
B22-C	77 (+15)	67 (+14)	53 (+12)	40 (+16)	27
B22-CT	84 (+22)	73 (+20)	60 (+19)	44 (+20)	30

Table 2.18. Melting temperatures (ºC) for the triplexes formed by B22 and derivatives with the RNA target WC-11mer/2'-OMe.

In this case the resulting triplexes showed single, cooperative melting transition with a pH dependent hyperchromicity ranging from 10% to 30% when pH decreases from pH 7.0 to pH 5.0.

Although the T_m for the triplex formed by the unmodified B22 clamp and the RNA target is lower than that of the triplex formed with the DNA target, the LNA-containing hairpins form a more stable triplex in the presence of complementary RNA strand. Previous studies showed that combination of RNA pyrimidine and DNA purine strands forms a highly stable triplex [80,81]. As LNA has a locked C3'-endo-sugar pucker it can be considered as an RNA analogue derivative. So, when a polypyrimidine target is an RNA strand and the Hoogsteen pyrimidine strand of the clamp contains LNA, the resulting triplex will contain this favourable combination. According to this, the B22-CT, with a higher LNA content and the most A-like (RNA) geometry, would form the most stable triplex, which is consistent with our experimental data.

2.8. Conclusions

We have shown that LNA-modified parallel clamps bind to their polypyrimidine target strands via triple-helix formation with greater affinity than hairpins containing only natural bases. In addition, the presence of LNA residues stabilizes the parallel duplex, as can be deduced from the T_m values of hairpins alone at pH 5.0. As LNA nucleotides have a C3'-*endo* sugar pucker, the backbone conformation seems to have a strong positive effect on triplex and parallel duplex structures. Triplex stabilization by LNA residues is even stronger when the polypyrimidine target strand is an RNA sequence. These results are relevant for the design of clamps for potential applications based on triplex formation such as triplex affinity capture [82,83] and antisense inhibition of gene expression [11,12].

2.9. References

[1]. Felsenfeld, G., Davies, D. R., and Rich, A. (1957) Formation Of A Three-Stranded Polynucleotide Molecule. *J. Am. Chem. Soc. 79*, 2023-2024.

[2]. Felsenfeld, G., and Rich, A. (1957) Studies on the Formation of Two- and Three-Stranded Polyribonucleotides. *Biochim. Biophys. Acta. 26*, 457-468.

[3]. Le Doan, T., Perrouault, L., Praseuth, D., Habhoub, N., Decout, J., Thuong, N. T., Lhomme, J., and Heene, C. (1987) Sequence-Specific Recognition, Photocrosslinking and Cleavage of the DNA Double Helix by an Oligo-({Alpha}]-Thymidylate Covalently Linked to an Azidoproflavine Derivative. *Nucl. Acids Res. 15*, 7749-7760.

[4]. Moser, H. E., and Dervan P B. (1987) Sequence-Specific Cleavage of Double Helical DNA by Triple Helix Formation. *Science. 238*, 645-650.

[5]. Duval-Valentin, G., Thuong, N. T., and Hélène, C. (1992) Specific Inhibition of Transcription by Triple Helix-Forming Oligonucleotides. *Proc. Natl. Acad. Sci. U. S. A. 89*, 504-508.

[6]. Grigoriev, M., Praseuth, D., Guieysse, A. L., Robin, P., Thuong, N. T., Hélène, C., and Harel-Bellan, A. (1993) Inhibition of Gene Expression by Triple Helix-Directed DNA Cross-Linking at Specific Sites. *Proc. Natl. Acad. Sci. U. S. A. 90*, 3501-3505.

[7]. Chan, P. P., and Glazer, P. M. (1997) Triplex DNA: Fundamentals, Advances, and Potential Applications for Gene Therapy. *J. Mol. Med. 75*, 267-282.

[8]. Neidle, S. (1997) Recent Developments in Triple-Helix Regulation of Gene Expression. *Anticancer Drug Des. 12*, 433-442.

[9]. Vasquez, K. M., and Wilson, J. H. (1998) Triplex-Directed Modification of Genes and Gene Activity. *Trends Biochem. Sci. 23*, 4-9.

[10]. Tang, J., Temsamani, J., and Agrawal, S. (1993) Self-Stabilized Antisense Oligodeoxynucleotide Phosphorothioates: Properties and Anti-HIV Activity. *Nucleic Acids Res. 21*, 2729-2735.

[11]. Kandimalla, E. R., Agrawal, S., Venkataraman, G., and Sasisekharan, V. (1995) Single Strand Targeted Triplex Formation: Parallel-Stranded DNA Hairpin Duplexes for Targeting Pyrimidine Strands. *J. Am. Chem. Soc. 117*, 6416-6417.

[12]. Kandimalla, E. R., and Agrawal, S. (1996) Hoogsteen DNA Duplexes of 3'-3'- and 5'-5' -Linked Oligonucleotides and Triplex Formation with RNA and DNA Pyrimidine Single Strands: Experimental and Molecular Modeling Studies. *Biochemistry* 35, 15332-15339.

[13]. Lee, J.S., Woodsworth, M.L., Latimer, L.J. and Morgan, A.R. (1984) Poly(Pyrimidine). Poly(Purine) Synthetic Dnas Containing 5-Methylcytosine Form Stable Triplexes At Neutral pH. *Nucleic Acids Res.*, 12, 6603–6614.

[14]. Froehler, B.C., Wadwani, S., Terhorst, T.J. and Gerrard, S.R. (1992) Oligodeoxynucleotides Containing C-5 Propyne Analogs Of 20-Deoxyuridine And 20-Deoxycytidine. *Tetrahedron Lett.*, 33, 5307–5310.

[15]. Bijapur, J., Keppler, M.D., Bergqvist, S., Brown, T., and Fox, K.R. (1999) 5-(1-propargylamino)-20-deoxyuridine (UP): a novel thymidine analogue for generating DNA triplexes with increased stability. *Nucleic Acids Res.*, 27, 1802–1809.

[16]. Sollogoub,M., Darby,R.A., Cuenoud,B., Brown,T. and Fox, K.R. (2002) Stable DNA Triple Helix Formation Using Oligonucleotides Containing 20-Aminoethoxy,5-Propargylamino-U. *Biochemistry*, 41, 7224–7231.

[17]. Brazier,J.A., Shibata,T., Townsley,J., Taylor,B.F., Frary,E., Williams,N.H. and Williams,D.M. (2005) Amino-Functionalized DNA: The Properties Of C5-Amino-Alkyl Substituted 20-Deoxyuridines And Their Application In DNA Triplex Formation. *Nucleic Acids Res.*, 33, 1362–1371.

[18]. Michel,T., Martinand-Mari,C., Debart,F., Lebleu,B., Robbins,I. and Vasseur,J.J. (2003) Cationic Phosphoramidate Alphaoligonucleotides Efficiently Target Single-Stranded DNA And RNA And Inhibit Hepatitis C Virus IRES-Mediated Translation. *Nucleic Acids Res.*, 31, 5282–5290.

[19]. Michel,T., Debart,F., Heitz,F. and Vasseur,J.J. (2005) Highly Stable DNA Triplexes Formed With Cationic Phosphoramidate Pyrimidine Alpha-Oligonucleotides. *Chembiochem.*, 6, 1254–1262.

[20]. Joseph, J., Kandala, J., Veerapanane, D., Weber, K., and Guntaka, R. (1997) Antiparallel Polypurine Phosphorothioate Oligonucleotides Form Stable Triplexes with the Rat alpha1(I) Collagen Gene Promoter and Inhibit Transcription in Cultured Rat Fibroblasts. *Nucl. Acids Res. 25*, 2182-2188.

[21]. Dempcy, R. O., Almarsson, O., and Bruice, T. C. (1994) Design and Synthesis of Deoxynucleic Guanidine: A Polycation Analogue of DNA. *Proc. Natl. Acad. Sci. USA. 91*, 7864-7868.

[22]. Knudsen, H., and Nielsen, P. (1996) Antisense Properties of Duplex- and Triplex-Forming PNAs. *Nucl. Acids Res. 24*, 494-500.

[23]. Lacroix, L., Arimondo, P. B., Takasugi, M., Hélène, C., and Mergny, J. (2000) Pyrimidine Morpholino Oligonucleotides Form a Stable Triple Helix in the Absence of Magnesium Ions. *Biochem. Biophys. Res. Commun. 270*, 363-369.

[24]. Escudé, C., Sun, J.S., Rougée, M., Garestier, T. and Hélène, C. (1992) Stable triple helices are formed upon binding of RNA oligonucleotides and their 2′-O-methyl derivatives to double-helical DNA. *C. R. Acad. Sci. Paris, Serie III*, 315, 521–525.

[25]. Shimizu,M., Konishi,A., Shimada,Y., Inoue,H. and Ohtsuka,E. (1992) Oligo(2′-O-methyl)ribonucleotides. Effective probes for duplex DNA. *FEBS Lett.,* 302, 155–158.

[26]. Seidman,M.M., Puri,N., Majumdar,A., Cuenoud,B., Miller,P.S. and Alam,R. (2005) The development of bioactive triple helix-forming oligonucleotides. *Ann. N Y Acad. Sci.*, 1058, 119–127.

[27]. Koshkin, A. A., Rajwanshi, V. K., and Wengel, J. (1998) Novel Convenient Syntheses of LNA [2.2.1]Bicyclo Nucleosides. *Tetrahedron Lett. 39*, 4381-4384.

[28]. Koshkin, A. A., Singh, S. K., Nielsen, P., Rajwanshi, V. K., Kumar, R., Meldgaard, M., Olsen, C. E., and Wengel, J. (1998) LNA (Locked Nucleic Acids): Synthesis of the Adenine, Cytosine, Guanine, 5-Methylcytosine, Thymine and Uracil Bicyclonucleoside Monomers, Oligomerisation, and Unprecedented Nucleic Acid Recognition. *Tetrahedron. 54*, 3607-3630.

[29]. Obika, S., Nanbu, D., Hari, Y., Andoh, J., Morio, K., Doi, T., and Imanishi, T. (1998) Stability and Structural Features of the Duplexes Containing Nucleoside Analogues with a Fixed N-Type Conformation, 2′-O,4′-C-Methyleneribonucleosides. *Tetrahedron Lett. 39*, 5401-5404.

[30]. Obika, S., Uneda, T., Sugimoto, T., Nanbu, D., Minami, T., Doi, T., and Imanishi, T. (2001) 2′-O,4′-C-Methylene Bridged Nucleic Acid (2′,4′-BNA): Synthesis and Triplex-Forming Properties. *Bioorg. Med. Chem. 9*, 1001-1011.

[31]. Sun, J. S., Giovannangeli, C., François, J. C., Kurfurst, R., Montenay-Garestier, T., Asseline, U., Saison-Behmoaras, T., Thuong, N. T., and Hélène, C. (1991) Triple-Helix Formation by Alpha Oligodeoxynucleotides and Alpha Oligodeoxynucleotide-Intercalator Conjugates. . *Proc. Natl. Acad. Sci. U. S. A.* 88, 6023-6027.

[32]. Novopashina, D.S., Sinyakov, A. N., Ryabinin, V. A., Venyaminova, A.G., Halby, L., Sun, J.S., and Boutorine, A.S. (2005) Sequence-Specific Conjugates of Oligo(2'-*O*-Methylribonucleotides) and Hairpin Oligocarboxamide Minor-Groove Binders: Design, Synthesis, and Binding Studies with Double-Stranded DNA. *Chemistry & Biodiversity. 2* (7), 936-952.

[33]. Duca, M., Vekhoff, P., Oussedik, K., Halby, L., and Arimondo, P. B. (2008) The Triple Helix: 50 Years Later, the Outcome. *Nucl. Acids Res. 36*, 5123-5138.

[34]. Robles, J., Grandas, A., Pedroso, E., Luque, F. J., Eritja, R., and Orozco, M. (2002) Nucleic Acid Triple Helices: Stability Effects of Nucleobase Modifications. *Curr Org Chem. 6*, 1333-1368.

[35]. Petersen, M., Nielsen, C. B., Nielsen, K. E., Jensen, G. A., Bondensgaard, K., Singh, S. K., Rajwanshi, V. K., Koshkin, A. A., Dahl, B. M., Wengel, J., and Jacobsen, J.P. (2000) The Conformations of Locked Nucleic Acids (LNA). *J. Mol. Recognit.* 13 (1), 44-53.

[36]. McTigue, P. M., Peterson, R. J., and Kahn, J. D. (2004) Sequence-Dependent Thermodynamic Parameters for Locked Nucleic Acid (LNA)-DNA Duplex Formation. *Biochemistry.* 43, 5388-5405.

[37]. Vester, B., and Wengel, J. (2004) LNA (Locked Nucleic Acid): High-Affinity Targeting of Complementary RNA and DNA . *Biochemistry.* 43, 13233-13241.

[38]. Wang, G., Gunic, E., Girardet, J., and Stoisavljevic, V. (1999) Conformationally Locked Nucleosides. Synthesis and Hybridization Properties of Oligodeoxynucleotides Containing 2′,4′-C-Bridged 2′-Deoxynucleosides. *Bioorg. Med. Chem. Lett. 9*, 1147-1150.

[39]. Bondensgaard, K., Petersen, M., Singh, S. K., Rajwanshi, V. K., Kumar, R., Wengel, J., and Jacobsen, J.P. (2000) Structural Studies of LNA: RNA Duplexes NMR: Conformations and Implications for RNase H Activity. *Chem – Eur. J.* 6, 2687-2695.

[40]. Wahlestedt, C., Salmi, P., Good, L., Kela, J., Johnsson, T., Hökfelt, T., Broberger, C., Porreca, F., Lai, J., Ren, K., Ossipov, M., Koshkin, A., Jakobsen, N., Skouv, J., Oerum, H., Jacobsen, M. H., and Wengel, J. (2000) Potent and Nontoxic Antisense Oligonucleotides Containing Locked Nucleic Acids. *Proc. Natl. Acad. Sci. U. S. A.* 97, 5633-5638.

[41]. Kumar, R., Singh, S. K., Koshkin, A. A., Rajwanshi, V. K., Meldgaard, M., and Wengel, J. (1998) The First Analogues of LNA (Locked Nucleic Acids): Phosphorothioate-LNA and 2'-Thio-LNA. *Bioorg. Med. Chem. Lett. 8*, 2219-2222.

[42]. Orum, H., Jakobsen, M. H., Koch, T., Vuust, J., and Borre, M. B. (1999) Detection of the Factor V Leiden Mutation by Direct Allele-Specific Hybridization of PCR Amplicons to Photoimmobilized Locked Nucleic Acids. *Clin. Chem. 45*, 1898-1905.

[43]. Obika, S., Hemamayi, R., Masuda, T., Sugimoto, T., Nakagawa, S., Mayumi, T., and Imanishi, T. (2001) Inhibition Of ICAM-1 Gene Expression By Antisense 2', 4'-BNA Oligonucleotides. *Nucleic Acids Res. Suppl.* 145-146.

[44]. Childs, J. L., Disney, M. D., and Turner, D. H. (2002) Oligonucleotide Directed Misfolding Of RNA Inhibits *Candida Albicans* Group I Intron Splicing. *Proc. Natl. Acad. Sci. U.S.A.* 99, 11091-11096.

[45]. Hansen, J. B., Westergaard, M., Thrue, C. A., Giwercman, B., and Oerum, H. (2003) Antisense Knockdown Of PKC-Alpha Using LNA-Oligos. *Nucleos Nucleot Nucl.* 22, 1607-1609.

[46]. Fluiter, K., ten Asbroek, A. L., de Wissel, M. B., Jakobs, M. E., Wissenbach, M., Olsson, H., Olsen, O., Oerum, H., and Baas, F. (2003) In Vivo Tumor Growth Inhibition And Biodistribution Studies Of Locked Nucleic Acid (LNA) Antisense Oligonucleotides. *Nucleic Acids Res.* 31, 953-962.

[47]. Zangemeister-Wittke, U. (2003) Antisense To Apoptosis Inhibitors Facilitates Chemotherapy And TRAIL-Induced Death Signaling, *Ann. N.Y. Acad. Sci.* 1002, 90-94.

[48]. Simoes-Wust, A. P., Hopkins-Donaldson, S., Sigrist, B., Belyanskaya, L., Stahel, R. A., and Zangemeister-Wittke, U. (2004) A Functionally Improved Locked Nucleic Acid Antisense Oligonucleotide Inhibits Bcl-2 And Bcl-Xl Expression And Facilitates Tumor Cell Apoptosis. *Oligonucleotides* 14, 199-209.

[49]. Nulf, C. J., and Corey, D. (2004) Intracellular Inhibition Of Hepatitis C Virus (HCV) Internal Ribosomal Entry Site (IRES)-Dependent Translation By Peptide Nucleic Acids (PNAs) And Locked Nucleic Acids (LNAs), *Nucleic Acids Res.* 32, 3792-3798.

[50]. Arzumanov, A., Walsh, A. P., Rajwanshi, V. K., Kumar, R., Wengel, J., and Gait, M. J. (2001) Inhibition Of HIV-1 Tatdependent Trans Activation By Steric Block Chimeric 2'-O-Methyl/LNA Oligoribonucleotides. *Biochemistry* 40, 14645-14655.

[51]. Arzumanov, A., Stetsenko, D. A., Malakhov, A. D., Reichelt, S., Sorensen, M. D., Babu, B. R., Wengel, J., and Gait, M. J. (2003) A Structure-Activity Study Of The Inhibition Of HIV-1 Tat-Dependent Trans-Activation By Mixmer 2'-O-Methyl Oligoribonucleotides Containing Locked Nucleic Acid (LNA), Alpha-L-LNA, Or 2'-Thio-LNA Residues. *Oligonucleotide* 13, 435-453.

[52]. Elmen, J., Zhang, H. Y., Zuber, B., Ljungberg, K., Wahren, B., Wahlestedt, C., and Liang, Z. (2004) Locked Nucleic Acid Containing Antisense Oligonucleotides Enhance Inhibition Of HIV-1 Genome Dimerization And Inhibit Virus Replication. *FEBS Lett.* 578 (3), 285-290.

[53]. Mong, J. A., Devidze, N., Goodwillie, A., and Pfaff, D. W. (2003) Reduction Of Lipocalin-Type Prostaglandin D Synthase In The Preoptic Area Of Female Mice Mimics Estradiol Effects On Arousal And Sex Behavior. *Proc. Natl. Acad. Sci. U.S.A.* 100, 15206-15211.

[54]. Thomsen, R., Nielsen, P. S., and Jensen, T. H. (2005) Dramatically Improved RNA In Situ Hybridization Signals Using LNA-Modified Probes. *RNA* 11, 1745-1748.

[55]. Kloosterman, W. P., Wienholds, E., de, B. E., Kauppinen, S., and Plasterk, R. H. (2006) In Situ Detection Of Mirnas In Animal Embryos Using LNA-Modified Oligonucleotide Probes. *Nat. Methods* 3, 27-29.

[56]. Torigoe, H., Hari, Y., Sekiguchi, M., Obika, S., and Imanishi, T. (2001) 2'-O,4'-C-Methylene Bridged Nucleic Acid Modification Promotes Pyrimidine Motif Triplex DNA Formation at Physiological pH. *J. Biol. Chem.. 276*, 2354-2360.

[57]. Sorensen, J. J., Nielsen, J. T., and Petersen, M. (2004) Solution Structure of a dsDNA:LNA Triplex. *Nucl. Acids Res. 32*, 6078-6085.

[58]. Sun, B., Babu, B. R., Sorensen, M. D., Zakrzewska, K., Wengel, J., and Sun, J. (2004) Sequence and pH Effects of LNA-Containing Triple Helix-Forming Oligonucleotides: Physical Chemistry, Biochemistry, and Modeling Studies. *Biochemistry* 43, 4160-4169.

[59]. Kumar, N., Nielsen, K. E., Maiti, S., and Petersen, M. (2006) Triplex Formation with alpha-L-LNA (alpha -Ribo-Configured Locked Nucleic Acid). *J. Am. Chem. Soc. 128*, 14-15.

[60]. Xodo, L. E., Manzini, G., and Quadrifoglio, F. (1990) Spectroscopic and Calorimetric Investigation on the DNA Triplex Formed by d(CTCTTCTTTCTTTTCTTTCTTCTC) and d(GAGAAGAAAGA) at Acidic pH. *Nucl. Acids Res.* 18, 3557-3564.

[61]. Xodo, L. E., Manzini, G., Quadrifoglio, F., van der Marel, G. A., and van Boom, J. H. (1991) Effect Of 5-Methylcytosine on the Stability of Triple-Stranded DNA--a Thermodynamic Study. *Nucl. Acids Res. 19*, 5625-5631.

[62]. Aviñó, A., Morales, J. C., Frieden, M., de la Torre, B. G., García, R. G., Cubero, E., Luque, F. J., Orozco, M., Azorín, F., and Eritja, R. (2001) Parallel-Stranded Hairpins Containing 8-Aminopurines. Novel Efficient Probes for Triple-Helix Formation. *Bioorg. Med. Chem. Lett. 11*, 1761-1763.

[63]. Cubero, E., Aviñó, A., de, l. T., Frieden, M., Eritja, R., Luque, F. J., González, C., and Orozco, M. (2002) Hoogsteen-Based Parallel-Stranded Duplexes of DNA. Effect of 8-Amino-Purine Derivatives. *J. Am. Chem. Soc. 124*, 3133-3142.

[64]. Aviño, A., Frieden, M., Morales, J. C., Garcia de la Torre, B., Guimil Garcia, R., Azorin, F., Gelpi, J. L., Orozco, M., Gonzalez, C., and Eritja, R. (2002) Properties of Triple Helices Formed by Parallel-Stranded Hairpins Containing 8-Aminopurines. *Nucl. Acids Res. 30*, 2609-2619.

[65]. Aviñó, A., Frieden, M., Morales, J. C., de la Torre, B. G., Güimil-García, R., Orozco, M., González, C., and Eritja, R. (2003) Properties of Triple Helices Formed Oligonucleotides Containing 8-Aminopurines. *Nucleos Nucleot Nucl.* 22, 645-648.

[66]. Beaucage, S. L., and Caruthers, M. H. (1981) Deoxynucleoside phosphoramidites—A New Class of Key Intermediates for Deoxypolynucleotide Synthesis. *Tetrahedron Lett.* 22, 1859-1862.

[67]. Beaucage, S. L., and Iyer, R. P. (1992) Advances in the Synthesis of Oligonucleotides by the Phosphoramidite Approach. *Tetrahedron.* 48, 2223-2311.

[68]. Asensio, J.L., Carr, R., Brown, T., and Lane, A.N. (1999). Conformational and thermodynamic properties of parallel intramolecular triple helices containing a DNA, RNA, or 2'-OMeDNA third strand. *J. Am. Chem. Soc.* 121, 11063–11070.

[69]. Mills, M., Arimondo, P., Lacroix, L., Garestier, T., Hélène, C., Klump, H.H., and Mergny, J.L. (1999). Energetics of strand displacement reactions in triple helices: A spectroscopic study. *J. Mol. Biol.* 291, 1035–1054.

[70]. Plum, G.E. (1998). Thermodynamics of oligonucleotide triple helices. *Biopolymers* 44, 241–256.

[71]. Plum, G.E., and Breslauer, K.J. (1995). Thermodynamics Of An Intramolecular DNA Triple Helix: A Calorimetric And Spectroscopic Study Of The Ph And Salt Dependence Of Thermally Induced Structural Transitions. *J. Mol. Biol.* 248, 679–695.

[72]. Plum, G.E., Park, Y.W., Singleton, S.F., Dervan, P.B., And Breslauer, K.J. (1990). Thermodynamic Characterization Of The Stability And The Melting Behavior Of A DNA Triplex: A Spectroscopic And Calorimetric Study. *Proc. Natl. Acad. Sci. USA* 87, 9436–9440.

[73]. Rougée, M., Faucon, B., Mergny, J.L., Barcelo, F., Giovannangeli, C., Garestier, T., and Hélène, C. (1992). Kinetics And Thermodynamics Of Triple-Helix Formation: Effects Of Ionic Strength And Mismatches. *Biochemistry* 31, 9269–9278.

[74]. Völker, J., Osborne, S.E., Glick, G.D., And Breslauer, K.J. (1997). Thermodynamic Properties Of A Conformationally Constrained Intramolecular DNA Triple Helix. *Biochemistry* 36, 756–767.

[75]. Wilson, W.D., Hopkins, H.P., Mizan, S., Hamilton, D.D., And Zon, G. (1994). Thermodynamics Of DNA Triplex Formation In Oligomers With And Without Cytosine Bases—Influence Of Buffer Species, pH, And Sequence. *J. Am. Chem. Soc.* 116, 3607–3608.

[76]. Aviño, A., Grimau, M.G., Frieden, M., and Eritja, R. (2004) Synthesis and Triple-Helix-Stabilization Properties of Branched Oligonucleotides Carrying 8-Aminoadenine Moieties. *Helv. Chim. Acta*. 87, 303-316.

[77]. Murphy, D., Eritja, R., and Redmond, G. (2004) Monitoring Denaturation Behaviour and Comparative Stability of DNA Triple Helices using Oligonucleotide-Gold Nanoparticle Conjugates. *Nucl. Acids Res. 32*, e65.

[78]. Liu, K., Miles, H. T., Frazier, J., and Sasisekharan, V. (1993) A Novel DNA Duplex. A Parallel-Stranded DNA Helix with Hoogsteen Base Pairing. *Biochemistry 32*, 11802-11809.

[79]. Mergny, J. L., and Lacroix, L. (2003) Analysis of Thermal Melting Curves. *Oligonucleotides. 13*, 515-537.

[80]. Roberts, R., and Crothers, D. (1992) Stability and Properties of Double and Triple Helices: Dramatic Effects of RNA Or DNA Backbone Composition. *Science. 258*, 1463-1466.

[81]. Han, H., and Dervan, P. B. (1993) Sequence-Specific Recognition of Double Helical RNA and RNA.DNA by Triple Helix Formation. *Proc. Natl. Acad. Sci. U. S. A.* 90, 3806-3810.

[82]. Nadal, A., Coll, A., Aviñó, A., Esteve, T., Eritja,R., and Pla, M. (2006) Efficient Sequence-Specific Purification of *Listeria Innocua* mRNA Species Triplex Affinity Capture with Parallel Tail-Clamps. *ChemBioChem. 7*, 1039-1047.

[83]. Ito, T., Smith, C. L., and Cantor, C. R. (1992) Sequence-Specific DNA Purification by Triplex Affinity Capture. *Proc. Natl. Acad. Sci. U. S. A.* 89, 495-498.

CHAPTER 3

Synthesis of Oligonucleotides Carrying 5'-5' Linkages Using Copper-Catalyzed Cycloaddition Reactions

3.1. Click chemistry

In 2001 Kolb, Finn and Sharpless published a landmark review [1] describing a new strategy for organic chemistry. They used the name 'click chemistry' to define a set of powerful, highly reliable, and selective reactions for the rapid synthesis of useful new compounds and through heteroatom links. This strategy is inspired by the way that nature performs combinatorial chemistry, making large oligomers from relatively simple building blocks with an overall preference for carbon-heteroatom bonds.

Chemical reactions must meet a set of requirements if they want to be considered in the context of click chemistry. These criteria have been defined by Sharpless *et al*., as reactions that are modular, wide in scope, high yielding, generate inoffensive byproducts that can be easily removed, are stereospecific, need simple conditions to be carried out, has readily available starting materials and reagents and require benign or easily removed solvent (preferably water).

These characteristics are commonly achieved by having a large thermodynamic driving force (usually greater than 20 kcal/mol) to favour a reaction highly selective for a single product. Although meeting all requirements of a click reaction is a tall order, several processes are considered to fit in this context. Some common examples are:

- Nucleophilic ring-opening reactions of strained heterocycles, such as epoxides or aziridines;

- Carbonyl chemistry of the "non-aldol" type, such as formation of ureas, thioureas, aromatic heterocycles, oxime ethers, hydrazones, etc;

- Additions to carbon-carbon multiple bonds such as oxidative additions (epoxidation, dihydroxylation…) and Michael additions;

- Cycloadditions reactions such as 1,3-dipolar cycloaddition or the Diels-Alder reaction.

The scheme in figure below (Figure 3.1) shows some of these reactions which match the click chemistry criteria.
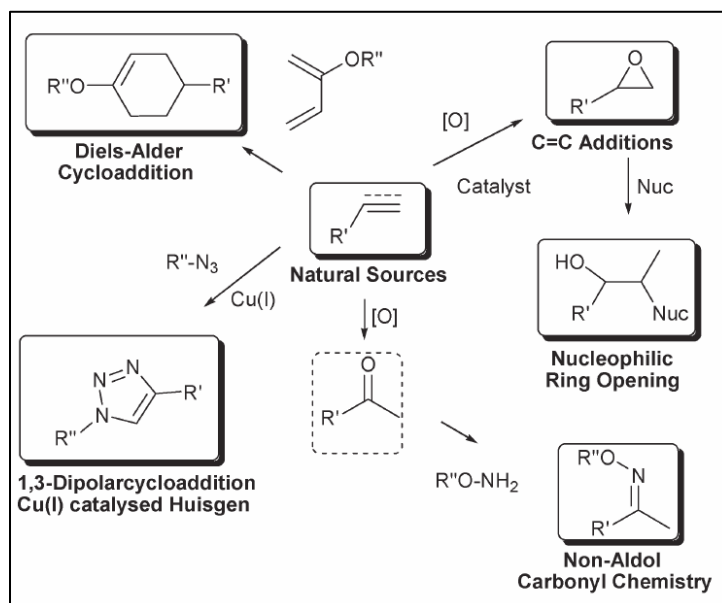
Figure 3.1. A selection of reactions which match the Click Chemistry criteria (extracted from reference [2]).

Among all of these reactions, the Huisgen 1,3-dipolar cycloaddition of alkynes and azides to yield 1,2,3-triazoles is undoubtly the premier example of a click reaction. In particular, the Cu(I)-catalyzed stepwise variant is often referred to simply as the "click reaction" and it will be explained in detail in the next section.

3.1.1. The Cu (I)-catalyzed azide-alkyne cycloaddition (CuAAC) reaction.

The formation of triazoles by addition of organic azides to acetylenes was discovered in the early 1900's by Dimroth but it was not until the 1960's when the generality, scope and mechanism of these cycloadditions was fully described by Rolf Huisgen [3,4].

The azide-alkyne Huisgen cycloaddition reaction is a 1,3-dipolar cycloaddition between an azide and an alkyne under thermal conditions to afford a 1,2,3-triazole as a mixture of 1,4- and 1,5- adduct (Figure 3.2).
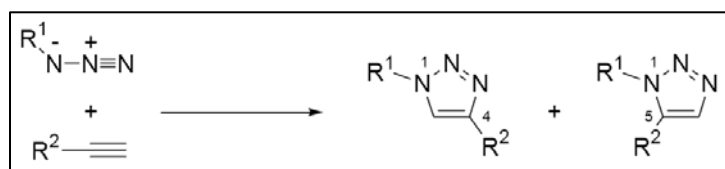
Figure 3.2. 1,2,3-Triazole Formation via Huisgen 1,3-Dipolar Cycloaddition.

The copper (I)-catalyzed variant was first reported in 2002 simultaeously by the group of Meldal [5] and Sharpless [6]. When catalyzed by Cu (I), the azide-alkyne cycloaddition is not only dramatically accelerated but yields the 1,4-

regioisomer as sole product in mild conditions (aqueous solvent and room temperature).

A stepwise mechanism was proposed by Fokin and Sharpless on the basis of calculations and kinetics studies [6,7]. Figure 3.3 shows the proposed scheme for the catalytic cycle.
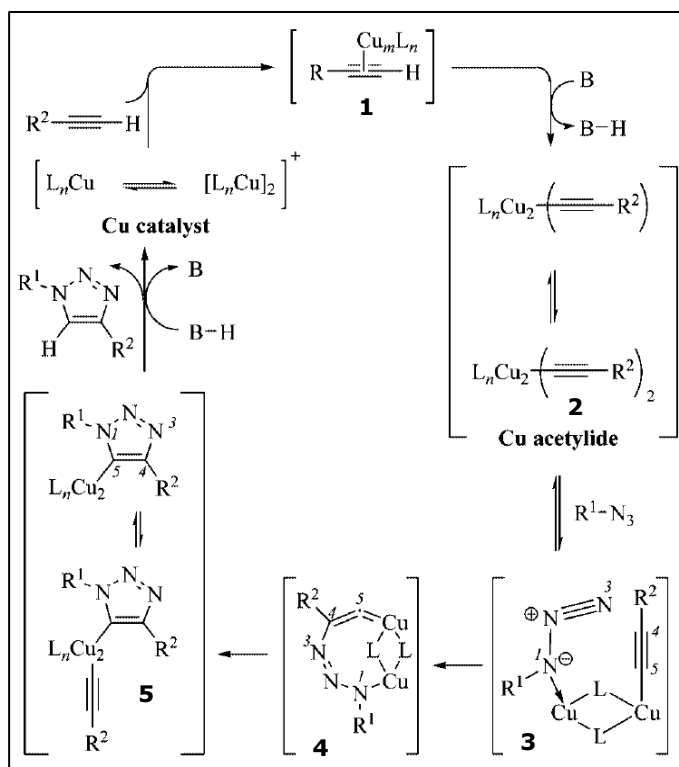
Figure 3.3. Proposed mechanism of Cu(I)-catalyzed alkyne-azide coupling, extracted from reference [8].

The stepwise catalytic cycle begins with formation of a Cu (I) acetylide species (**2**) via the π complex **1**. Although questions about the nature of these complexes still exist, the current evidence indicates that the copper acetylide species involved in catalysis require two metal centers, one or two alkyne ligands, and other labile ligands that allow for competitive azide binding. Different intermediates can exist depending on the reaction conditions.

The next step is the azide displacement of one ligand to generate a copper acetylide-azide complex (**3**), which facilitates nucleophilic attack of acetylide carbon C(4) at N(3) of the azide forming metallocycle **4**. This metallocycle positions the bound azide properly for subsequent ring contraction to give the triazole-copper derivative **5.** Protonation of this intermediate followed by dissociation of the product ends the reaction and regenerates the catalyst.

Following the discovery of the Cu (I) catalyzed alkyne-azide cycloaddition, a high number of studies have been carried out for the further investigation of the

reaction. Reported conditions have varied widely among successful examples published in the literature. Results from a multitude of works over the last years suggest that alkyne–azide coupling affords triazoles in high yield under a variety of conditions, proving the robustness of this reaction.

A variety of copper (I) sources have been tested. Different copper (I) salts have been used directly. Among them, CuI is the most popular [5] but others have also given good results such as Cu(OTf)$_2$ [9], [Cu (CH$_3$CN)$_4$][PF$_6$] [10,11], (Ph$_3$P)$_3$CuBr [12] or (EtO)$_3$PCuI [12]. In this case the reaction usually requires water and acetonitrile as co-solvent and one equivalent of a nitrogen base (e.g. triethylamine, N-ethyldiisopropylamine or 2,6-lutidine) and is usually performed under inert conditions.

One of the most commonly used Cu(I) catalyst is generated in-situ by reduction of Cu(II) salts, usually CuSO$_4$·5H$_2$O. As the reductant ascorbic acid and/or sodium ascorbate at a 3- to 10- fold excess over the catalyst have proved to afford products in high purity and yielding with a 2-5 mol% catalyst loading [6,13]. Tris(2-carboxyethyl)phosphine (TCEP) has also been used as reducing agent in studies using CuAAC in biological systems [14-17]. When using Cu(II) salts , the reaction is commonly performed in a water/alcohol mixture. Mixtures of water and organic co-solvents such as DMSO have proven to produce equally good results [18]. Another alternative is the formation of Cu(I) catalyst by oxidation of Cu metal. Some groups have performed addition of excess copper turnings to azides and alkynes in water/alcohol mixtures obtaining the corresponding triazoles in good yield[7]. Other protocols are based on the use of nanosize Cu(0) powder [19] or Cu(0) nanoclusters [20].

Some years ago the use of stabilizing ligands for Cu(I) to prevent its oxidation and enhance the catalytic activity was reported [18,21,22]. Among various N-based compounds, polytriazolylamines and specially TBTA (Figure 3.4) appeared to give the best results [18].
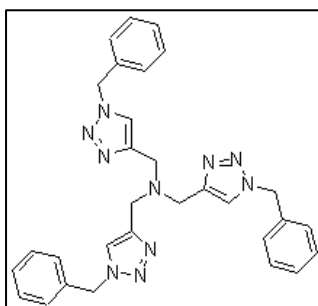
Figure 3.4. Tris-[(1-benzyl-1H-1,2,3-triazol-4-yl)methyl]amine, also known as TBTA is a stabilizing ligand for Cu(I) developed by Sharpless group. It protects Cu(I) from oxidation and disproportionation, while enhancing its catalytic activity.

Steric factors and electronic effects have also proved to play an important role in the success of CuAAC. This is reflected in some studies of biomolecular

labelling through CuAAC, where it became apparent that the steric shielding of the alkyne contributes to low the yield of the reaction [23].On the other hand, some studies have noted that electron-deficient alkynes react most quickly [5,24], likely due to facile formation of the Cu (I) acetylide species and increased rate of electrophilic attack by the bound azide.

Although CuAAC coupling often requires no additional heating, microwave chemistry can dramatically reduce reactions times in many cases [12,25,26]. Regarding the reaction phase, CuAAC has been performed in both solution and solid phase. The latter has allowed the efficient synthesis of combinatorial libraries using the split and combine method to screen a high variety of triazole containing compounds against relevant biological targets [27].

Wang and coworkers broadened even more the scope of CuAAC with in-situ azide generation prior to cycloaddition [28]. Such one-pot procedures avoid isolation of azides, hazardous for their potential risk of exothermal decomposition and explosion.

3.1.2. Applications of the CuAAC reaction.

The ease with which azides and alkynes are introduced into organic compounds, their inertness towards functional groups typically found in biomolecules (termed as bioorthogonal properties) and the mild conditions employed in the CuAAC reaction make it ideal for bioconjugation purposes as well as drug discovery or use in materials science. Some examples of these applications are given below.

- Application of CuAAC in drug discovery

The discovery of Cu(I) catalyzed variant of Huisgen's 1,3-dipolar cycloaddition reaction triggered the generation of chemical libraries with a high level of simplicity. Two building blocks are easily joined by formation of a 1,4-disubstituted 1,2,3-triazole linkage. The reliability and high yield of the reaction allows the screening of compounds directly from the reaction mixture. Furthermore, the generated triazoles have been revealed in several studies not just as a passive linker but as a very active pharmacophore with favourable physicochemical properties [29-33].

As examples worth mentioning the work by Wong *et al*. who used the CuAAC in a high throughput screening which led to the discovery of a novel and selective inhibitor of human α-1,3-fucosyltransferase [34].

Brik *et al.* prepared a library of potential HIV protease inhibitors conjugating azide-bearing scaffolds with acetylenes via click chemistry [35]. Over 100 triazole compounds were screened directly, without product isolation, against wild type

HIV-1 protease and three mutants. Potent inhibitors, active at nanomolar concentrations, were identified.

Novel means of lead discovery approaches have been achieved by target-guided synthesis (TGS) in which the biological target is actively involved in the synthesis of its own inhibitory compound (Figure 3.5). In this approach the biological target acts as a template for the assembly of building blocks. Only small compounds that interact with the active site of the protein will be in close proximity to react with one another and form potent inhibitors.
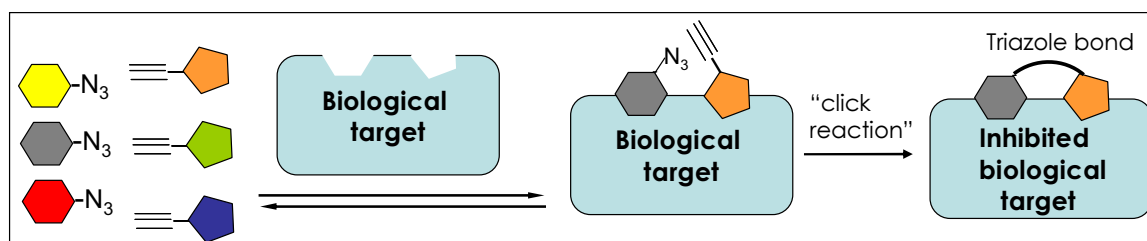
Figure 3.5. Schematic representation of the use of click chemistry in target-guided synthesis.

Sharpless and collaborators described the use of acetylcholinesterase, an enzyme involved in neurotransmitter hydrolysis, in the application of TGS [36,37]. After screening from a mixture of fragments decorated with azide and alkyne functionalities, substantial rate acceleration was observed for certain azide-acetylene reagent combinations in the presence of the enzyme.

- Application of CuAAC in bioconjugation

Following the discovery and development of click reaction numerous biomolecules including DNA, peptides, proteins, oligosaccharides and glycoconjugates have been labelled with different compounds. Many of these new molecular entities are extremely useful for the study of biological systems.

As successful examples, Eichler *et al.* performed ligation of peptides to form assembled and scaffolded peptides [38]. The group of Kirshenbaum has described an efficient protocol for the multisite modification of peptoids on solid phase using click chemistry, allowing the generation of complex peptidomimetic compounds [39,40].

High-density postsynthetic functionalization of DNA was carried out by Carell *et al.* who used the CuAAC for the multiple labelling of alkyne-modified DNA [23]. This reaction was also successfully used to produce FAM-labelled ssDNA (Figure 3.6.C) as a primer for the Sanger DNA sequencing [41].

One particularly striking application of click chemistry is the chemical tagging of live organisms and proteins (Figure 3.6.A). A few years ago Finn *et al.* succeeded in using the CuAAC for labelling Cowpea mosaic virus particles (CPMV)

with fluorescein [42]. Tirrell and Link forced *E.coli* cells to display an azide-bearing outer membrane protein C (OmpC), which were successfully biotinylated with a biotin-alkyne reagent [43]. The Schultz laboratory then reported that their method for incorporation of azide groups into proteins of *S. cerevisiae* could be followed up by coupling of dyes [44], as optimized by Finn *et al.* for *in situ* bioconjugations [16].

Bioconjugation has also proved particularly fruitful in the field of activity based protein profiling (ABPP). In this technique affinity labels are used to profile proteins on the basis of their function in biological systems. Small azide reactive probes can be easily up taken by cells and covalently label specific classes of enzymes. Subsequent coupling of a chemical tag such as rhodamine allows for rapid detection and isolation of these enzymes from a complex mixture of proteins (Figure 3.6.B). By using this approach the *in vivo* profiling of glutathione S-transferases, aldehyde dehydrogenases, and enoyl CoA hydratases has been probed [15].

In the figure 3.6 some of these bioconjugation applications are highlighted.
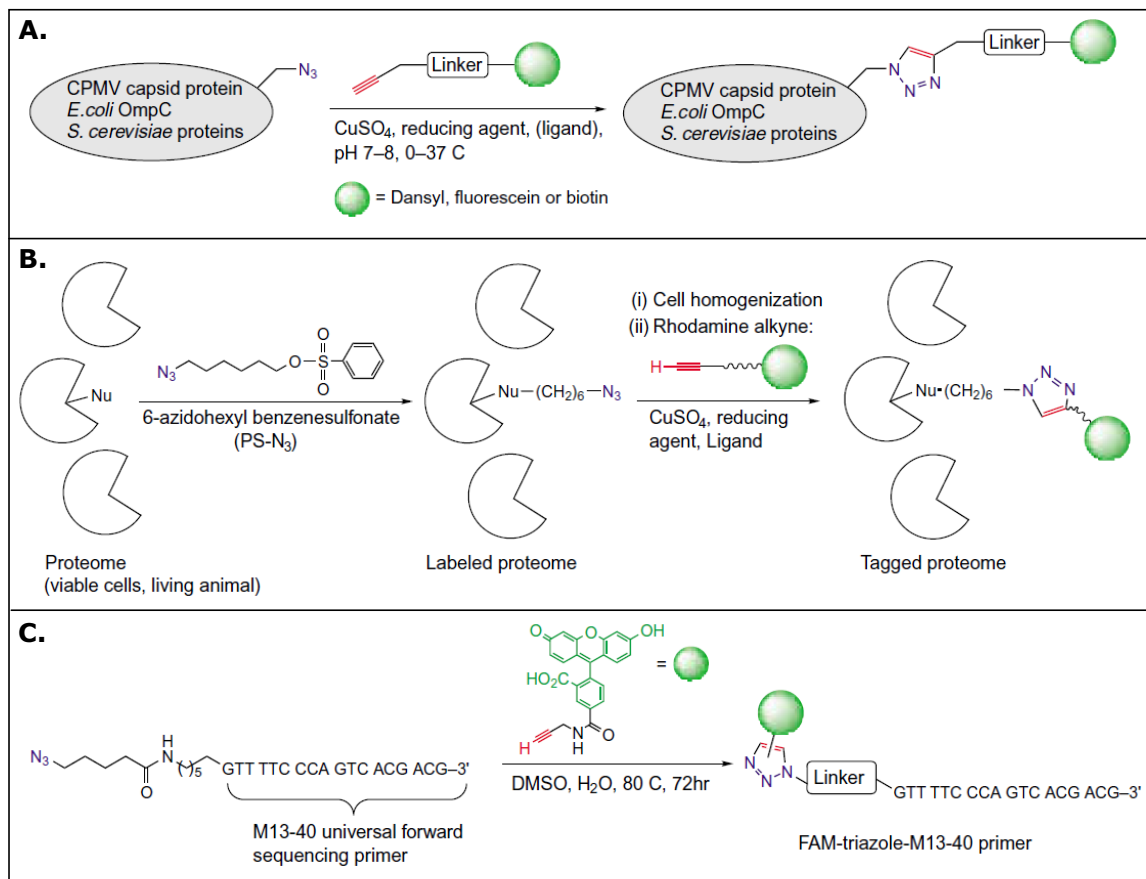
Figure 3.6. Bioconjugation applications using the azide-alkyne cycloaddition reaction. A) Virus, cell and protein tagging. B) *In vivo* activity-based protein profiling. C) DNA labelling to enable sequencing by the Sanger method.

- Application of CuAAC in materials science and nanotechnology

Materials chemistry is a rich beneficiary of the click reaction thanks to its ability to make molecular connections with high fidelity. Hawker, Fokin and Sharpless first synthesized triazole-linked dendrimers of high purity using Cu(I)-catalyzed coupling of acetylenes and azides [25]. Since then several groups have studied the synthesis of polymers *via* click chemistry, as reviewed by Binder and Sachsenhofer [45,46].

The reaction has been also used to functionalize surfaces coated with alkyne or azide containing molecules. Self-assembled monolayers (SAMs) such as alkyne-terminated SAM on gold [47] and azide-terminated SAM on silica [48,49] have been employed in different works.

CuAAC is ideally suited for immobilization of biomolecules onto surfaces [50,51], which has many potential applications in the development of microarrays, microbeads or biosensor chips. Nanoparticles and nanotubes have also been functionalized with different molecules using this reaction [52-55].

The figure 3.7 shows several applications of the Cu(I) catalyzed alkyne-azide cycloaddition in the field of material science.
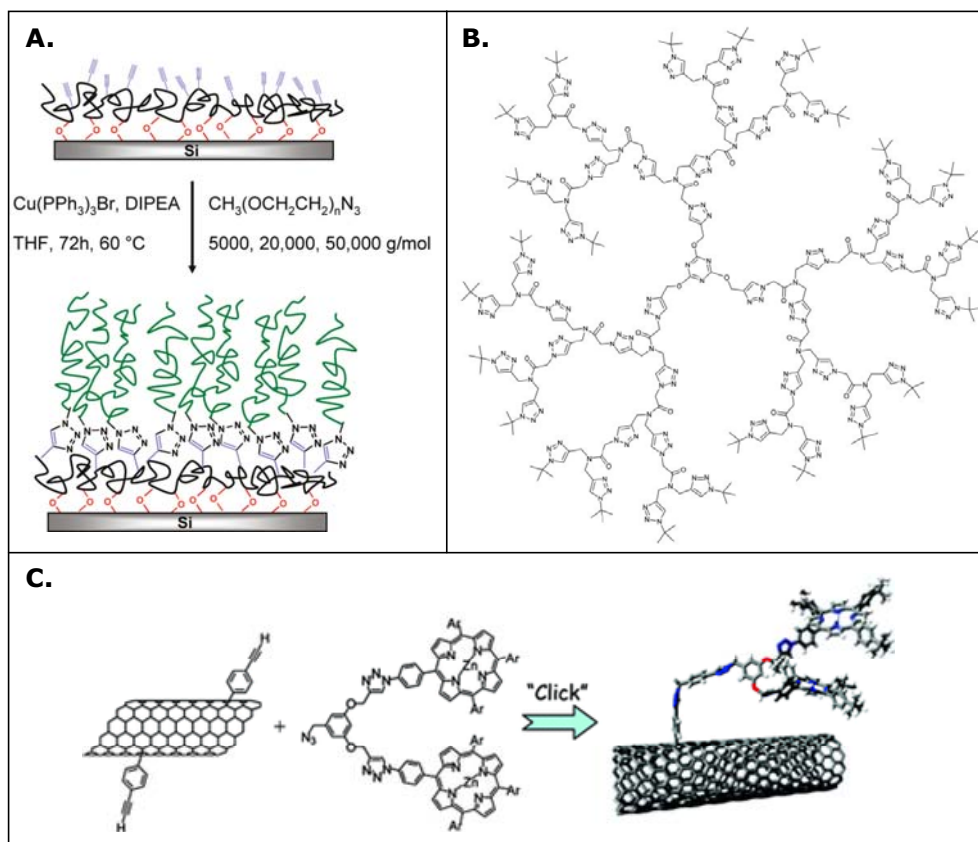
Figure 3.7. Examples of applications of CuAAC in materials science and nanotechnology A). Grafting of azide-terminated polymer chains to alkyne-

functionalized surfaces. B). Dendrimer synthesized by Fokin *et al*. using click chemistry. C). Functionalization of carbon nanotubes with porphyrin dendrons.

3.2. Aim of the work

In the previous chapter the synthesis of parallel hairpins was described. The LNA substitutions were introduced in the polypyrimidine strand, which was synthesized in the 3' to 5' direction, with commercially available phosphoramidites. For the natural polypurine strand (synthesized from 5' to 3' end) commercially available A and G reverse phosphoramidites were used. The problem arises if we wished to introduce modifications also in this second strand. In that case we would need to dispose of the corresponding modified reverse phosphoramidite (not commercially available), which means a strong synthetic effort.

An alternative method to synthesize parallel clamps without need of reverse phosphoramidites consists in using branching units and has been previously described by our group [56] and others [63]. In this method the hairpins are synthesized from the middle of the molecule by the extension of one branch of an asymmetric branching molecule, followed by assembly of the next branch (figure 3.8). The combination of an acid-labile group (dimethoxytrityl, DMT) and a base-labile group ((9H-fluoren-9-ylmethoxy)carbonyl; Fmoc) allowed assembly of the desired molecule without the need of reverse phosphoramidites.
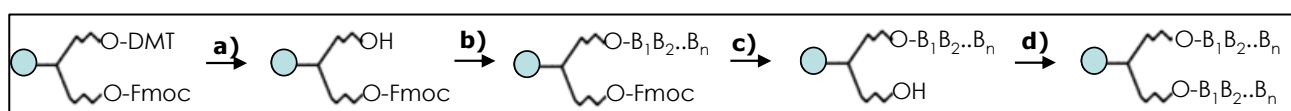
Figure 3.8. Scheme for the synthesis of parallel clamps using a branching molecule. a) deprotection of the DMT group with mild acidic conditions; b) elongation of the first chain with standard phosphoramidites; c) Fmoc removal with basic conditions; d) assembly of the second chain with standard phosphoramidites.

This approach implies the removal of the Fmoc group in the middle of the synthesis to allow the second strand to grow. In this step, not only the Fmoc group, but also the 2-cyanoethyl groups of the phosphate moieties of the first assembled DNA strand are removed. In addition to premature removal of the 2-cyanoethyl groups of phosphates, other difficulties need to be taken into account when using this strategy. Results found during synthesis of branched DNA indicate that steric hindrance and electron-withdrawing effects of the groups at the branching site slow the coupling reactions. Thus, increasing the coupling time and/or the phosphoramidite concentration is required [57,58].

In this work we propose a novel strategy to obtain parallel clamps using the non-templated chemical ligation of two oligonucleotides by 5'-5' linkages. This

chapter addresses the linking of two DNA strands using the Cu (I)-catalyzed azide-alkyne cycloaddition reaction (Figure 3.9).
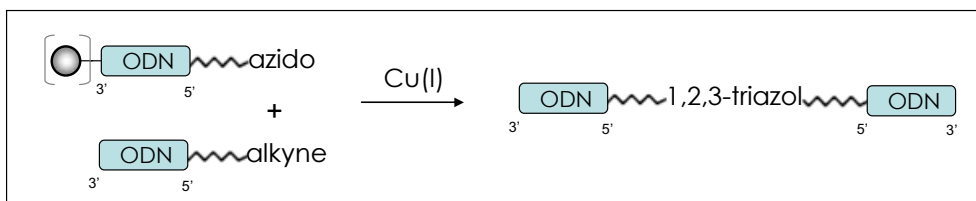
Figure 3.9. Scheme of chemical ligation of two oligonucleotide strands by a 5'-5' linkage.

The development of efficient protocols for the introduction of azido and alkyne moieties in oligonucleotides as well as identification of optimal conditions for ligation of these strands by CuAAC are reported.

The last part of the chapter covers the work carried out during a FPI predoctoral short-term staying in the laboratory of Dr. Grøtli, in the Medicinal Chemistry Department at Göteborg University. The aim of the research at Dr. Grøtli's group was the synthesis of novel non-natural aminoacids by click chemistry that can be used for the modification of peptides with histidine analogues.

3.3. Design of oligonucleotide sequences

Azido and alkyne moieties were introduced in the 5'-end of different oligonucleotides, mainly in homopurine and homopyrimidine sequences so that the modified DNA strands could form a parallel hairpin after their chemical ligation by click chemistry.

Oligonucleotide sequences are based on the parallel clamp which was synthesized for triplex studies in the chapter 2. Other sequences, such as polyadenine and polythymidine were synthesized for preliminary studies. 5'-modified oligonucleotides used for click reactions and their intermediates are listed in table 3.10. Numbers and abbreviations used to identify them along this work are indicated in the first and second column, respectively.

N$_o$.	Oligonucleotide	Sequence[a]
1	8T	$^{3'}$-TTTTTTTT-$^{5'}$
2	8A	$^{3'}$-AAAAAAAA-$^{5'}$
3	CT	$^{3'}$-TCTCCTCCTTC-$^{5'}$
4	GA	$^{3'}$-AGAGGAGGAAG-$^{5'}$
5	CT$_{long}$	$^{3'}$-TTTTTTCTCCTCCTTC-$^{5'}$
6	pyr-CT	pyr-thr-OPO$_3$-$^{3'}$-TCTCCTCCTTC-$^{5'}$
7	GT$_{10}$	$^{3'}$-GTTTTTTTTTTT-$^{5'}$
8	8T-$^{5'}$aminohexyl	$^{3'}$-TTTTTTTT-$^{5'}$OPO$_3$-(CH$_2$)$_6$-NH$_2$
9	8T-$^{5'}$propargylglutaryl	$^{3'}$-TTTTTTTT-$^{5'}$OPO$_3$-(CH$_2$)$_6$-NHCO-(CH$_2$)$_3$-CONH-CH$_2$-C≡CH
10	8T-$^{5'}$COONHS	$^{3'}$-TTTTTTTT-$^{5'}$OPO$_3$-(CH$_2$)$_9$-COONHS
11	8T-$^{5'}$propargyl	$^{3'}$-TTTTTTTT-$^{5'}$OPO$_3$-(CH$_2$)$_9$-CONH- CH$_2$-C≡CH
12	8A-$^{5'}$COONHS	$^{3'}$-AAAAAAAA-$^{5'}$OPO$_3$-(CH$_2$)$_9$-COONHS
13	8A-$^{5'}$propargyl	$^{3'}$-AAAAAAAA-$^{5'}$OPO$_3$-(CH$_2$)$_9$-CONH- CH$_2$-C≡CH
14	CT-$^{5'}$COONHS	$^{3'}$-TCTCCTCCTTC-$^{5'}$OPO$_3$-(CH$_2$)$_9$-COONHS
15	CT-$^{5'}$propargyl	$^{3'}$-TCTCCTCCTTC-$^{5'}$OPO$_3$-(CH$_2$)$_9$-CONH- CH$_2$-C≡CH
16	pyr-CT-$^{5'}$COONHS	pyr-thr-OPO$_3$-$^{3'}$-TCTCCTCCTTC-$^{5'}$-OPO$_3$-(CH$_2$)$_9$-COONHS
17	pyr-CT-$^{5'}$propargyl	pyr-thr-OPO$_3$-$^{3'}$-TCTCCTCCTTC-$^{5'}$-OPO$_3$-(CH$_2$)$_9$-CONH-CH$_2$-C≡CH
18	CT$_{long}$-$^{5'}$COONHS	$^{3'}$-TTTTTTCTCCTCCTTC-$^{5'}$OPO$_3$-(CH$_2$)$_9$-COONHS
19	CT$_{long}$-$^{5'}$propargyl	$^{3'}$-TTTTTTCTCCTCCTTC-$^{5'}$OPO$_3$-(CH$_2$)$_9$-CONH- CH$_2$-C≡CH
20	CT-$^{5'}$hexynyl	$^{3'}$-TCTCCTCCTTC-$^{5'}$OPO$_3$-(CH$_2$)$_4$-C≡CH
21	GA-$^{5'}$hexynyl	$^{3'}$-AGAGGAGGAAG-$^{5'}$OPO$_3$-(CH$_2$)$_4$-C≡CH
22	8T-$^{5'}$azidobutyryl	$^{3'}$-TTTTTTTT-$^{5'}$OPO$_3$-(CH$_2$)$_6$-NHCO-(CH$_2$)$_4$-N$_3$
23	CT-$^{5'}$iodo	$^{3'}$-TCTCCTCCTTC-$^{5'}$–I
24	CT-$^{5'}$azido	$^{3'}$-TCTCCTCCTTC-$^{5'}$–N$_3$
25	GA-$^{5'}$iodo	$^{3'}$-AGAGGAGGAAG-$^{5'}$–I
26	GA-$^{5'}$azido	$^{3'}$-AGAGGAGGAAG-$^{5'}$–N$_3$
27	GT$_{10}$-$^{5'}$azido	$^{3'}$-GTTTTTTTTTTT-$^{5'}$–N$_3$
28	CT-$^{5'}$bromohexyl	$^{3'}$-TCTCCTCCTTC-$^{5'}$OPO$_3$-(CH$_2$)$_6$-Br
29	CT-$^{5'}$azidohexyl	$^{3'}$-TCTCCTCCTTC-$^{5'}$OPO$_3$-(CH$_2$)$_6$-N$_3$
30	GA-$^{5'}$bromohexyl	$^{3'}$-AGAGGAGGAAG-$^{5'}$OPO$_3$-(CH$_2$)$_6$-Br
31	GA-$^{5'}$azidohexyl	$^{3'}$-AGAGGAGGAAG-$^{5'}$OPO$_3$-(CH$_2$)$_6$-N$_3$

Table 3.10. Oligonucleotides used in this work to obtain parallel hairpins through CuAAC. [a] NHS: N-hydrosuccinimide ester; pyr: pyrene; thr:threoninol.

The different methods for introducing the azido and alkyne groups at the 5' end of oligonucleotides will be explained in detail in the next section, as well as derivatization at the 3' with a pyrene molecule using CPG functionalized with L-threoninol.

3.4. Synthesis of oligonucleotides carrying alkynyl groups

3.4.1. Synthesis of 5'-alkyne-ODNs from 5'-amino-ODNs

A wide spectrum of non-standard phosphoramidites can be used in conventional automated synthesis to insert certain modifications at a desired position, such as the 5' or 3' ends, the internucleotidic linkages or the nucleobases. Multiple examples of phosphoramidite building blocks derived from a desired conjugate group have been widely reported for derivatization and oligonucleotides labelling [59-61].

A common method for introducing different molecules at the 5'-end of DNA strands involves the reaction of 5'-amino-oligonucleotides with a compound carrying a carboxylic acid group [62].

In this work the commercially available 5'-Amino-Modifier C6 phosphoramidite (figure 3.11) has been used to functionalize different sequences with a monomethoxytrityl (MMT)-protected amino group. This phosphoramidite is a derivative of 6-aminohexanol, in which the amino group has been protected with the MMT group and the alcohol functionalized with the phosphoramidite group.
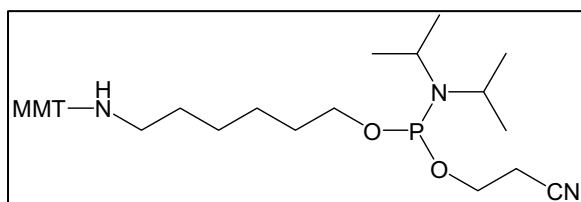
Figure 3.11. 5'-Amino-Modifier C6 phosphoramidite used in this work for the introduction of a primary amino group at the 5'-terminus of the oligonucleotides.

On the other hand, a molecule containing both a propargyl and an activated ester group was synthesized and used for the preparation of alkyne-modified oligonucleotides. The compound succinimidyl N-propargyl glutariamidate was obtained according to the scheme 3.12.
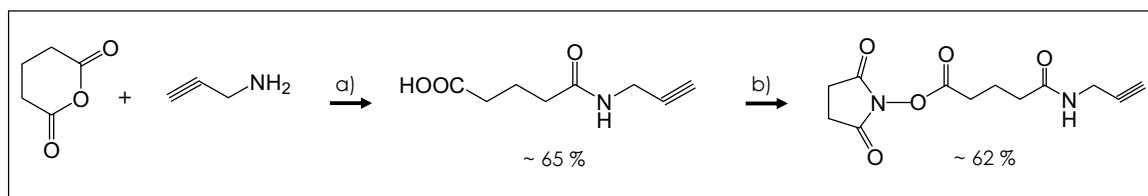
Scheme 3.12. Synthesis of the succinimidyl N-propargyl glutariamidate used for the preparation of 5'-propargyl-oligonucleotides. a) 1eq. NEt$_3$/DCM, 12h at r.t, b) 1 eq. N-Hydroxysuccinimide, 1eq. EDC, DCM, 8h at r.t.

Both intermediate and final product were characterized by ^{1}H-NMR and ^{13}C-NMR. The NMR spectra of the intermediate N-propargyl glutaric acid showed impurification with triethylamine, which was successfully removed after purification of the final desired product.

An oligonucleotide containing eight thymidines was synthesized in an automatic synthesizer and the phosphoramidite indicated above was coupled in the last cycle. After removing the MMT group, the resulting amino-oligonucleotide-support was treated with succinimidyl N-propargyl glutariamidate, followed by deprotection and cleavage from the support by aqueous ammonia treatment (scheme 3.13).
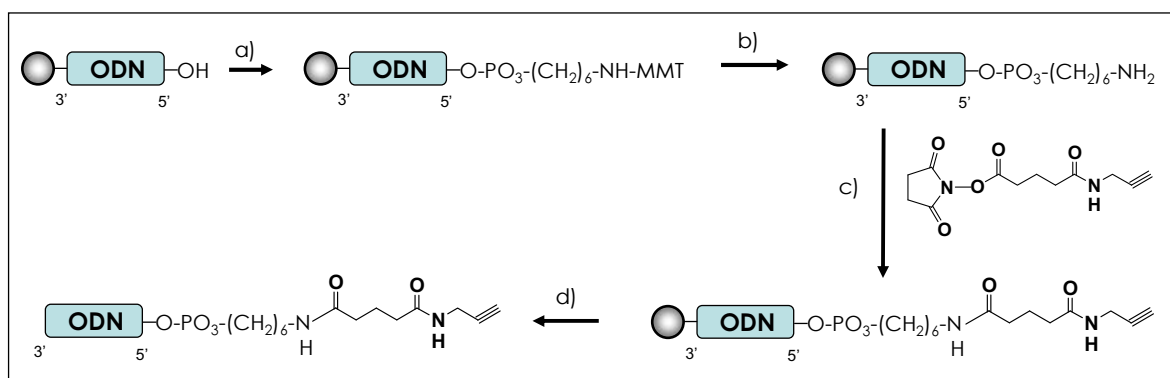
Scheme 3.13. Synthesis of 5'-propargyl-oligonucleotides based on the conjugation of 5'-amino-oligonucleotides. a) 5'-Amino-Modifier C6 phosphoramidite in ACN b) 3% TCA/DCM, c) succinimidyl N-propargyl glutariamidate in dioxane d) NH$_3$ (aq) 55ºC.

The hydrophobicity of the incorporated alkyne moiety allowed the purification of the modified DNA sequence by reverse-phase HPLC. The desired propargyl oligonucleotides were obtained in a yield of about 65 %, as can be seen in chromatogram of figure 3.14.
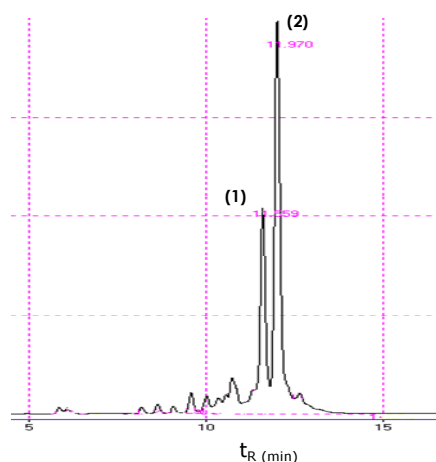
Figure 3.14. HPLC analysis of the product resulting from conjugation of CPG-supported 8T-$^{5'}$-aminohexyl ODN with succinimidyl N-propargyl glutariamidate. Two

major peaks were observed, the last of which corresponds to the desired **ODN 9**. Gradient: 0→ 50% B in 20 min (A: 5% ACN in 0.1 M TEAAc pH 6.5; B: 70% ACN in 0.1 M TEAAc pH 6.5).

The peak (2) corresponds to the desired 8T-5'-propargyl (**ODN 9**) meanwhile the MW found for the peak (1) agrees with N-acetylation of the primary amino group of the starting 8T-5'-aminohexyl oligonucleotide. Previous studies [64,65] have shown that MMT protection does not completely prevent the reactivity of the 5'-amino group toward N-acetylation (coming from capping reagents) which consequently reduces the efficiency of oligonucleotide functionalization.

3.4.2. Synthesis of 5'-alkyn-ODNs from 5'-carboxy-ODNs

Alternatively, the commercially available phosphoramidite of 10-hydroxydecanoic acid N-hydroxysuccinimide ester (figure 3.15) was used for the introduction of the N-hydroxysuccinimide ester group at the 5'-end (Scheme 3.17).
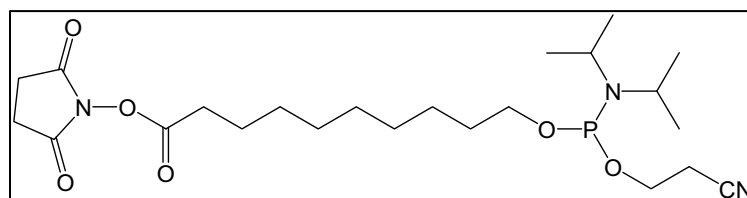
Figure 3.15. 5'-Carboxy-Modifier C10 used for the preparation of 5'-NHS-oligonucleotides.

This molecule is designed to be added at the 5' terminus of an oligonucleotide synthesis and enables conjugation with molecules containing a primary amine, resulting in a stable amide linkage. Conjugation must be done before ammonia deprotection, as ammonium hydroxide would lead to the ammonolysis of the NHS ester to form a carboxamide group.

Oligonucleotide sequences were synthesized both on a 1 μmol (CPG) and 0.2 μmol (PS) scale and 5'-Carboxy-Modifier C10 was coupled using the conventional coupling cycle for each support.

Conjugation with amines must be carried out immediately after the coupling of the 5'-Carboxy-Modifier C10 phosphoramidite to avoid extent of NHS-ester hydrolysis. A small fraction of a 5'-NHS-ODN-support was kept refrigerated, cleaved after several days and analyzed by HPLC. HPLC profile revealed partial hydrolysis of the product that was more pronounced the more time it had been stored. Figure 3.16.A shows a chromatogram corresponding to a partially hydrolyzed CT-5'-COONHS sample (**ODN 14**) and its comparison with the HPLC analysis of the same sequence when the cleavage is performed immediately after the ODN synthesis (Figure 3.16.B). In this latter case yield was around 87 %.
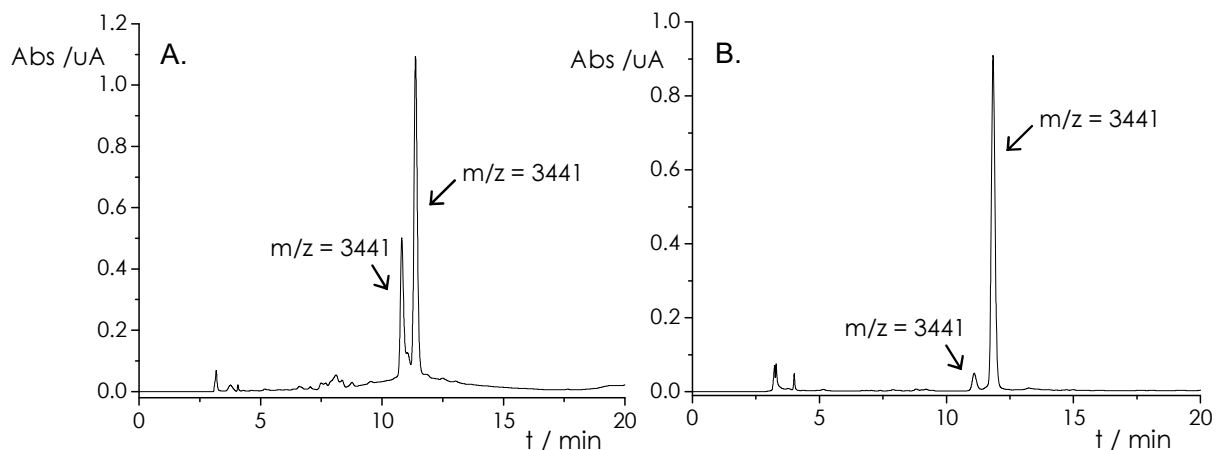
Figure 3.16. A) HPLC analysis of a partially hydrolyzed CT-5′-COONHS sample after one-week storage period. B) HPLC analysis of CT-5′-COONHS cleaved immediately after the synthesis. In both chromatograms the first eluting product is caused by hydrolysis of the NHS ester. The m/z values obtained by MALDI-TOF are indicated next to each peak. Gradient: 5→ 35% B in 20 min (A: 5% ACN in 0.1 M TEAAc pH 6.5; B: 70% ACN in 0.1 M TEAAc pH 6.5).

Similar MW values were found by MALDI-TOF for the two different peaks, which seems to indicate that the first one corresponds to the 5′-carboxy-oligonucleotide (hydrolysis of the NHS ester by moisture in the storage period) and the second one to the 5′-carboxamide-oligonucleotide (ammonolysis of the NHS ester during cleavage process). Only this latter peak comes from the product which would have enabled conjugation with amines.

Thus, the 5′-NHS-oligonucleotide-supports were treated promptly with propargylamine dissolved in dichloromethane with 10% triethylamine, followed by deprotection and cleavage from the support by aqueous ammonia treatment (scheme 3.17).
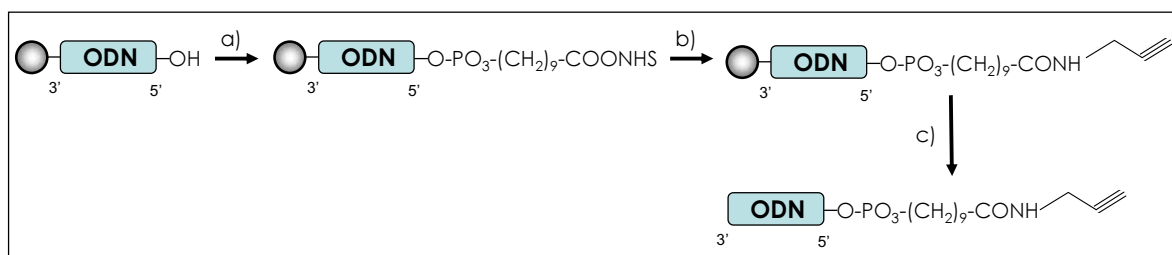
Scheme 3.17. Synthesis of 5′-propargyl-oligonucleotides based on the conjugation of 5′-carboxy-oligonucleotides. a) 5'-Carboxy-Modifier C10 in ACN, b) propargylamine in NEt_3/DCM (1/9), c) NH_3 (aq) 55ºC.

Propargyl-oligonucleotides were purified by reverse-phase HPLC and obtained in high yield, ranging from 70 to 85 % according to the relative peak areas. For all sequences, HPLC chromatograms presented a major peak which was collected, desalted by NAP-10, quantified by measuring the absorbance at 260nm

and analyzed by mass spectrometry. In figure 3.18 an example of HPLC analysis for **ODN 15** is shown. Small peaks eluting before the desired products were also analyzed by MALDI-TOF and were found to correspond to the 5'-carboxy-oligonucleotide (1) and to the 5'-carboxamide-oligonucleotide (2).
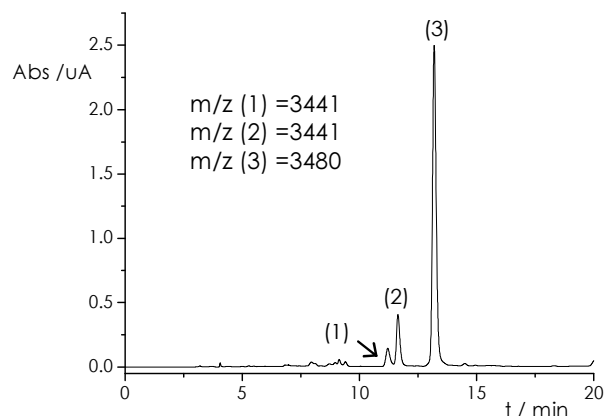
Figure 3.18. HPLC profile of **ODN 15.** The m/z values obtained for each peak by MALDI-TOF are indicated in the graphic. The major peak (3) corresponds with the desired product. Gradient: 5→ 35% B in 20 min (A: 5% ACN in 0.1 M TEAAc pH 6.5; B: 70% ACN in 0.1 M TEAAc pH 6.5).

As it will be explained later, some 5'-alkynyl oligonucleotides were fluorescently labelled at the 3' with a pyrene moiety. For this purpose, a solid support previously modified with a pyrene molecule was prepared by Dr. Alvaro Somoza from L-threoninol and 1-pyrenecarboxylic acid according to the scheme 3.19, as detailed in reference [66]. This modified CPG support was introduced in the automatic DNA synthesized and the desired sequences were assembled as usual.
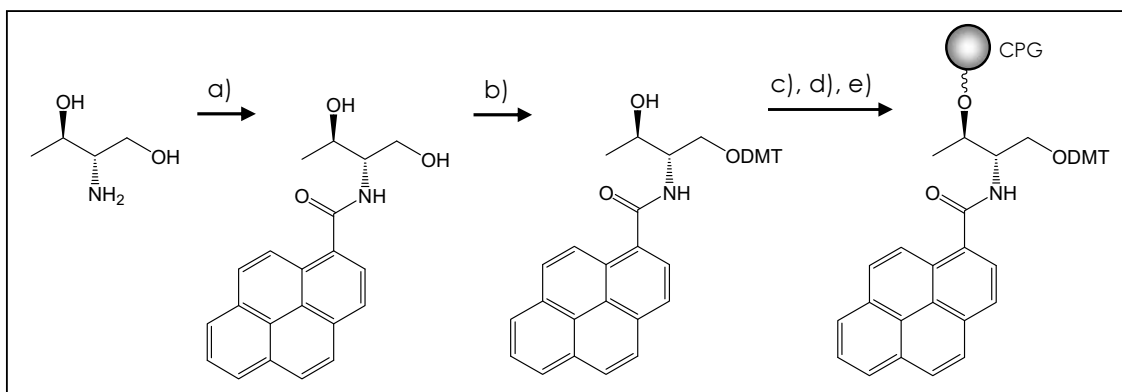
Scheme 3.19. a) 1-Pyrenecarboxylic acid, N,N'-Diisopropylcarbodiimide, HOBt, DMF, r.t, 24h ; b) DMTrCl, DIPEA, DMAP, pyridine, r.t 24h; c) succinic anhydride, DMAP, DIPEA, DCM r.t, 24h; d) DMAP, DTNP, P(Ph$_3$), ACN; e) CPG.

For all products, the molecular weight values found by MALDI-TOF were in agreement with the expected mass. In table 3.20 the measured masses of the

purified ODNs, their calculated theorical values and the retention time on HPLC are listed.

ODN	Sequence	t_R (min)	Found MW	Expected MW
12	8A-$^{5'}$COONHS	8.9[a]	2691	2692
13	8A-$^{5'}$propargyl	10.8[a]	2728	2730
14	CT-$^{5'}$COONHS	11.8	3441	3442
15	CT-$^{5'}$propargyl	13.4	3479	3481
16	pyr-CT-$^{5'}$COONHS	15.7	3837	3839
17	pyr-CT-$^{5'}$propargyl	17	3873	3877
18	CT$_{long}$-$^{5'}$COONHS	11.8	4961	4965
19	CT$_{long}$-$^{5'}$propargyl	13.1	4999	5003

Table 3.20. MALDI-TOF analysis of oligonucleotides used in this work after HPLC purification. Retention time corresponds to a gradient of 5→ 35% B in 20 min (A: 5% ACN in 0.1 M TEAAc pH 6.5; B: 70% ACN in 0.1 M TEAAc pH 6.5), except for the values marked with an [a], in which case 0→ 50% B in 20 min was employed.

The use of the 5'-carboxy-ODNs to obtain 5'-alkynyl-ODNs was simpler than the route using 5'-amino-ODNs described previously.

3.4.3. Synthesis of 5'-alkyn-ODNs with an alkyne-containing phosphoramidite

As a further step in the simplification process, the phosphoramidite derivative of an alcohol carrying a terminal alkyne was prepared. Commercially available 5-hexyn-1-ol was reacted with chloro-N,N-diisopropylamino-O-(2-cyanoethoxy) phosphine yielding the desired phosphoramidite (Scheme 3.21).
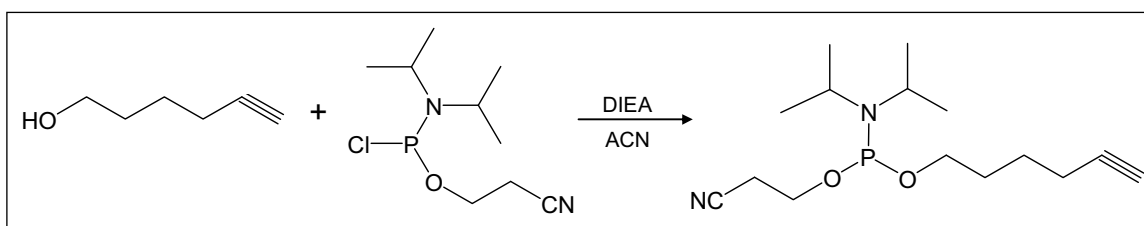
Scheme 3.21. Synthesis of the 2-cyanoethyl hex-5-ynyl N,N-diisopropyl phosphoramidite.

This molecule was used to directly introduce an alkynyl group at the 5'-end of oligonucleotides through a conventional coupling cycle in the automatic synthesizer (Scheme 3.22).
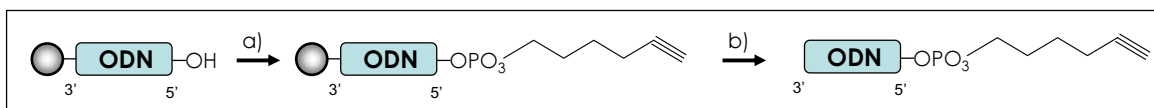
Scheme 3.22. Synthesis of 5'-propargyl-oligonucleotides based on the coupling of an alkyne containing phosphoramidite. a) 2-cyanoethyl hex-5-ynyl N,N-diisopropyl phosphoramidite in ACN, b) NH$_3$ (aq) 55ºC.

Alkynyl-oligonucleotides were obtained in excellent yields (88-93%) as can be seen in the HPLC analysis in figure 3.23. Characterization by mass spectrometry was in agreement with the expected values.
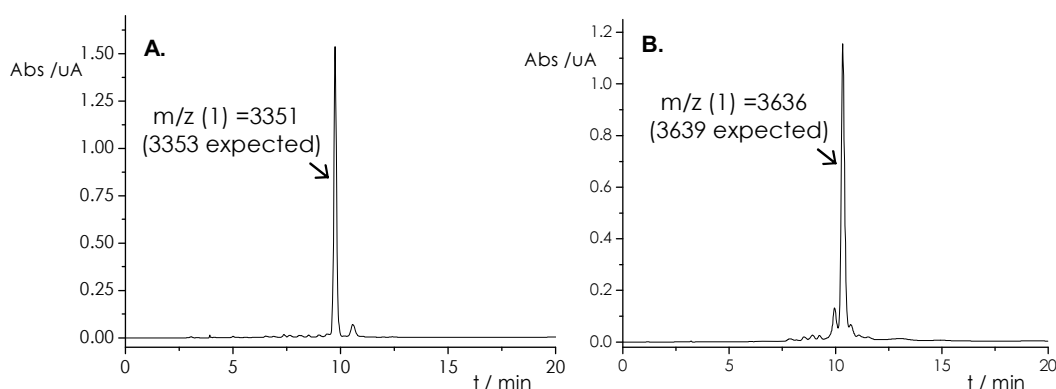
Figure 3.23. HPLC profile of **ODN 20** (A) and **ODN 21** (B). The m/z values obtained by MALDI-TOF are indicated next to each peak. The gradient used to obtained these profiles were 5→ 35% B in 20 min for the figure A and 0→ 50% B in 20 min for the figure B (A: 5% ACN in 0.1 M TEAAc pH 6.5; B: 70% ACN in 0.1 M TEAAc pH 6.5).

3.5. Synthesis of oligonucleotides carrying azido groups.

The azido group is not compatible with the phosphoramidite group because azido groups react with phosphites yielding phosphoramidates, according to the Staudinger reaction [67]. For this reason azido groups need to be introduced in the oligonucleotide after the completion of the sequence. The synthesis of oligonucleotides carrying azidonucleosides has also shown that azido groups attached to the nucleobases are stable to ammonia solutions only at room temperature, but not at higher temperature [68-70]. Thus, most of the times the CuAAC reactions were carried out with the 5'-azido-oligonucleotides on the solid support. For those cases in which 5'-azido-oligonucleotides were used in solution the dimethylformamidine group was employed as protecting group for the guanine bases which requires milder deprotection conditions than the standard isobutyryl group. While the traditional purine protecting groups require at least 6 hours at 55°C for deprotection in ammonia, oligonucleotides with the dimethylformamidine group require only 1 hour at 55°C or 8 hours at room temperature for complete deprotection [71].

3.5.1. Synthesis of 5'-azido-ODNs from 5'-amino-ODNs

The first method for the synthesis of the 5'-azido-oligonucleotides was based in a protocol described by Seo *et al*. [41]. In this work a molecule containing both an azide and an activated ester group was synthesized and used for the conjugation with 5'-amino-oligonucleotides. Succinimidyl 5-azido-valerate was obtained according to the scheme 3.24. Both intermediate and final product were characterized by ^{1}H-NMR and ^{13}C-NMR.
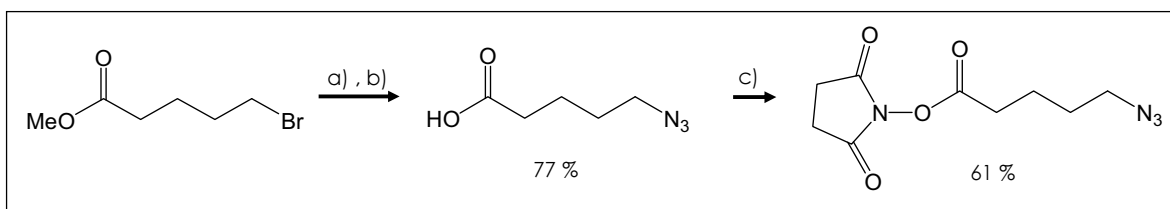
Scheme 3.24. Synthesis of the succinimidyl 5-azido-valerate used for the preparation of 5'-azido-oligonucleotides. a) 5 eq. NaN$_3$/DMF, o.n at r.t, b) 4 eq. LiOH in THF/H$_2$O (1/2), c) 1 eq. N-Hydroxysuccinimide, 1eq. EDC, DCM, o.n at r.t.

The desired 8T-$^{5'}$-aminohexyl sequence was synthesized using the 5'-amino-modifier C6, as indicated in the previous section. After the removal of the MMT group the resulting amino-oligonucleotide-support was conjugated with succinimidyl 5-azido-valerate (scheme 3.25). The resulting support was treated for one hour with concentrated ammonia at room temperature to avoid azide decomposition and the cleavage product was subsequently purified by HPLC. These mild cleavage conditions can only be used in this case, as a polythymidine strand have all its bases deprotected, but longer times are required for sequences containing nucleobases with protecting groups.
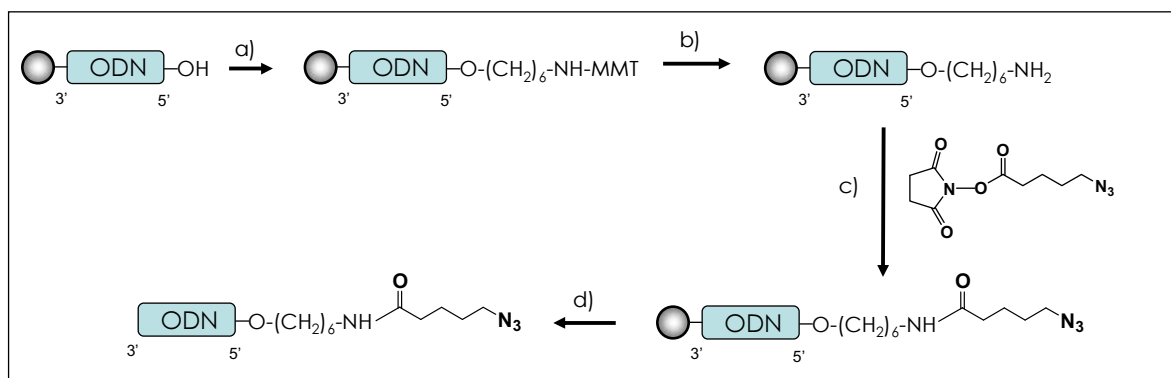
Scheme 3.25. Synthesis of 5'-azido-oligonucleotides based on the conjugation of 5'-amino-oligonucleotides. a) 5'-Amino-Modifier C6 phosphoramidite in ACN b) 3%TCA/DCM, c) succinimidyl 5-azido-valerate in dioxane d) NH$_3$ (aq), r.t.

The desired 8T-$^{5'}$-azidobutyryl sequence (**ODN 22**) was obtained in a yield of about 40 %, as determined by HPLC analysis (figure 3.26).
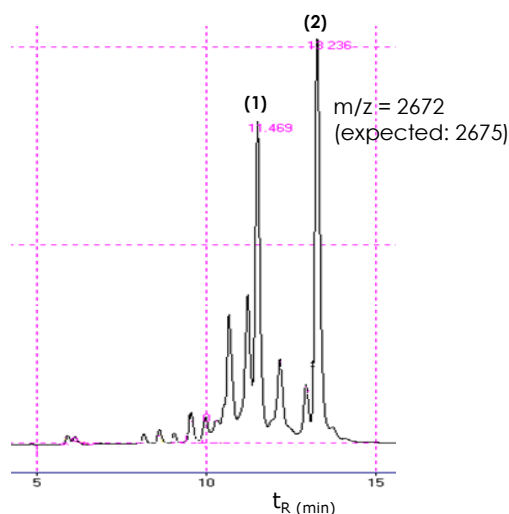
Figure 3.26. HPLC analysis of the product resulting from conjugation of CPG-supported 8T-$^{5'}$-aminohexyl ODN with 5-azidopentanoic acid N-hydroxysuccinimide ester. Two major peaks were observed, the last of which corresponds to the desired **ODN 22**. Gradient: 0→ 50% B in 20 min (A: 5% ACN in 0.1 M TEAAc pH 6.5; B: 70% ACN in 0.1 M TEAAc pH 6.5).

In this case a considerable proportion corresponding to N-acetylated product was also observed (peak 1). Analysis by ESI-MS was in agreement with the expected value for the MW of the desired product (peak 2).

3.5.2. Synthesis of 5'–azido-ODNs from 5'–iodo-ODNs

In 2002 the group of Kool *et al*. described a simple and versatile method for placing an iodo group at the 5' end of oligonucletides [72]. Because the iodo is an efficient leaving group in S$_N$2 displacement reactions, its introduction at the 5'-position allows for facile ligation to molecules containing a strongly nucleophilic group. In addition it can be easily converted to a wide variety of other functional groups. In this work a protocol based on the iodination of the 5'-end of the desired sequences followed by azide displacement was studied.

The reaction was carried out using an iodination reagent while the protected oligonucleotides remain on the solid support. The desired sequences were synthesized on a 1 μmol scale and the last DMT group was removed. The resulting support was treated with triphenoxymethylphosphonium iodide to yield the 5'-iodo-oligonucleotides which were reacted with sodium azide while still attached to the support (Scheme 3.27).
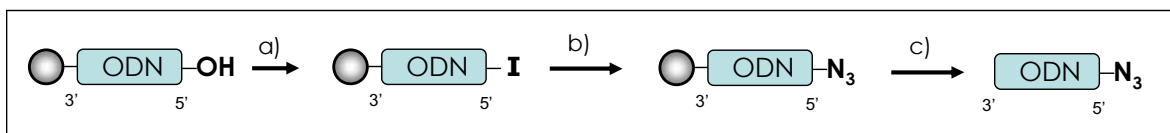
Scheme 3.27. Synthesis of 5'-azido-oligonucleotides based on their 5'-iodination. a) $(PhO)_3PCH_3I$ in DMF b) NaN_3/DMF c) NH_3 (aq) r.t.

A small amount of resin was cleaved before undergoing each reaction to determine the yield of every step. In addition these samples can be used as HPLC references to determine the retention time of starting and intermediate materials. Finally, ammonia cleavage gave the 5'-azido-oligonucleotide in excellent yields (around 70% of final conversion) as determined by HPLC analysis. In figure 3.28 an example of HPLC profile obtained after injection of **ODN 26** is shown. The desired product eluted as a major peak. Small peaks on both sides were identified as the starting unmodified oligonucleotide (**ODN 4**) and the iodinated intermediate (**ODN 25**) respectively.
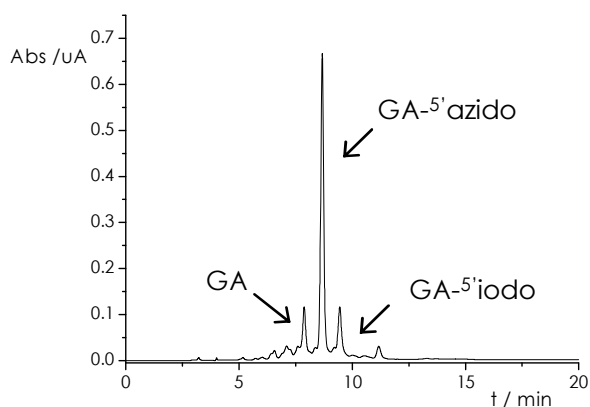
Figure 3.28. HPLC profile of **ODN 26.** The products corresponding to each peak are indicated in the graphic. The major peak corresponds with the desired product. Gradient: 5→ 35% B in 20 min (A: 5% ACN in 0.1 M TEAAc pH 6.5; B: 70% ACN in 0.1 M TEAAc pH 6.5).

The purified azido oligonucleotides as well as their intermediates were characterized by mass spectrometry. MWs obtained by MALDI-TOF are listed in Table 3.29, together with the retention time and the relative peak areas reported in the HPLC chromatograms of final products.

ODN	Sequence	t_R (min)	% area	Found MW	Expected MW
3	CT	9.5 [a)]	14	3194	3194
23	CT-5'iodo	10.9[a)]	13	3302	3304
24	CT-5'azido	10.4 [a)]	73	3217	3219
4	GA	7.9 [b)]	15	3476	3479
25	GA-5'iodo	9.4 [b)]	16	3586	3589
26	GA-5'azido	8.7 [b)]	69	3502	3504

Table 3.29. MALDI-TOF analysis of oligonucleotides used in this work after HPLC purification. Retention time corresponds to a gradient of 0→ 50% B in 20 min

for the values marked with an [a)] and to 5→ 35% B in 20 min for the case of [b)]. (A: 5% ACN in 0.1 M TEAAc pH 6.5; B: 70% ACN in 0.1 M TEAAc pH 6.5). MW found by MALDI-TOF showed a good correlation with the expected values.

3.5.3. Synthesis of 5'-azido-ODNs with a bromine-containing phosphoramidite

The success of the previous method suggested the preparation of a phosphoramidite to introduce the halohexyl group directly at the 5'-end of the oligonucleotide, avoiding the previous iodination step. It was decided to study the potential use of the bromohexyl group as an intermediate in the introduction of the azido function group in DNA. In addition the hexyl linker would provide less steric hindrance to the azido group than the previous 5'-azido-2'-deoxynucleoside derivative.

Starting from commercially available 6-bromohexanol, the phosphoramidite derivative was prepared (scheme 3.30).
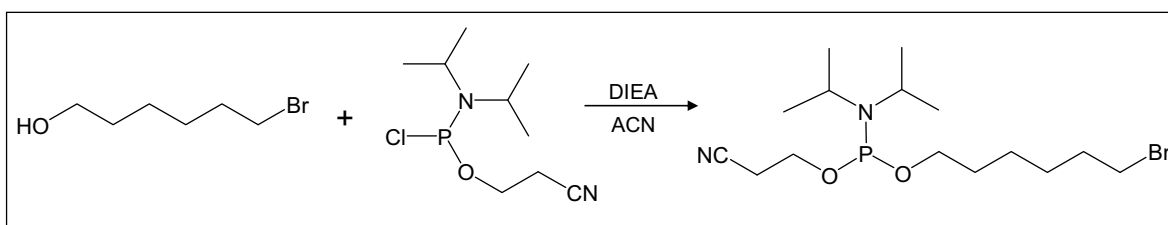
Scheme 3.30. Synthesis of the 6-bromohexyl-(2-cyanoethyl)-(N, N-diisopropyl)-phosphoramidite.

This phosphoramidite was introduced in the DNA synthesizer and incorporated into the desired sequences. The support carrying the 5'-bromo oligonucleotide was treated with sodium azide (scheme 3.31) and the resulting product was cleaved from the resin with concentrated ammonia at room temperature, giving the desired 5'-azido-oligonucleotides in good yields.
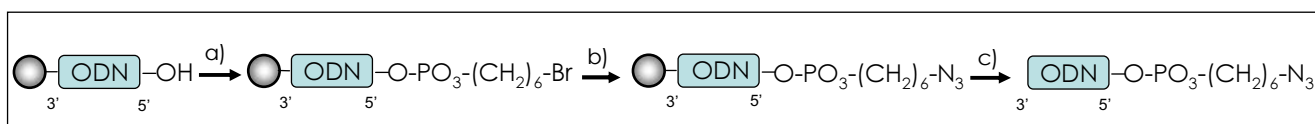
Scheme 3.31. Synthesis of 5'-azido-oligonucleotides based on azide substitution on 5'-bromohexyl-oligonucleotides. a) 6-bromohexyl (2-cyanoethyl) (N,N-diisopropyl) phosphoramidite in ACN b) NaN$_3$/DMF c) NH$_3$ (aq) r.t.

HPLC analysis of the synthesized molecules is shown below. The purified oligonucleotides were obtained in 75-94 % yield and had the expected mass, as revealed by MALDI-TOF analysis.
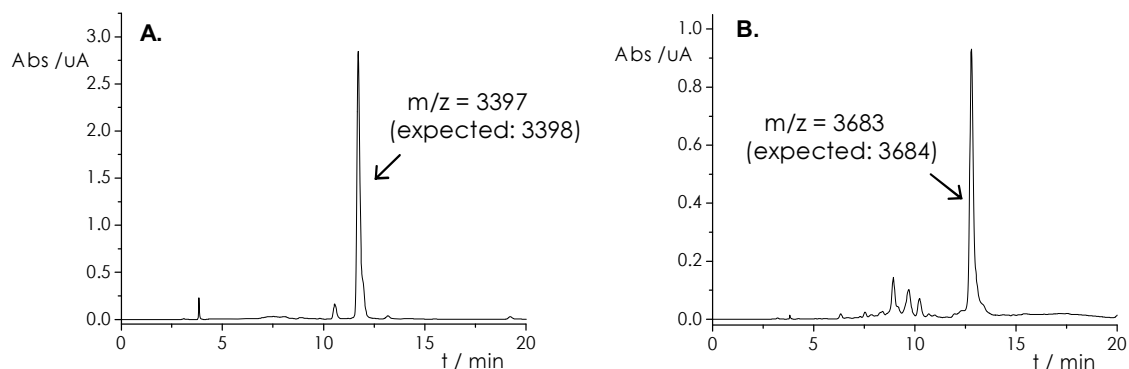
Figure 3.32. HPLC analysis after cleavage **ODN 29** (A) and **31** (B) from the support. Treatment of **ODN 28** and **30** with sodium azide causes nucleophilic substitution of bromine atom by an azido group. MW calculated for the sequences CT and GA containing an azidohexyl group at the 5′ end were in agreement with the values found in MALDI-TOF analysis. Gradient: 5→ 35% B in 20 min (A: 5% ACN in 0.1 M TEAAc pH 6.5; B: 70% ACN in 0.1 M TEAAc pH 6.5).

The 6-bromohexyl phosphoramidite was also studied as an intermediate to obtain 5′-aminohexyl oligonucleotides after ammonia cleavage from the support. A small amount of CPG beads carrying the 5′-bromohexyl oligonucleotides were treated with concentrated ammonia at 55 ºC which resulted in nucleophilic substitution of bromine atom to give the desired 5′-aminohexyl oligonucleotides as the major product (Figure 3.33).
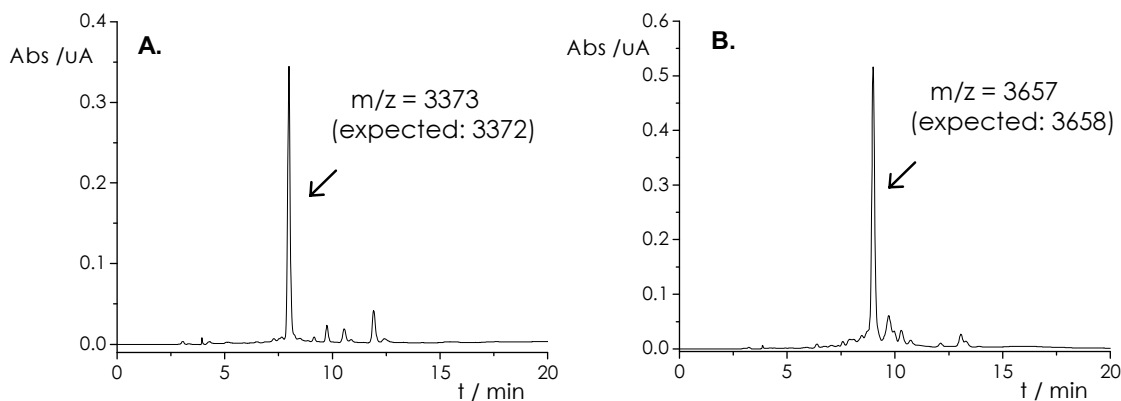
Figure 3.33. HPLC analysis after cleavage **ODN 28** (A) and **30** (B) from the support. Treatment with ammonia causes nucleophilic substitution of bromine atom by an amino group. MW calculated for the sequences CT and GA containing an aminohexyl group at the 5′ end were in agreement with the MALDI-TOF analysis. Gradient: 5→ 35% B in 20 min (A: 5% ACN in 0.1 M TEAAc pH 6.5; B: 70% ACN in 0.1 M TEAAc pH 6.5).

It should be mentioned, however, that a loss of efficiency in nucleophilic substitution was observed after a long-term storage of 5′-bromohexyl-oligonucleotides-CPG and secondary peaks were obtained in HPLC analysis (unidentified products). For this reason ODNs containing the bromohexyl linker should be reacted as soon as possible after their synthesis.

To confirm that the purified products contained the amino terminal group and that the obtained mass does not come from a substitution of bromine with an hydroxyl group (in which case the oligomer would be expected to have a similar mass) it was decided to couple a ligand with a carboxylic group that would lead to an easily detectable conjugate.

5(6)-carboxyfluorescein N-hydroxysuccinimide ester was coupled to the 5'-aminohexyl-CT oligonucleotide, as depicted in Scheme 3.34.
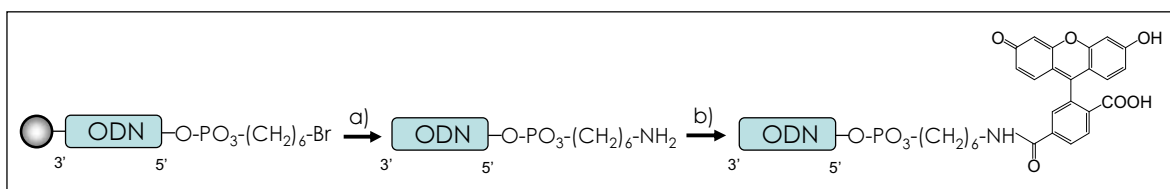
Scheme 3.34. Conjugation of a 5'-aminohexyl oligonucleotide with a fluoresceine derivative. a) NH_3 55ºC o.n, b) 5(6)-carboxyfluorescein N-hydroxysuccinimide ester in sodium carbonate buffer (pH 9) with 20% dioxane, o.n. at r.t.

Prior to fluorescein conjugation, the ammonia deprotected oligonucleotides were eluted through a Dowex Na^+ ion exchange resin to replace ammonium ions (which would react with the ester moiety preventing the amino group of the ODN to conjugate with the fluorescein) by sodium ions.

HPLC analysis of the ODN CT-[5']aminohexyl after conjugation with 5(6)-carboxyfluorescein N-hydroxysuccinimide ester is shown in Figure 3.35. The desired fluorescein labelled oligonucleotide was obtained as a major product (peak 3). The peak eluting before (peak 2) corresponds to the coupling of the oligomer with one of the isomers of the fluorescein (as the commercial reagent is a mixture of 5- and 6-carboxyfluorescein isomers).
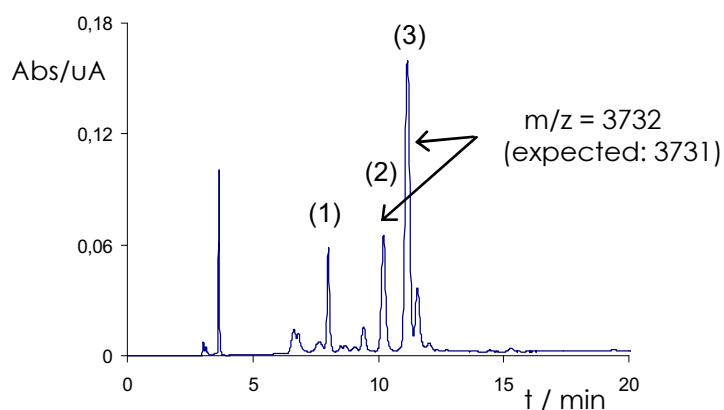
Figure 3.35. HPLC profile of conjugation reaction between CT-[5']aminohexyl and 5(6)-carboxyfluorescein N-hydroxysuccinimide ester. Peak (1) corresponds to the starting material while the peaks (2) and (3) come from the desired conjugation reaction. Gradient: 5→ 35% B in 20 min (A: 5% ACN in 0.1 M TEAAc pH 6.5; B: 70% ACN in 0.1 M TEAAc pH 6.5).

Both products (peaks 2 and 3) presented a maximum of absorbance at 498 nm at HPLC UV-detector. MWs found by MALDI-TOF were in agreement with the expected mass.

Thus, it has been demonstrated that the bromohexyl linker provides a straightforward protocol to incorporate an aminohexyl linker at the 5' terminus of an oligonucleotide [73]. The use of this intermediate for the introduction of the nucleophilic amino group can be used to overcome the disadvantages presented by the MMT protected amino modifier phosphoramidite named above, as the N-acetylation observed previously.

In the next section the use of these azide and alkyne containing oligonucleotides to prepare parallel-stranded DNA clamps will be investigated.

3.6. Cu(I)-catalyzed cycloaddition of azido- and alkynyl-oligonucleotides

3.6.1. Preliminary studies

First of all, click reaction was performed between 0.2 mmol of 5'-azido-thymidine and two equivalents of propargylamine (scheme 3.36) using different conditions, as indicated in table 3.37.
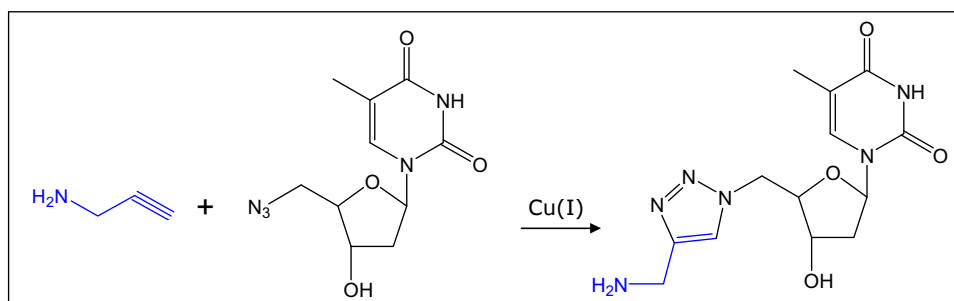
Scheme 3.36. Cu(I) catalyzed 1,3-dipolar cycloaddition of propargylamine and 5'-azidothymidine.

	Cu source	Other reactives	Solvent	Conditions
A	0.01 eq. CuSO$_4$	0.05 eq. ascorbic acid	3 ml H$_2$O/tBuOH (2:1)	r.t, stirring
B	0.5 eq. CuI	0.5 eq. DIPEA	3 ml H$_2$O/ACN (2:1)	r.t, Ar, stirring
C	0.01 eq. CuSO$_4$	0.05 eq. ascorbic acid	1.5 ml H$_2$O/tBuOH (2:1)	r.t, Ar, stirring

Table 3.37. Different conditions used in the copper-catalyzed cycloaddition reactions between 5'-azido-thymidine and propargylamine.

Reaction was followed by TLC. UV and ninhydrin test confirmed that reaction was completed after 15-20 hours using conditions B and C (quantitative yield).

When oxygen was not excluded (conditions A) the starting azido nucleoside was still observed even after two days. Final products were also analyzed by HPLC (Figure 3.38) and characterized by electrospray ionization mass spectrometry.
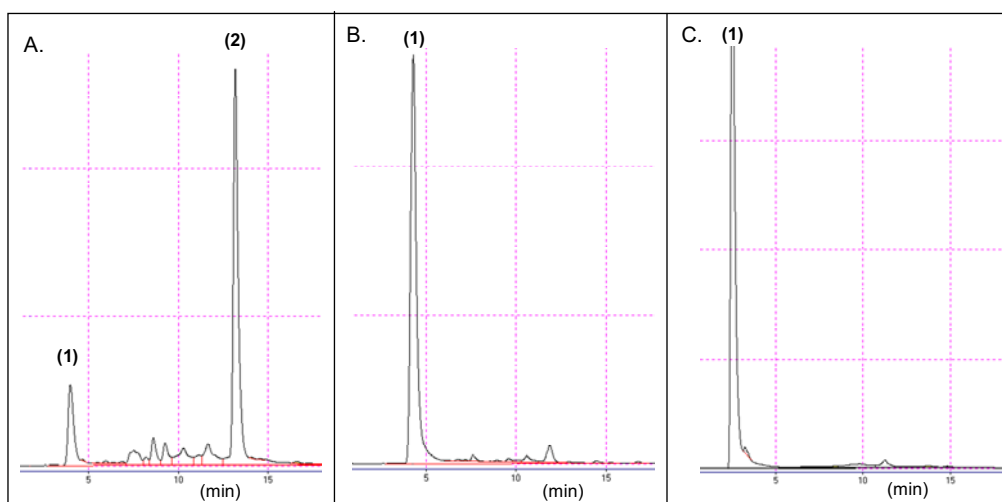
Figure 3.38. HPLC profiles obtained using conditions A, B and C respectively. Peak (1) corresponds to the desired product while the peak (2) corresponds to the starting 5'-azido-thymidine. Gradient: 0 → 50% B in 20 min (A: 5% ACN in 0.1 M TEAAc pH 6.5; B: 70% ACN in 0.1 M TEAAc pH 6.5).

Chromatograms obtained when using argon atmosphere (Figure 3.38.B and 3.38.C) showed one single peak, corresponding to the desired product. When reaction was not carried out under inert conditions, yield dropped to about 20 %, as can be seen in chromatogram of figure 3.38.A, whose profile displays two main peaks, the major of them (peak 2) corresponding to the azido starting material.

When a Cu(I) catalyst is used directly (as in B conditions), exclusion of oxygen is required to prevent disproportionation or oxidation to catalytically inactive Cu(II). Reduction of a copper (II) salt using ascorbate has been considered sometimes as an alternative to oxygen-free conditions. Although click reactions have been performed in some cases using $CuSO_4$/ascorbate without exclusion of atmospheric oxygen, the experiments described above (conditions A *vs*. C) demonstrate that using argon atmosphere is strongly recommended for both systems.

3.6.2. CuAAC reactions to chemically ligate two oligonucleotide strands in solution phase

Next, the use of copper-catalyzed cycloaddition reactions to chemically ligate two oligonucleotides in solution was studied. In order to find the optimal conditions for the coupling reaction, a small excess of 8T-5'propargylglutaryl (**ODN 9**) was mixed with 8T-5'azidobutyryl (**ODN 22**) in the presence of either $CuSO_4$/ascorbic acid or CuI , using the conditions detailed in table 3.39.

Due to poor solubility of CuI in aqueous systems a large excess of this reagent was added to the solution (1 mg contains about 300 equivalents respect to the starting ODNs). When working with such small amounts of material (15-30 nmol of ODNs), handling equimolar amounts or little excess of CuI is quite difficult, specially when solubility is so poor that accurate dilutions can not be prepared.

	5'-azido-ODN	5'-alkyn-ODN	Cu source	Other reactives	Solvent	Conditions
A	15 nmol	20 nmol	0.1 eq. CuSO$_4$	0.5 eq. ascorbic acid	70 µl H$_2$O/tBuOH (2:1)	r.t, Ar, 72h
B	15 nmol	20 nmol	10 eq. CuSO$_4$	50 eq. ascorbic acid	75 µl H$_2$O/tBuOH (2:1)	r.t, Ar, 72h stirring
C	15 nmol	30 nmol	300 eq. CuI	400 eq. DIPEA	60 µl H$_2$O/ACN (1:1)	r.t, Ar, 40h stirring

Table 3.39. Conditions used in the copper-catalyzed cycloaddition reactions between two polythymidine strands in solution.

The resulting products were analyzed by HPLC. Figure 3.40 shows the different HPLC profiles obtained after using the reaction conditions indicated above. The length of the cycloaddition product was confirmed by gel electrophoresis.
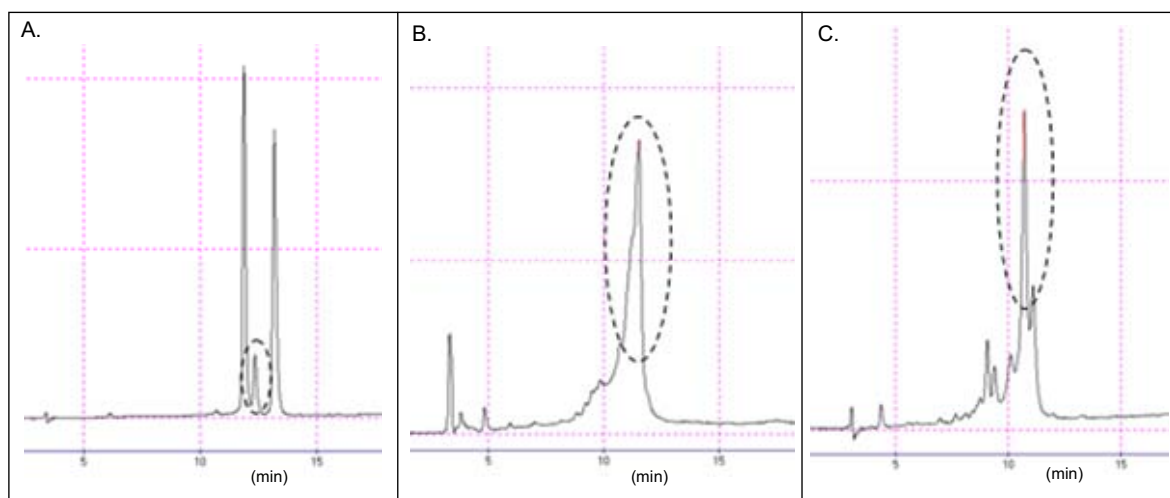
Figure 3.40. HPLC profiles obtained using conditions A, B and C of Table 3.39 respectively. Dotted line circles indicate elution of the cycloaddition product. Gradient: 0 → 50% B in 20 min (A: 5% ACN in 0.1 M TEAAc pH 6.5; B: 70% ACN in 0.1 M TEAAc pH 6.5).

Higher yield was achieved when an excess of copper, rather than catalytic amounts, was used. Although the preliminary studies explained previously with nucleosides as well as most studies concerning CuAAC in literature reported the use of small amount of copper, best results were obtained in this case when a high number of equivalents were added. This may be because some of the copper ions are "captured" by the phosphate groups of the oligonucleotide backbone thus

reducing the efficiency of this metal to catalyze the click reaction. This electrostatic interaction may be likely also responsible for the problems encountered in analysis and purification of cycloaddition products, as is the case of HPLC chromatograms showing not well resolved peaks (figure 3.40.B and C) and mass spectrometry giving a higher mass than expected.

3.6.3. CuAAC reactions to chemically ligate two oligonucleotide strands in solid phase

In order to facilitate the removal of copper ions, Cu-catalyzed cycloaddition reactions on solid phase were studied. First of all, stability of triazoles in the cleavage conditions was assessed. The cycloaddition product of propargylamine and 5'-azido-thymidine was characterized by electrospray ionization mass spectrometry before and after treatment with concentrated aqueous ammonia. The triazole was shown to be stable after overnight ammonia treatment both at room temperature and at 55 ⁰C. This enables the use of CuAAC for ligation of two DNA strands in solid phase.

The solid support carrying oligonucleotide sequence 8T-[5']azidobutyryl (**ODN 22**) was treated with 2 equivalents of 8A-[5']propargyl (**ODN 13**) using 150 and 170 equivalents of CuI and DIPEA respectively in 100 µl of H_2O/ACN (1:1). The resulting product was extensively washed with an EDTA solution while still attached to the support in order to eliminate copper ions. Finally, it was treated with concentrated ammonia and analyzed by HPLC (Figure 3.41).
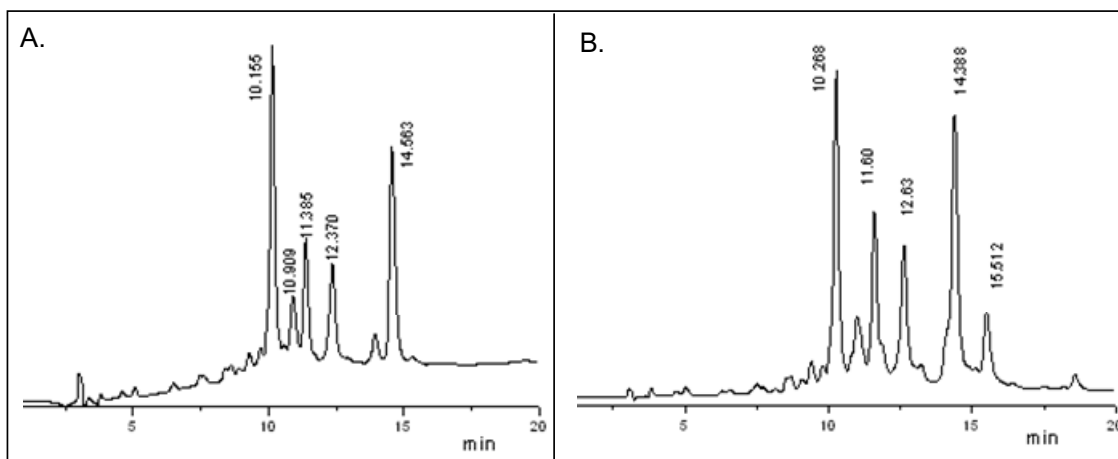
Figure 3.41. HPLC profile obtained after cleavage of A) 8T-[5']azidobutyryl and B) cycloaddition reaction product between 8T-[5']azidobutyryl and 8A-[5']propargyl. Gradient: 5→ 35% B in 20 min (A: 5% ACN in 0.1 M TEAAc pH 6.5; B: 70% ACN in 0.1 M TEAAc pH 6.5).

Although at first sight no appreciable change in the chromatogram profile of the product is observed respect to the starting material (Figure 3.41), it can be observed from the UV spectra registered for each peak that the desired product

eluted with a similar retention time (14.4 min) as the azido starting material (14.6 min).

To confirm this hypothesis enzymatic digestion of a HPLC purified sample was performed. Compositional analysis of oligonucleotides can be provided upon their complete digestion down to their constituent dNs with snake venom phosphodiesterase and alkaline phosphatase (Figure 3.42).
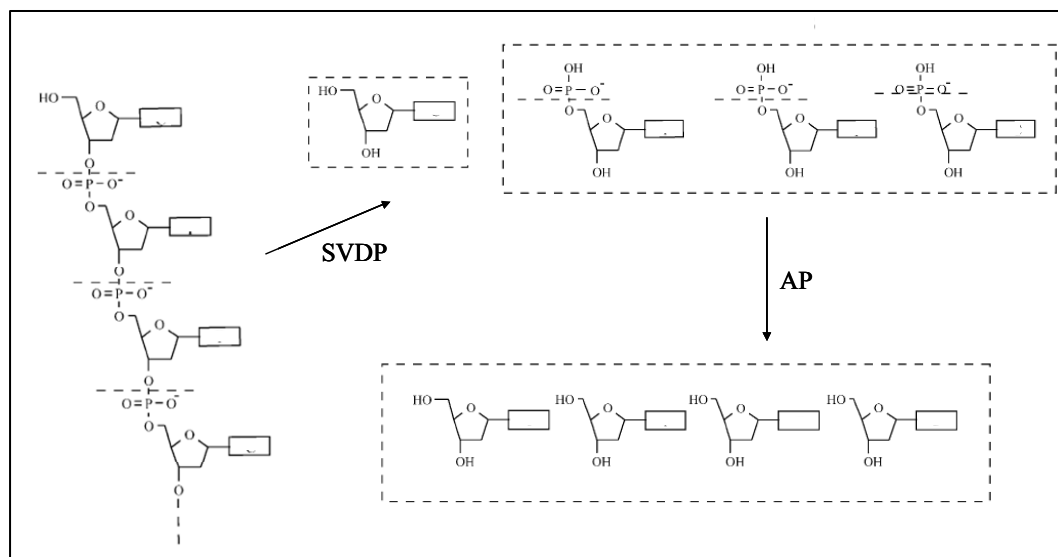
Figure 3.42. Enzymatic digestion of an oligonucleotide. Snake venom phosphodiesterase (SVDP) digestion of the oligonucleotide produces nucleotides and one nucleoside from the 5' terminal residue, which is not phosphorylated. Alkaline phosphatase (AP) digestion removes the phosphate group from the nucleotides. (The rectangles represent the bases). Extracted from reference [74].

Separation and analysis of the digestion products by reversed-phase HPLC allows to ascertain the relative ratios of each nucleotide after normalize the absorbance of the different peaks by dividing by the ε_{260}.

Enzymatic digestion of the product eluting at 14.4 min showed the presence of both thymidines and adenines (Figure 3.43), these latter coming from the 8A-5'propargyl sequence which has been successfully linked to the polythymidine attached to CPG.
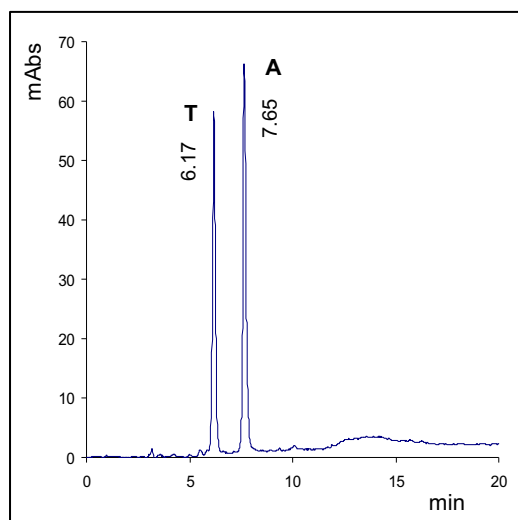
Figure 3.43. HPLC analysis of nucleosides coming from enzymatic digestion of oligonucleotide obtained by click reaction between **ODN 13** and **ODN 22.** Gradient: 0 → 50% B in 20 min (A: 5% ACN in 0.1 M TEAAc pH 6.5; B: 70% ACN in 0.1 M TEAAc pH 6.5).

Since the molar extinction coefficient (ε) of pdA and pdT at 260 nm is 15400 and 8700 $M^{-1}\cdot cm^{-1}$ respectively, the polyadenine chain was coupled with an efficiency of around 50%.

Next, the use of CuAAC was studied to chemically ligate two oligonucleotides capable to form a parallel-stranded clamp similar to the one employed for the triplex studies in the previous chapter, based on the sequences studied by Xodo *et al.* [75,76].

For this purpose the solid support carrying oligonucleotide sequence CT-5'azido (**ODN 24**) was treated with GA-5'hexynyl (**OND 21**) using similar conditions as those indicated above. Thus, the solid support carrying oligonucleotide sequence CT-5'azido was treated at r.t during 40h with 4 equivalents of GA-5'hexynyl using 200 and 240 equivalents of CuI and DIPEA respectively in 100 μl of H_2O/ACN (1:1). However, in this case the cycloaddition reaction resulted in low yields, and the final product could not be isolated. To investigate if low yield was due to steric hindrance caused for the direct attachment of azido group to the ribose ring, the same CuAAC was performed using the ODN CT-5'azidohexyl (**ODN 29**) which possess a less hindered azide moiety. In this latter case no product formation was also observed.

It has been previously reported that alkynes possessing an electron-withdrawing group, such as an amide or carboxylic ester, are much more reactive in dipolar cycloadditions than their alkyl counterpart [77-79]. This is consistent with the mechanism explained in section 3.1.1 in which a nucleophilic attack of acetylide carbon C(4) by N(3) of the azide takes place after formation of the active copper acetylide-azide complex.

To investigate the influence of this factor, benzylazide was reacted with an oligonucleotide modified with an alkyne with and without an electron-withdrawing group (**ODN 11** and **20**, figure 3.44). Both reactions gave the expected cycloaddition product in quantitative yield. Thus, the hex-5-ynyl group can be used for linking small azide compounds to DNA strands in solid phase, in which case a high excess of azide reactant can be used. Nevertheless, it might be not reactive enough to link two large molecules such as these oligonucleotide strands.
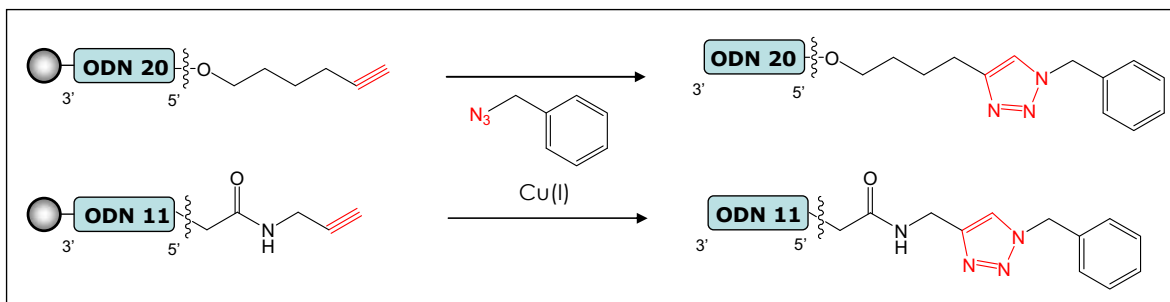
Figure 3.44. Reactions of **ODNs 11** and **20** with benzylazide.

Next, the electrodeficient alkyne containing sequence 8T-$^{5'}$propargyl (**ODN 11**) was reacted with both CPG-supported CT-$^{5'}$azido (**ODN 24**) and CT-$^{5'}$azidohexyl (**ODN 29**). Nine and five equivalents of alkyne containing sequence were added respectively using CuI as Cu(I) source and similar conditions as before. In addition, although performing the reaction under argon atmosphere, it was decided in this case to add 100 equivalents of ascorbic acid, for a better prevention of Cu(I) oxidation through the long reaction time. In both cases, analysis of the reaction by HPLC showed the successful formation of the cycloaddition product as the major component (Figure 3.45).
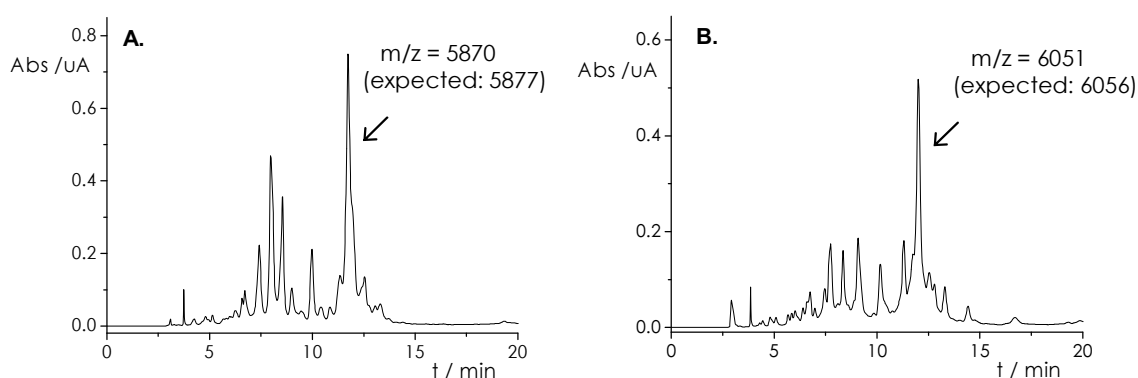
Figure 3.45. HPLC profile of CuAAC reaction between: A) 8T-$^{5'}$propargyl (**ODN 11**) and CT-$^{5'}$azido (**ODN 24**); B) 8T-$^{5'}$propargyl (**ODN 11**) and CT-$^{5'}$azidohexyl (**ODN 29**). MW calculated for the cycloaddition products were in agreement with the MALDI-TOF found values. Gradient: 5→ 35% B in 20 min (A: 5% ACN in 0.1 M TEAAc pH 6.5; B: 70% ACN in 0.1 M TEAAc pH 6.5).

The final yield was around 40 %, according to the relative peak areas. Analysis by mass spectrometry and gel electrophoresis confirmed the synthesis of the desired products. This demonstrates that the alkyne group of **ODN 11** is mildly activated for the CuAAC reaction by the neighbouring amide moiety. In addition, the use of ascorbic acid seems to improve the yield, likely due to preventing Cu(I) oxidation.

Reaction between CPG-supported-**ODN 29** and **ODN 11** was also performed in the presence of TBTA, the Cu(I) ligand reported to enhance speed and prevent DNA damage, but not very significant improvement was observed. HPLC profile of the reaction is shown in figure 3.46 below and should be compared with figure 3.45.B.
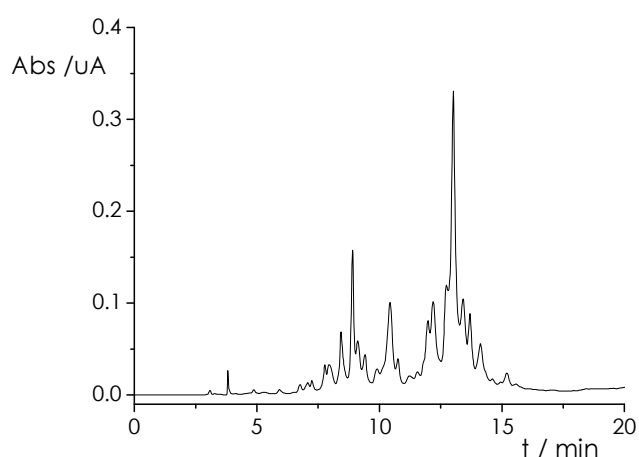
Figure 3.46. HPLC profile of CuAAC reaction between 8T-$^{5'}$propargyl (**ODN 11**) and CT-$^{5'}$azidohexyl (**ODN 29**) using TBTA. Gradient: 5→ 35% B in 20 min (A: 5% ACN in 0.1 M TEAAc pH 6.5; B: 70% ACN in 0.1 M TEAAc pH 6.5).

The CuAAC reaction was also performed with an azide containing ODN linked on a support different from the CPG.

ChemMatrix supports are 100 % polyethylene glycol supports that present good swelling properties in both polar and apolar solvents and have been extensively reported to facilitate the preparation of highly structured peptides [80-82]. This resin has been recently studied in Dr. Eritja's group for the synthesis of oligonucleotide-peptide conjugates, showing advantages over CPG support [83]. In this work the efficacy of Chem Matrix support for the ligation of two oligonucleotide strands by CuAAC was analyzed.

A ChemMatrix support carrying oligonucleotide sequence $^{5'}$-TTTTTTTTTTTG-$^{3'}$ (**ODN 27**) was converted to the 5'-azido ODN via the 5'-iodo derivative as described previously. The resulting product was reacted with **ODN 11** (8T-$^{5'}$propargyl) to yield the 5'-5'-linked oligonucleotide. Only 1.5 equivalents of alkyne were added in this case. Figure 3.47 shows the analysis by reversed-phase HPLC of

the azido starting sequence as well as the subsequent cycloaddition product. A major peak was obtained that corresponded to the expected mass.
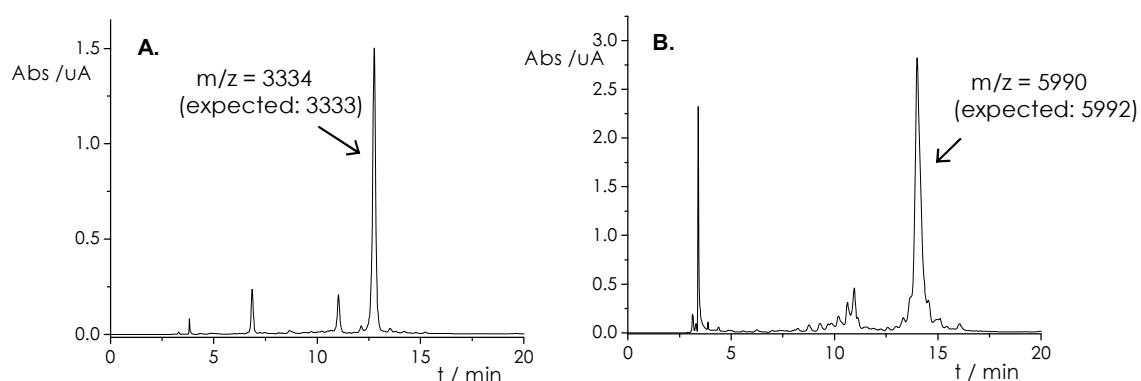
Figure 3.47. HPLC analysis of the A) GT$_{10}$-$^{5'}$azido sequence (**ODN 27**) after cleavage from the matrix support and B) solid-phase CuAAC reaction between **ODN 27** and alkyn-containing sequence 8T-$^{5'}$propargyl (**ODN 11**). Gradient: 5→ 35% B in 20 min (A: 5% ACN in 0.1 M TEAAc pH 6.5; B: 70% ACN in 0.1 M TEAAc pH 6.5).

The crude from the click chemistry on ChemMatrix was better as judged by the lower amount of impurities eluting before the desired compound. The success of the cycloaddition reaction on ChemMatrix supports is likely the result of the good swelling properties of this support in polar solvents.

The next step was to use CuI, DIPEA and ascorbic acid in H$_2$O/ACN to ligate supported GA-$^{5'}$azidohexyl (**ODN 31**) with the sequence CT-$^{5'}$propargyl (**ODN 15**) which contains an electrodeficient alkyne. Surprisingly in this case no cycloaddition products could be isolated, nor on CPG or the CM support. Figure 3.48 shows an example of unsuccessful reaction between **ODN 15** and CPG-supported **ODN 31**.
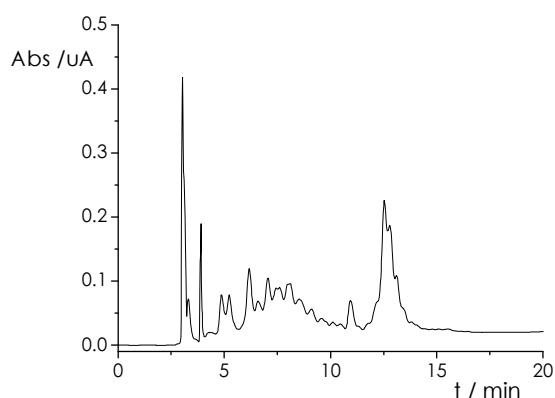
Figure 3.48. HPLC analysis of cycloaddition reaction between **ODN 15** and **ODN 31.** Gradient: 5→ 35% B in 20 min (A: 5% ACN in 0.1 M TEAAc pH 6.5; B: 70% ACN in 0.1 M TEAAc pH 6.5).

Multiple peaks eluting at short retention times may come from degradation of DNA or depurination of **GA** strand caused by ascorbic acid. In addition, some studies in the literature have reported sodium ascorbate to induce oxidative damage of DNA in presence of mono and divalent copper [84-87]. Chiou *et al.* demonstrated that mixing of ascorbic acid and Cu(II) efficiently generate reactive oxygen species with protein and DNA scission activities [85]. DNA cleavage was strongly affected by the sequence and conformation as they found certain degree of cleavage preference toward purine-containing DNA segments while pyrimidine clusters were least susceptible to cleavage. In other study, Kanan *et al.* performed DNA directed CuAAC reactions and observed moderate yields due to DNA degradation in the presence of a large excess of Cu(I) and sodium ascorbate [87].

So from now on, ascorbic acid will be avoided when using polypurine sequences and TBTA will be used in some cases as the only Cu(I) stabilizer.

Figure 3.49 shows the HPLC analysis of the reaction between CPG-GA-$^{5'}$azidohexyl (**ODN 31**) and 3 equivalents of CT-$^{5'}$propargyl (**ODN 15**) using 70 equivalents of CuI, 135 of DIPEA and without adding ascorbic acid. Besides, denaturing PAGE shows formation of the cycloaddition product.
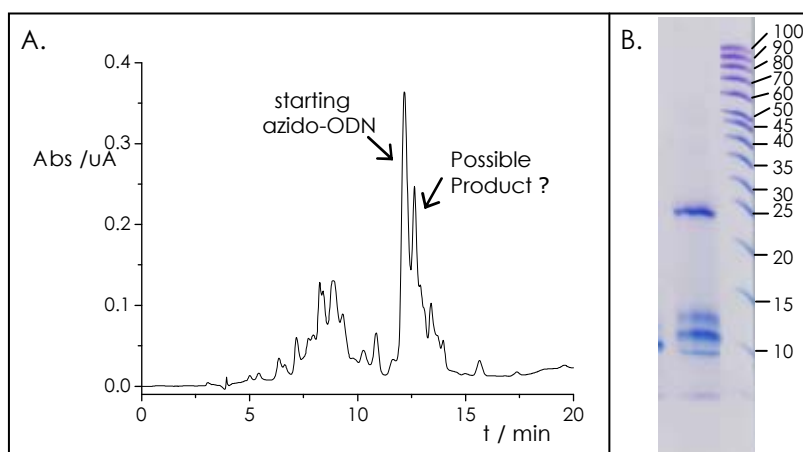
Figure 3.49. A) HPLC analysis of cycloaddition reaction between **ODN 15** and **ODN 31** using CuI and DIPEA without adding ascorbic acid. Gradient: 5→ 35% B in 20 min (A: 5% ACN in 0.1 M TEAAc pH 6.5; B: 70% ACN in 0.1 M TEAAc pH 6.5). B) Denaturing PAGE analysis of the crude reaction. Upper band in the first lane corresponds to the expected length for the parallel clamp.

Analysis by denaturing PAGE shows clearly the formation of the desired parallel hairpin (upper lane) but an intense band corresponding to the starting azido sequence is also observed. However, the similarity in retention times of both products makes the purification by reverse phase HPLC and subsequent analysis difficult.

In order to facilitate isolation of the desired hairpin product by HPLC, two new alkyne containing sequences were designed: the longer sequence CT$_{long}$-

$^{5'}$propargyl (**ODN 19**), which contains 16 bases and the pyr-CT-$^{5'}$propargyl (**ODN 17**), which is fluorescently labelled with a pyrene moiety and was synthesized as explained previously in the section 3.4.2. Derivatization with pyrene is expected to produce not only a fluorescent label for easy detection of the cycloaddition product but also an increase of the hydrophobicity and a delay in the retention time of the hairpin which should facilitate its purification by reverse phase HPLC.

This new alkyne containing oligonucleotides were reacted with three different azido-containing sequences, as indicated in table 3.50. In all reactions CuI/DIPEA system was used to accelerate alkyne-azide cycloaddition reaction and TBTA was used as the only Cu(I) stabilizer.

Reaction	Azido-ODN (nmol)	Alkyn-ODN (equiv)	CuI/DIPEA (equiv)	TBTA (equiv)
1	97 nmol GA-$^{5'}$azidohexyl (**ODN 31**)	1.9 eq. CT-$^{5'}$propargyl (**ODN 15**)	80/440	--
2	60 nmol GA-$^{5'}$azidohexyl (**ODN 31**)	1.6 eq. CT$_{long}$-$^{5'}$propargyl (**ODN 19**)	113/622	22
3	64 nmol GA-$^{5'}$azidohexyl (**ODN 31**)	1.6 eq. pyr-CT-$^{5'}$propargyl (**ODN 17**)	122/672	30
4	45 nmol GA-$^{5'}$azido (**ODN 26**)	2.6 eq. CT-$^{5'}$propargyl (**ODN 15**)	105/577	21
5	48 nmol GA-$^{5'}$azido (**ODN 26**)	2 eq. CT$_{long}$-$^{5'}$propargyl (**ODN 19**)	109/598	20
6	58 nmol GA-$^{5'}$azido (**ODN 26**)	1.8 eq. pyr-CT-$^{5'}$propargyl (**ODN 17**)	118/648	23
7	150 nmol CT-$^{5'}$azido (**ODN 24**)	1.3 eq. pyr-CT-$^{5'}$propargyl (**ODN 17**)	70/380	54

Table 3.50. Reagents used in different CuAAC reactions performed in this work.

Below, the figure 3.51 shows denaturing PAGE analysis of some of the reactions indicated above.
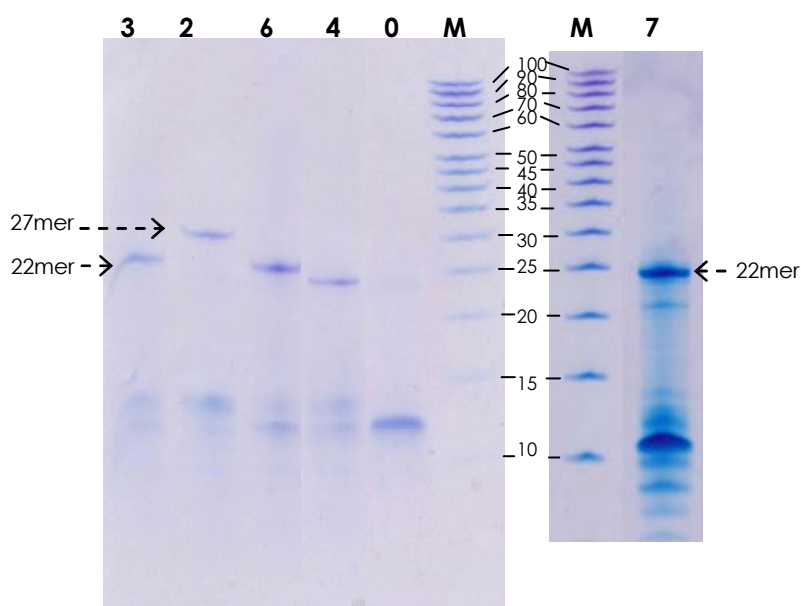
Figure 3.51. Denaturing PAGE analysis of some of the reactions. From left to right: reaction **3**, **2**, **6**, **4**, lane **0** corresponds to the starting **ODN 31**, **M** to the marker and the last lane to reaction **7**.

In the case of reaction **2** an oligonucleotide of 27 bases length is obtained, as expected from the ligation of **ODN 31** with the 16mer sequence CT_{long}-$^{5'}$propargyl (**ODN 19**). In all cases denaturing PAGE analysis showed slight formation of the desired product (upper lane), but a high amount of starting material is still present as deduced from the intense bands corresponding to 11 bases and shorter lengths.

Surprisingly, the new alkyne containing sequences still did not allow isolation by reverse-phase HPLC and analysis resulted in complex chromatographic profiles, with a high number of peaks, as it is shown in the examples of figure 3.52.
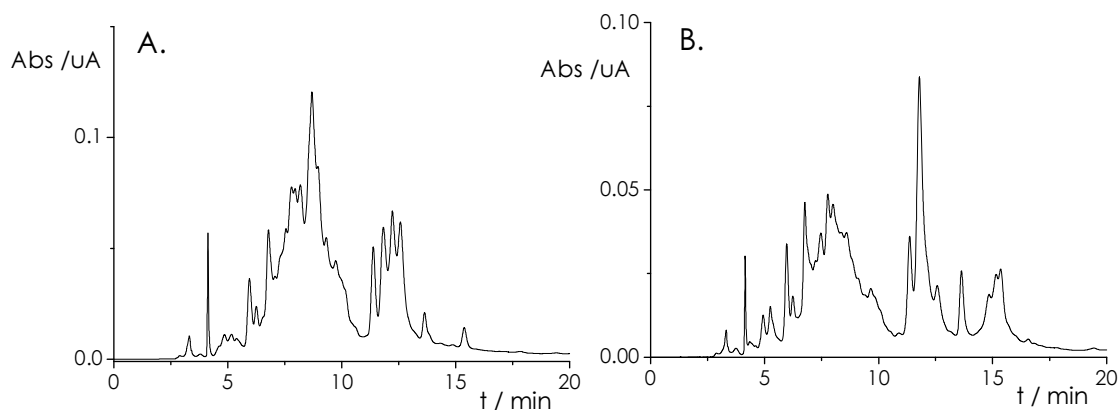
Figure 3.52. A) HPLC analysis of cycloaddition reaction between **ODN 31** and **ODN 19** (reaction **2** in table 3.50). B) HPLC analysis of cycloaddition reaction

between **ODN 31** and **ODN 17** (reaction **3** in table 3.50). Gradient: 5→ 35% B in 20 min (A: 5% ACN in 0.1 M TEAAc pH 6.5; B: 70% ACN in 0.1 M TEAAc pH 6.5).

When the pyr-CT-$^{5'}$propargyl sequence was used, the crude of CuAAC reactions showed a fluorescent emission with a maximum at 400 nm when irradiated at 345 nm (Figure 3.53.A), characteristic of the pyrene moiety. Figure 3.53.B. shows a picture of the vial containing the cleavage ammonia solution of product coming from reaction **7** when exposed under a 345 nm lamp.
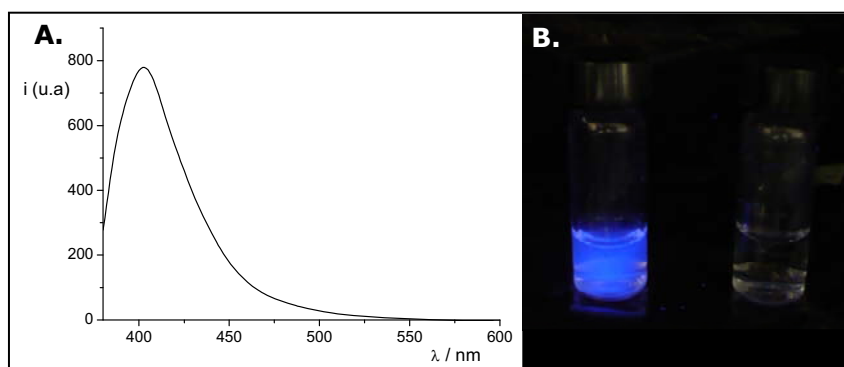
Figure 3.53. A) Fluorescence spectrum of the crude coming from "reaction **3**" irradiated at 345 nm. B) Vial containing the cleavage ammonia solution of product coming from "reaction **7**".

Fluorescence observed when sample was irradiated at 345 nm is an unequivocal signal that some of the pyr-CT-$^{5'}$propargyl sequence was covalently attached to the solid supported azido oligonucleotide.

In order to estimate the yield of the different reactions, enzymatic degradation studies were performed. Compositional analysis of oligonucleotides was performed by reverse-phase HPLC after their complete digestion with snake venom phosphodiesterase and alkaline phosphatase to determine the relative ratios of each nucleotide.

Enzymatic digestion of crude coming from different reactions are showed in figure 3.54. Analysis of degraded CT-$^{5'}$propargyl (ODN **15**) and GA-$^{5'}$azido (ODN **26**) was previously performed for t_R comparison.
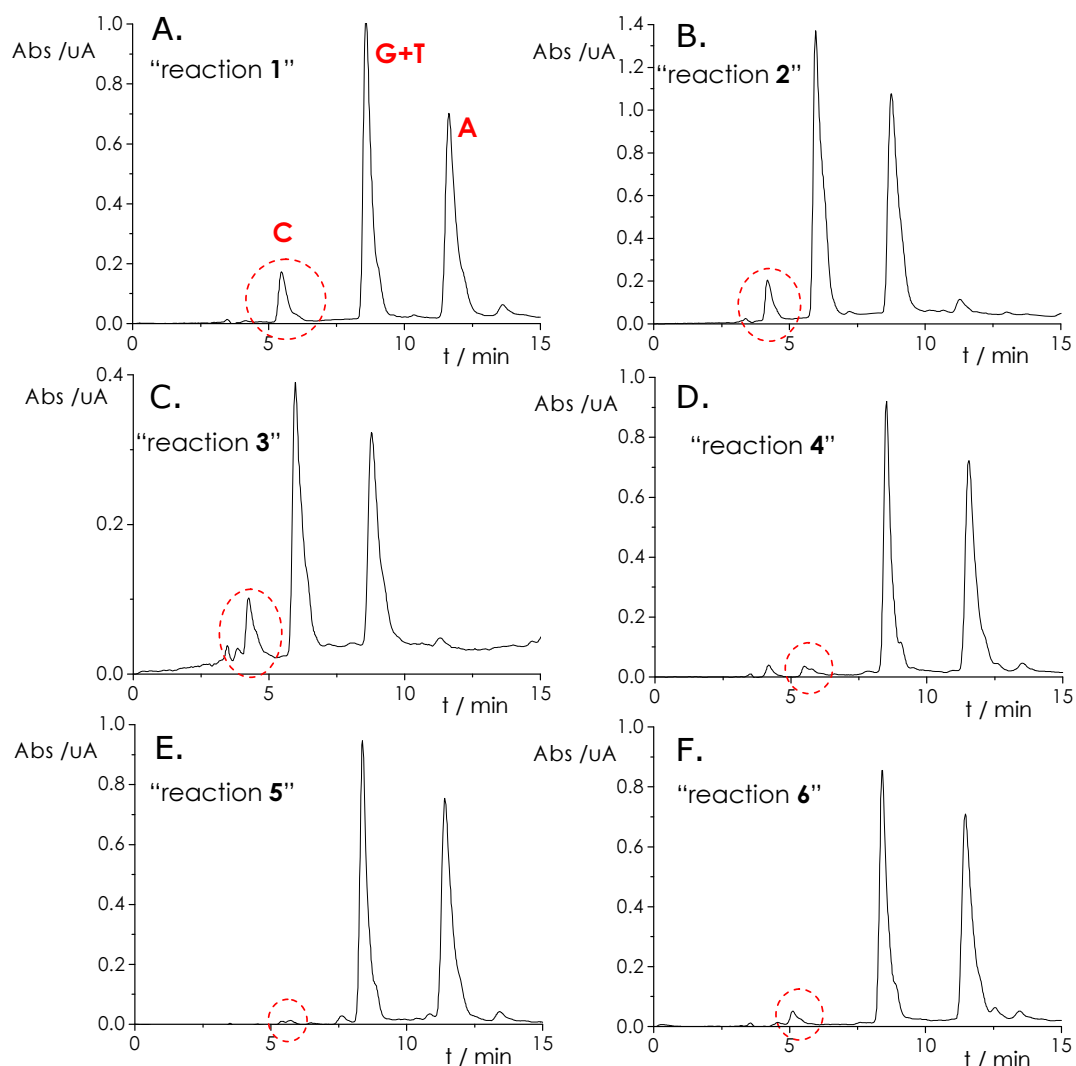
Figure 3.54. Chromatographic profiles obtained after enzymatic degradation of the crudes coming from reactions **1-6** of table 3.50. Gradient: 0→ 50 % B in 20 min (A: 5% ACN in 0.1 M TEAAc pH 6.5; B: 70% ACN in 0.1 M TEAAc pH 6.5).

The cytidine peak elutes first and comes from the propargyl containing oligonucleotide which has been successfully linked to the solid supported azido containing oligonucleotide. Its relative area can be used to make an estimation of the CuAAC yield after normalize the absorbance of the different peaks by dividing by the ε_{260}.

Since the molar extinction coefficient (ε) of pdA and pdC at 260 nm is 15400 and 7400 $M^{-1}\cdot cm^{-1}$ respectively, it can be estimated that the polypyrimidine chain was coupled with an efficiency of around 45% in the best cases (reactions **1-3**).

When using GA-$^{5'}$azido as the supported sequence (reactions **4-6**), the yield was very poor (less than 15%) as observed in chromatograms D-F of figure 3.54. This may be due to sterical hindrance caused by close proximity of the azide group respect to the nucleoside (figure 3.55). In the cases where hexyl group is the linker

between azido group and C5 yields were much better under similar conditions. This effect might be critical for guanine terminated oligonucleotides but not so important if the nuclebase if a pyrimidine, as shown in previous cases.
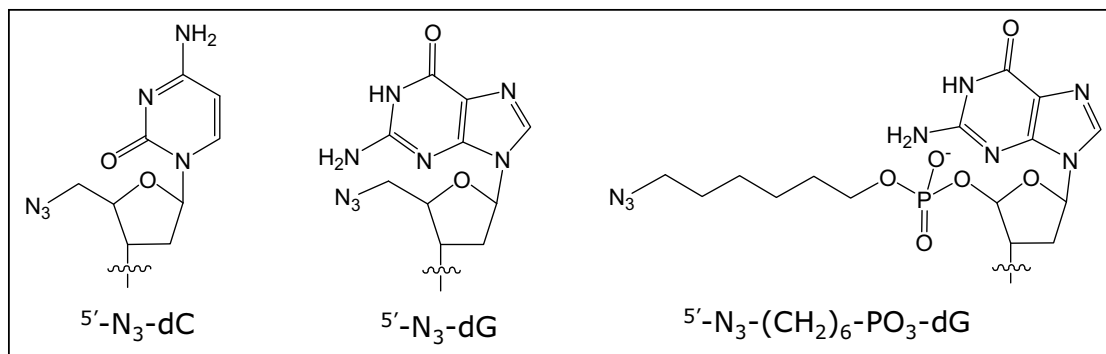
Figure 3.55. From left to right, last azido modified nucleosides contained in the DNA sequences CT-⁵′azido (**ODN 24**), GA-⁵′azido (**ODN 26**), and GA-⁵′azidohexyl (**ODN 31**).

The next step was looking for another technique that allows isolation of the ligation product. It is known that self-complementary sequences and G-rich ODN strands can result in intra and intermolecular associations to form secondary DNA structures which could prevent efficient ODN separation under non-denaturing conditions. This could be the reason why in this work denaturing PAGE shows two well-resolved bands while HPLC analysis results in multiple elution peaks.

Anion-exchange separations under denaturing conditions have been reported to be particularly useful for the resolution of oligonucleotides with high guanine content or with regions of complementary sequences [88,89].

Anion exchange chromatography (AEC) is an ionic exchange chromatographic technique that allows the separation of ions and polar molecules based on their charge. In AEC the stationary phase surface displays cationic functional groups that interact with negatively charged analyte samples. The strength of the interaction is determined by the number and location of the charges on the molecule and solid support. The mobile phase is generally a low to medium conductivity (salt concentration) solution. By increasing the salt concentration (generally with a linear gradient) the molecules with the weakest ionic interactions are disrupted first and elute earlier in the salt gradient. Those molecules that have a very strong ionic interaction require a higher salt concentration and elute later in the gradient.

In this work a 1 ml RESOURCE™ Q (GE Healthcare; 15 μm, 6.4 x 30 mm) was used. Oligonucleotides of different lengths can be separated because negatively charged phosphate groups on the DNA interact with the tetraalkylammonium cations contained on the column. A gradient of increasing ionic strength (0 to 1M NaCl in 20 min) was used to elute oligonucleotides in order of increasing chain length. The pH of the buffer should be at least 1 pH unit above the

pI of the analyte molecules so that they are negatively charged and bind to the matrix. In this work buffer 20 mM tris·HCl (pH 8.0) was employed without and with 50 % formamide as denaturing agent. Addition of formamide has been previously proved to give good results with oligonucleotide conjugates that are prone to aggregate or precipitate [90,91] and its use has been recommended for highly self-complementary sequences and/or rich in deoxyguanosine residues [88-90].

Several conditions and elution profiles were tested until an acceptable resolution was achieved. Figure 3.56.A shows different anion exchange chromatographic profiles corresponding to the 11mer sequences GA-$^{5'}$azidohexyl (**ODN 31**) and CT-$^{5'}$propargyl (**ODN 15**) and to the longer 16mer DNA strand CT$_{long}$-$^{5'}$propargyl (**ODN 19**). It can be observed that 16mer is eluted almost one minute later than the shorter 11mer, so this gradient would be useful to separate the desired parallel hairpins (22 or 27mer) from the rest of sequences (16 or 11mer and shorter). However HPLC analysis of the product resulting from ligation of GA-$^{5'}$azidohexyl and CT$_{long}$-$^{5'}$propargyl resulted in multiple elution peaks (figure 3.56.B).
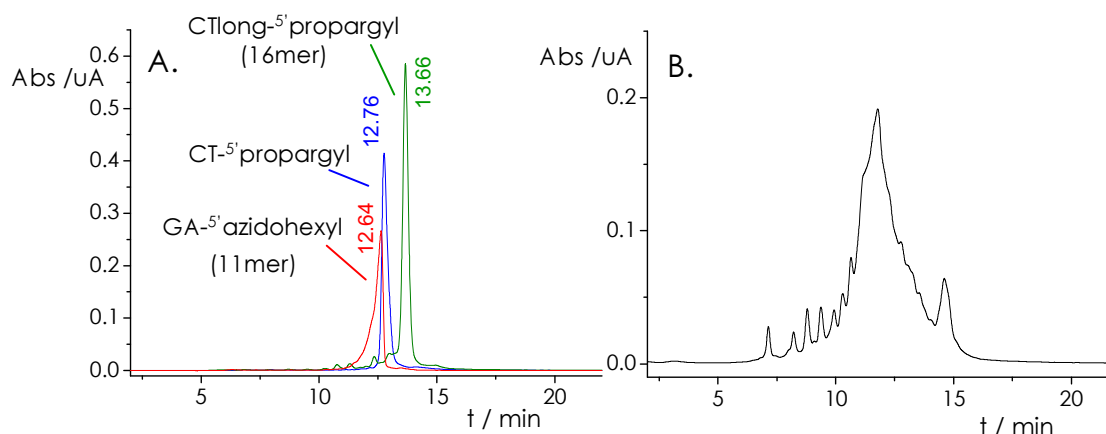
Figure 3.56. A) Superposition of anion exchange chromatographic profiles of the 11mer GA-$^{5'}$azidohexyl (red), CT-$^{5'}$propargyl (blue) and the 16mer CTlong-$^{5'}$propargyl (green). B) AEC analysis of the product coming from CuAAC between GA-$^{5'}$azidohexyl and CT$_{long}$-$^{5'}$propargyl. (Gradient: 0→ 50 % B in 20 min (A: 20 mM tris·HCl (pH 8.0); B: 20 mM tris·HCl (pH 8.0), 2M NaCl)

The same samples were analyzed by AEC using buffers containing formamide and resulting HPLC analysis is shown below. Figure 3.57.B shows that in this case resolution was better, which means that when no denaturing agent is added secondary structures are probably formed. In this case 2-3 major peaks elute in the zone of 11 and 16mer. The last eluting peak could be the desired hairpin but further evidence could not be obtained by subsequent analysis due to the poor yield.
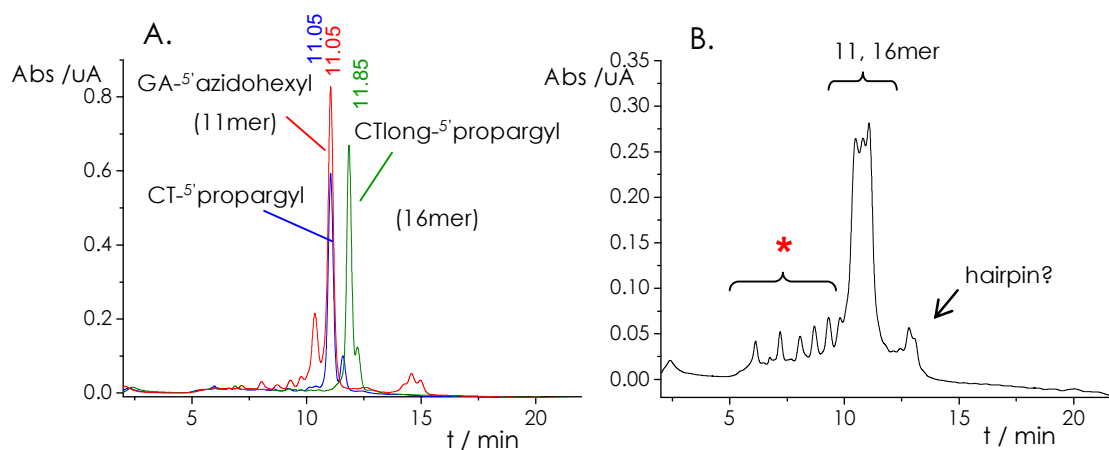
Figure 3.57. A) Superposition of anion exchange chromatographic profiles of the 11mer GA-5'azidohexyl (red), CT-5'propargyl (blue) and the 16mer CT$_{long}$-5'propargyl (green). B) AEC analysis of the product coming from CuAAC between GA-5'azidohexyl and CTlong-5'propargyl. (Gradient: 0 → 100% B in 20 min (A: 20 mM tris·HCl (pH 8.0), 50% formamide; B: 20 mM tris·HCl (pH 8.0), 1M NaCl, 50% formamide)

The ladder of small peaks eluting in the first ten minutes (marked with a red asterisk in figure 3.57.B) may be due either to DNA degradation or to DNA complexation with Cu^{2+} ions. Although oligonucleotides degradation is unlikely due to the conditions used in this case (absence of ascorbic acid and use of TBTA), this process would result in the production of smaller DNA fragments that were less retained in the cationic column and eluted earlier. The same effect would be observed if copper was complexed to undamaged DNA. Despite washing extensively the solid-supported products with EDTA prior to their cleavage from the resin, copper traces may be remain tightly bound. This would change the net charge of the oligonucleotides and therefore their retention properties, making difficult the isolation and characterization of desired products.

Interaction of Cu^{2+} with nucleic acids has been extensively studied over several decades using different methods and techniques [92-100]. It has been reported that at very low metal concentrations Cu^{2+} binds nonspecifically to the phosphate groups (figure 3.58.**a**) while upon increasing concentration also binds to the nitrogen bases and with much higher affinity than for the phosphate groups [93,98,100]. The most widely accepted model is chelation of Cu^{2+} with N7 of guanines and oxygen of the closest phosphate group on the same strand (figure 3.58.**b**) but other binding sites have been proposed [100], as depicted in schemes **c-f** of the same figure.
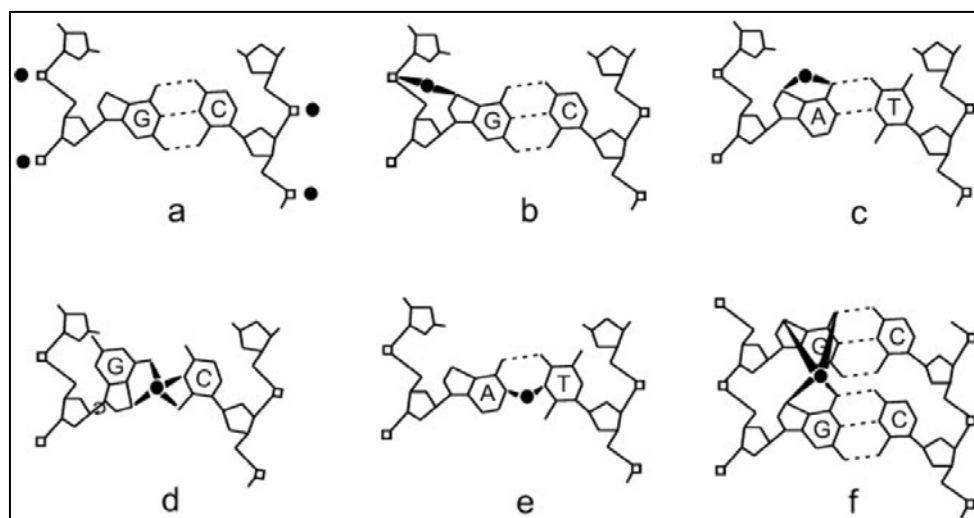
Figure 3.58. The possible binding sites for Cu^{2+} ions on DNA (extracted from reference [100]).

This complex interaction of copper with DNA might be the reason why purification and characterization of the ligation products has presented so many difficulties in this work when using guanine-rich sequences.

Regarding the moderate yields, a last attempt to improve the cycloaddition reaction between GA-5'azidohexyl and CT-5'propargyl consisted in performing the ligation with the reactants inversely immobilized. A few studies had reported a decrease in CuAAC reaction because of alkyn cross-coupling. Meldal and coworkers originally reported difficulty with coupling alkynes onto an azide-substituted resin, due to excessive alkyne homocoupling [5]. Although triazole formation on azide-substituted resins has proceeded in high yield in a lot of studies, [101-103], for resins with more sterically hindered azide functionalities alkyne homocoupling may dominate and dramatically reduce yields. To rule out this possible limitation, the CuAAC was performed with the azide in solution and the alkyne on the resin. In this case the GA-5'azidohexyl sequence was synthesized using G^{dmf} to avoid harsh cleavage conditions.

Figure 3.59.A shows analysis by anion exchange chromatography with denaturing buffer of the reaction between GA-5'azidohexyl and CT-5'propargyl when this latter is attached to the CPG support. Analysis of peaks **1-3** by denaturing PAGE (figure 3.59.B) shows that product **3** eluting at 12.5 min is the desired ligation product while the major peak **1** (10.7 min) corresponds to the starting CT-5'propargyl sequence.
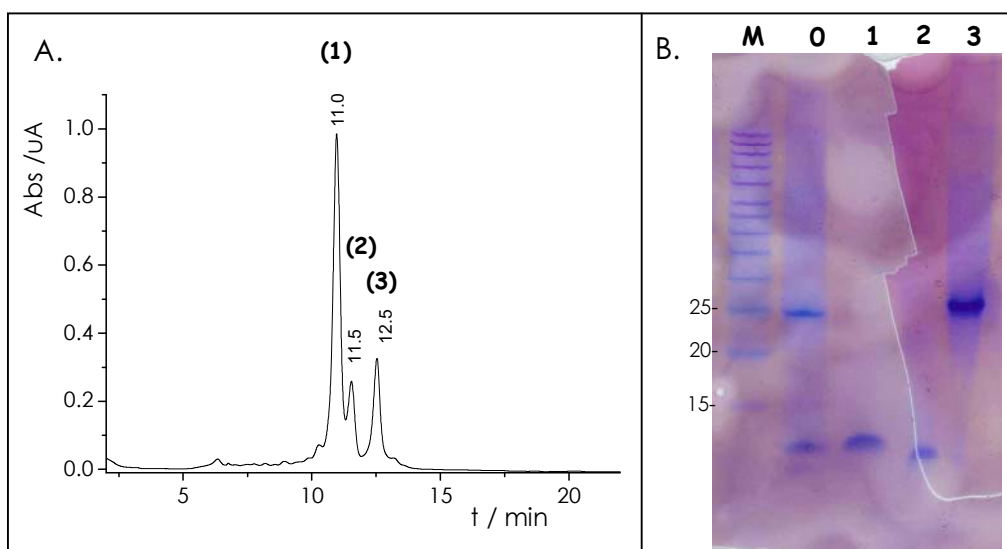
Figure 3.59. A) AEC analysis of the product coming from CuAAC between GA-$^{5'}$azidohexyl (**ODN 31**) and CT-$^{5'}$propargyl (**ODN 15**) with this latter attached to the CPG support (Gradient: 0 → 100% B in 20 min (A: 20 mM tris·HCl (pH 8.0), 50% formamide; B: 20 mM tris·HCl (pH 8.0), 1M NaCl, 50% formamide). B) Denaturing PAGE analysis of the eluted products. **M**: marker (10-100 nt); **0**: crude reaction product; **1,2,3**: peaks (1),(2),(3).

In this case, chromatogram presents a much cleaner profile than in previous experiments. While in the other experiments the unreacted supported GA-$^{5'}$azidohexyl sequence could retain more copper ions, the fact that the starting material attached to CPG is now a homopyrimidine sequence might be the reason why profile presents few and very well resolved peaks.

However, according to the relative peak areas and taking into account the ε_{260} of both starting material and ligation product, it was estimated that the yield of the CuAAC reaction was only 20 %. This means that inverse immobilization of the reactants did not cause a substantial improvement of the cycloaddition reaction in this case.

Moderate yields and the complex interaction of copper with DNA explained before might be the reason why not so many examples of CuAAC reactions between two DNA oligonucleotides have been published. While click chemistry has been widely used for labeling of oligonucleotides with small molecules [23,41,104], conjugation with carbohydrates [105,106], lipids [107], peptides [108], proteins [109] and DNA immobilization to surfaces [50,110,111] without problems, the ligation of two DNA strands has proved difficult in some cases.

Several successful examples in which highly efficient non-enzymatic DNA strand ligations have been achieved were those in which an alkyne–DNA conjugate and an azide–DNA conjugate, in low concentrations are brought in close proximity either by direct hybridization or by hybridization of the two conjugates to a complementary DNA template (Figure 3.60).
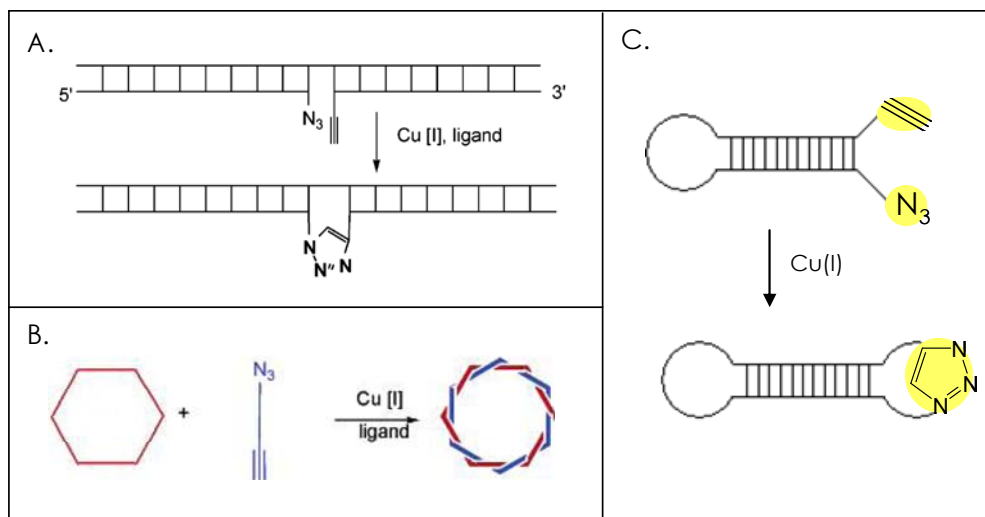
Figure 3.60. A) Scheme of template-mediated click-ligation of two ODNs employed by Kumar *et al*. [112]. B) Formation of double-stranded pseudohexagon from a single stranded cyclic template and a linear ODN modified with an azide and an alkyne group; adapted from reference [112]. C) Formation of triazole cross-linked dumbbell-like ODNs by the CuAAC reaction, performed by Nakane *et al*. [113].

Interestingly, the importance of template-assisted CuAAC reactions for DNA ligation has been recently demonstrated by Jacobsen *et al.* [114] who reported small-molecule-induced control in duplex and triplex DNA-directed CuAAC reactions (Figure 3.61) and confirmed the distance dependence of the reaction.
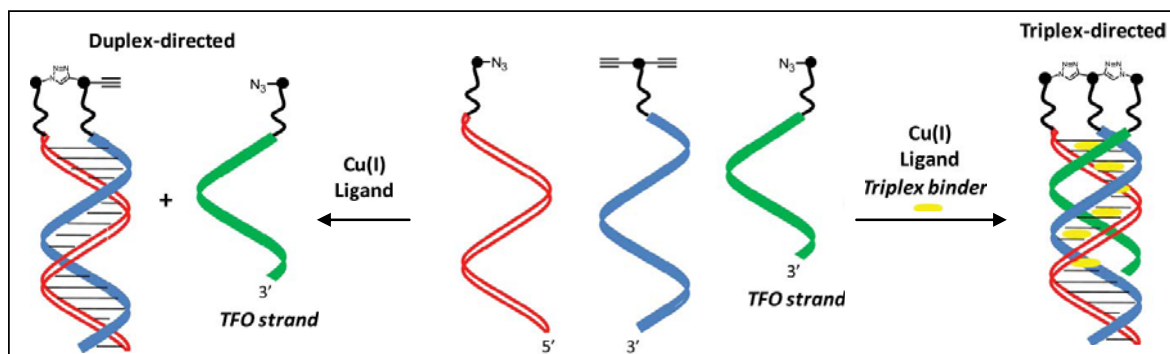
Figure 3.61. Scheme followed by Jacobsen et al. for controlling nucleic acid-directed chemical reactions with triplex DNA binders. Adapted from reference [114].

Click chemistry has also given good results to ligate azido and alkynyl groups intramolecularly. Lietard *et al.* synthesized cyclic, branched and bicyclic ODNs by introducing alkyne and azido functions in the same DNA strand and performing CuAAC assisted by microwaves [115].

Low yield of some of the CuAAC reactions carried out in this thesis may be also due to the lacking of proximity between azido and alkynyl groups.

3.7. Synthesis of novel unnatural amino acids by click chemistry.

In this section the utility of Cu(I)-catalyzed cycloaddition reaction has been examined to generate novel non natural amino acids that can be incorporated simply in peptides. This work was carried out during a FPI predoctoral short-term staying in the laboratory of Dr. Grøtli, in the Medicinal Chemistry Department at Göteborg University.

The first objective was the synthesis of amino acids whose side chain was terminated with an azide or an alkyne group. Two different protocols were employed to prepare the amino acids depicted in figure 3.62.
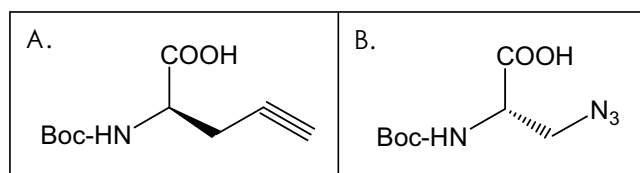
Figure 3.62. A) (S)-Nα-t-Boc-propargylglycine B) Nα-t-Boc-β-azido-L-alanine

These molecules can be used in solid phase peptide synthesis. Their side chain will allow regioespecific introduction of triazole moieties if the introduction of the amino acids is followed by Huisgen [3+2]-cycloaddition reactions before the peptide synthesis is continued. This can be used as a powerful technique for chemical peptide labelling with a high variety of molecules just by performing the cycloaddition reaction with diverse azido and alkyne derivatives to obtain for example glycopeptides or fluorescent-tagged peptides.

In addition these two amino acids can be used as starting materials to prepare a variety of novel amino acids by click chemistry reactions with azido or alkynes derivatives. In this work an *in-situ* generated azido-containing alanine (figure 3.62.B) will be used to create a small library of non natural amino acids by performing CuAAC with different acetylenic partners.

On the other hand the generated [1,2,3]-triazole may be used as an analogue of the histidine imidazole ring because of its structural similarity. The side chain imidazole group of histidine has great importance in the activity and properties of several enzymes and peptides in most cases due to its ability to take part in acid-base catalysis [116] so introduction of unnatural amino acids with different chemical characteristics to the original histidine such as acidity, nucleophilicity or sterical factors can be of great interest to get new properties [117].

3.7.1. Stereoselective synthesis of an alkyne containing amino acid

One of the most established methods for the asymmetric synthesis of mono- or disubstituted α-aminoacids has been reported to be the alkylation of chiral glycine and alanine enolates [118]. Many different cyclic glycine and alanine chiral templates have been described, with Schöllkopf's bis-lactim ethers being one of the most used, due to their high diastereofacial enolate bias [119]. In this work the bislactim ether shown below in figure 3.63 was used. In general, these chiral templates need strong bases for deprotonation and strictly anhydrous conditions together with very low reaction temperatures. Treatment with *n*-butyllithium at -78 ºC caused deprotonation at C5 and gave an almost planar dihydropyrazine anion, which can easily undergo electrophilic attack by an alkyl halide. The electrophilic group attacks preferentially the pyrazine ring in a trans-relationship to the isopropyl group to minimize steric interactions which results in a high diastereoselective alkylation with an acceptable chemical yield.

All the different steps to finally obtain the (S)-Nα-t-Boc-propargylglycine are depicted in scheme of figure 3.63. The starting 2,5-diketopiperazine was synthesized previously in the group of Dr. Grøtli with a microwave-assisted protocol developed in his laboratory [120].
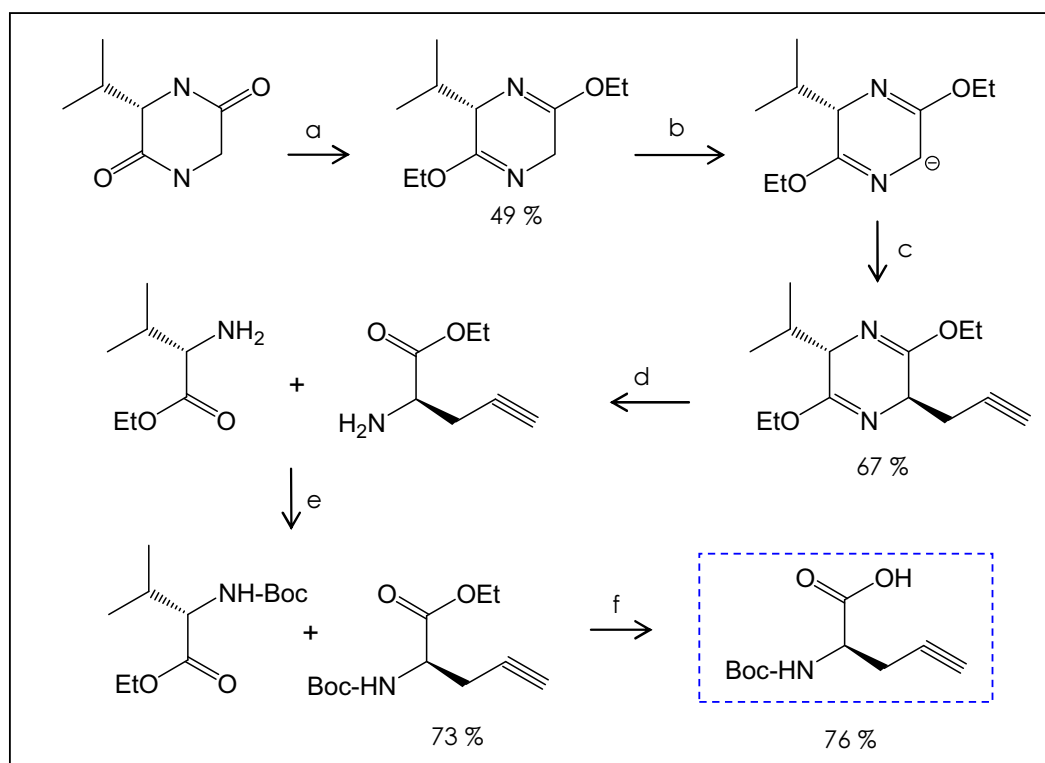
Figure 3.63. a) $Et_3O_3 \cdot BF_4$, N_2, DCM, r.t, 6 days; b) *n*-BuLi, THF, -78ºC, 45 min; c) propargyl bromide, THF, o.n; d) TFA, H_2O/ACN (1:1), MW, 60 ºC, 5 min; e) Boc_2O, THF, reflux, o.n; f) LiOH, H_2O/THF (1:1), MW, 60 ºC, 20 min.

The final product as well as the intermediate compounds were characterized by ^{1}H-NMR and ^{13}C-NMR.

3.7.2. Synthesis of an azide containing amino acid and subsequent click chemistry reactions

As azides are difficult to handle and tend to be explosive, a protocol described by Beckmann *et al.* [121] was employed. This protocol is a one-pot procedure for generating triazoles starting from amines avoiding the isolation of the azide intermediates.

In this work, the starting amine was Nα-t-Boc-α-amino-L-alanine, which was synthesized from the comercially available Nα-t-Boc-L-asparagine through the Hoffmann rearrangement [122] with iodosobenzene diacetate (more commonly named as phenyliodonium diacetate or PIDA), as illustrated in figure 3.64.
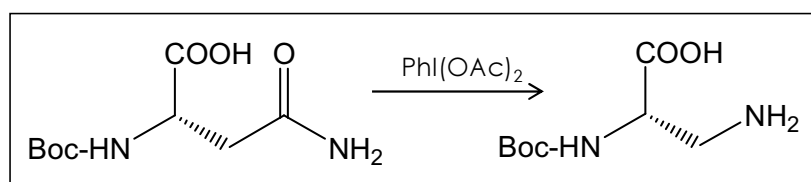
Figure 3.64. Synthesis of Nα-t-Boc-α-amino-L-alanine.

Nα-t-Boc-α-amino-L-alanine was used as starting material for generating azide followed by azide-alkyne cycloaddition with commercially available alkynes, to synthesize novel amino acids (Figure 3.65).
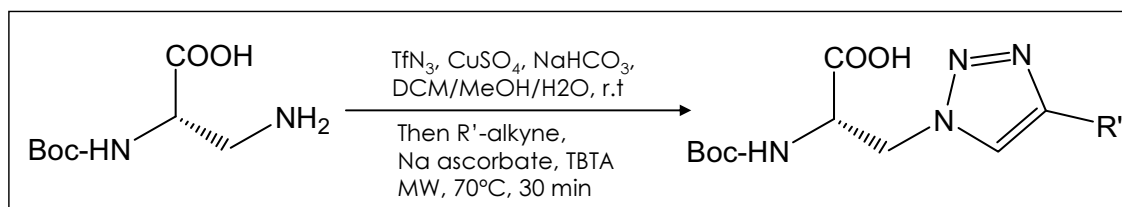
Figure 3.65. One-pot procedure used for generating triazole-linked structures starting from Nα-t-Boc-α-amino-L-alanine, based on the protocol reported by Beckmann *et al*. [121].

The diazo transfer was performed using literature-known conditions [123] at room temperature but with sodium bicarbonate as base. After complete conversion of the starting amine, one equivalent of the desired alkyne-containing compound together with the reducing sodium ascorbate and the Cu(I)-stabilizing ligand TBTA were added directly without any work-up procedure. Heating to 70ºC by MW irradiation was required to obtain high yields within reasonable reaction times.

Table 3.66 shows the different starting alkynes and the resulting triazole containing products as well as the yield for each reaction.
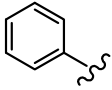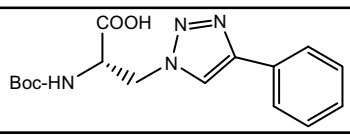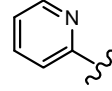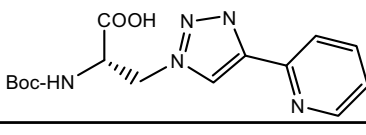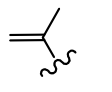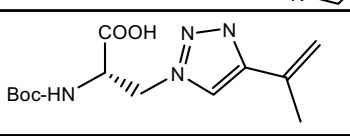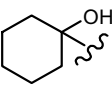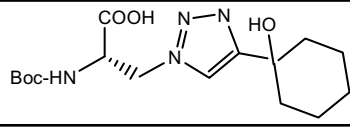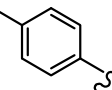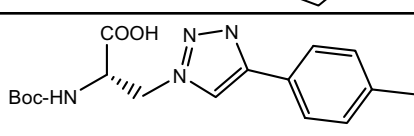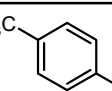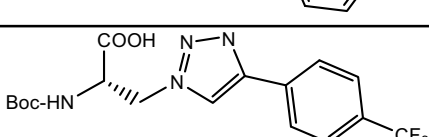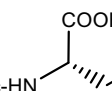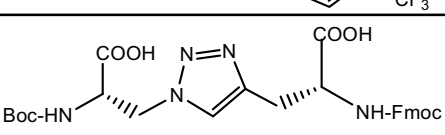
R' (R'——≡)	amino acid	yield
(phenyl)	Boc-HN, COOH, N=N, N, triazole-phenyl	97
(2-pyridyl)	Boc-HN, COOH, N—N, N, triazole-(2-pyridyl)	86
(isopropenyl)	Boc-HN, COOH, N—N, N, triazole-isopropenyl	86
(1-hydroxycyclohexyl, OH)	Boc-HN, COOH, N—N, N, HO, triazole-cyclohexanol	quant
(p-tolyl)	Boc-HN, COOH, N—N, N, triazole-(p-tolyl)	quant
F$_3$C-(phenyl)	Boc-HN, COOH, N—N, N, triazole-phenyl-CF$_3$	quant
Fmoc-HN, COOH (alkyne amino acid)	Boc-HN, COOH, N=N, N, triazole, COOH, NH-Fmoc	95

Table 3.66. Unnatural amino acids synthesized from alkynes indicated in the first column by click chemistry with Nα-t-Boc-α-azido-L-alanine. The yield is indicated in the third column. (quant=quantitative yield)

All these synthesized amino acids were purified by flash chromatography and characterized by ^{1}H-NMR, ^{13}C-NMR and IR. In all cases, the triazole products were isolated in very good yields.

The introduction of these amino acids in several peptides is currently been studied in the group of Dr. Grøtli.

3.8. Conclusions

A novel strategy to obtain parallel clamps using the non-templated chemical ligation of two oligonucleotides by 5'-5' linkages has been reported.

Efficient protocols for introducing azido and alkyne functionalities at the 5' end of oligonucleotides have been developed. The chemical ligation of such

structures by Cu(I)-catalyzed cycloaddition reaction has been performed and the following remarks have been noted:

An excess of copper ions (and not a catalytic amount) is required, likely due to the retention of this cation by phosphate groups of DNA

Exclusion of atmospheric oxygen is essential to avoid oxidation of Cu(I), even when using the CuSO$_4$/ascorbate system. Adding ascorbic to CuI for preventing its oxidation gave very good results for ligation of homopyrimidine sequences but several problems were encountered when using this reducing agent and guanine rich DNA sequences. TBTA was employed thence as the only Cu(I) stabilizer when working with homopurine strands.

Hex-5-ynyl group was found to be very useful for linking small molecules to oligonucleotides but presented poor reactivity in the CuAAC ligation of two DNA strands. On the other hand, the alkyne activated by a neighbouring electrowithdrawing amide moiety gave good results.

Direct attachment of the azido group to the C5 of ribose ring (from 5'-iodinated precursor) gave lower CuAAC yields than those cases in which a hexyl chain is the linker between azido group and C5, especially for purine terminated oligonucleotides.

The use of ChemMatrix support for the synthesis of oligonucleotides and subsequent click reaction gave higher yields than CPG in the case of linking two polypyrimidine sequences, probably due to the hydrophilic nature of this support.

Synthesis of parallel hairpins has been achieved but purification and characterization of the ligation products has presented difficulties when using guanine-rich sequences (especially when these are attached to the solid support), probably due to interaction with copper and formation of secondary structures.

Moderate yields of some CuAAC reactions carried out in this thesis may be due to the lacking of proximity between azido and alkynyl groups, according to several studies reporting the distance dependence of the reaction.

Cu (I)-catalyzed azide-alkyne cycloaddition reaction has been also used to synthesize novel unnatural aminoacids. A small library of compounds was synthesized from different alkynes by click chemistry with Nα-t-Boc-α-azido-L-alanine and the triazole products were isolated in very good yields.

3.9. References

[1]. Kolb, H.C., Finn, M.G., and Sharpless, K.B. (2001) Click Chemistry: Diverse Chemical Function from a Few Good Reactions. *Angew. Chem. Int. Ed.* 40, 2004-2021.

[2]. Moses, J. E., and Moorhouse, A. D. (2007) The Growing Applications of Click Chemistry. *Chem. Soc. Rev. 36*, 1249-1262.

[3]. Huisgen, R. (1963) 1,3-Dipolar Cycloadditions Past and Future. *Angew. Chem. Int. Ed. Engl.* 2, 565-598.

[4]. Huisgen, R. (1963) Kinetics and Mechanism of 1,3-Dipolar Cycloadditions. *Angew. Chem. Int. Ed. Engl.* 2, 633-645.

[5]. Tornøe, C. W., Christensen, C., and Meldal, M. (2002) Peptidotriazoles on Solid Phase: [1,2,3]-Triazoles by Regiospecific Copper(I)-Catalyzed 1,3-Dipolar Cycloadditions of Terminal Alkynes to Azides. *J. Org. Chem. 67*, 3057-3064.

[6]. Rostovtsev, V.V., Green, L.G., Fokin, V.V., and Sharpless, K.B. (2002) A Stepwise Huisgen Cycloaddition Process: Copper(I)-Catalyzed Regioselective "Ligation" of Azides and Terminal Alkynes. *Angew. Chem. Int. Ed.* 114, 2708-2711.

[7]. Himo, F., Lovell, T., Hilgraf, R., Rostovtsev, V. V., Noodleman, L., Sharpless, K. B., and Fokin, V. V. (2005) Copper(I)-Catalyzed Synthesis of Azoles. DFT Study Predicts Unprecedented Reactivity and Intermediates. *J. Am. Chem. Soc. 127*, 210-216.

[8]. Bock, V. D., Hiemstra, H., and van Maarseveen, J.H. (2006) Cu^I-Catalyzed Alkyne-Azide "Click" Cycloadditions from a Mechanistic and Synthetic Perspective. *Eur. J. Org.Chem. 1*, 51-68.

[9]. Fukuzawa, S., Shimizu, E., and Kikuchi, S. (2007) Copper (II) Triflate as a Double Catalyst for the One-Pot Click Synthesis of 1, 4-Disubstituted 1, 2, 3-Triazoles from Benzylic Acetates. *Synlett. 18*, 2436-2438.

[10]. Malkoch, M., Schleicher, K., Drockenmuller, E., Hawker, C.J., Russell, T.P., Wu, P., and Fokin, V.V. (2005) Structurally Diverse Dendritic Libraries: A Highly Efficient Functionalization Approach Using Click Chemistry. *Macromolecules* 38, 3663–3678.

[11]. Broggi, J., Joubert, N., Aucagne, V., Zevaco, T., Berteina-Raboin, S., Nolan, S. P., and Agrofoglio, L. A. (2007) Study of Different Copper (I) Catalysts for the "Click Chemistry" Approach to Carbanucleosides. *Nucleos Nucleot Nucl. 26*, 779-783.

[12]. Pérez-Balderas, F., Ortega-Muñoz, M., Morales-Sanfrutos, J., Hernández-Mateo, F., Calvo-Flores, F., Calvo-Asín, J. A., Isac-García, J., and Santoyo-González, F. (2003) Multivalent Neoglycoconjugates by Regiospecific Cycloaddition of Alkynes and Azides using Organic-Soluble Copper Catalysts. *Org. Lett. 5*, 1951-1954.

[13]. Hansen, T. V., Wu, P., Sharpless, W. D., and Lindberg, J. G. (2005) Just Click It: Undergraduate Procedures for the Copper (I)-Catalyzed Formation of 1, 2, 3-Triazoles from Azides and Terminal Acetylenes. *J. Chem. Educ. 82*, 1833-1836.

[14] Zhan, W.-h., Barnhill, H. N., Sivakumar, K., Tian, H., and Wang, Q. (2005) Synthesis Of Hemicyanine Dyes For 'Click' Bioconjugation. *Tetrahedron Lett*. 46, 1691–1695.

[15]. Speers, A. E., Adam, G. C., and Cravatt, B. F. (2003) Activity-Based Protein Profiling In Vivo Using A Copper (I)-Catalyzed Azide-Alkyne [3+ 2] Cycloaddition. *J. Am. Chem. Soc*. 125, 4686–4687.

[16]. Wang, Q., Chan, T. R., Hilgraf, R., Fokin, V. V., Sharpless, K. B., and Finn, M. G. (2003) Bioconjugation By Copper (I)-Catalyzed Azide-Alkyne [3+ 2] Cycloaddition. *J. Am. Chem. Soc.* 125, 3192–3193.

[17]. Speers, A. E., and Cravatt, B. F. (2004) Profiling Enzyme Activities In Vivo Using Click Chemistry Methods. *Chem. Biol*. 11, 535–546.

[18]. Lewis, W. G., Magallon, F. G., Fokin, V. V., and Finn, M. G. (2004) Discovery And Characterization Of Catalysts For Azide-Alkyne Cycloaddition By Fluorescence Quenching. *J. Am. Chem. Soc*. 126, 9152–9153.

[19] Orgueira, H. A., Fokas, D., Isome, Y., Chane, P. C.-M., and Baldino, C. M. (2005) Regioselective Synthesis Of [1, 2, 3]-Triazoles Catalyzed By Cu (I) Generated In Situ From Cu (0) Nanosize Activated Powder And Amine Hydrochloride Salts. *Tetrahedron Lett*., 46, 2911–2914.

[20]. Pachón, L. D., van Maarseveen, J. H., and Rothenberg, G. (2005) Click Chemistry: Copper Clusters Catalyse the Cycloaddition of Azides with Terminal Alkynes. *Adv. Synth. Catal*. 347, 811–815.

[21]. Chan, T.R., Hilgraf, R., Sharpless, K.B., and Fokin, V.V. (2004) Polytriazoles As Copper(I)-Stabilizing Ligands In Catalysis. *Org. Lett.* 6, 2853–2855.

[22]. Donnelly, P. S., Zanatta, S. D., Zammit, S. C., White, J. M., and Williams, S. J. (2008) 'Click' Cycloaddition Catalysts: Copper(I) and Copper(II) Tris(Triazolylmethyl) Amine Complexes. *Chem. Commun*. 21, 2459–2461.

[23]. Gierlich, J., Burley, G. A., Gramlich, P. M. E., Hammond, D. M., and Carell, T. (2006) Click Chemistry as a Reliable Method for the High-Density Postsynthetic Functionalization of Alkyne-Modified DNA. *Org. Lett. 8*, 3639-3642.

[24]. Collman, J. P., Devaraj, N. K., and Chidsey, C. E. D. (2004) "Clicking" Functionality onto Electrode Surfaces. *Langmuir* 20, 1051–1053.

[25] Wu, P., Feldman, A. K., Nugent, A. K., Hawker, C. J., Scheel, A., Voit, B., Pyun, J., Fréchet, J. M. J., Sharpless, K. B., and Fokin, V. V. (2004) Efficiency and Fidelity in a Click-Chemistry Route to Triazole Dendrimers by the Copper(I)-Catalyzed Ligation of Azides and Alkynes. *Angew. Chem. Int. Ed. Engl*. 43, 3928–3932.

[26]. Khanetskyy, B., Dallinger, D., Kappe, C. O. (2004) Combining Biginelli Multicomponent And Click Chemistry: Generation Of 6-(1, 2, 3-Triazol-1-Yl)-Dihydropyrimidone Libraries. *J. Comb. Chem*. 6, 884–892.

[27]. Tornøe, C. W., Sanderson, S. J., Mottram, J. C., Coombs, G. H., and Meldal, M. (2004) Combinatorial Library of Peptidotriazoles: Identification of [1,2,3]-Triazole Inhibitors Against a Recombinant Leishmania Mexicana Cysteine Protease. *J. Comb. Chem.* 6, 312-324.

[28]. Chittaboina, S., Xie, F., and Wang Q. (2005) One-Pot Synthesis Of Triazole-Linked Glycoconjugates. *Tetrahedron Lett*. 46, 2331–2336.

[29]. Brik, A., Alexandratos, J., Lin, Y.C., Elder, J.H., Olson, A.J., Wlodawer, A., Goodsell, D.S., and Wong, C.H. (2005) 1,2,3-Triazole As A Peptide Surrogate In The Rapid Synthesis Of HIV-1 Protease Inhibitors. *Chem. Bio. Chem*. 6, 1167–1169.

[30]. Pagliai, F., Pirali, T., Del Grosso, E., Di Brisco, R., Tron, G.C., Sorba, G., and Genazzani, A.A. (2006) Rapid synthesis of triazole-modified resveratrol analogues via click chemistry. *J. Med. Chem*. 49, 467–470.

[31]. Srinivasan, R., Uttamchandani, M., and Yao, S.Q. (2006) Rapid assembly and in situ screening of bidentate inhibitors of protein tyrosine phosphatases. *Org. Lett*. 8, 713–716.

[32]. Oh, K., and Guan, Z. (2006) A convergent synthesis of new β-turn mimics by click chemistry. *Chem. Comm*. 29, 3069–3071.

[33]. Pirali, T,, Gatti, S., Di Brisco, R., Tacchi, S., Zaninetti, R., Brunelli, E., Massarotti, A., Sorba, G., Canonico, P.L., Moro, L., Genazzani, A.A., Tron. G.C., and Billington, R.A. (2007) Estrogenic Analogues Synthesized Via Click Chemistry. *Chem. Med. Chem*. 2, 437 – 440.

[34]. Lee, L.V., Mitchell, M.L., Huang, S.J., Fokin, V.V., Sharpless, K.B., and Wong, C.H. (2003) A Potent And Highly Selective Inhibitor Of Human α-1,3-Fucosyltransferase Via Click Chemistry. *J. Am. Chem. Soc*. 125, 9588–9589.

[35]. Brik, A., Muldoon, J., Lin, Y.C., Elder, J.H., Goodsell, D.S., Olson, A.J., Fokin, V.V., Sharpless, K.B., and Wong, C-H. (2003) Rapid Diversity-Oriented Synthesis in Microtiter Plates for in Situ Screening of HIV Protease Inhibitors. *Chem. Bio. Chem*. 4, 1246-1248.

[36]. Lewis, W.G., Green, L.G., Grynszpan, F., Radi, Z., Carlier, P.R., Taylor, P., Finn, M.G., and Sharpless, K.B. (2002) Click Chemistry in Situ: Acetylcholinesterase as a Reaction Vessel for the Selective Assembly of a Femtomolar Inhibitor from an Array of Building Blocks. *Angew. Chem. Int. Ed.* 114, 1095 – 1099.

[37]. Krasinski, A., Radic, Z., Manetsch, R., Raushel, J., Taylor, P., Sharpless, K. B., and Kolb, H. C. (2005) In Situ Selection of Lead Compounds by Click Chemistry: Target-Guided Optimization of Acetylcholinesterase Inhibitors. *J. Am. Chem. Soc*. 127, 6686-6692.

[38]. Franke, R., Doll, C., and Eichler, J. (2005) Peptide Ligation through Click Chemistry for the Generation of Assembled and Scaffolded Peptides. *Tetrahedron Lett. 46*, 4479-4482.

[39]. Jang, H., Fafarman, A., Holub, J. M., and Kirshenbaum, K. (2005) Click to Fit: Versatile Polyvalent Display on a Peptidomimetic Scaffold. *Org. Lett. 7*, 1951-1954.

[40]. Holub, J. M., Jang, H., and Kirshenbaum, K. (2006) Clickity-Click: Highly Functionalized Peptoid Oligomers Generated Sequential Conjugation Reactions on Solid-Phase Support. *Org. Biomol. Chem*. 4, 1497 – 1502.

[41]. Seo, T. S., Li, Z., Ruparel, H., and Ju, J. (2003) Click Chemistry to Construct Fluorescent Oligonucleotides for DNA Sequencing. *J. Org. Chem. 68*, 609-612.

[42]. Wang, Q., Chan, T. R., Hilgraf, R., Fokin, V. V., Sharpless, K. B., and Finn, M. G. (2003) Bioconjugation by Copper(I)-Catalyzed Azide-Alkyne [3 + 2] Cycloaddition. *J. Am. Chem. Soc. 125*, 3192-3193.

[43]. Link, A.J., and Tirrell, D.A. (2003) Cell surface labeling of Escherichia coli via copper(I)-catalyzed [3+2] cycloaddition. *J. Am. Chem. Soc*. 125, 11164–11165.

[44]. Deiters, A., Cropp, T.A., Mukherji, M., Chin, J.W., Anderson, J.C., and Schultz, P.G. (2003) Adding amino acids with novel reactivity to the genetic code of Saccharomyces cerevisiae. *J. Am. Chem. Soc*. 125, 11782–11783.

[45]. Binder, W. H., and Sachsenhofer, R. (2007) 'Click'Chemistry in Polymer and Materials Science. *Macromol. Rapid Commun*. 28, 15-54.

[46]. Binder, W. H., and Sachsenhofer, R. (2008) 'Click'Chemistry in Polymer and Material Science: An Update. *Macromol. Rapid Commun.* 29, 952-981.

[47] Lee, J. K., Chi, Y. S., and Choi, I. S. (2004) Reactivity of Acetylenyl-Terminated Self-Assembled Monolayers on Gold:Triazole Formation. *Langmuir* 20, 3844-3847.

[48] Lummerstorfer, T., and Hoffmann, H. J. (2004) Click chemistry on surfaces: 1,3-dipolar cycloaddition reactions of azide-terminated monolayers on silica. *Phys. Chem. B.,* 108, 3963-3966.

[49]. Ciampi, S., Bocking, T., Kilian, K. A., James, M., Harper, J. B., and Gooding, J. J. (2007) Functionalization of acetylene terminated monolayers on Si(100) surfaces: a click chemistry approach. *Langmuir* 23, 9320–9329.

[50]. Devaraj, N. K., Miller, G. P., Ebina, W., Kakaradov, B., Collman, J. P., Kool, E. T., and Chidsey, C. E. D. (2005) Chemoselective Covalent Coupling of Oligonucleotide Probes to Self-Assembled Monolayers. *J. Am. Chem. Soc*. 127, 8600-8601.

[51]. Sun, X., Stabler, C. L., Cazalis, C. S., and Chaikof, E. L. (2006) Carbohydrate and Protein Immobilization Onto Solid Surfaces by Sequential Diels-Alder and Azide-Alkyne Cycloadditions. *Bioconjug. Chem. 17*, 52-57.

[52]. Li, H., Cheng, F., Duft, A. M., and Adronov, A. (2005) Functionalization of single-walled carbon nanotubes with well defined polystyrene by"click" coupling. *J. Am. Chem. Soc*. 127, 14518–14524.

[53]. Brennan, J. L., Hatzakis, N. S., Tshikhudo, T. R., Razumas, V., Patkar, S., Vind, J., Svendsen, A., Nolte, R. J. M., Rowan, A. E., and Brust, M. (2006) Bionanoconjugation Via Click Chemistry:The Creation of Functional Hybrids of Lipases and Gold Nanoparticles. *Bioconjug. Chem. 17*, 1373-1375.

[54]. von Maltzahn, G., Ren, Y., Park, J., Min, D., Kotamraju, V. R., Jayakumar, J., Fogal, V., Sailor, M. J., Ruoslahti, E., and Bhatia, S. N. (2008) In Vivo Tumor Cell Targeting with "Click" Nanoparticles. *Bioconjug. Chem*. 19, 1570-1578.

[55]. Polito, L., Monti, D., Caneva, E., Delnevo, E., Russo, G., and Prosperi, D. (2008) One-Step Bioengineering of Magnetic Nanoparticles Via a Surface Diazo transfer/azide-Alkyne Click Reaction Sequence. *Chem. Comm.* 5, 621-623.

[56]. Aviño, A., Grimau, M.G., Frieden, M., and Eritja, R. (2004) Synthesis and Triple-Helix-Stabilization Properties of Branched Oligonucleotides Carrying 8-Aminoadenine Moieties. *Helv. Chim. Acta.* 87, 303-316.

[57]. Grøtli, M., Eritja, R. and Sproat, B. (1997) Solid-phase Synthesis of Branched RNA and Branched DNA/RNA Chimeras. *Tetrahedron* 53, 11317-11346.

[58]. Frieden, M., Aviñó, A., Tarrasón, G., Escorihuela, M., Piulats, J., and Eritja, R. (2004) Synthesis of Oligonucleotide-Peptide Conjugates Carrying the c-myc Peptide Epitope as Recognition System. *Chem. Biodiversity* 1, 930–938.

[59]. Roget, A., Bazin, H., and Teoule, R. (1989) Synthesis and use of Labelled Nudeoside Phosphoramidite Building Blocks Bearing a Reporter Group: Biotinyl, Dinitrophenyl, Pyrenyl and Dansyl. *Nucl. Acids Res. 17*, 7643-7651.

[60]. Theisen, P., McCullum, C., Upadhya, K., Jacobson, K., Vu, H., and Andrus, A. (1992) Fluorescent Dye Phosphoramidite Labelling of Oligonucleotides. *Tetrahedron Lett. 33*, 5033-5036.

[61]. Venkatesan, N., Kim, S. J., and Kim, B. H. (2003) Novel Phosphoramidite Building Blocks in Synthesis and Applications Toward Modified Oligonucleotides. *Curr. Med. Chem. 10*, 1973-1991.

[62]. Vinayak, R. (1999) A Convenient, Solid-Phase Coupling of Rhodamine Dye Acids to 5' Amino-Oligonucleotides. *Tetrahedron Lett. 40*, 7611-7613.

[63]. De Napoli, L., Di Fabio, G., Messere, A., Montesarchio, D., Musumeci, D. and Piccialli, G. (1999) Synthesis And Characterization Of New 3'-3' Linked Oligodeoxyribonucleotides For Alternate Strand Triple Helix Formation. *Tetrahedron* 55, 9899-9914.

[64]. Zaramella, S., Yeheskiely, E., and Strömberg, R. (2004) A Method for Solid-Phase Synthesis of Oligonucleotide 5'-Peptide-Conjugates Using Acid-Labile α-Amino Protections. *J. Am. Chem. Soc.* 126, 14029–14035.

[65]. Ocampo, S. M., Albericio, F., Fernández, I., Vilaseca, M., and Eritja, R. (2005) A Straightforward Synthesis Of 5'-Peptide Oligonucleotide Conjugates Using N$^\alpha$-Fmoc-Protected Amino Acids. *Org. Lett.* 7, 4349–4352.

[66]. Somoza, A., Terrazas, M., and Eritja, R. (2010) Modified siRNAs For The Study Of The PAZ Domain. *Chem. Commun.* 46, 4270 – 4272.

[67]. Köhn, M., and Breinbauer, R. (2004) The Staudinger Ligation - A Gift to Chemical Biology. *Angew. Chem. Int. Ed.* 43, 3106 – 3116.

[68]. Liu, J., Fan, Q.R., Sodeoka, M., Lane, W.S., and Verdine, G.L. (1994) DNA Binding By An Amino Acid Residue In The C-Terminal Half Of The Rel Homology Region. *Chem. Biol.* 1, 47-55.

[69]. Fàbrega, C., Güimil García, R., Díaz, A.R., and Eritja, R. (1998) Studies on the Synthesis of Oligonucleotides Containing Photoreactive Nucleosides: 2-Azido-2'-Deoxyinosine and 8-Azido-2'-Deoxyadenosine. *Biol. Chem*., 379, 527-533.

[70]. Frieden, M., Aviñó, A., and Eritja, R. (2003) Convenient Synthesis of 8-Amino-2'-deoxyadenosine. *Nucleos Nucleot Nucl.* 22, 193-202.

[71]. Vu, H., McCollum, C., Jacobson, K., Theisen, P., Vinayak, R., Spiess, E., and Andrus, A. (1990) Fast Oligonucleotide Deprotection Phosphoramidite Chemistry for DNA Synthesis. *Tetrahedron Lett.* 31, 7269-7272.

[72]. Miller, G. P., and Kool, E. T. (2002) A Simple Method for Electrophilic Functionalization of DNA. *Org. Lett*. 4, 3599-3601.

[73]. Alvira, M., Quinn, S.J., Aviñó, A., Fitzmaurice, D. and Eritja, R. (2008) Synthesis of Oligonucleotide Conjugates Carrying Viologen and Fluorescent Compounds. *The Open Organic Chemistry Journal* 2, 41-45.

[74]. Donald, C. E., Stokes, P., O'Connor, G., and Woolford, A. J. (2005) A Comparison of Enzymatic Digestion for the Quantitation of an Oligonucleotide by Liquid chromatography–isotope Dilution Mass Spectrometry. *J Chromatogr. B.* 817, 173-182.

[75]. Xodo, L. E., Manzini, G., and Quadrifoglio, F. (1990) Spectroscopic and Calorimetric Investigation on the DNA Triplex Formed by d(CTCTTCTTTCTTTTCTTTCTTCTC) and d(GAGAAGAAAGA) at Acidic pH. *Nucl. Acids Res.* 18, 3557-3564.

[76]. Xodo, L. E., Manzini, G., Quadrifoglio, F., van der Marel, G. A., and van Boom, J. H. (1991) Effect Of 5-Methylcytosine on the Stability of Triple-Stranded DNA--a Thermodynamic Study. *Nucl. Acids Res. 19*, 5625-5631.

[77]. Demko, Z. P., and Sharpless, K. B. (2001) Preparation of 5-Substituted 1H-Tetrazoles from Nitriles in Water . *J. Org. Chem.* 66, 7945-7950.

[78]. Demko, Z. P., and Sharpless, K. B. (2002) A Click Chemistry Approach to Tetrazoles by Huisgen 1,3-Dipolar Cycloaddition: Synthesis of 5-Acyltetrazoles from Azides and Acyl Cyanides. *Angew. Chem. Int. Ed.*. 41, 2113-2116.

[79]. Li, Z., Seo, T. S., and Ju, J. (2004) 1,3-Dipolar Cycloaddition of Azides with Electron-Deficient Alkynes Under Mild Condition in Water. *Tetrahedron Lett*. 45, 3143-3146.

[80]. Camperi, S. A., Marani, M. M., Iannucci, N. B., Côté, S., Albericio, F., and Cascone, O. (2005) An Efficient Strategy for the Preparation of One-Bead-One-Peptide Libraries on a New Biocompatible Solid Support. *Tetrahedron Lett*. 46, 1561-1564.

[81] García-Martín, F., White, P., Steinauer, R., Côté, S., Tulla-Puche, J., and Albericio, F. (2006) The synergy of ChemMatrix resin® and pseudoproline building blocks renders Rantes, a complex aggregated chemokine. *Peptide Science* 84, 566-575.

[82] García-Martín, F., Quintanar-Audelo, M., García-Ramos, Y., Cruz, L. J., Gravel, C., Furic, R., Côté, S., Tulla-Puche, J., and Albericio, F. (2006) ChemMatrix, a Poly(ethylene glycol)-Based Support for the Solid-Phase Synthesis of Complex Peptides. *J. Comb. Chem.* 8, 213-220.

[83]. Mazzini, S., García-Martin, F., Alvira, M., Aviñó, A., Manning, B., Albericio, F., and Eritja, R. (2008) Synthesis of Oligonucleotide Derivatives using ChemMatrix Supports. *Chem. Biodiversity* 5, 209-218.

[84]. Chiou, S. (1984) DNA-Scission Activities of Ascorbate in the Presence of Metal Chelates. J Biochem. 96, 1307-1310.

[85]. Chiou, S., Chang, W., Jou, Y., Chung, H. M., and Lo, T. (1985) Specific Cleavages of DNA by Ascorbate in the Presence of Copper Ion Or Copper Chelates. *J Biochem*. 98, 1723-1726.

[86]. Wang, Y., and Van Ness, B. (1989) Site-Specific Cleavage of Supercoiled DNA by ascorbate/Cu(II). *Nucl. Acids Res*. 17, 6915-6926.

[87]. Kanan, M.W., Rozenman, M. M., Sakurai, K., Snyder, T. M., and Liu, D. R. (2004) Reaction discovery enabled by DNA-templated synthesis and in vitro selection. *Nature* 431, 545-549.

[88]. Newton, C. R., Greene, A. R., Heathcliffe, G. R., Atkinson, T. C., Holland, D., Markham, A. F., and Edge, M. D. (1983) Ion-Exchange High-Performance Liquid Chromatography of Oligodeoxyribonucleotides using Formamide. *Anal. Biochem*. 129, 22-30.

[89]. Haupt, W., and Pingoud, A. (1983) Comparison Of Several High-Performance Liquid Chromatography Techniques For The Separation Of Oligodeoxynucleotides According To Their Chain Lengths. *J. Chromatogr*.260, 419–427.

[90]. Turner, J. J., Arzumanov, A. A., and Gait, M. J. (2005) Synthesis, Cellular Uptake and HIV-1 Tat-Dependent Trans-Activation Inhibition Activity of Oligonucleotide Analogues Disulphide-Conjugated to Cell-Penetrating Peptides. *Nucl. Acids Res*. 33, 27-42.

[91]. Alam, M.R., Dixit, V., Kang, H., Li, Z-B., Chen, X., Trejo, J., Fisher, M. and Juliano, R.L. (2008) Intracellular Delivery Of An Anionic Antisense Oligonucleotide Via Receptor-Mediated Endocytosis. *Nucl. Acids Res.*, 36, 2764-2776.

[92]. Eichhorn, G.L., Clark, P. and Becker, E.D. (1966) Interactions of Metal Ions with Polynucleotides and Related Compounds. VII. The Binding of Copper(II) to Nucleosides, Nucleotides, and Deoxyribonucleic Acids. *Biochemistry* 5, 245–253

[93]. Zimmer, C., Luck, G., Fritzsche, H., and Triebel, H. (1971) DNA-Copper (II) Complex And The DNA Conformation. *Biopolymers* 10, 441–463.

[94]. Chao, Y-Y.H., and Kearns, D.R. (1977) Magnetic Resonance Studies Of Copper (II) Interaction With Nucleosides And Nucleotides. *J. Am. Chem. Soc*. 99, 6425–6434.

[95]. Tajmir-Riahi, H.A., Langlais, M. and Savoie, R. (1988) A Laser Raman Spectroscopic Study Of The Interaction Of Calf-Thymus DNA With Cu(II) And Pb(II) Ions: Metal Ion Binding And DNA Conformational Changes. *Nucl. Acids Res*. 16, 751-762.

[96]. Sagripanti, J. L., Goering, P. L., and Lamanna, A. (1991) Interaction Of Copper With DNA And Antagonism By Other Metals. *Toxicol. Appl. Pharmacol.* 110, 477–485.

[97]. Duguid, J., Bloomfield, V. A., Benevides, J., Thomas, J. G., Jr. (1993) Raman spectroscopy of DNA-metal complexes. I. Interactions and conformational effects of the divalent cations: Mg, Ca, Sr, Ba, Mn, Co, Ni, Cu, Pd, and Cd. *Biophys. J.* 65, 1916–1928.

[98]. Tajmir-Riahi, H. A., Naoui, M., and Ahmad, R. (1993). The effects of Cu2+ and Pb2+ on the solution structure of calf thymus DNA: DNA condensation and denaturation studied by Fourier transform IR difference spectroscopy. *Biopolymers* 33, 1819–1827.

[99]. Sorokin, V. A., Valeev, V. A., Gladchenko, G. O., Sysa, I. V., Blagoi, Y. P., and Volchok, I. V. (1996) Interaction of bivalent copper, nickel, manganese ions with native DNA and its monomers. *J. Inorg. Biochem.* 63, 79–98.

[100]. Andrushchenko, V., Van De Sande, J. H., and Wieser, H. (2003) Vibrational Circular Dichroism and IR Absorption of DNA Complexes with Cu2+ Ions. *Biopolymers* 72, 374–390.

[101]. Löber, S., Rodriguez-Loaiza, P., and Gmeiner, P. (2003) Click Linker: Efficient And High-Yielding Synthesis Of A New Family Of SPOS Resins By 1, 3-Dipolar Cycloaddition. *Org. Lett*. 5, 1753–1755.

[102]. Löber, S., and Gmeiner, P. (2004) Click Chemistry On Solid Support: Synthesis Of A New REM Resin And Application For The Preparation Of Tertiary Amines. *Tetrahedron* 60, 8699–8702.

[103]. Bettinetti, L., Löber, S., Hübner, H., and Gmeiner, P. (2005) Parallel Synthesis and Biological Screening of Dopamine Receptor Ligands Taking Advantage of a Click Chemistry Based BAL Linker. *J. Comb. Chem*. 7, 309–316.

[104]. Gramlich, P.M. E., Warncke, S., Gierlich, J., and Carell, T. (2008) Click–Click–Click: Single to Triple Modification of DNA. *Angew. Chem. Int. Ed*. 47, 3442–3444.

[105]. Bouillon, C., Meyer, A., Vidal, S., Jochum, A., Chevolot, Y., Cloarec, J.P., Praly, J.P., Vasseur, J.J., and Morvan, F. (2006) Microwave Assisted "Click" Chemistry for the Synthesis of Multiple Labeled-Carbohydrate Oligonucleotides on Solid Support. *J. Org. Chem*. 71, 4700–4702.

[106]. Pourceau, G., Meyer, A., Vasseur, J.J., and Morvan, F. (2009) Synthesis of Mannose and Galactose Oligonucleotide Conjugates by Bi-click chemistry. *J. Org. Chem.* 74, 1218–1222.

[107]. Godeau, G. Staedel, C., and Barthélémy, P. (2008) Lipid-Conjugated Oligonucleotides via "Click Chemistry" Efficiently Inhibit Hepatitis C Virus Translation. *J. Med. Chem.* 51, 4374–4376

[108]. Gogoi, K., Mane, M. V., Kunte, S. S., and Kumar, V. A. (2007) A Versatile Method For The Preparation Of Conjugates Of Peptides With DNA/PNA/Analog By Employing Chemo-Selective Click Reaction In Water. *Nucleic Acids Res*. 35, e139.

[109]. Humenik, M., Huang, Y., Wang, Y., and Sprinzl, M. (2007) C-Terminal Incorporation Of Bio-Orthogonal Azide Groups Into A Protein And Preparation Of Protein-Oligodeoxynucleotide Conjugates By Cui Catalyzed Cycloaddition. *ChemBioChem* 8, 1103–1106.

[110]. Seo, T. S., Bai, X., Kim, D. H., Meng, Q., Shi, S., Ruparel, H., Li, Z., Turro, N. J., and Ju, J. (2005) Four-color DNA sequencing by synthesis on a chip using photocleavable fluorescent nucleotides. *Proc. Natl. Acad. Sci. U.S.A*. 102, 5926–5931.

[111]. Rozkiewicz, D.I., Gierlich, J., Burley, G.A., Gutsmiedl, K., Carell, T., Ravoo, B.J., and Reinhoudt, D.N. (2007) Transfer Printing of DNA by "Click" Chemistry. *Chem.Bio.Chem.* 8, 1997–2002.

[112]. Kumar, R., El-Sagheer, A., Tumpane, J., Lincoln, P., Wilhelmsson, L. M., and Brown, T. (2007) Template-Directed Oligonucleotide Strand Ligation, Covalent Intramolecular DNA Circularization and Catenation Using Click Chemistry. *J. Am. Chem. Soc*. 129, 6859–6864.

[113]. Nakane, M., Ichikawa, S., Matsuda, A. (2008) Triazole-Linked Dumbbell Oligodeoxynucleotides with NF-κB Binding Ability as Potential Decoy Molecules. *J. Org. Chem*. 73, 1842–1851.

[114]. Jacobsen, M.F., Ravnsbæk, J. B., and Gothelf, K.V. (2010) Small Molecule Induced Control In Duplex And Triplex DNA-Directed Chemical Reactions. *Org. Biomol. Chem*. 8, 50–52.

[115]. Lietard, J., Meyer, A., Vasseur, J.J., and Morvan, F. (2008) New Strategies for Cyclization and Bicyclization of Oligonucleotides by Click Chemistry Assisted by Microwaves. J. Org. Chem. 73, 191–200.

[116]. Cleland, W. W., Frey, P.A., and Gerlt, J.A. (1998) The Low Barrier Hydrogen Bond in Enzymatic Catalysis. J. Biol. Chem. 273, 25529-2553.

[117]. Ikeda, Y., Kawahara, S., Taki, M., Kuno, A., Hasegawa, T., Taira, K. (2003). Synthesis Of A Novel Histidine Analogue And Its Efficient Incorporation Into A Protein In Vivo. *Protein Eng.* 16, 699-706.

[118]. Abellán, T., Chinchilla, R., Galindo, N., Guillena, G., Nájera, C., and Sansano, J. M. (2000). Glycine And Alanine Imines As Templates For Asymmetric Synthesis Of α-Amino Acids. *Eur. J. Org. Chem.* 15, 2689-2697.

[119]. Kristolaitytè, S., Sackus, A., and Undheim, K. (2001). Alkylation Of Schöllkopf's Bislactim Ether Chiral Auxiliary With 4-Bromo-1,2-Butadiene. *Chemistry; The Lithuanian Acad. Sciences* 12, 76-79.

[120]. Carlsson, A., Jam, F., Tullberg, M., Pilotti, Å., Ioannidis, P., and Luthman, K. (2006). Microwave-Assisted Synthesis Of The Schöllkopf Chiral Auxiliaries: (3S)- And (3R)-3,6-Dihydro-2,5-Diethoxy-3-Isopropyl-Pyrazine. *Tetrahedron Lett., 47*, 5199-5201.

[121]. Beckmann, H. S. G., and Wittmann, V. (2007). One-Pot Procedure For Diazo Transfer And Azide-Alkyne Cycloaddition: Triazole Linkages From Amines. *Org. Lett. 9*, 1-4.

[122]. Zhang, L., Kauffman, G. S., Pesti, J. A., and Yin, J. (1997). Rearrangement Of Nα-Protected L-Asparagines With Iodosobenzene Diacetate. A Practical Route To β-Amino-L-Alanine Derivatives. *J. Org. Chem. 62*, 6918-6920.

[123]. Nyffeler, P. T., Liang, C., Koeller, K. M., and Wong, C. (2002). The Chemistry Of Amine-Azide Interconversion: Catalytic Diazotransfer And Regioselective Azide Reduction. *J. Am. Chem. Soc. 124*, 10773-10778.

CHAPTER 4

Oligonucleotides Conjugates Carrying Cu(II)

Complexes: Synthesis and Electrochemical Study

4.1. Introduction and aim of the work

The work described throughout this chapter covers the synthesis of oligonucleotide conjugates carrying Cu(II) complexes and the first steps in their electrochemical characterization using classical electrochemical techniques such as cyclic voltammetry. This latter part was carried out during a FPI predoctoral short-term staying in the laboratory of Dr. Schiffrin, in the Centre for Nanoscale Science at the University of Liverpool.

This work is a collaborative effort financed by the European Communities under the project DYNAMO. Our group's task is to construct molecular scaffolds made from DNA molecules to support and link arrays of electrochemical oscillators. The oscillatory devices are based on periodical switching between coordination geometry of inorganic copper complexes. Cyclic tetradentate ligands with N or S donor atoms can be accommodated by tetrahedral Cu(I) complexes as well as octahedral Cu(II) complexes [1-6]. By reducing externally the Cu(II) state, the coordination geometry changes from octahedral to tetrahedral which results in a change in electron transfer properties. By allowing the chemical reoxidation of the Cu(I) complex a periodic behaviour is expected.

The work developed in this thesis covers the linking of Cu(II) complexes with oligonucleotides and the initial electrochemical characterization of the conjugates.

4.2. Design of oligonucleotides

In order to perform electrical measurements on DNA a method to link the oligonucleotides to the electrode surface is needed. In this work oligonucleotides conjugated to tetradentate copper ligands will be immobilized onto gold electrodes. The most common strategy for covalent DNA attachment on gold surfaces involves the use of gold-thiol self-assembled monolayer (SAM) chemistry. Thus, modification of DNA strands with an alkane thiol enables their chemisorption to gold electrodes.

Commercially available reagents shown in figure 4.1 have been used to introduce a disulfide group at the 3' or the 5' end of ODNs. The disulfide group may be reduced to thiol groups which are capable to form sulfur-gold bonds. Disulfide modified ODNs can be also anchored directly (without previous reduction) to gold surfaces as proposed by some authors [7,8].
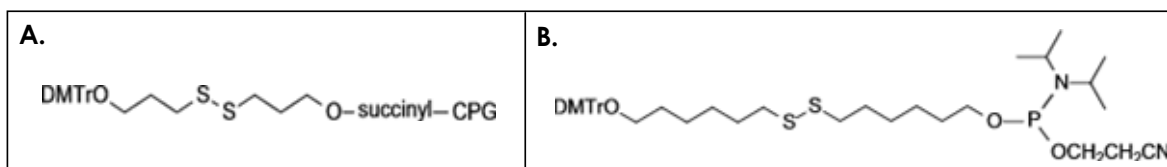
Figure 4.1. Chemical structure of the molecules used for derivatization of oligonucleotides with thiol groups. A) 3'-Thiol-modifier C3 S-S CPG. B) Thiol-modifier C6 S-S cyanoethyl (CE) phosphoramidite.

The 3'-Thiol-Modifier C3 S-S CPG support was used directly in the automatic synthesizer. After the first detritylation step oligonucleotides were assembled as usual. For the synthesis of sequences with the thiol group at the 5' end the thiol-modifier C6 S-S CE phosphoramidite was coupled in the last cycle using standard conditions.

A 15-mer oligonucleotide sequence containing the four nucleobases (**ODN 15C**) was synthesized together with its complementary sequence (**ODN 15Ccompl**). Thiol groups were inserted in position 3' or 5' as indicated in Table 4.2. Reduction of disulfide bonds to thiol groups will be explained later.

N_o.	ODN	Sequence
1	15C	$3'$-CGTTACCTCGGAGAT-$5'$
2	15Ccompl	$3'$-ATCTCCGAGGTAACG-$5'$
3	$3'$-disulfide-15C	HO-$(CH_2)_3$-S-S-$(CH_2)_3$-OPO_3-$3'$CGTTACCTCGGAGAT-$5'$
4	15Ccompl-$5'$-disulfide	$3'$-ATCTCCGAGGTAACG-$5'OPO_3$-$(CH_2)_6$-S-S-$(CH_2)_6$-ODMT
5	$3'$-thiol-15C	HS-$(CH_2)_3$-OPO_3-$3'$CGTTACCTCGGAGAT-$5'$
6	15Ccompl-$5'$-thiol	$3'$-ATCTCCGAGGTAACG-$5'OPO_3$-$(CH_2)_6$-SH

Table 4.2. Oligonucleotides used for electrochemistry studies.

Oligonucleotides **15C** and **$3'$-disulfide-15C** were functionalized with a copper tetradentate ligand. In this way, three different systems could be used for electrochemical studies, as represented in Scheme 4.3.
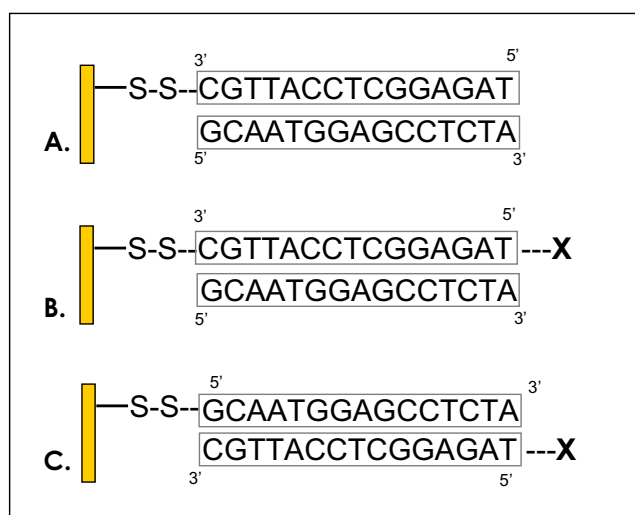
Scheme 4.3. Different systems used in electrochemical studies, where **X** represents the copper ligand. A) Control system to study copper interaction with a double strand DNA (dsDNA) that does not contain the chelating unit. B) The copper ligand is tethered to an ODN attached to the gold surface. C) The copper ligand is tethered to an ODN hybridized with the covalently gold-attached strand.

The copper chelating units were the aza- and thio-crown ethers depicted in Figure 4.4. The 1,4,8,11-Tetraazacyclotetradecane (A), known also as "cyclam", is commercially available meanwhile 1,5-diaza-9,13-dithiacyclohexadecane (B) was prepared by the group of Professor Håkansson, a partner of DYNAMO with extensive experience in organometallic synthesis and study of metal complexes and coordination compounds.
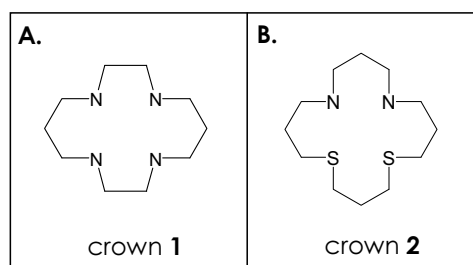
Figure 4.4. A) Commercially available 1,4,8,11-Tetraazacyclotetradecane or "cyclam". B) 1,5-diaza-9,13-dithiacyclohexadecane, synthesized in the group of Dr. Håkansson.

4.3. Synthesis of oligonucleotides carrying copper-chelating units

For tethering the cyclic ligands to the 5' end of the desired sequences two coupling chemistries were tested. In the first approach the formation of an amide bond between one of the secondary amines of the copper chelate and an activated ester in the 5' end of the oligonucleotide was studied. To this end, the N-hydroxysuccinimide ester group of the C10 carboxy modifier phosphoramidite was used (Scheme 4.5)
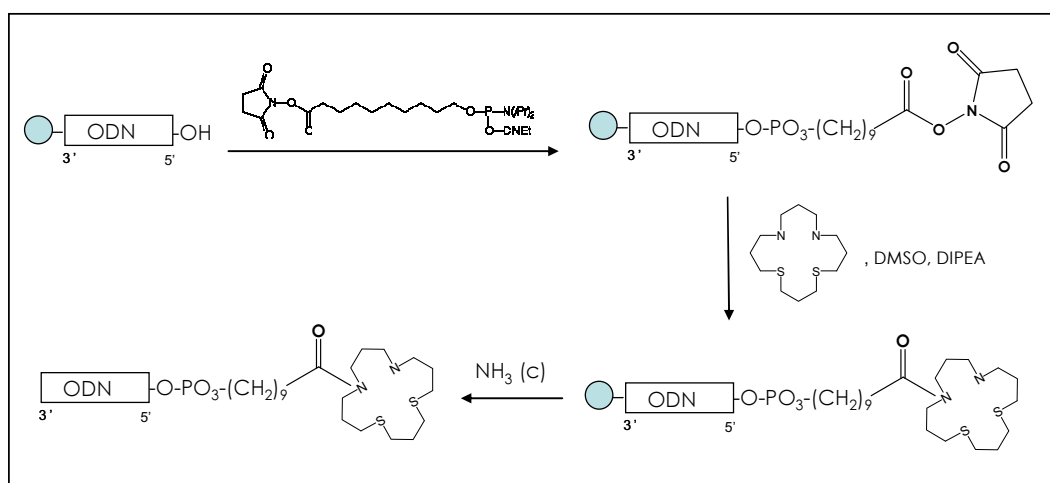
Scheme 4.5. First protocol used for the conjugation of oligonucleotides with the desired copper chelates.

The second method (scheme 4.6) consists in an alkylation reaction between the secondary amino groups of the copper chelates and an alkyl bromide moiety previously inserted in the oligonucleotide chain using the phosphoramidite synthesized in chapter 3.
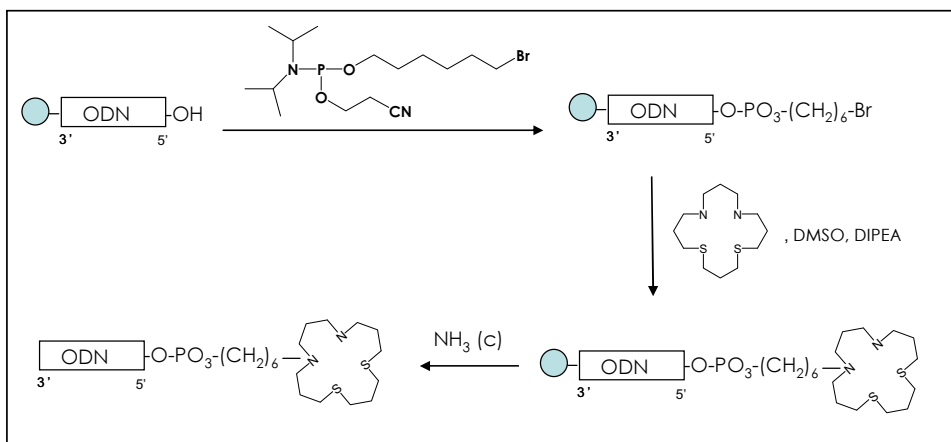
Scheme 4.6. Second protocol used for the conjugation of oligonucleotides with the desired copper chelates.

Only this second approach allowed the obtention of the desired products. Problems encountered in the first protocol as well as the synthesis of the modified sequences using the second protocol are explained below.

ODNs 15C and [3'-disulfide-15C] were synthesized on a 1 μmol scale and the C10 carboxy modifier phosphoramidite was coupled using the conventional coupling cycle. A small fraction of the 5'-NHS-ODN-supports was cleaved with concentrated aqueous ammonia and analyzed by HPLC. Chromatograms presented a major peak which was collected, desalted by NAP-5 and analyzed by MALDI-TOF (Figure 4.7). Molecular weight values were in agreement with the expected mass. As NH_3 hydrolyses the NHS group, MWs correspond to the values calculated for sequences with a carboxamide group (ODN-[5']-OPO_3-$(CH_2)_9$-$CONH_2$).
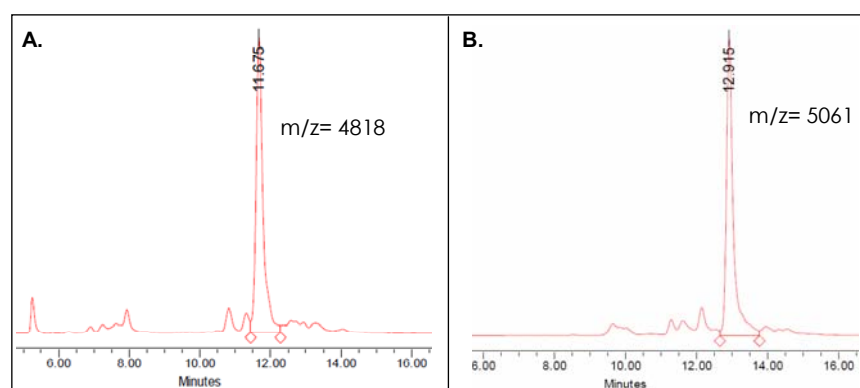
Figure 4.7. HPLC analysis of the ODNs modified with the C10 carboxy modifier phosphoramidite. A) 15C and B) [3']-disulfide-15C. The m/z values obtained by MALDI-TOF are indicated next to each peak. Gradient: 5 → 35% B in 20 min (A: 5% ACN in 0.1 M TEAAc pH 6.5; B: 70% ACN in 0.1 M TEAAc pH 6.5).

Later on, the 5'-NHS-ODN-supports were treated during 4-5 hours at 55ºC with a high excess of the cyclic copper ligands (50-100 equivalents) dissolved in DMSO (for the case of crown **2**) or DCM (for 'cyclam') with 5% of DIPEA. After elimination of the reagents by filtration, the resulting supports were treated with aqueous ammonia to remove the protecting groups and release the oligonucleotides from the supports. A subsequent analysis by HPLC revealed the formation of several products, as can be seen in the chromatographic profiles in Figure 4.8.
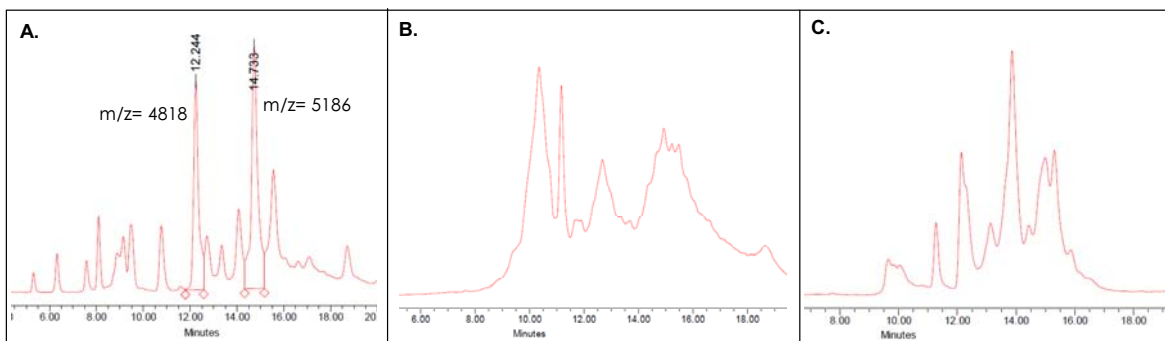
Figure 4.8. HPLC profiles of A) 15C-5'-NHS solid support reacted with crown **2**. B) 3'-disulfide-15C-5'-NHS solid support reacted with crown **2** and with C) *cyclam*. Gradient: 5 → 35% B in 20 min (A: 5% ACN in 0.1 M TEAAc pH 6.5; B: 70% ACN in 0.1 M TEEAc pH 6.5).

Only the chromatogram of figure 4.8.A presented enough resolution to collect some product and analyze them by MALDI-TOF. However the m/z obtained for the first peak corresponds to the starting material and the second peak gave a MW 95 units higher than expected.

Analysis of the resulting products was performed by denaturing PAGE. Figure 4.9 shows the results. Below, Table 4.10 indicates the samples that were run in each lane.
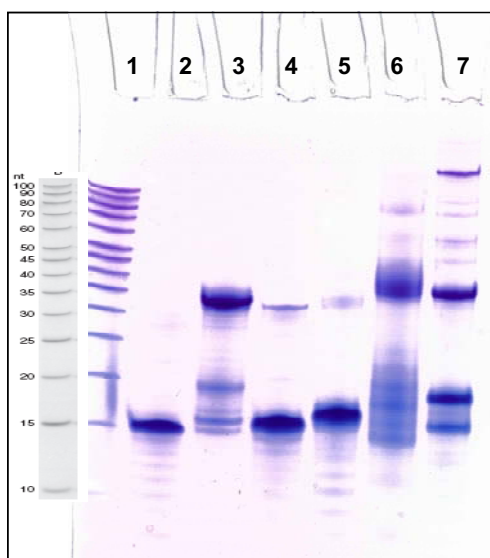
Figure 4.9. PAGE analysis (20% polyacrylamide, TBE buffer) of samples indicated in Table 4.10.

Lane	Sample
1	Marker (10-100 nt)
2	15Ccompl
3	$15C^{5'}$-OPO_3-$(CH_2)_9$-CONH-crown**2** (HPLC; t_R=14.7min)
4	HO-$(CH_2)_3$-S-S-$(CH_2)_3$-OPO_3-$^{3'}15C$
5	HO-$(CH_2)_3$-S-S-$(CH_2)_3$-OPO_3-$^{3'}15C^{5'}$-OPO_3-$(CH_2)_9$-$CONH_2$
6	HO-$(CH_2)_3$-S-S-$(CH_2)_3$-OPO_3-$^{3'}15C^{5'}$-OPO_3-$(CH_2)_9$-CONH-crown**2**
7	HO-$(CH_2)_3$-S-S-$(CH_2)_3$-OPO_3-$^{3'}15C^{5'}$-OPO_3-$(CH_2)_9$-CONH-*cyclam*

Table 4.10. Oligonucleotide samples loaded in the different lanes of the denaturing gel.

Lanes 3, 6 and 7 showed a band corresponding to oligonucleotides with a length twice than expected. It seems as if one crown had been conjugated through more than one nitrogen atom, resulting in two DNA strands attached to the same single tetradentate ligand. As the reaction was performed using a 50-100 excess of the copper chelate, this could be only explained for an increase in nucleophilic character of the rest of donor atoms once one of the nitrogens has formed an amide bond.

Analysis by anion exchange chromatography (AEC) also confirmed that oligonucleotides longer than 15 bases were obtained. Figure 4.11 shows a comparison between the 5'-NHS-15C injected before and after the reaction with crown **2**.
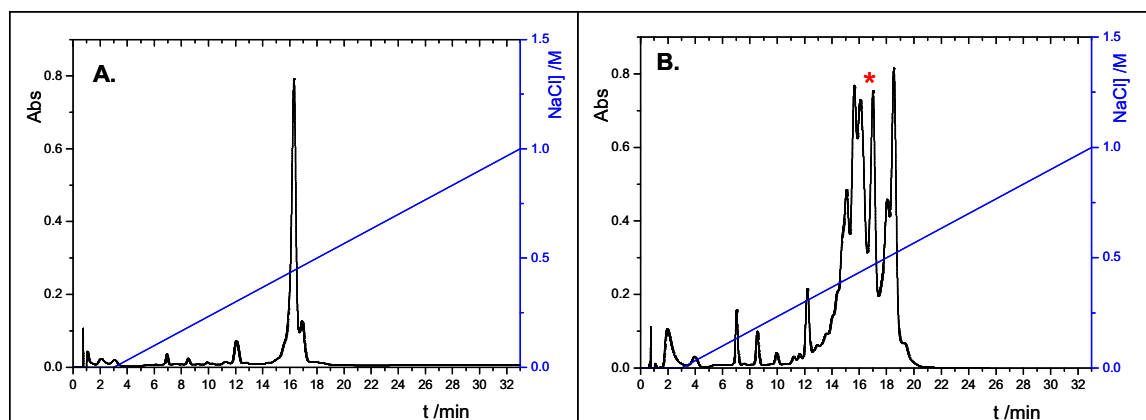
Figure 4.11. Anion exchange chromatography (AEC) profiles of A) 5'-NHS-15C and B) 5'-NHS-15C conjugated with crown **2.** Gradient: 0 → 50% B in 30 min (A: 20 mM tris·HCl, pH=8, 50% formamide; B: 20 mM tris·HCl, pH=8, 50% formamide, 2M NaCl).

In figure 4.11.B peaks eluting before the starting material are suggested to correspond to the 5'-crown-oligonucleotide complexed with HPLC buffer cations, e.g. NEt_4^+. ODNs eluting later than 16' (marked with an *) correspond to strands longer than the starting material, as the higher t_R implies a higher content in negative charges.

The failure of this method for functionalization of oligonucleotides with copper ligands led to think of a second procedure. A paper published by Wu and Pitsch [9], in which described the reaction between a bromopentyl-substituted nucleoside and 1-aza-18-crown-6, led to consider the use of the 6-bromohexyl-phosphoramidite (used previously in chapter 3 for azide group introduction) as an intermediate for the introduction of our copper chelating compounds.

15C and **3'-disulfide-15C** were functionalized with a bromohexyl group as described previously (section 3.5.3 of chapter 3). Then, 0.2 μmol of each $^{5'}$Br-$(CH_2)_6$-ODN-support was incubated with a solution of 100 equivalents of crown in DCM (in the case of 'cyclam') or DMSO (for crown **2**) with 5% of DIPEA at 55ºC for one day. After deprotection and cleavage from the support, products were examined by HPLC. Chromatographic profiles are shown in figure 4.12.
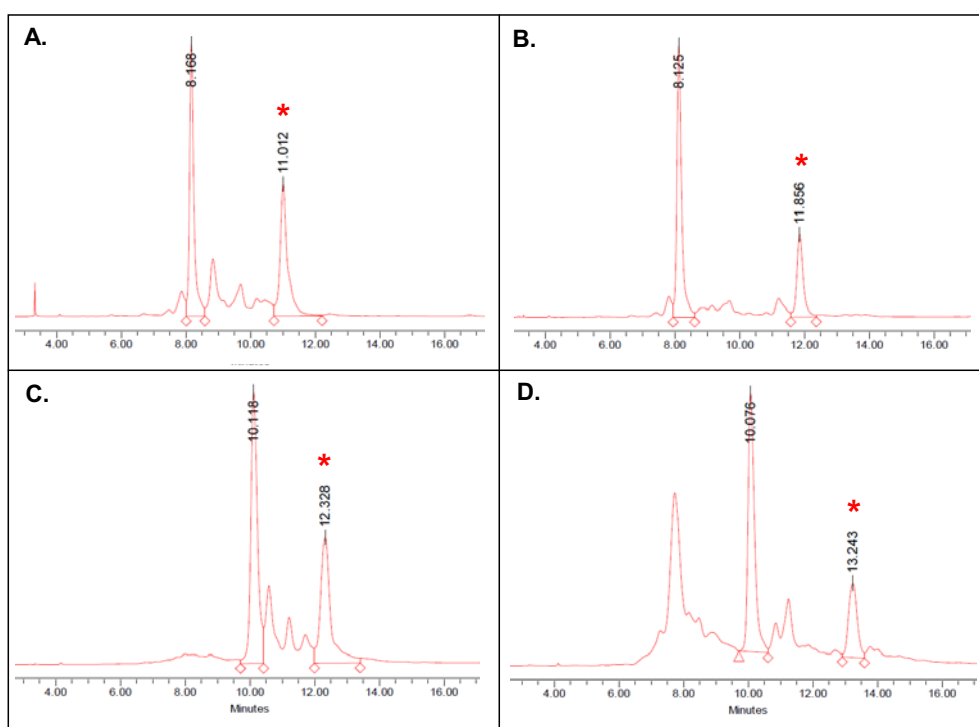
Figure 4.12. HPLC profiles of A) 15C-OPO$_3$-$(CH_2)_6$-Br conjugated with crown **1**. B) 15C-OPO$_3$-$(CH_2)_6$-Br conjugated with crown **2**. C) $^{3'}$-disulfide-15C-OPO$_3$-$(CH_2)_6$-Br conjugated with crown **1**. D) $^{3'}$-disulfide-15C-OPO$_3$-$(CH_2)_6$-Br conjugated with crown **2**. Gradient: 5 $\rightarrow$ 35% B in 20 min (A: 5% ACN in 0.1 M TEAAc pH 6.5; B: 70% ACN in 0.1 M TEAAc pH 6.5).

In all cases, the highest peak comes from the nucleophilic substitution of bromine atom by NH$_3$ to give 5'-aminohexyl-oligonucleotides. But in all chromatograms a new peak was observed (marked with an * in figure above) that was collected and analyzed by MALDI-TOF spectrometry, having the desired molecular weight. Although the desired compounds were obtained in moderate yields (≤30%), the functionalization of oligonucleotides with the crown molecules was achieved.

Measured masses of the purified ODNs, their calculated theorical values and the yield calculated from relative peak areas are listed in Table 4.13.

Sample	t_R (min)	Yield (%)	Found MW	Expected MW
15C-$^{5'}$-crown**1**	11.01	31	4929.7	4927.9
15C-$^{5'}$-crown**2**	11.86	23	4988.5	4991.9
$^{3'}$-disulfide-15C-$^{5'}$-crown**1**	12.33	25	5168.8	5171.9
$^{3'}$-disulfide-15C-$^{5'}$-crown**2**	13.24	10	5228.1	5235.9

Table 4.13. Retention time on HPLC, yield and molecular weight (MW) obtained by MALDI-TOF of the oligonucleotides conjugated with the copper chelating compounds.

4.4. Copper chelation studies with the 5'-crown-oligonucleotides

In order to analyze the copper complexation properties of the oligonucleotide carrying copper complexes a preliminary study was carried out. Firstly, UV spectra of 1 mM crown solutions in absence and presence of Cu(II) was registered. For both crowns an absorption band with a maximum around 370 nm was observed only in the presence of copper, which indicates that this metal is coordinated by the tetradentate ligands. However, concentration of ligand required to give an acceptable UV signal is too high to study copper complexed in crowns tethered to DNA (as oligonucleotide solutions are in the range of micromolar concentration).

In order to study the ability of crowns linked to DNA for chelating copper (II) the modified sequences were incubated with a solution containing this cation and analyzed by MALDI-TOF after removing the excess of copper by molecular sieve filtration. Therefore, 1 O.D of each 5'-crown-ODN was incubated overnight with 10 equivalents of $CuCl_2$ in 0.5 ml of milliQ water at 4ºC. The excess of copper was removed by passing the solution through a NAP-5 (Sephadex G-25) column. MW obtained after this step are listed in table 4.14.

Sample	Found MW	Expected MW[a]
15C-$^{5'}$-crown**1** /Cu^{2+}	4996.5	4991.4
15C-$^{5'}$-crown**2** /Cu^{2+}	5000.2	5055.4
$^{3'}$-disulfide-15C-$^{5'}$-crown**1** /Cu^{2+}	5243.4	5235.4
$^{3'}$-disulfide-15C-$^{5'}$-crown**2** /Cu^{2+}	5243.1	5299.4

Table 4.14. MW obtained by MALDI-TOF of the oligonucleotides conjugated with crowns after chelation of copper. [a] The theoretical MW values are calculated for the case of chelation of one Cu^{2+} atom per strand.

Oligonucleotides derivatized with crown **2** did not appear to chelate Cu (II) or at least not strong enough to remain bound after passing through the desalting cartridge.

In the case of DNA strands conjugated to *cyclam*, MALDI spectra presented a major peak that was in agreement with the MW calculated for 5'-*cyclam*-ODN with one copper atom. However, minor peaks corresponding to the ODN with more than one copper atom were also observed. This was attributed to unspecific adsorption of copper ions on the DNA strand (e.g. electrostatic interaction with the backbone phosphate groups or guanine coordination) since a ladder of small peaks corresponding to the product with several copper atoms was also present in the MALDI spectra of oligonucleotides without crown.

Finally, purified oligonucleotides modified with *cyclam* were aliquoted in different fractions, concentrated to dryness and kept frozen until performing electrochemical studies at Liverpool University. Samples used for copper chelation studies are kept separately, to compare the electrochemical behaviour of copper inserted using this protocol and copper that will be chelated once the ODNs have been immobilized on the electrodes.

4.5. Overview of Electrochemistry fundamentals

In this section basic principles of electrochemistry will be overviewed before describing the electrochemical methods applied to the study of our systems. Although the most relevant equations will be presented throughout this chapter, reference [10] must be consulted for a rigorous mathematical analysis.

Electrochemistry is the branch of science that deals with the study of chemical reactions which involve electron transfer processes and that take place at the interface between an electrode (electronic conductor) and an electrolyte (ionic conductor). These processes in which electrons are transferred between molecules are called oxidation (loss of electrons) or reduction (gain of electrons) reactions.

Experimentally, electrochemical systems are defined generally as two electrodes where reductions (cathode) and oxidations (anode) occur, separated by at least one electrolyte phase and connected by an external electric circuit integrated in a device known as electrochemical cell. The overall chemical reaction taking place in this cell is comprised of two independent half-reactions each of which responds to the interfacial potential difference at the corresponding electrode. Thus, measurement and control of cell potential is one of the most important aspects of experimental electrochemistry.

Most of the time, only one of these half-reactions is the focus of interest and the electrode at which it occurs is called the working electrode (W.E). The other half of the cell is standardized by using a reference electrode (R.E) which is comprised of phases having essentially constant composition and has a fixed potential. In many electrochemical experiments three-electrode cells are used. In this arrangement a third electrode known as auxiliary (or counter) electrode (C.E) is used to supply electrons needed to balance the current observed at the working

104

electrode and to ensure that current does not run through the reference electrode which would disturb its potential.

The different electrodes used in electrochemical experiments performed in this work are described below:

- Working electrode

There are various types of working electrodes but disk electrodes are the most popular. Common materials used for disk electrodes are platinum, silver, gold, glassy carbon, graphite, etc. In this work a gold disk embedded in an insulating Teflon cylinder was used.

- Reference electrode

Internationally accepted primary reference is the standard hydrogen electrode (SHE), or normal hydrogen electrode (NHE) based on the redox of hydrogen occurring at a platinum electrode which is written schematically as $Pt/H_2/H^+$. However, potentials are often measured with respect to reference electrodes other than NHE which is not very convenient from an experimental point of view.

A widely used reference electrode is the saturated calomel electrode (SCE), which is $Hg/Hg_2Cl_2/KCl$ (saturated in water) and has a potential of 0.242 V *versus* NHE. In table 4.15 the reference electrodes used in this work with their potential values respect to the NHE and SCE are listed.

Reference electrode	Potential	
	vs NHE	*vs* SCE
Hg/Hg_2Cl_2, KCl (saturated in H_2O)	0.242	**0**
Ag/AgCl, NaCl (3M in H_2O)	0.209	-0.035
Hg/Hg_2SO_4, K_2SO_4 (saturated in H_2O)	0.64	0.40

Table 4.15. Reference electrodes used in this work and their potential value *vs* NHE and SCE at 25ºC.

- Counter electrode

A platinum wire was used as auxiliary electrode. Its surface area must be larger than that of the working electrode to ensure that the reactions occurring on the working electrode are not surface area limited by the auxiliary electrode.

These three electrodes are inserted in an electrochemical cell, and immersed in the electrolyte solution, as represented in scheme 4.16.
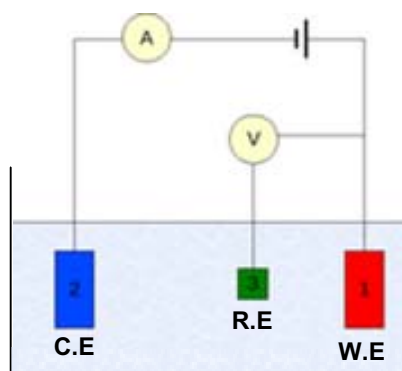
Scheme 4.16. Three-electrode setup: (1) working electrode; (2) auxiliary electrode; (3) reference electrode.

In a typical electrochemical experiment the potential difference between the working electrode and the reference electrode is varied by means of an external power supply. This is equivalent to controlling the energy of the electrons within the working electrode. By driving the electrode to more negative potentials the energy of electrons is raised. If they reach a level high enough to transfer into vacant electronic states on species in the electrolyte, a reduction current will flow from electrode to solution (figure 4.17.A). Similarly, the energy of electrons can be lowered by imposing a more positive potential, and at a certain point electrons of electrolyte species will find a more favourable energy on the electrode and will transfer there (oxidation current, figure 4.17.B)
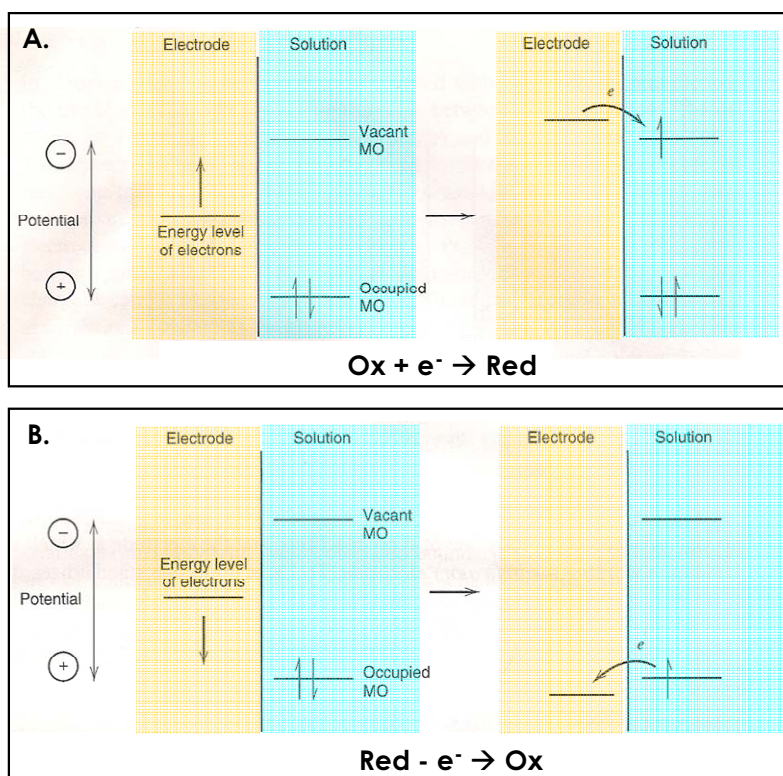
Figure 4.17. Schematic representation of A) reduction and B) oxidation process of a species in solution. A depiction of highest occupied molecular orbital (MO) and lowest vacant MO is shown.

These electron transfer processes are governed by Faraday's law (the amount of chemical reaction caused by the flow of current is proportional to the amount of electricity passed) that is, the passage of 96485,4 Coulombs ($1C=6,24\cdot10^{18}$ electrons) produces 1 mole of product in a one-electron transfer reaction. The current (i) is the rate of flow of coulombs and its fundamental unit according to the SI is the ampere (1 A=1 $C\cdot s^{-1}$).

The critical potentials at which these processes occur are related to the standard potentials, E^0, which is specific for each redox couple and is related to the electrode potential by the Nerst equation:

$$E = E^0 + \frac{RT}{nF} \ln \frac{a_{Ox}}{a_{Red}}$$

where R is the universal gas constant (R = 8.314 $J\cdot K^{-1}\cdot mol^{-1}$), T is the temperature (K), n is the number of electrons involved in the process, F is the Faraday constant (the number of coulombs per mole of electrons; F = 96485,4 $C\cdot mol^{-1}$), and a_{ox} and a_{red} are the activities of *ox* and *red*, respectively. In terms of concentrations of ox and red species, the equation can be also written as follows:

$$E = E^{0\prime} + \frac{RT}{nF} \ln \frac{[Ox]}{[Red]}$$

where $E^{0\prime}$ is the potential at [Ox]=[Red] and is often called the formal potential.

However, the potential at which the redox event is experimentally observed does not always match with the value one would predict from thermodynamics. The additional potential (beyond the thermodynamic requirement) needed to drive a reaction at a certain rate is called the overpotential, and is described by the following equation:

$$\eta = E - E_{eq}$$

When the overpotential (η) is very small (e.g. <5 mV) for the entire current region to be measured, the electrode process is said to be **reversible**, and the redox couple exhibits a Nerstian behaviour at the electrode surface. On the other hand, if a large overpotential is needed for the current to flow, the electrode process is said to be **irreversible**.

Not only electron transfer processes but also transport of the electroactive species from the bulk of the solution to the electrode and vice versa must be considered. For example, when a reduction current flows, Ox at the electrode surface is consumed to generate Red and the surface concentration of Ox becomes lower than that in the bulk of the solution. Then, a concentration gradient is formed near the electrode surface and Ox is transported from the bulk of the solution toward the electrode surface. Inversely, the surface concentration of Red becomes

higher than that in the bulk of the solution and Red is transported away from the electrode surface.

Others factors affecting electrode reaction rate include chemical reactions preceding or following the electron transfer or surface reactions such as adsorption or desorption. Scheme of figure 4.18 shows the possible steps involved in the pathway of a general electrode redox reaction.
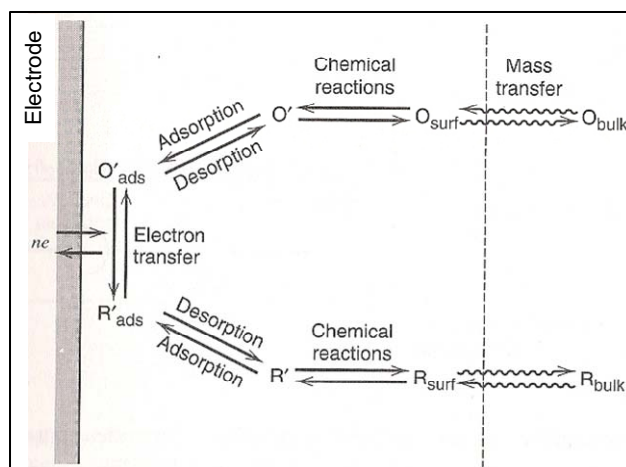
Figure 4.18. Steps involved in a general electrode reaction, O + ne^- → R.

When a steady-state current is obtained, the rates of all the reaction steps are the same. The magnitude of this current is limited by the rate of the slowest reaction called rate-determining step.

Regarding the mass transfer from the bulk solution to the electrode surface, three modes of contribution can be remarked: diffusion, caused by the movement of species due to a concentration gradient; migration: caused by the movement of charged species due to a gradient of electrical potential and convection, caused by the movement of species due to external mechanical forces, as stirring or by temperature gradient in the solution.

Usually laboratory electrochemical experiments are designed so that one or more of the contributions to mass transfer are negligible. Two types of conditions predominate:

- Unstirred solutions (to eliminate convection mode) with a large excess of a base electrolyte (to reduce migration mode, because ions of the base electrolyte will, rather than charged species, which migrate). Thus, mass transfer will be mainly diffusion controlled.

- Experiments carried out with a well defined convective regime, as in the case of voltammetry with rotating disk electrode.

In the next section electrochemical techniques used in this thesis will be outlined as well as their application for the study of different electrochemical systems, including an insight into the redox properties of copper within the crown conjugated to a DNA strand.

4.6. Electrochemical techniques used in electrochemical analysis

4.6.1. Cyclic voltammetry

Cyclic voltammetry (CV) is perhaps the most widely used electrochemical technique, and is frequently used for the characterization of a redox system. In this method the current at the working electrode is measured while the potential is swept linearly versus time like in linear sweep voltammetry (LSV). The rate of change of potential with time is referred to as the scan rate (v, in V/s). In CV, when a set potential is reached the working electrode's potential ramp is inverted, as it is show in the waveform of figure 4.19. This cycle can happen multiple times during a single experiment.
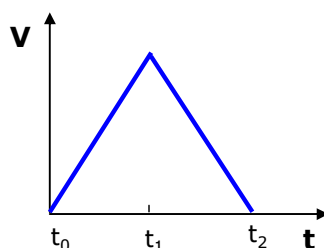
Figure 4.19. Typical triangular waveform applied potential in CV experiments.

For an example where only the reduced form of the species is initially present the basic shape of the current response for a cyclic voltammetry experiment is shown in figure 4.20.
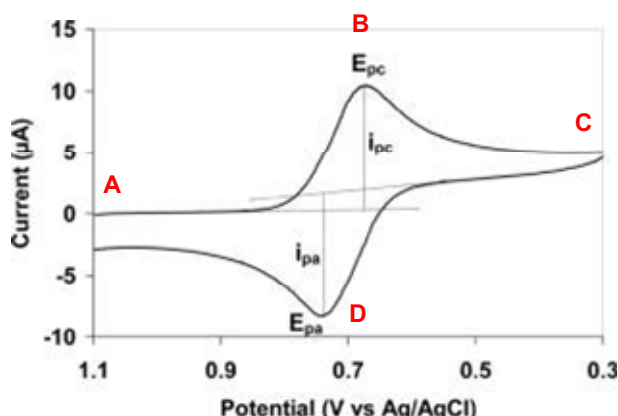
Figure 4.20. Typical cyclic voltammogram for a reversible process.

At the start of the experiment, the bulk solution contains only the reduced form of the redox couple (Red) so that at potentials lower than the redox potential,

i.e. the initial potential, there is no net conversion of Red into Ox, the oxidised form (point **A**). As the redox potential is approached, there is a net anodic current which increases exponentially with potential. As Red is converted into Ox, concentration gradients are set up for both Red and Ox, and diffusion occurs down these concentration gradients. At the anodic peak (point **B**), the redox potential is sufficiently positive that any Red that reaches the electrode surface is instantaneously oxidised to Ox. Therefore, the current now depends upon the rate of mass transfer to the electrode surface and its intensity decreases as the concentration of the analyte is depleted close to the electrode surface (and thickness of the diffusion layer increases with time) which results in an asymmetric peak shape.

Upon reversal of the scan (point **C**), the current continues to decay until the potential nears the redox potential. At this point, a net reduction of Ox to Red occurs which causes a cathodic current and produces a peak shaped response (point **D**).

For a reversible process, the cathodic and anodic peak currents are equal in magnitude ($|i_{pc}| = |i_{pa}|$) and its value increases linearly with the square root of the scan rate (ν), as expressed by the Randles-Sevcik equation:

$$i_{\mathrm{p}} = (2.69 \times 10^5) n^{3/2} A D^{1/2} \nu^{1/2} C \quad [25^\circ C]$$

where n is the number of electrons involved in the redox process, A is the area of the electrode (cm^2), D is the diffusion coefficient ($cm^2 \cdot s^{-1}$) and C the concentration ($mol \cdot cm^{-3}$) of the electroactive species. i_p and ν units are amperes and $V \cdot s^{-1}$, respectively.

In a reversible system, E_p is independent of scan rate and the peak potential separation ($\Delta E_p = E_{pa} - E_{pc}$) observed in the cyclic voltammogram is equal to $57/n$ mV, where n is the number of electron equivalents transferred in the redox process. By decreasing the reversibility, the difference between the two peak potentials increases.

4.6.2. Linear sweep voltammetry at Rotating Disk Electrodes

Rotating disk electrode (RDE) is a disk of electrode material imbedded in a rod of insulating material that is attached to a motor so it can be rotated at a certain frequency (usually described in terms of angular velocity). In this system, the solution away from the electrode is uniformly pumped towards the disk (figure 4.21.A), so that the convective regime is well defined. Thus, the mass transfer to and from the electrode can be treated theoretically by hydrodynamics.

The rotation of the electrode keeps the thickness of the diffusion layer time-independent, so a steady limiting current is obtained. Hence, the current-potential curve at the RDE is S-shaped and has a potential-independent limiting current region, as shown in the graphic of figure 4.21.B.
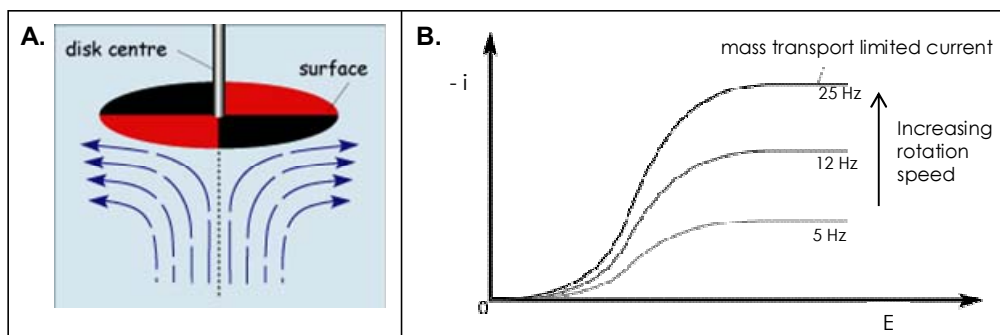
Figure 4.21. A) Schematic representation of the flow near a rotating disk. B) Typical current-potential curve for a voltammetry with rotating disk electrode.

The limiting current i_l (A) is expressed by Levich equation if it is controlled by mass transfer:

$$i_l = 0.62\, nF\pi r^2 \omega^{1/2} \nu^{-1/6} D^{2/3} C$$

where n is the number of electrons involved in the redox process, F is the Faraday's constant, r (cm) is the radius of the disk electrode, ω (rad·s^{-1}) is its angular velocity, ν (cm^2·s^{-1}) is the kinematic viscosity of the solution, D (cm^2·s^{-1}) is the diffusion coefficient of electroactive species, and C (mol·cm^{-3}) is its concentration. The limiting current is proportional to the square root of the rate of rotation.

4.6.3. Staircase voltammetry and differential pulse voltammetry

Differential pulse voltammetry (DPV) is considered as a derivative of staircase voltammetry, in which the potential sweep is a series of stair steps. Thus, the applied waveform involves a series of potential pulses, as shown in figure 4.22.A. The current is measured immediately before each potential pulse is applied (i_a) and immediately before the pulse ends (i_b), and the difference between these current responses (i_b-i_a) is used to produce the voltammogram (Figure 4.22.B)
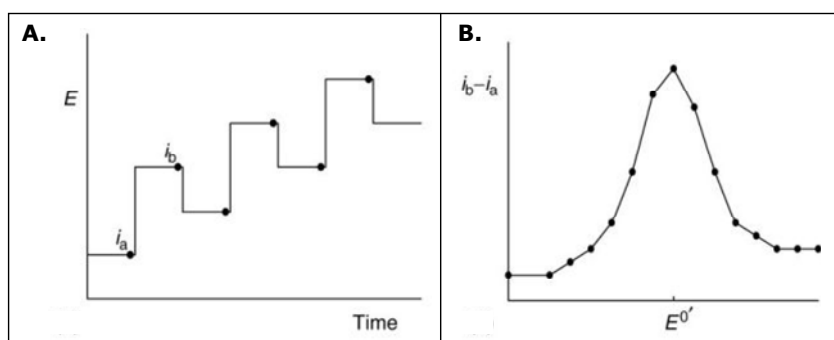
Figure 4.22. A) Diagram of the potential waveform used in DPV. B) Differential pulse voltammogram.

With this technique the charging current (noise) at the electrode is minimized so a high sensitivity is achieved.

111

Differential pulse voltammograms show symmetrical peaks for reversible reactions and the peak current is proportional to the concentration.

4.6.4. Chronoamperometry

Chronoamperometry is an electrochemical technique in which the potential of the working electrode is stepped largely enough to cause an electrochemical reaction and the resulting current is monitored as a function of time. Diagram of the excitation waveform used in chronoamperometry is shown in figure 4.23.A. Figure 4.23.B shows the current vs time response generated in this type of experiments.
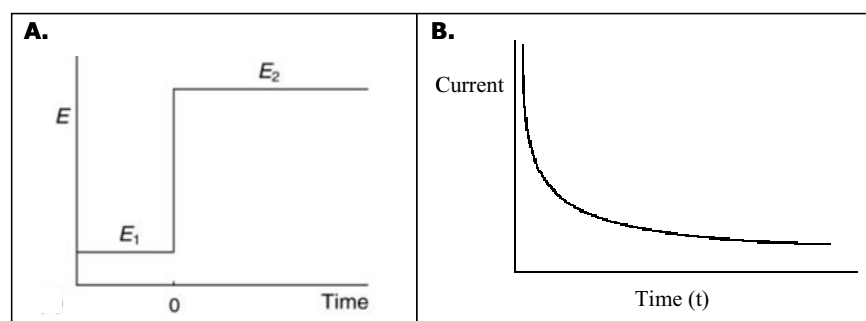
Figure 4.23. A) Diagram of the step potential used in chronoamperometry. B) Current vs. time response generated in a chronoamperometric experiment.

The electrode is initially held at a potential E_1 that does not cause oxidation or reduction of molecules in the solution. The potential is stepped to a value (E_2) that causes the immediate and complete reaction of any molecule in contact with the electrode. Hence, the concentration of the substance at the electrode surface goes immediately to zero, creating a concentration gradient between the electrode surface and the bulk solution that initiates diffusion of the substance towards the electrode. For diffusion controlled reactions the current-time relationship is known as Cottrell equation:

$$i = nFAD^{1/2}C\pi^{1/2}t^{-1/2}$$

where all the variables have the same meaning as before.

4.7. Considerations before getting started

For a successful electrochemical measurement several aspects should be considered before starting an experiment.

An important factor when using gold electrodes is the dependence of the response (in terms of activity, stability and reproducibility) on the electrode surface features such as lattice system, topography and roughness. In addition properties of gold substrate play also an important role in the self-assembly process of thiol

monolayers. Accordingly, the use of such electrodes requires precise and specific surface electrode pretreatment in order to obtain good results.

A great number of thermal [11,12], mechanical [13,14] and electrochemical [11-13,15-17] gold electrode pretreatment procedures have been described in the literature. In this work a mechanical polishing with alumina was firstly applied followed by an electrochemical cleaning under acidic conditions.

Cycling the electrode potencial in a 0.1 M sulfuric acid solution until a stable CV scan is achieved is a very common electrochemical cleaning technique [18,19]. Potential was cycled from -0.35 to 1.5 V (vs. SCE) at a rate of 4 V·s^{-1} until the CV becomes stable. Between these limits the cyclic voltammogram of clean gold shows an oxidation peak at $+1.3$V (vs. SCE) and a reduction peak at $+0.9$V (vs. SCE) corresponding to gold oxide formation and reduction (Figure 4.24). Furthermore, any residue of organic adsorbed material is removed during repeated oxidation and reduction of the gold. By finishing the scan at a negative (or low enough) potential an oxide-free gold surface was ensured.

In addition oxygen adsorption measurement can be used as a reliable method to calculate the electrochemical surface area of gold electrodes [20-22]. Usually, calculations of the real surface area, commonly expressed as a roughness factor, are based on the assumption that a monolayer of chemisorbed oxygen with a gold:oxygen ratio of 1:1 has been formed. The charge required for the reduction of this monolayer (Q_{Std}) is about 400 μC·cm^{-2} for polycrystalline gold [23-25]. Then, real electrochemical surface area is expressed as the ratio between the charge of the gold oxide reduction presented on the studied electrode surface (Q_{AuO}, determined by integration of the gold oxide stripping peak from the voltammetric curves) and Q_{Std}.

In figure 4.24 a voltammetric curve of a gold electrode in 0.1 M H_2SO_4 is shown. In the case illustrated in this graphic the scan was registered between 0.2 and 1.5 V (vs SCE) at a scan rate of 100 mV·s^{-1} after the multiple cycling explained above.
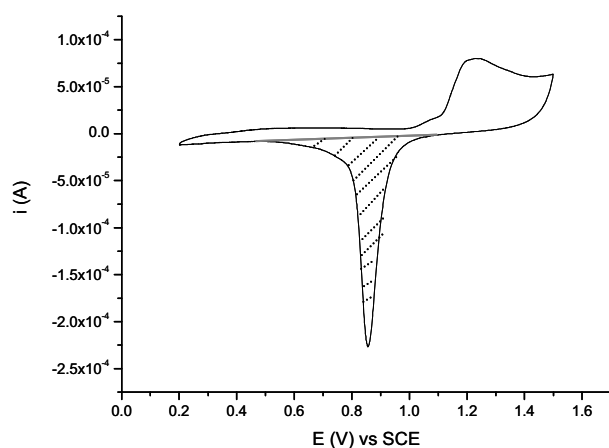
Figure 4.24. CV of a cleaned gold electrode in 0.1 M H_2SO_4 at 0.1 V·s^{-1}.

The area of the section marked with dotted lines corresponds to the charge required for stripping of the gold oxide monolayer formed. In this example a gold disk electrode of 5 mm of diameter was used and the roughness factor calculated as mentioned before gave a value of 2.5.

Before running any cyclic voltammetry study of electroactive species, it is very important to deaerate the electrolyte solution to avoid formation of oxide in the gold surface. Extensively bubbling of electrolyte solution with argon was performed before each experiment.

4.8. Study of a reversible redox reaction with different electrochemical techniques

In order to be properly introduced to theoretical electrochemical responses, the behaviour of a reversible redox reaction was studied with the techniques explained before. One of the most common redox reaction used to illustrate a reversible electrochemical response is the reduction of the ferricyanide ion to ferrocyanide:

$$[Fe(CN)_6]^{3-}_{(aq)} + e- \rightarrow [Fe(CN)_6]^{4-}_{(aq)}$$
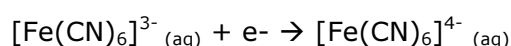
It is known that for this redox process, kinetics of electron transfer are fast and the mass transport is the major component which determines the reaction rate.

Firstly, cyclic voltammetry experiments of 10 mM $K_3Fe(CN)_6$ in 1 M $KNO_{3\,(aq)}$ supporting electrolyte were run between 0.3 and -0.4 V (*vs* Hg/Hg_2SO_4, K_2SO_4) at different scan rates. In figure 4.25 the cyclic voltammogram obtained at a sweep rate of 20 mV·s^{-1} is shown.
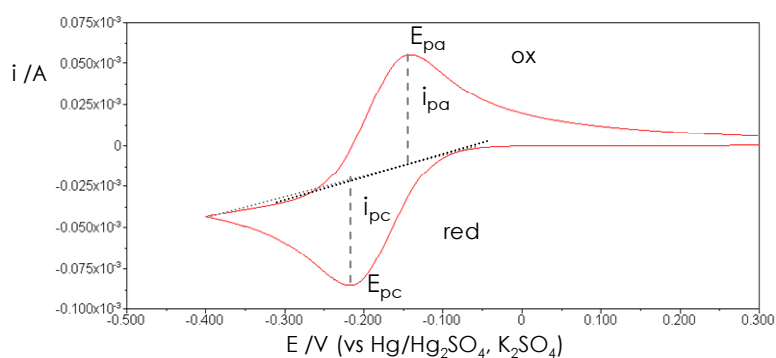
Figure 4.25. CV of 10 mM $K_3Fe(CN)_6$ in 1 M $KNO_{3\,(aq)}$ at 20 mV·s^{-1}.Parameters calculated for each voltammogram are depicted in the graphic.

Peak separation as well as ratio between cathodic and anodic peak current can be used to determine the reversibility of the redox reaction. As mentioned before, for a reversible process where one electron is transferred (n=1) the ΔE_p

must be 59 mV and i_{pc}/i_{pa} equal to one. In this case, ΔE_p = 70 mV and i_{pc}/i_{pa} = 0.96, which means that the system presents a small deviation from reversibility.

On the other hand, the Randles-Sevcik equation predicts that the peak current of a reversible redox process plotted against the square root of the scan rate must vary in a linear fashion. Figure 4.26 indicates that the voltammetric response of hexacyanoferrate (II/III) is indeed linearly dependent on the square root of the scan rate between 10 and 500 $mV \cdot s^{-1}$.
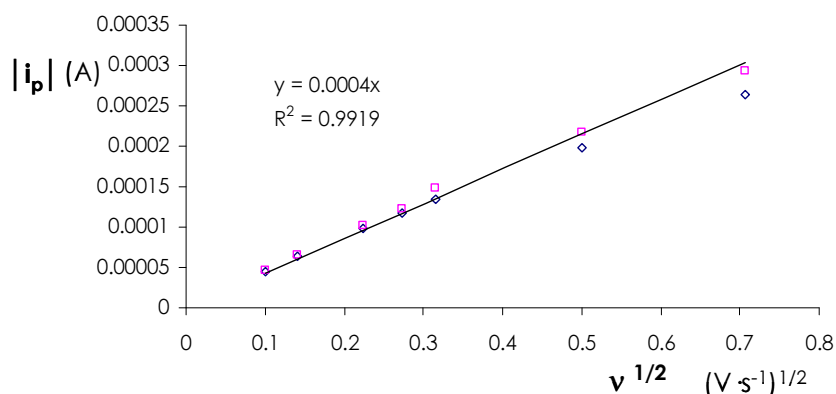
Figure 4.26. Voltammetric peak current dependence on sweep rate. Cathodic peak current is represented by blue diamond square data markers and anodic peak current by pink square data markers. Linear fit for these latter is shown in the graphic but nearly identical slope from linear regression analysis of the cathodic peak current was obtained.

The slope of the resulting line is proportional to the diffusion coefficient, which can be calculated from the Randles-Sevcik equation. D was determined to be $4.4 \cdot 10^{-6}$ $cm^2 \cdot s^{-1}$, which is not very different from the literature value reported of $6.5 \cdot 10^{-6}$ for 2 mM ferricyanide in 1M KNO_3 [26,27].

In the following experiment, chronoamperometry was also used to determine the diffusion coefficient. Potential was stepped from 0.3 V (*vs* Hg/Hg_2SO_4, K_2SO_4), where all the molecules are in the oxidized state, that is $[Fe(CN)_6]^{3-}$, to -0.4 V. This latter value is almost 200 mV more negative than the E_{pc} so species at the electrode surface will be immediately reduced and rate reaction will be controlled by diffusion. When this factor governs the system, the current is proportional to the inverse of the square root of time and D can be calculated by simply rearranging the Cottrell equation. Figure 4.27.A shows the chronoamperogram obtained after the step potential. In figure 4.27.B the plot of **i** *vs* $t^{-1/2}$ shows a linear relationship.
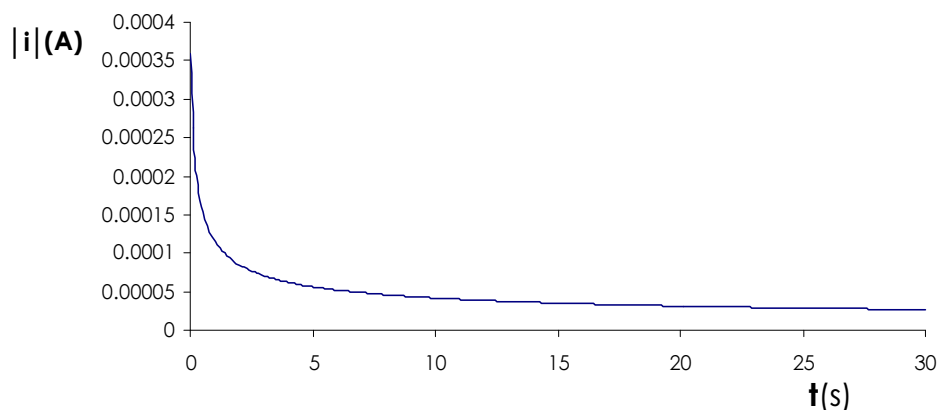
Figure 4.27.A. Chronoamperogram obtained after the potential was stepped from 0.3 V to -0.4 V (*vs* Hg/Hg$_2$SO$_4$, K$_2$SO$_4$).
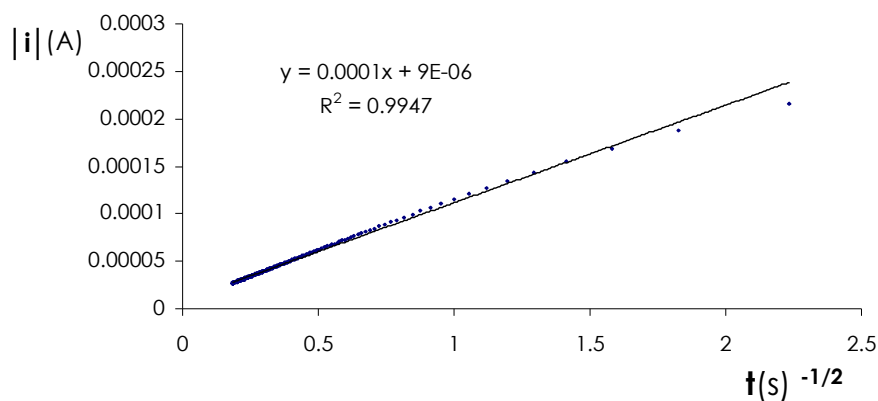
Figure 4.27.B. Plot of **i** *vs* **t$^{-1/2}$** and the linear regression analysis determined for the data set.

Calculation of ***D*** from the slope of the graphic above and Cottrell equation gave a value of 6.7 cm$^2 \cdot$s^{-1}, which in this case is almost identical to the literature value.

Finally, the reduction of ferricyanide in this system was investigated by linear sweep voltammetry at a rotating disk electrode. Potential was linearly ramped between 0.3 and -0.4 V (*vs* Hg/Hg$_2$SO$_4$, K$_2$SO$_4$), with a scan rate of 20 mV$\cdot$s^{-1} in a series of experiments in which the electrode was rotated at different frequencies (from 100 to 3000 r.p.m). As predicted by Levich equation, for a simple mass-transport-limited electron transfer the current depends on the angular rotational velocity (ω). In figure 4.28.A the current-potential curves registered at different angular velocities are shown. In graphic of figure 4.28.B it can be seen that the value of the steady limiting current increases linearly with the square root of the angular velocity, as predicted for a mass transport controlled reaction.
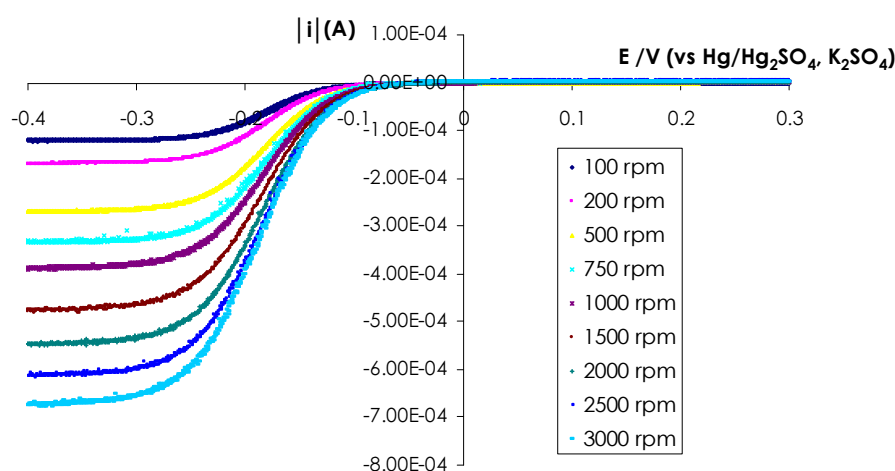
Figure 4.28.A. Graphic showing the current-potential curves registered at different angular velocities.
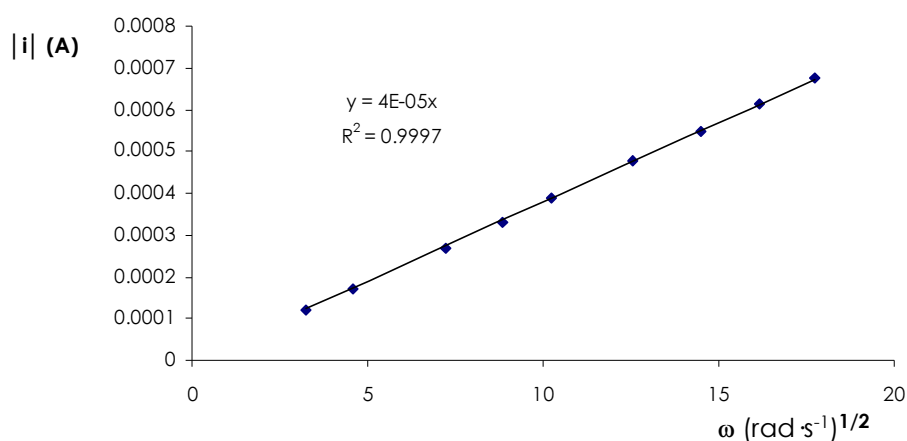
Figure 4.28.B. Plot of the steady limiting current versus the square root of the angular velocity. The linear dependence was clearly observed, as expected.

In this case, the value of **D** was calculated from the slope of the graphic of **i** vs $\omega^{1/2}$ after rearranging the Levich equation and resulted in 9.2 cm^2·s^{-1}.

4.9. Formation and electrochemical characterization of a thiol self-assembled monolayer on gold.

In this section the modification of a gold electrode with an alkanethiol self-assembled monolayer (SAM) and their electrochemical characterization will be addressed. Scheme 4.29 illustrates the SAM of thioctic acid (TA; 1,2-dithiolane-3-pentanoic acid) on a gold electrode exploited in this study.

117
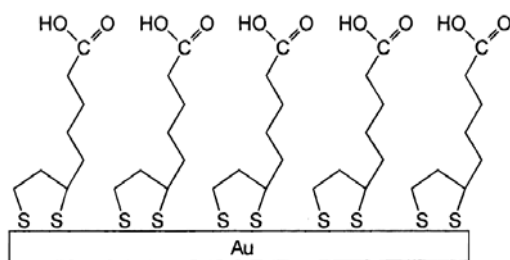
Scheme 4.29. Thioctic acid self-assembled monolayer on a gold surface.

Thioctic acid was covalently bound to the gold surface via the chemisorption of thiol groups to gold. The SAM was prepared by simple dipping of the gold electrode in a 1 mM solution of thioctic acid in EtOH during 24 hours. After the self-assembly step the electrode was thoroughly rinsed with EtOH to remove physisorbed molecules.

The electrodes covered with thioctic monolayers were subjected to voltammetric studies in the presence of a standard redox system to obtain information on the compactness of the monolayer and the presence of functional groups. Since electron transfer of ferricyanide is highly sensitive to the coverage of the gold surface, the redox couple $Fe(CN)_6^{3-}$/ $Fe(CN)_6^{4-}$ was selected as a probe to study the adsorption of the thioctic SAM at the gold electrode.

Figure 4.30 shows the response of 1 mM $Fe(CN)_6^{3-}$, in 0.1 M KH_2PO_4 at pH 7.4, on the bare and on the TA-modified gold electrode. Cyclic voltammetry shows a reversible response on bare gold while no electrochemical response is observed in the case of thioctic-modified electrode showing the complete blocking of the surface by the attached SAM and demonstrating that this layer is almost defect-free. At this pH the monolayer carboxylate head groups are predominantly negatively charged so the access of $Fe(CN)_6^{3-}$ to the gold electrode is efficiently inhibited by electrostatic repulsion which completely prevents the electron transfer in the reduction peak current.
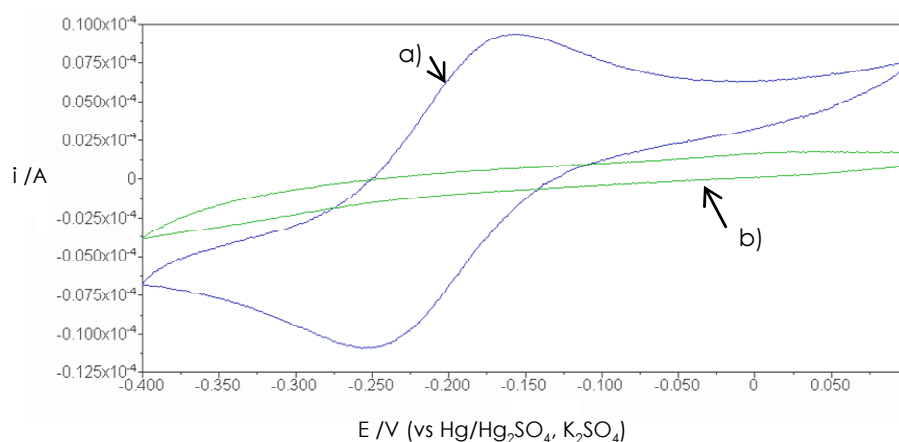
Figure 4.30. Comparison of cyclic voltammetric response for 1 mM $Fe(CN)_6^{3-}$, in 0.1 M KH_2PO_4 at pH 7.4 at a gold electrode with (b, green line) and without a thioctic monolayer (a, blue line). Scan rate: 50 mV·s^{-1}.

It has been reported in literature, that the permselectivity (defined here as the ability to suppress the response of electroactive ions present in solution) of the TA monolayer electrodes can be controlled by the solution pH and the charge density at the monolayer/solution interface [28-30]. Thus, TA monolayers display different permselectivity depending on the degree of protonation of the carboxylic acid group in agreement with a pKa of ~ 6.5 for TA in a SAM [31,32].

When CV is performed with 1 mM $Fe(CN)_6^{3-}$, in 0.1 M KH_2PO_4 at pH 5 the probe molecules were only partially prevented from penetrating through the monolayer and a weak cathodic and anodic peak current were observed. Due to the partial blocking effect, the electrochemical reversibility of the $Fe(CN)_6^{3-}$/ $Fe(CN)_6^{4-}$ redox couple is greatly diminished, as is reflected in voltammogram of figure 4.31.
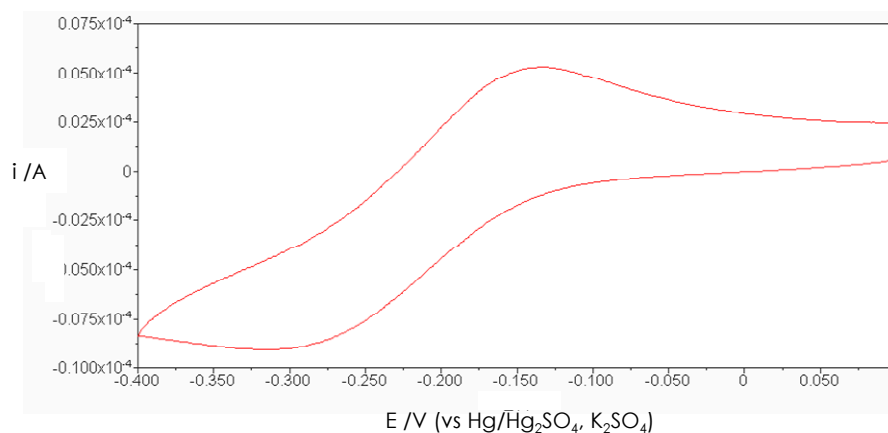
Figure 4.31. Cyclic voltammogram for 1 mM $Fe(CN)_6^{3-}$, in 0.1 M KH_2PO_4 at pH 5 at a gold electrode with a thioctic monolayer. Scan rate: 50 mV·s^{-1}.

The surface coverage (Γ) of SAM-forming molecules can be estimated by their electrochemical reductive desorption under basic conditions. The electrochemical reduction of thiols from gold electrodes has been extensively studied [33-36]. The covalent bond formed between gold and the thiol group is electrochemically reducible according to the following reaction:

$$R\text{-}S\text{-}Au + e^- \rightarrow Au^0 + R\text{-}S^-$$
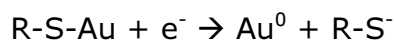
Electrochemical desorption was performed by cyclic voltammetry of a freshly prepared TA SAM in a deaerated 0.50 M KOH solution from -1.2 to -1.8 V (*vs* Hg/Hg$_2$SO$_4$, K$_2$SO$_4$). The voltammogram obtained (figure 4.32) exhibits one wave characterized by a peak potential of -1.4 V, which is in good agreement with earlier studies [37].
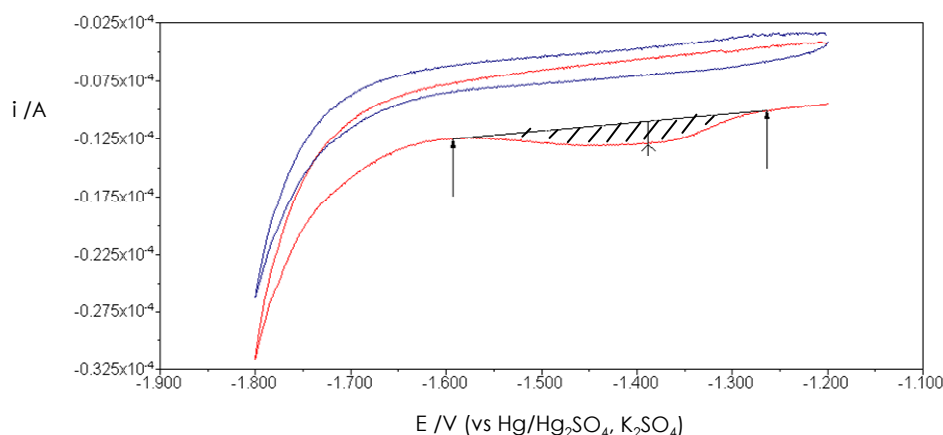
Figure 4.32. First (red line) and second (blue line) cyclic voltammograms for the reduction of the Au-S bond in the thioctic SAM in a 0.50 M KOH aqueous solution at 50 mV·s^{-1}. Area under reduction peak is illustrated by parallel lines.

By repetitive scans, the current intensity decreased, reflecting the reduction of sulfur-gold bonds and consequently, the loss of material assembled to the surface.

The surface coverage (Γ) was calculated by integrating charges (Q) passing on the reduction peak (first scan), according to the following equation:

$$\Gamma = Q/nFA$$

where A is the electrode surface area, F is Faraday's constant, and n is the number of electrons involved in the electrode reaction [10].

Γ was determined to be $9,8·10^{-10}$ mol·cm^{-2}, which is within the range for a typical adsorbate coverage of a SAM modified surface (10^{-10} to 10^{-9} mol·cm^{-2}).

4.10. Immobilization of oligonucleotides on gold electrodes

Reported conditions for modification of gold surfaces with thiol-modified oligonucleotides have varied widely among different examples published in the literature. Hence, very different DNA concentration, saline buffer conditions and incubation time have shown to give good results for DNA-SAMs formation [38-42].

On the other hand, it has been previously pointed out by some authors that not only thiol but also disulfide-modified oligonucleotides are suitable for covalent linking to gold surfaces. Disulfide bonds are cleaved spontaneously during the process of adsorption and gold-sulfur bonds are formed [7,8].

Thus, in early experiments in this work, oligonucleotides were used directly for gold functionalization without performing previous disulfide bond reduction. Self-assembly of disulfide-modified oligonucleotides was carried out by treating gold

electrodes with ODN (**3'-disulfide-15C** and **15Ccompl-5'-disulfide**) solutions at two different concentrations (30 and 300 μM) in phosphate buffered saline (PBS; 0.1 M phosphate, pH 7.4) at room temperature during 20 hours. Several studies have reported the use of Mg^{2+} to create densely packed DNA films by screening the electrostatic repulsion between phosphate backbones of adjacent strands. In this work immobilization in both absence and presence of Mg^{2+} (4 mM) was examined. All used conditions are summarized in Table 4.33. The electrodes were extensively rinsed with water to remove physisorbed molecules.

Sequence	[ODN] / μM	MgCl$_2$	KCl
15Ccompl-5'-disulfide	300	--	--
15Ccompl-5'-disulfide	300	4 mM	--
15Ccompl-5'-disulfide	30	--	--
15Ccompl-5'-disulfide	30	4 mM	--
3'-disulfide-15C	300	4 mM	--
3'-disulfide-15C	30	4 mM	--
3'-disulfide-15C	30	4 mM	1 M

Table 4.33. Different immobilization conditions used in this study.

Adsorption of oligonucleotides was studied by CV and the redox behaviour of the $Fe(CN)_6^{3-}$/ $Fe(CN)_6^{4-}$ couple was used to probe the packing structure of the monolayer, based on the fact that DNA strands can inhibit electron transfer by electrostatic repulsion between their phosphate groups and ferricyanide. In figure 4.34 a comparison of cyclic voltammograms for 1 mM $K_3[Fe(CN)_6]$ in 0.1 M PBS of pH 7.4 at a bare gold electrode and at one with the DNA-modified surface is shown.
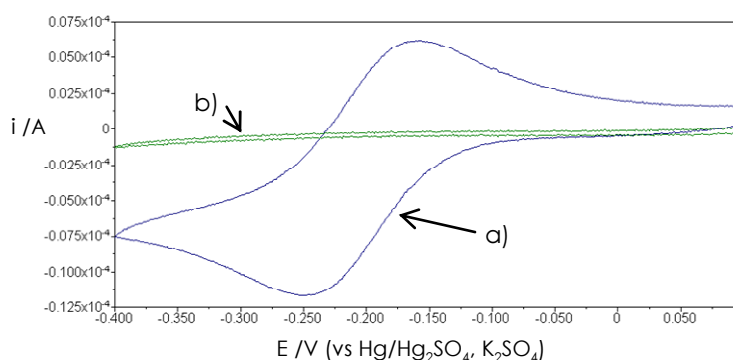
Figure 4.34. Cyclic voltammograms a) at a bare gold electrode and b) at a gold electrode incubated with a 30 μM solution **15Ccompl-5'-disulfide** in 0.1 M PBS of pH 7.4 containing 4 mM MgCl$_2$. The electron transfer is clearly inhibited in the case of DNA-modified gold. Scan rate: 50 mV·s^{-1}.

For all immobilization tested conditions no signal of redox reaction was observed which means that access of $Fe(CN)_6^{3-}$ to the gold electrode is efficiently prevented by the film, which causes a complete inhibition of electron transfer.

According to other authors this implies essentially complete coverage by the thiol-terminated DNA.

However, electrochemical reductive desorption of the DNA SAMs showed no appreciable peak in the zone of the sulfur-gold reduction potential. This suggested that in all cases the blocking layer was might formed mostly by ODNs that were bound non-specifically to the gold surface.

In a study published by Herne and Tarlov [43] it is pointed out that DNA can be adsorbed nonspecifically on gold surfaces via nitrogen interactions of nucleotide bases. The authors observed that non thiolated DNA is adsorbed strongly on gold surface and it can not be removed by extensive rinsing with buffer or water or even heating the gold to 75ºC, as other authors had proposed [44].

In this work, study of unspecific adsorption was assessed with nonthiolated oligonucleotides. Immobilization of the same sequence without disulfide group (**ODN 15Ccompl**) was performed using the same conditions as before. Incubation of gold electrodes with non modified DNA also resulted in a blockage of electron transfer and consequent suppression of ferricyanide response (figure 4.35, blue line), which demonstrates that surface was completely covered by non-specifically bound DNA. This unspecific adsorbed DNA still remained after rinse extensively with high ionic strength solution (3M KCl), in agreement with Herne and Tarlov observations.
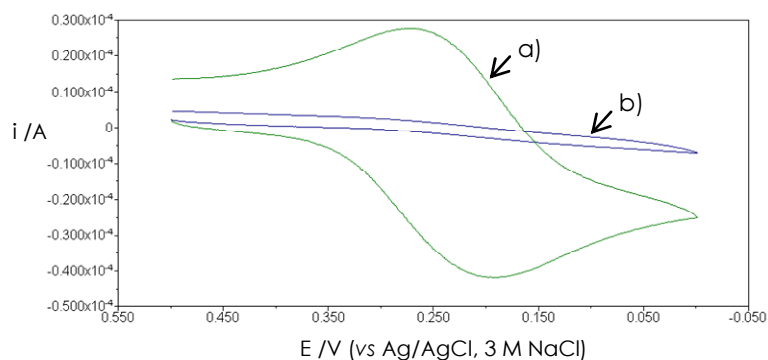
Figure 4.35. Cyclic voltammograms a) at a bare gold electrode (ø=5 mm) and b) at a gold electrode treated with a 30 μM solution of nonthiolated ODN (**15Ccompl**) in 0.1 M PBS of pH 7.4 containing 4 mM $MgCl_2$. Suppression of ferricyanide redox wave is clearly observed. Scan rate: 100 mV·s^{-1}.

In order to remove the nonspecifically bound ssDNA the nonthiolated-modified gold surfaces were exposed to an aqueous solution of 2 mM mercaptoethanol (MCE) for 2h. Previous studies have reported that short chain alkanethiols displace nonspecifically adsorbed DNA but they do not alter thiolated-oligonucleotides covalently bound through the sulfur atom [43]. On the other hand, SAMs of short chain thiols with polar groups facing the solution allow the ferricyanide to approach to the gold surface and are permeable to electron transfer.

The CV obtained with a 1 mM $K_3[Fe(CN)_6]$ in 0.1 M PBS of pH 7.4 at nonthiolated-DNA modified gold electrodes showed a reversible wave after treatment with MCE (Figure 4.36, blue line) which demonstrates that nonspecifically bound oligonucleotides have been efficiently removed and a MCE SAM has been formed. The use of mercaptohexanol (MCH) gave also good results.
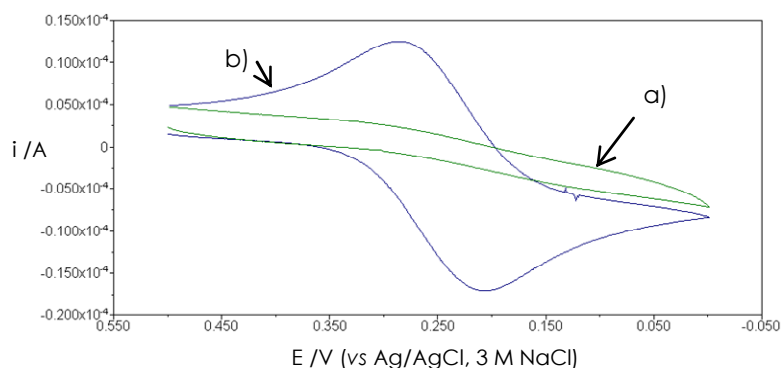
Figure 4.36. Cyclic voltammograms obtained at a gold electrode modified with nonthiolated oligonucleotides a) before and b) after MCE treatment. Scan rate: 100 mV·s⁻¹.

Thus, MCH was used after immobilization of R-S-S-ODNs to replace the weaker adsorptive contacts between nitrogenated DNA bases and gold surface and to leave the ODNs tethered primarily through the thiol groups, as represented schematically in figure 4.37. In addition, this approach promotes the vertical orientation of the covalently bound oligonucleotides.
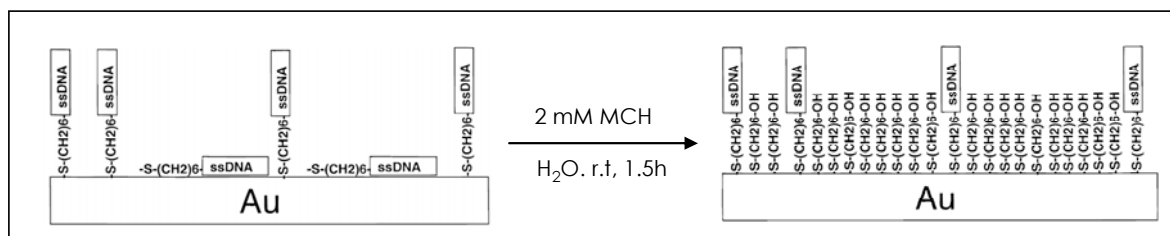
Figure 4.37. Schematic representation of the displacement of non specific interactions between DNA and gold surface by MCH treatment.

According to this scheme, mixed SAMs containing a high proportion of covalently attached DNA should result in a diminished ferricyanide redox response. However, cyclic voltammetry of the ferricyanide solution at the gold electrodes that had been firstly incubated with disulfide-oligonucleotides and secondly with MCH resulted in a quasi-reversible redox wave which implies that immobilization protocol used in this work gave very low DNA density SAMs and most of the surface was functionalized with MCH (which allows electron transfer). Some studies also reported low surface coverage when using disulfide modified ODNs [44].

So a second protocol for DNA SAM formation was probed, which consisted in reduction of the disulfide bridges with tris[2-carboxyethyl] phosphine (TCEP) immediately before oligonucleotide immobilization on cleaned gold electrodes. A similar procedure to the one employed by Plaxco *et al.* [45] with small variations was used. Thus, 1 μl of 300 μM disulfide-modified DNA sequences was mixed with 2 μl of 10 mM TCEP and incubated at r.t. for 2.5 hours to reduce the disulfide bond. Then, samples were diluted to a total volume of 20 or 200 μl with PBS (pH=7.2; 10 mM KH_2PO_4 with 1M KCl and 1 mM Mg^{2+}).

In this case the ferricyanide redox reaction was blocked even after treatment of gold electrodes with MCH which means that most of the DNA had been attached through thiol-gold bonds.

Effect of TCEP pretreatment on disulphide-protected ssDNA in immobilization efficiency was also analyzed by reductive desorption in 0.5 M KOH. In this case a more prominent reduction peak was observed at sufficiently negative potentials (figure 4.38).

E /V (*vs* Ag/AgCl, 3 M NaCl)
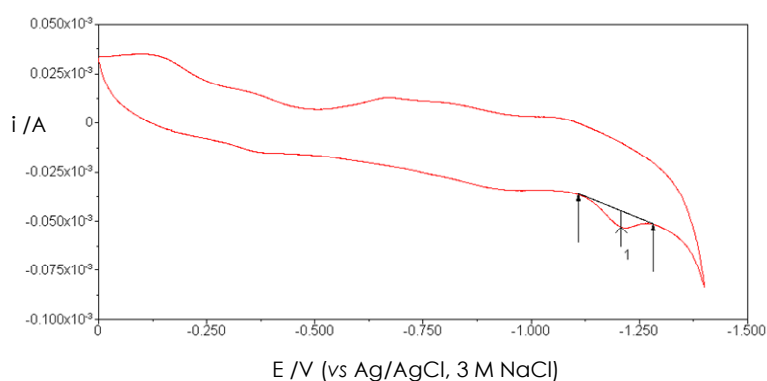
Figure 4.38. Reductive desorption of **3'-thiol-15C** in 0.5 M KOH from a gold electrode. Scan rate: 100 mV·s^{-1}.

The surface coverage was calculated by integration of reduction peak and it was determined to give a value of 9.5·10^{-10} mol/cm^2.

This technique, although useful to verify and quantify SAM formation, is destructive and does not allow the further use of the electrodes, so it was only used to probe the SAM formation and assume that equivalent SAMs were formed in subsequent experiments when using the same conditions.

The next step was the hybridization of the immobilized oligonucleotides with their complementary strand and electrochemical detection of the formed duplexes, as detailed in the following section.

4.11. Electrochemical study of DNA hybridization

After treatment with MCH, ssDNA-modified electrodes (ssDNA/Au) were hybridized with a 30 μM solution of complementary strand (ODN **15Ccompl**) in PBS (pH=7.2; 10 mM KH_2PO_4 with 1M KCl and 1 mM Mg^{2+}) for a minimum of 4 h and a maximum of 24h at room temperature. Thus, the dsDNA modified electrode (dsDNA/Au) was obtained. The dsDNA/Au was rinsed with water and subsequent electrochemical detection of hybridization was performed.

There are several electrochemical methods to detect DNA hybridization, the use of electroactive hybridization indicators being the most commonly used. These indicators are cationic metal complexes, like $Co(bpy)_3^{3+}$ [46], $Co(phen)_3^{3+}$ [47-49] and $Ru(bpy)_3^{3+}$ [39,50], or intercalating organic compounds, like daunomycin [51,52] or methylene blue [38,53-57]. The electrochemical responses of these labels or indicators change upon DNA hybridization.

In this work the hybridization with complementary DNA on gold electrodes was studied using methylene blue (MB), which has received considerable attention in previous studies as an electroactive indicator of DNA hybridization [38,53-57] showing good voltammetric behaviour. This aromatic heterocycle binds dsDNA through intercalation and its electrochemical reduction to leucomethylene blue (LB) occurs over electron transfer mediated by DNA double helix (Figure 4.39).
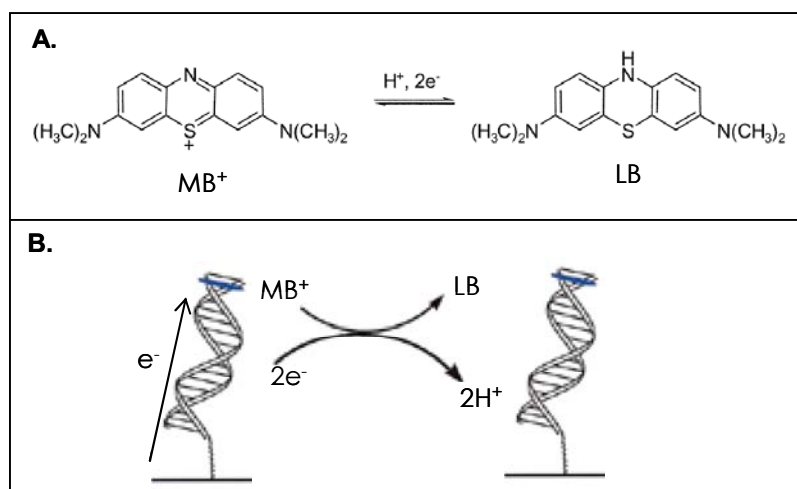
Figure 4.39. A) Redox reaction of methylene blue (MB^+) to give the reduced leucomethylene blue (LB). B) Schematic representation of intercalated MB reduction.

Other interaction modes between DNA and MB have been described. The cationic charge of MB causes DNA binding affinity by electrostatic interaction with anionic phosphate backbone. Strong interaction with the guanine bases has also been reported by some groups [54,58]. Possibly due to the existence of such different interactions, some reports in the literature concerning MB-based DNA

sensing strategies are even contradictory. Thus, Ozsoz *et al*. observed a decrease in the current signal of MB when hybridization reaction occurs due to inaccessibility of MB to the guanines [54]. In contrast, Ju *et al*. reported an increase of MB redox signal after DNA hybridization, due to the intercalation process [55].

It must be considered that conformations of DNA strands at surfaces are critical for MB electrochemistry [59], what might be the reason for the discrepancy in literature. For example in the report of Ozsoz, DNA lays down on carbon paste electrodes whereas that other studies reporting increase of MB signal upon hybridization work with DNA assembled in a vertical disposition, as is likely the case of the densely packed DNA SAMs employed in this work. Maybe for this reason, experiments performed in this section are in agreement with the results reported in these latter studies, as it is explained below.

Firstly, accumulation process of MB was performed at ssDNA/Au. Reaction with MB was carried out by immersing the DNA-modified gold electrodes into PBS (pH=7.2; 10 mM KH_2PO_4 with 1M KCl and 1 mM Mg^{2+}) containing 1 mM MB for 2,5h. After accumulation of MB, electrodes were rinsed thoroughly with water to remove physically adsorbed molecules.

The reduction signal of MB was measured in 0.1 M PBS of pH 7.4 electrolyte solution by differential pulse voltammetry (DPV). Then, the modified electrode was removed from the electrochemical cell, washed with water and hybridization with the complementary strand was performed as detailed before. DPV was registered after the hybridization step.

Figure 4.40 shows a comparison between the peak reduction current of MB accumulated at **3'-thiol-15C/Au** before and after hybridization (4h at r.t) with the **15Ccompl** ODN strand.
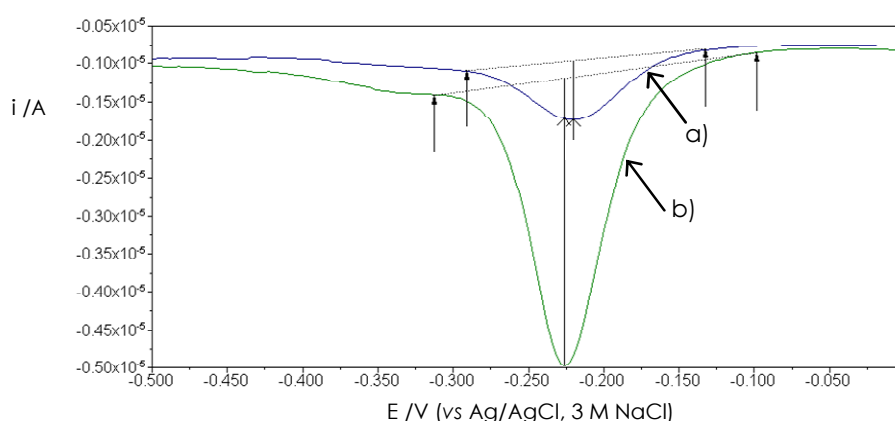
Figure 4.40. Differential pulse voltammograms of MB accumulated at a) ssDNA/Au and at b) dsDNA/Au. Hybridization of **3'-thiol-15C** attached to gold was carried out with a 30 μM solution of **15Ccompl** in PBS (pH=7.2; 10 mM KH_2PO_4 with 1M KCl and 1 mM Mg^{2+}) for 4 h.

It was found that the peak current of MB at dsDNA/Au was 3-fold higher than at ssDNA. This is in agreement with a situation concerning electrostatic interaction of MB with ssDNA and both electrostatic and intercalative binding with dsDNA. Interestingly, the redox potential shifted slightly to more negative values at dsDNA modified electrode, which suggested that MB binds more strongly to dsDNA than to ssDNA as had been previously reported in other studies [59].

Once electrochemistry of MB bound to DNA-modified electrodes was studied and hybridization was probed, the electrochemical behaviour of copper within cyclam-modified ODNs at gold electrodes was subsequently analyzed.

4.12. Electrochemical study of copper interaction with *cyclam*-modified DNA

Although charge transport through DNA has been extensively studied over the last years [60-64], an understanding of the exact conduction mechanism is still required. Hence, different observations among studies found in literature have reported DNA to display metal-like conductivity properties [65,66], to behave as a semiconductor [62,67] or even as an insulator [68]. Electrical conductance measurements to the single molecule level carried out previously in the group of Dr. Schiffrin demonstrated that electrical conductance can be performed on both single- and double-stranded structures, but the marked increase in this latter indicates that base pairing and stacking that occurs in DNA duplexes plays a vital role in the charge transport phenomenon. The sensitivity of electron transfer to base stacking has also provided the basis for sensors applications and electrochemical DNA mismatches detection [69-71].

Concerning the importance of different electron transfer properties through different DNA structures the redox behaviour of copper bound to cyclam-modified oligonucleotides was studied in both ssDNA/Au and dsDNA/Au systems.

Thus, single DNA strands attached to gold electrodes were incubated with $CuSO_4$ and analyzed by CV prior to the hybridization step. In the same way that occurs with methylene blue, the cationic Cu^{2+} could interact with *cyclam*-ODNs not only by chelation with the crown but also through guanine coordination or electrostatic interaction with phosphate backbone.

Figure 4.41 summarizes the different steps that have been followed in order to get a first insight into electrochemical behaviour of copper bound to cyclam-modified oligonucleotides attached to gold surfaces.
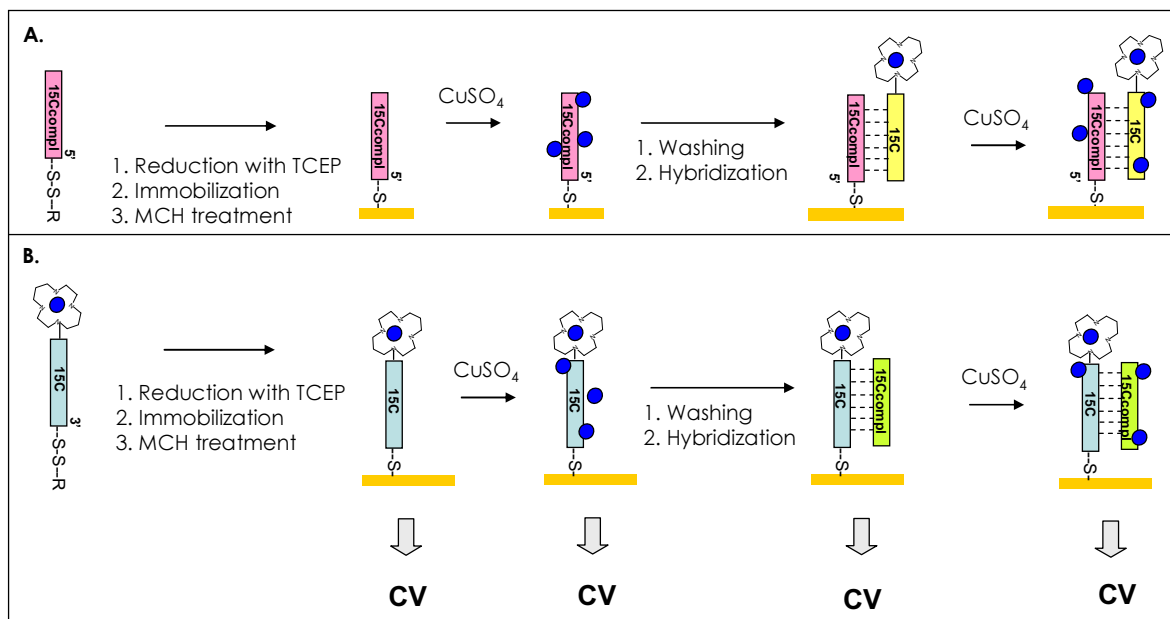
Figure 4.41. Two different systems have been used in this study. A) The cyclam is tethered to the ODN that is complementary to the one that is covalently linked to the electrode. B) The cyclam is tethered to the ODN that is directly linked to the electrode.

According to the scheme indicated above, several redox processes could be expected:

$$Cu^{2+} + e- \rightleftarrows Cu^+$$
$$Cu^+ + e- \rightleftarrows Cu$$
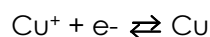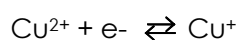
which in addition can take place within different environments, depending on if copper ions are coordinated to nitrogen atoms of cyclam, interacting with guanines or unspecific bound to negative DNA backbone.

Before performing any CV experiment, it must be taken into account that reversibility criteria are different for electroactive species bound to electrode surfaces that for species dissolved in electrolyte solution. It has been described that for an ideal nerstian adsorbate layer $E_{pa}=E_{pc}$, and that the width at half-height of either redox peak is given by 90.6/n mV. The peak current is proportional to the scan rate (v), in contrast to the $v^{1/2}$ dependence observed for nerstian waves of diffusing species, and is expressed by the following equation:

$$i_{p} = \frac{n^2F^2}{4RT} vA\Gamma_{O}^{*}$$

where Γo* is the coverage of the adsorbed monolayer and the rest of the variables have the same meaning as before (section 4.5).

Firstly, gold electrodes were functionalized with thiol-modified oligonucleotides with and without crown. Hence, 15Ccompl-5'-disulfide and 3'-disulfide-15C-5'-crown**1** (from the sample complexed previously with Cu^{2+}) were

treated with TCEP to reduce disulfide bonds and attached to gold electrodes. After treatment with MCH to remove nonspecific bound DNA strands, cyclic voltammetry was performed between 0.5 to -0.5 V (vs Ag/AgCl, 3M NaCl) in 0.1 M KH_2PO_4 at pH 7.4.

In neither case redox waves were obtained. The absence of signals for the case of cyclam-15C/Au can be due to inefficient electron transfer through ssDNA or to a loss of the chelated copper during the modified electrode preparation.

Secondly, both electrodes were incubated with a 10 mM solution of $CuSO_4$ in H_2O during 4 hours at room temperature and rinsed finally with water. Cyclic voltammetry after this step showed also no signal. However, a change of capacitance (related to the charging current observed in absence of electron transfer) was observed (figure 4.42), likely due to electrostatic interaction with ODN backbone and the consequent increase of the dielectric constant of the monolayer.
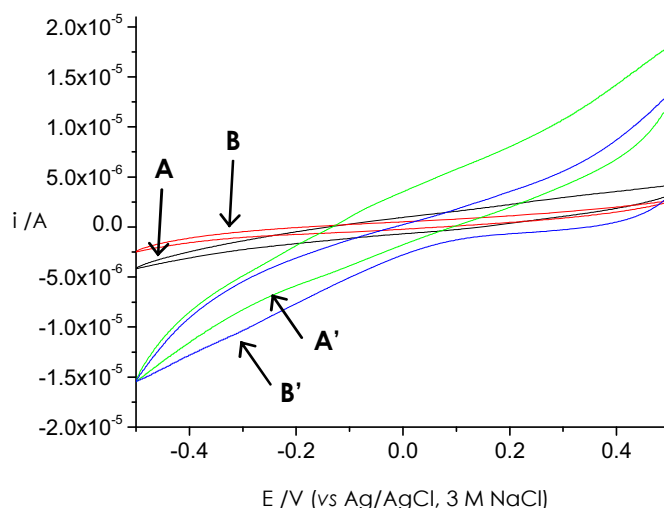
Figure 4.42. Comparison of CV obtained at gold electrodes modified with system **A** and **B** before (**A** and **B** lines) and after (**A'** and **B'** lines) treatment with copper sulphate. Although no redox wave signal is observed an increase in capacitance is shown.

Similar observations were made by Rubinstein and co-workers who prepared SAMs of bishydroxamate ligands that are able to bind Cu^{2+} [72] as well as by Reinhoudt *et al.*, who reported an increase of the capacitance of self-assembled monolayers of crown ether adsorbates after complexation of metal ions [73].

The next step consisted in hybridization of ODN strands attached to gold electrodes with their complementary targets. In this way, cyclam will be linked to gold surface through dsDNA, so a better electron transfer from electrode to chelated Cu^{2+} is expected.

Prior to incubation of the new dsDNA/Au with a 10 mM $CuSO_4$ solution no signal is observed. After treatment with the copper sulphate solution, a weak signal is observed for the case of system **B**, where cyclam is linked to the ODN that is directly attached to the gold surface, but it disappears after the first scan. By contrast, a pronounced cathodic peak is observed in the case of system **A**, where cyclam is tethered to the hybridized strand. Two small anodic peaks were also observed in the reverse scan which may be associated with the oxidation of copper metal.

In figure 4.43 the cyclic voltammograms at gold electrode modified with system **A** registered at different scan rates between 0.5 to -0.5 V (vs Ag/AgCl, 3M NaCl) in 0.1 M KH_2PO_4 at pH 7.4 is shown.
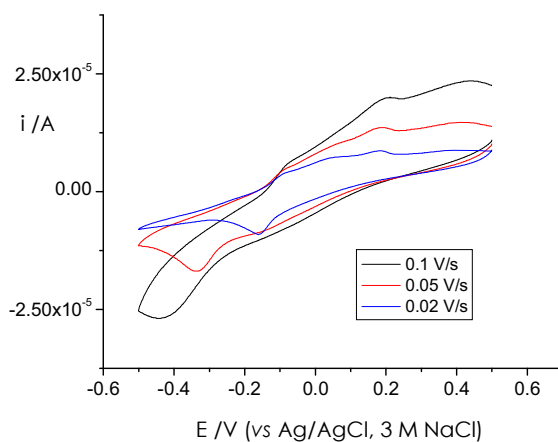
Figure 4.43. CV at gold electrode modified with system **A.** Cathodic peak appears at different potential values depending of the applied scan rate.

Whereas no shifting in anodic peaks potential is observed in all registered CV experiments, the potential value of the cathodic peak presents a high variability as function of the scan rate.

The high separation between peaks and change of E_p as a function of scan rate indicates the presence of a chemically irreversible electrochemical reaction. Reduction in size of anodic peaks in the reverse scan respect to the cathodic peak seems to indicate little reconversion of reduced species to the oxidized state. This could be due for example to metallic copper deposition onto electrode surface which is not entirely dissolved back.

Results obtained from multiple cycling showed that the peak current in the first scan cycle was significantly different from those in the subsequent cycles. Figure 4.44 shows a comparison between the first and second scan at different sweep rates. It can be seen that this difference is more pronounced the higher the scan rate is.
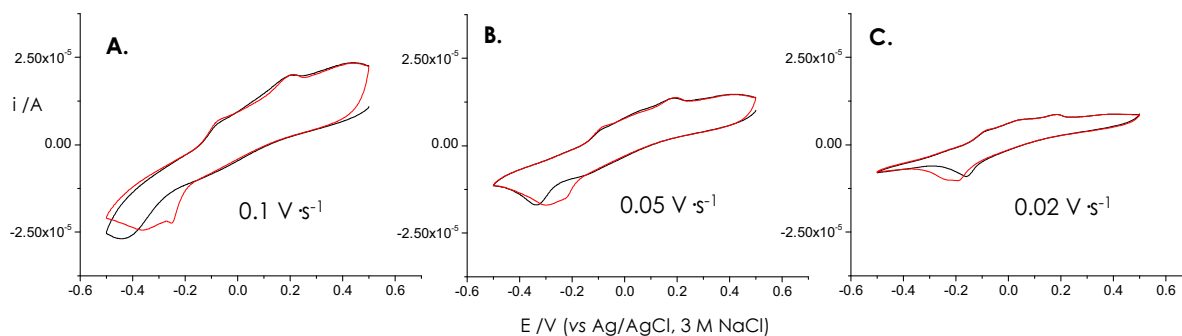
Figure 4.44. Comparison between the first (black line) and second scan (red line) at A) 0.1 V·s^{-1}, B) 0.05 V·s^{-1} and C) 0.02 V·s^{-1}.

It should also be commented that a slight increase in cathodic peak current with repeat scanning was observed (Figure 4.45) which seems to support the hypothesis of formation of metallic copper film.
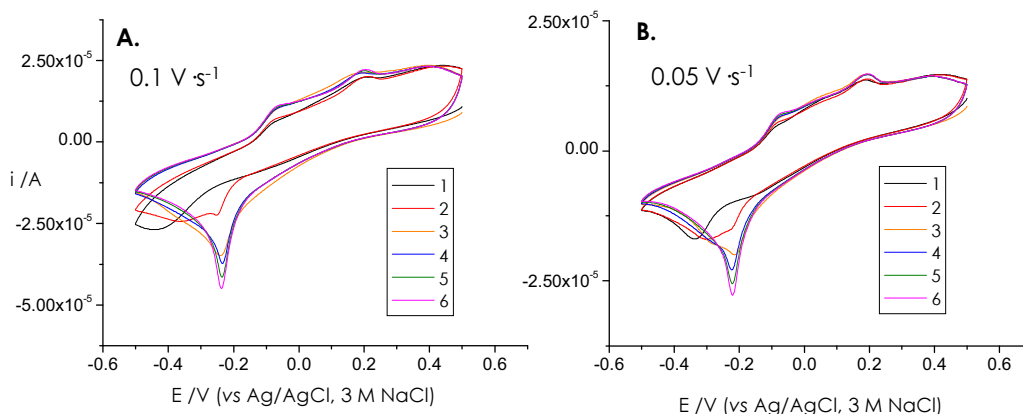
Figure 4.45. Increase in cathodic peak with sequential scanning. CV was performed at 0.1 V·s^{-1} (A) and at 0.05 V·s^{-1} (B).

A second set of experiments were performed in which the potential window was shortened and applied from 0.1 V to -0.5 V (vs vs Ag/AgCl, 3M NaCl). In this case a large displacement of E_{pc} was revealed (figure 4.46). On the other hand, the effect of multiple cycling is different. While a slight increase in cathodic peak had been previously observed, in this case the second scan made the peak to decrease, as is shown in voltammograms of figure 4.46.
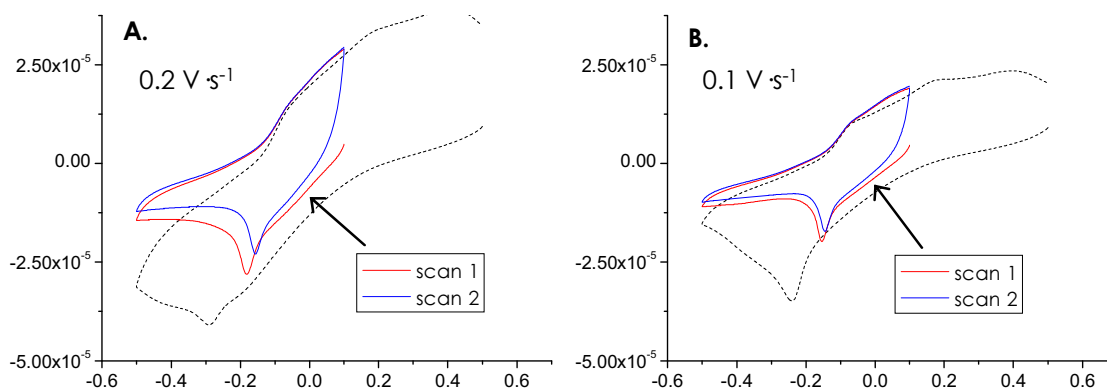
Figure 4.46. Cyclic voltammograms obtained when using a shorter potential range at 0.2 V·s⁻¹ (A) and at 0.1 V·s⁻¹ (B). Redox response obtained when using the large potential window is shown for comparison (dashed black line).

These differences could be related with the fact that reverse scan ends before the second anodic peak appears so reoxidation of reduced species is incomplete.

After collection and analysis of all these electrochemical data it seems that copper ions clearly showed an electrochemical signal after binding with our system but the complexity of voltammetric response at the cyclam-dsDNA/Au electrodes does not allow a good and reliable characterization of the system. Thus, a further detailed study is needed to get a deep understanding of copper-cyclam-DNA interaction mode.

Cyclic voltammetry technique presents some limitations that could be important for this project. For example, as electron transfer rate between gold and copper ions are usually thought to decrease exponentially with distance [72], the change in measured voltammetric response after multiple cycling could be also due to small changes in the orientation of the SAM, caused by high voltage variation.

Another serious limitation is that the possible processes should show redox response in the accessible potential range which, in the system used in this project, is quite restricted. If the voltage would be swept further to very negative values the thiolated ODNs could be desorbed from the gold surface. On the other hand if a very positive potential was applied electrochemical oxidation of DNA could occur [74-77].

In addition, cyclic voltammetric data for the reduction of copper inserted within cyclam are only available as diffusing species in non-aqueous solution. Due to poor solubility of cyclam in water, 0.1M TBAHP in ACN was used as supporting electrolyte in previous studies where the redox behaviour of copper-*cyclam* in solution was studied. Hence, these data can not be used as a reference to ensure that the interesting redox processes occur in our potential range. To solve this

132

problem, CV experiments should be performed with the cyclam crown covalently attached to gold electrodes through a thiolated arm and compare the copper behaviour in this SAM with the one in which cyclam is linked to gold through DNA. Currently, the synthesis of cyclam whith a pending thiolated alkyl arm is being addressed by a PhD student at Dr. Schiffrin research group.

4.13. Conclusions

The synthesis of ODNs carrying Cu(II) complexes has been described. Several sequences were functionalized with a bromohexyl group and conjugated to two different copper tatradentate ligands by nucleophilic substitution.

These modified DNA strands were immobilized to gold electrodes either directly, by covalent attachment though sulfur-gold bonds or indirectly, through hybridization with a complementary strand linked to the electrode surface. Electrochemical studies were performed with both systems.

Only cyclic voltammetry with the latter presented electrochemical signals corresponding to redox processes of copper ions, probably due to a better electron transfer through this system. However electrochemical response changed significantly depending on measurement conditions (number of scans, scan rate, applied potential range) so a further detailed analysis is needed for a better characterization of the different redox processes.

A SAM of thiolated copper ligands attached to gold surface without DNA linkers should be studied and ongoing research is focused in this point.

4.14. References

[1]. Suh, M. P., and Kang, S. G. (1988) Synthesis and Properties of Nickel(II) and Copper(II) Complexes of 14-Membered Hexaaza Macrocycles, 1,8-Dimethyl- and 1,8-Diethyl-1,3,6,8,10,13-Hexaazacyclotetradecane. *Inorg. Chem. 27*, 2544-2546.

[2]. Lu, Q., Reibenspies, J. J., Martell, A. E., and Motekaitis, R. J. (1996) Copper(II) Complexes of the Hexaaza Macrocyclic Ligand 3,6,9,16,19,22-Hexaaza-27,28-Dioxatricyclo[22.2.1.111,14]Octacosa-1(26),11,13,24-Tetraene and their Interaction with Oxalate, Malonate, and Pyrophosphate Anions. *Inorg. Chem. 35*, 2630-2636.

[3]. Eriksson, H., Håkansson, M., and Jagner, S. (1998) Pentamethylphenylcopper(I): A Square-Planar Tetranuclear Cluster. *Inorg. Chim. Acta. 277*, 233-236.

[4]. Håkansson, M., Vestergren, M., Gustafsson, B., and Hilmersson, G. (1999) Isolation and Spontaneous Resolution of Eight-Coordinate Stereoisomers. *Angew. Chem. Int. Ed.* 38, 2199-2201.

[5]. Chattopadhyay, S., Drew, M. G. B., and Ghosh, A. (2006) Synthesis, Characterization, and Anion Selectivity of Copper(II) Complexes with a Tetradentate Schiff Base Ligand. *Inorg. Chim. Acta. 359*, 4519-4525.

[6]. Rodríguez, L., Labisbal, E., Sousa-Pedrares, A., García-Vázquez, J. A., Romero, J., and Sousa, A. (2010) Electrochemical Synthesis and Crystal Structure of Iron(II), Cobalt(II), Nickel(II) and Copper(II) Complexes of Dianionic Tetradentate N4 Schiff Base Ligand. *Inorg. Chim. Acta. 363*, 1284-1288.

[7]. Wackerbarth, H., Marie, R., Grubb, M., Zhang, J., Hansen, A., Chorkendorff, I., Christensen, C. V., Boisen, A., and Ulstrup, J. (2004) Thiol- and Disulfide-Modified Oligonucleotide Monolayer Structures on Polycrystalline and Single-Crystal Au(111) Surfaces. *J. Solid State Electrochem. 8*, 474-481.

[8]. Luderer, F., and Walschus, U. (2005) Immobilization of Oligonucleotides for Biochemical Sensing by Self-Assembled Monolayers: Thiol-Organic Bonding on Gold and Silanization on Silica Surfaces. *Top. Curr. Chem.* 260, 37-56.

[9]. Wu, X., and Pitsch, S. (1998) Synthesis and Pairing Properties of Oligoribonucleotide Analogues Containing a Metal-Binding Site Attached to Beta-D-Allofuranosyl Cytosine. *Nucl. Acids Res. 26*, 4315-4323.

[10]. Bard, A. J., and Faulkner, L. R. Electrochemical Methods: Fundamental and Applications, 2nd ed.; J. Wiley & Sons: New York, 2000.

[11]. Burke, L. D., Collins, J. A., Horgan, M. A., Hurley, L. M., and O'Mullane, A. P. (2000) The Importance of the Active States of Surface Atoms with Regard to the Electrocatalytic Behaviour of Metal Electrodes in Aqueous Media. *Electrochim. Acta. 45*, 4127-4134.

[12]. Burke, L. D., Hurley, L. M., Lodge, V. E., and Mooney, M. B. (2001) The Effect of Severe Thermal Pretreatment on the Redox Behaviour of Gold in Aqueous Acid Solution. *J. Solid State Electrochem. 5*, 250-260.

[13]. Yang, Z., Gonzalez-Cortes, A., Jourquin, G., Viré, J., Kauffmann, J., and Delplancke, J. (1995) Analytical Application of Self Assembled Monolayers on Gold Electrodes: Critical Importance of Surface Pretreatment. *Biosens. Bioelectron. 10*, 789-795.

[14]. Subramanian, R., Lakshminarayanan, V. (1999) Effect Of Surface Roughness On The Self-Assembly Of Octadecanethiol Monolayer On To Polycrystalline Noble Metal Surfaces. *Curr. Sci*. 76, 665-669.

[15]. Lee, M., Hsueh, C., Freund, M. S., and Ferguson, G. S. (1998) Air Oxidation of Self-Assembled Monolayers on Polycrystalline Gold: The Role of the Gold Substrate. *Langmuir* 14, 6419-6423.

[16]. Burke, L.D., and O'Mullane, A. P. (2000) Generation of Active Surface States of Gold and the Role of such States in Electrocatalysis. *J. Solid State Electrochem. 4*, 285-297.

[17]. Fischer, L. M., Tenje, M., Heiskanen, A. R., Masuda, N., Castillo, J., Bentien, A., Émneus, J., Jakobsen, M. H., and Boisen, A. (2009) Gold Cleaning Methods for Electrochemical Detection Applications. *Microelectron. Eng. 86*, 1282-1285.

[18]. Liu, G., Böcking, T., and Gooding, J. J. (2007) Diazonium Salts: Stable Monolayers on Gold Electrodes for Sensing Applications. *J Electroanal Chem. 600*, 335-344.

[19]. Noh, M., and Tothill, I. (2006) Development and Characterisation of Disposable Gold Electrodes, and their use for Lead(II) Analysis. *Anal. Bioanal. Chem.. 386*, 2095-2106.

[20]. Gordon, J. S., and Johnson, D. C. (1994) Application of an Electrochemical Quartz Crystal Microbalance to a Study of Water Adsorption at Gold Surfaces in Acidic Media. *J. Electroanal. Chem. 365*, 267-274.

[21]. Juodkazis, K., Juodkazytė, J., Juodienė, T., and Lukinskas, A. (1998) Determination of Au(III) in the Surface Layers Formed Anodically on the Gold Electrode. *J. Electroanal. Chem. 441*, 19-24.

[22]. Sarapuu, A., Nurmik, M., Mändar, H., Rosental, A., Laaksonen, T., Kontturi, K., Schiffrin, D. J., and Tammeveski, K. (2008) Electrochemical Reduction of Oxygen on Nanostructured Gold Electrodes. *J. Electroanal. Chem. 612*, 78-86.

[23]. Trasatti, S., and Petrii, O. A. (1991) Real Surface Area Measurements In Electrochemistry. *Pure Appl.Chem.* 63, 711-734.

[24]. Hoogvliet, J. C., Dijksma, M., Kamp, B., and van Bennekom, W. P. (2000) Electrochemical Pretreatment of Polycrystalline Gold Electrodes To Produce a Reproducible Surface Roughness for Self-Assembly: A Study in Phosphate Buffer pH 7.4. *Anal. Chem*. 72, 2016–2021.

[25]. Carvalhal, R.F., Freire, R.S., and Kubota, L.T. (2005) Polycrystalline Gold Electrodes: A Comparative Study of Pretreatment Procedures used for Cleaning and Thiol Self-Assembly Monolayer Formation. *Electroanalysis. 17*, 1251-1259.

[26]. Bucur, R. V., Bartes, A., and Mecea, V. (1977) Kinetic Measurements on a Stationary Disk Electrode in a Uniformly Rotating Fluid. *Electrochim. Acta. 23*, 641.

[27]. Akram, M., Stuart, M. C., and Wong, D. K. Y. (2004) Direct Application Strategy to Immobilise a Thioctic Acid Self-Assembled Monolayer on a Gold Electrode. *Anal. Chim. Acta. 504*, 243-251.

[28]. Cheng, Q., and Brajter-Toth, A. (1992) Selectivity And Sensitivity Of Self-Assembled Thioctic Acid Electrodes. *Anal. Chem.* 64, 1998-2000.

[29]. Cheng, Q., and Brajter-Toth, A. (1995) Permselectivity and High Sensitivity at Ultrathin Monolayers. Effect of Film Hydrophobicity. *Anal. Chem.* 67, 2767-2775.

[30]. Cheng, Q., and Brajter-Toth, A. (1996) Permselectivity, Sensitivity, and Amperometric pH Sensing at Thioctic Acid Monolayer Microelectrodes *Anal. Chem*. 68, 4180-4185.

[31]. Madoz, J., Kuznetzov, B. A., Medrano, F. J., Garcia, J. L., and Fernandez, V. M. (1997) Functionalization of Gold Surfaces for Specific and Reversible Attachment of a Fused β-Galactosidase and Choline-Receptor Protein. *J. Am. Chem Soc*. 119, 1043-1051.

[32]. Wang, Y., and Kaifer, A. E. J. (1998) Interfacial Molecular Recognition. Binding of Ferrocenecarboxylate to β-Aminocyclodextrin Hosts Electrostatically Immobilized on a Thioctic Acid Monolayer. *Phys. Chem. B* 102, 9922-9927.

[33]. Widrig, C. A., Chung, C., and Porter, M. D. (1991) The Electrochemical Desorption of n-Alkanethiol Monolayers from Polycrystalline Au and Ag Electrodes. *J. Electroanal. Chem. 310*, 335-359.

[34]. Yang, D. F., Wilde, C. P., and Morin, M. (1996) Electrochemical Desorption and Adsorption of Nonyl Mercaptan at Gold Single Crystal Electrode Surfaces. *Langmuir* 12, 6570-6577.

[35]. Shin-ichiro Imabayashi, Minehiko Iida, Daisuke Hobara, Zhi Qiang Feng, Katsumi Niki, and Takashi Kakiuchi. (1997) Reductive Desorption of Carboxylic-Acid-Terminated Alkanethiol Monolayers from Au(111) Surfaces. *J. Electroanal. Chem. 428*, 33-38.

[36]. Sumi, T., Wano, H., and Uosaki, K. (2003) Electrochemical Oxidative Adsorption and Reductive Desorption of a Self-Assembled Monolayer of Decanethiol on the Au(111) Surface in KOH+ethanol Solution. *J. Electroanal. Chem. 550-551*, 321-325.

[37]. Dong, Y., Abaci, S. and Shannon, C. (2003) Self-Assembly and Electrochemical Desorption of Thioctic Acid Monolayers on Gold Surfaces. *Langmuir* 19, 8922-8926.

[38]. Kelley, S. O., Barton, J. K., Jackson, N. M., and Hill, M. G. (1997) Electrochemistry of Methylene Blue Bound to a DNA-Modified Electrode. *Bioconjug. Chem. 8*, 31-37.

[39]. Steel, A.B., Herne, T.M., and Tarlov, M.J. (1998) Electrochemical Quantitation Of DNA Immobilized On Gold. *Anal. Chem.* 70, 4670–4677.

[40]. Takenaka, S., Yamashita, K., Takagi, M., Uto, Y., and Kondo, H. (2000) DNA Sensing on a DNA Probe-Modified Electrode using Ferrocenylnaphthalene Diimide as the Electrochemically Active Ligand. *Anal. Chem. 72*, 1334-1341.

[41]. Liu, S., Li, Y., Li, J., and Jiang, L. (2005) Enhancement of DNA Immobilization and Hybridization on Gold Electrode Modified by Nanogold Aggregates. *Biosens Bioelectron. 21*, 789-795.

[42]. Ishige, Y., Shimoda, M., and Kamahori, M. (2006) Immobilization of DNA Probes Onto Gold Surface and its Application to Fully Electric Detection of DNA Hybridization using Field-Effect Transistor Sensor. *Japan. J. Appl. Phys. 45*, 3776-3783.

[43]. Herne, T. M., and Tarlov, M. J. (1997) Characterization of DNA Probes Immobilized on Gold Surfaces. *J. Am. Chem. Soc. 119*, 8916-8920.

[44]. Anne, A., Bouchardon, A., and Moiroux, J. (2003) 3'-Ferrocene-Labeled Oligonucleotide Chains End-Tethered to Gold Electrode Surfaces: Novel Model Systems for Exploring Flexibility of Short DNA using Cyclic Voltammetry. *J. Am. Chem. Soc. 125*, 1112-1113.

[45]. Xiao, Y., Lai, R. Y., and Plaxco, K. W. (2007) Preparation of Electrode-Immobilized, Redox-Modified Oligonucleotides for Electrochemical DNA and Aptamer-Based Sensing. *Nat. Protocols. 2*, 2875-2880.

[46]. Millan, K. M., and Mikkelsen, S. R. (1993) Sequence-Selective Biosensor for DNA Based on Electroactive Hybridization Indicators. *Anal. Chem. 65*, 2317-2323.

[47]. Wang, J., Cai, X., Rivas, G., Shiraishi, H., Farias, P. A. M., and Dontha, N. (1996) DNA Electrochemical Biosensor for the Detection of Short DNA Sequences Related to the Human Immunodeficiency Virus. *Anal. Chem. 68*, 2629-2634.

[48]. Wang, J., Palecek, E., Nielsen, P. E., Rivas, G., Cai, X., Shiraishi, H., Dontha, N., Luo, D., and Farias, P. A. M. (1996) Peptide Nucleic Acid Probes for Sequence-Specific DNA Biosensors. *J. Am. Chem. Soc. 118*, 7667-7670.

[49]. Erdem, A., Meric, B., Kerman, K., Dalbasti, T., and Ozsoz, M. (1999) Detection of Interaction between Metal Complex Indicator and DNA using Electrochemical Biosensor. *Electroanalysis* 11, 1372 – 1376.

[50]. Napier, M. E., Loomis, C. R., Sistare, M. F., Kim, J., Eckhardt, A. E., and Thorp, H. H. (1997) Probing Biomolecule Recognition with Electron Transfer: Electrochemical Sensors for DNA Hybridization. *Bioconjug. Chem. 8*, 906-913.

[51]. Sun, X., He, P., Liu, S., Ye, J., and Fang, Y. (1998) Immobilization Of Single-Stranded Deoxyribonucleic Acid On Gold Electrode With Self-Assembled Aminoethanethiol Monolayer For DNA Electrochemical Sensor Applications. *Talanta* 47, 487–495.

[52]. Boon, E.M., Salas, J.E., and Barton, J.K. (2002) An Electrical Probe Of Protein–DNA Interactions On DNA-Modified Surfaces. *Nat. Biotechnol*. 20, 282–286.

[53]. Erdem, A., Kerman, K., Meric, B., Akarca, U. S., and Ozsoz, M. (2000) Novel Hybridization Indicator Methylene Blue for the Electrochemical Detection of Short DNA Sequences Related to the Hepatitis B Virus. *Anal. Chim. Acta. 422*, 139-149.

[54]. Erdem, A., Kerman, K., Meric, B, and Ozsoz, M. (2001) Methylene Blue as a Novel Electrochemical Hybridization Indicator. *Electroanalysis. 13*, 219-223.

[55]. Gu, J., Lu, X., and Ju, H. (2002) DNA Sensor for Recognition of Native Yeast DNA Sequence with Methylene Blue as an Electrochemical Hybridization Indicator. *Electroanalysis 14*, 949 – 954.

[56]. Zhu, N., Zhang, A., Wang, Q., He, P., and Fang, Y. (2004) Electrochemical Detection of DNA Hybridization using Methylene Blue and Electro-Deposited Zirconia Thin Films on Gold Electrodes. *Anal. Chim. Acta. 510*, 163-168.

[57]. Jin, Y., Yao, X., Liu, Q., and Li, J. (2007) Hairpin DNA Probe Based Electrochemical Biosensor using Methylene Blue as Hybridization Indicator. *Biosens. Bioelectron. 22*, 1126-1130.

[58]. Yang, W., Ozsoz, M., Hibbert, D. B., and Gooding, J. J. (2002) Evidence for the Direct Interaction Between Methylene Blue and Guanine Bases Using DNA-Modified Carbon Paste Electrodes. *Electroanalysis* 14, 1299-1302.

[59]. Pan, D., Zuo, X., Wan, Y., Wang, L., Zhang, J., Song, S., and Fan, C. (2007) Electrochemical Interrogation of Interactions between Surface-Confined DNA and Methylene Blue. *Sensors* 7, 2671-2680.

[60]. Kelley, S.O., Jackson, N.M., Hill, M.G., and Barton, J.K. (1999) Long-range electron transfer through DNA films. *Angew. Chem. Int. Ed*. 38, 941–945.

[61]. Giese, B. (2000) Long-Distance Charge Transport in DNA: The Hopping Mechanism. *Acc. Chem. Res. 33*, 631-636.

[62]. Porath, D., Bezryadin, A., De Vries, S., and Dekker, C. (2000) Direct Measurement Of Electrical Transport Through DNA Molecules. *Nature* 403, 635–638.

[63]. Elias, B., Shao, F., and Barton, J. K. (2008) Charge Migration Along the DNA Duplex: Hole Versus Electron Transport. *J. Am. Chem. Soc. 130*, 1152-1153.

[64]. Genereux, J. C., and Barton, J. K. (2010) Mechanisms for DNA Charge Transport. *Chem. Rev. 110*, 1642-1662.

[65]. Arkin, M. R., Stemp, E. D. A., Holmlin, R. E., Barton, J. K., Hörmann, A., Olson, E. J. C., and Barbara, P. F. (1996) Rates Of DNA-Mediated Electron Transfer Between Metallointercalators. *Science* 273, 475–480.

[66]. Fink, H.W., Schönenberger, C. (1999) Electrical Conduction Through DNA Molecules. *Nature* 398, 407– 410.

[67]. Nogues, C., Cohen, S. R., Daube, S., Apter, N., and Naaman, R. (2006) Sequence Dependence of Charge Transport Properties of DNA. *J. Phys. Chem. B. 110*, 8910-8913.

[68] Lewis, F. D., Wu, T., Zhang, Y., Letsinger, R. L., Greenfield, S. R., and Wasielewski, M. R. (1997) Distance-Dependent Electron Transfer In DNA Hairpins. *Science* 277, 673– 676.

[69]. Kelley, S.O., Boon, E.M., Barton, J.K., Jackson, N.M., and Hill, M.G. (1999) Single-Base Mismatch Detection Based On Charge Transduction Through DNA. *Nucleic Acids Res*. 27, 4830–4837.

[70]. Boon, E.M., Ceres, D.M., Drummond, T.G., Hill, M.G., and Barton, J.K. (2000) Mutation Detection By Electrocatalysis At DNA-Modified Electrodes. *Nat. Biotechnol*. 18, 1096–1100.

[71]. Yu, C. J., Wan, Y., Yowanto, H., Li, J., Tao, C., James, M.D., Tan, C.L., Blackburn, G.F., and Meade, T.J. (2001) Electronic Detection Of Single-Base Mismatches In DNA With Ferrocene modified Probes. *J. Am. Chem. Soc*. 123, 11155–11161.

[72]. Gafni, Y., Weizman, H., Libman, J., Shanzer, A., and Rubinstein, I. (1996) Biomimetic Ion-Binding Monolayers on Gold and their Characterization by AC-Impedance Spectroscopy. *Chem – Eur J.* 2, 759 – 766.

[73]. Flink, S., van Veggel, F.C.J.M, and Reinhoudt, D.N. (1999) Recognition of Cations by Self-Assembled Monolayers of Crown Ethers. *J. Phys. Chem. B* 103, 6515-6520.

[74]. Oliveira Brett, A.M. and Matysik, F.M. (1997). Voltammetric And Sonovoltammetric Studies On The Oxidation Of Thymine And Cytosine At A Glassy Carbon Electrode. *J. Electroanal. Chem.* 429, 95–99.

[75]. Wang, Z., Liu, D.D., and Dong, S. (2002) Study On Adsorption And Oxidation Of Calf Thymus DNA At Glassy Carbon Electrode. *Electroanalysis* 5, 1419–1421.

[76]. Ferapontova, E. E.., and Domínguez, E. (2003) Direct Electrochemical Oxidation of DNA on Polycrystalline Gold Electrodes. *Electroanalysis* 15, 629 – 634.

[77]. Li, Q., Batchelor-McAuley, C., and Compton, R. G. (2010) Electrochemical Oxidation of Guanine: Electrode Reaction Mechanism and Tailoring Carbon Electrode Surfaces to Switch between Adsorptive and Diffusional Responses. *J. Phys. Chem. B.* 114, 7423-7428.

CHAPTER 5

**Synthesis of a Novel DNA Structure Able to Form
Stable Monomolecular Quadruplexes:
Effect of 8-amino-guanine Substitutions**

5.1. Introduction

Guanine-rich DNA sequences are able of forming a non-canonical four-stranded topology called the G-quadruplex. These structures are based in the G-tetrad or G-quartet, which consists of a planar arrangement of four guanine bases associated through a cyclic array of Hoogsteen hydrogen bonds in which each guanine both accepts and donates two hydrogen bonds (Figure 5.1).
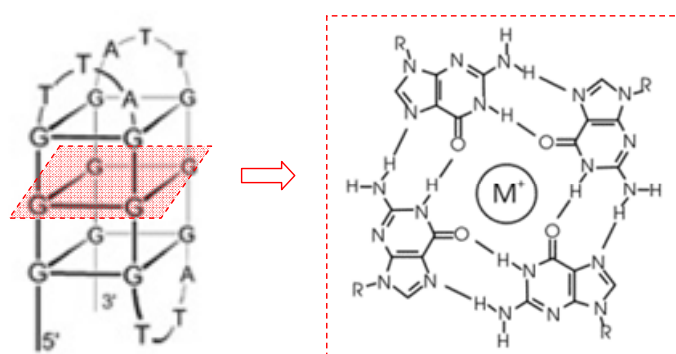
Figure 5.1. Chemical structure of a G-tetrad of a quadruplex DNA

G-quadruplex is originated by the superposition of G-tetrads which can form four-stranded structures by stacking interactions. The tetrads are stacking in such a way that adopts a right-handed helix (figure 5.2) with a central cavity with specific binding sites for metal ions.
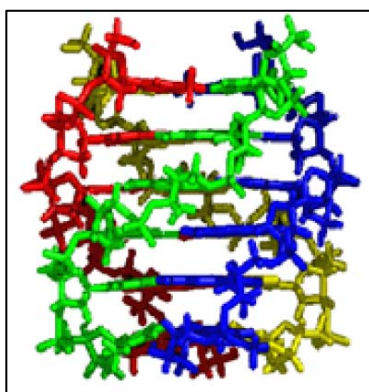
Figure 5.2. Stacking of G-quartets forms a right-handed helix

The first evidence of such architectures dates back to the 70's and comes from spectroscopic and fiber diffraction studies of poly(dG) and polyinosinic acid [1,2]. Attention to these motifs was highly renewed some years later, when Williamson *et al*. [3] showed that telomeric sequences can form G-quartets in vitro. Since then, a high number of studies have shown that guanine-rich repeats appear not only in telomeres but are also adopted in other key biological contexts, including some oncogenic promoter elements [4-12], and within RNA 5'-untranslated regions (UTR) in close proximity to translation start sites [13]. Thus,

quadruplex motifs may act as topological switches that are coupled to the initiation of transcription. In addition the number of reports describing specific quadruplex binding proteins is now considerable [14-21]. For all these reasons, G-quadruplex DNA structures are a potential target for drug design.

Quadruplex structures have also an increasing interest for their applications in supramolecular chemistry or nanotechnology. High-order structures such as G-wires [22,23], DNA nanodevices based on quadruplex-duplex interconversion [24] or biosensors [25] have been described in the literature.

5.2. Structural features of G-quadruplexes

5.2.1. Topological classification of G-Quadruplex.

The first structures of a G-quadruplex were reported in 1992 for the sequence of $d(G_4T_4G_4)$ from the 3' overhang of *Oxytricha* telomere by both X-ray crystallography [26] and NMR spectroscopy [27,28]. Subsequent NMR and crystallographic studies of different sequences have shown that guanine-rich DNA fragments form quadruplexes with different topologies and strand orientations, depending on the sequence and the number of strands.

Quadruplex can be tetramolecular (when formed by four strands), bimolecular (referred to as hairpin dimers) and unimolecular (one single strand folds by itself to form G-tetrads intramolecularly). Within these groups, they can be classified attending to the relative orientation of the chains (parallel or antiparallel) and to the way the loops connect the different strands. There are three different types of loop, as depicted in the bottom scheme (Scheme 5.3). **Lateral** loops (also known as edgewise) link bases of the same tetrad that share hydrogen bonds. In contrast, **diagonal** loops link bases of the same tetrad that do not share hydrogen bonds. **Propeller** loops (also known as double-chain reversal), link guanines that are not in the same tetrad but share a groove.
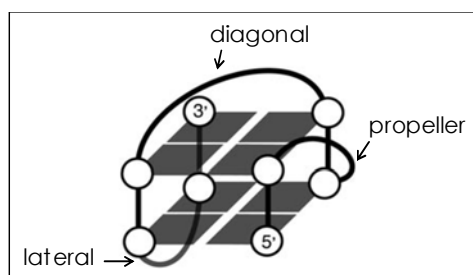
Scheme 5.3. Different types of loops linking strands in a G- quadruplex.

The figure below (figure 5.4) shows a classification of the different quadruplex topologies according to the number of DNA strands and to the way the loops connect them.

tetramolecular	bimolecular	unimolecular
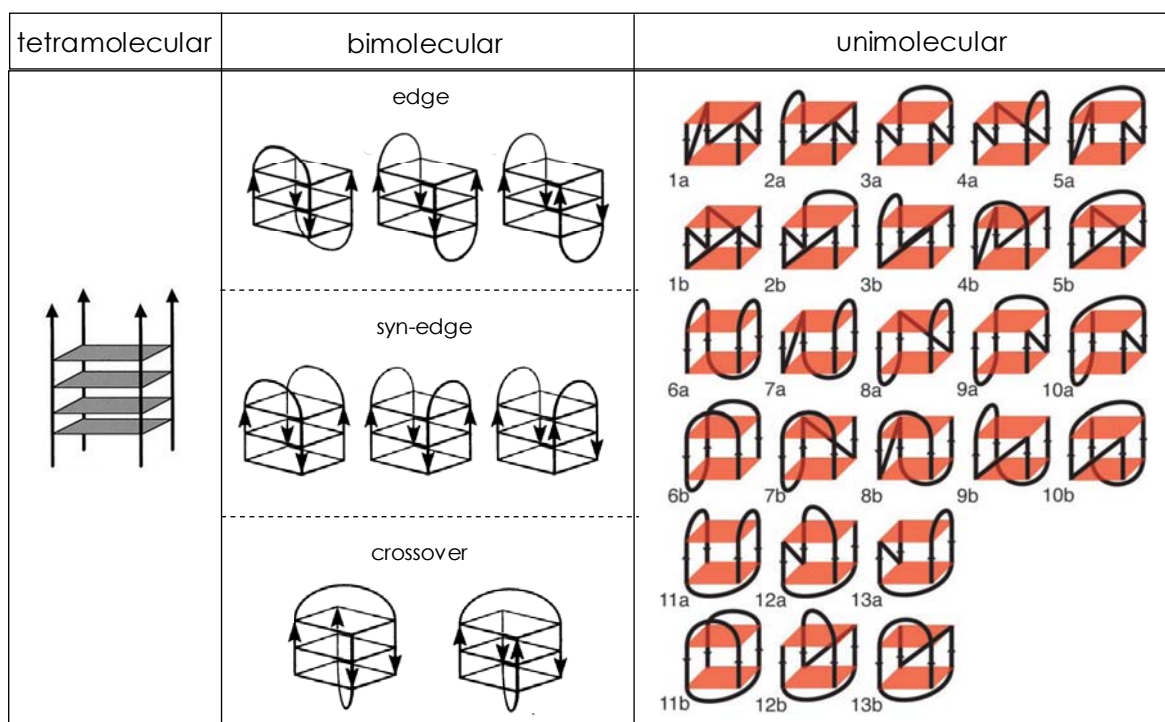
Figure 5.4. Different topological forms of tetramolecular, bimolecular and unimolecular G-quadruplex structures.

Tetramolecular quadruplexes have usually their four strands in a parallel orientation. In the case of bimolecular quadruplexes, different topologies have been observed. In the *edge* form, two lateral loops connect adjacent DNA strands. If the loops lie on the same face of the G-tetrad stacking the structure is called *syn-edge*. The *crossover* form is characterized by diagonal loops that connect opposite strands transversely.

In the case of unimolecular quadruplexes, since their topology can be defined by three loops, and there are three loop types, 27 theoretical loop combinations are possible. However, many of these are sterically not permissible. The exclusion of these combinations results in 13 possible combinations starting from a clockwise loop, and 13 from an anticlockwise loop. Thus, there are 26 permissible looping combinations, which have been recently reviewed by Webba da Silva *et al*. [29,30] and are represented above.

The most common topologies are the *chair* (schemes 6a, 6b in figure 5.4) and the *basket* form (11a, 11b in figure 5.4). While the *chair* presents three lateral loops, in the *basket* form one of the loops connects two strands diagonally. Other combinations of strand directionalities and connections have been observed, such is the case of the *dog-eared* structure [31] which contains two lateral loops and a

propeller loop that runs diagonally across the faces that are perpendicular to the G-tetrads (9a, 9b in figure 5.4).

5.2.2. G-quadruplex grooves

In a quadruplex structure, the phosphodiester backbones of stacked tetrads delimit four cavities or grooves, which have different dimensions depending on the glycosidic bond angles (GBA) of the guanosine nucleotides. These can adopt either an *anti* or a *syn* conformation, which differ in the relative disposition of the guanine aromatic ring respect to the deoxyribose ring. The chemical structures of the *anti* and *syn* conformers of 2'-deoxy-guanosine are depicted in figure 5.5.
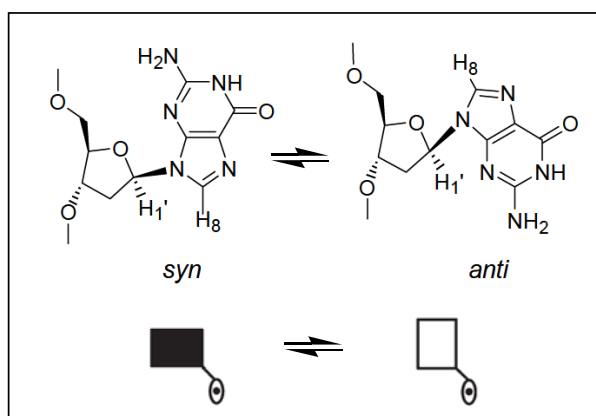
Figure 5.5. Relative disposition of the aromatic ring respect to the deoxyribose ring in the *syn* and *anti* guanine conformers.

Thus, there are 16 possible GBA positions for (G:G:G:G) tetrads, as can be seen in the figure 5.6 below.
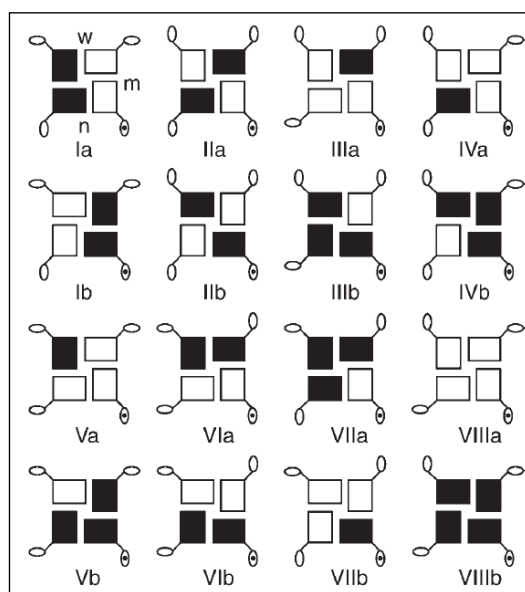
Figure 5.6. All possible combinations of glycosidic bond angles for a G-tetrad. Extracted from reference [29].

The distinct distribution of these glycosidic conformations in the G-tetrads results in the distinct nature of grooves. Depending of their width they are classified in three types: wide (w), medium (m) and narrow (n). If contiguous bases in a tetrad have the same GBA, they form a medium groove. In contrast, narrow and wide grooves are the result of hydrogen-bond-aligned bases with different GBA. Combination Ia of figure 5.6 shows the type of groove (w,m,n) according to the adjacent disposition of GBA.

For example, tetramolecular parallel quadruplexes have four equivalent grooves of medium width with all the guanines in *anti* conformation [32,33]; quadruplexes formed with alternating *anti-syn-anti-syn* dG within each quartet have two narrow and two wide grooves [15]; moreover, quadruplexes formed with *anti-anti-syn-syn* alternation within each quartet have one wide, one narrow and two medium width grooves [34]. The G-tetrads included in these examples are represented in the figure 5.7.
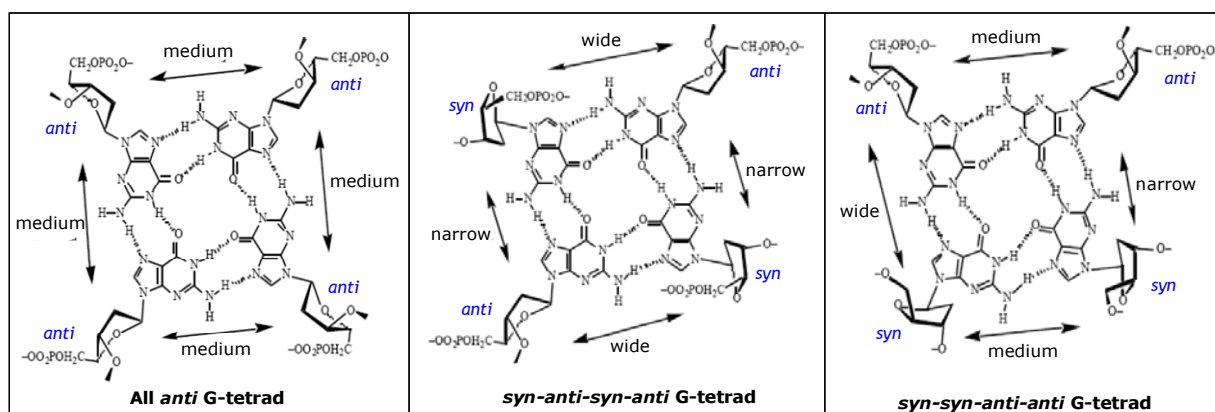
Figure 5.7. Glycosidic angles of guanines and their effects on the width of quadruplex grooves.

The specific manner of alternating groove widths in these structures could provide a way of selectively targeting specific topological and conformational forms of G-quadruplex DNA.

5.2.3. G-quadruplexes and cation binding

In G-quadruplex DNA the central cavity formed by stacked G-tetrads serves as a host to a variety of cations [35]. Numerous studies have investigated the localization and effect of different monovalent cations on quadruplex structures and have clearly shown that they play an important role in the folding and stability of quadruplexes. In fact, in most cases these structures do not form in the absence of such ions.

The central core of the G-quartet produces a specific geometric arrangement of lone pairs of electrons from the four guanine oxygen atoms (O6), which can coordinate a monovalent ion of the correct size, such as Na^+ or K^+. The smaller Na^+

ion can sit in the plane formed by these atoms, whereas the larger K^+ requires a nonplanar component, which may lie between two G-quartets [36], as shown in Figure 5.8. This allows additional coordination of the metal ions, and satisfies their usual hexacoordinate stereochemistry.
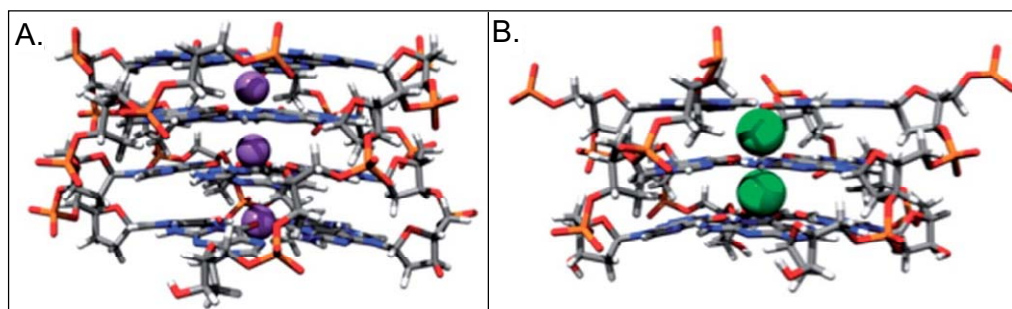
Figure 5.8. Ion-binding sites in quadruplex. A) Parallel stacked quartets with Na^+ stabilization (purple spheres) from (d(TGGGGT)$_4$). B) Parallel stacked quartets with K^+ stabilization (green spheres) from (dA(GGGTTA)$_3$GGG). Extracted from reference [36].

Some works in the literature have revealed significant differences not just in the stability but also in the structure of the same sequence depending on the counterion present in solution. In some cases an interconversion between different conformations can be modulated by the type of cation [37-39]. For example Feigon and co-workers [39] have used ^{1}H-NMR to study the competition between Na^+ and K^+ for coordination by G quartets using the oligonucleotide d(G$_3$T$_4$G$_3$) as a model system and they have monitored the conversion between the sodium and potassium forms under equilibrium conditions.

Most of the studies conducted so far have been carried out with Na^+ or K^+ as they are the most common cations in cells, but other ions have shown affinity for quadruplex structures as is the case of NH_4^+ [40, 41], Li^+ [42], Sr^{2+} [43, 44] or Ca^{2+} [38]. The binding affinity of metal ions follows the trend $K^+ \sim Sr^{2+} >> Rb^+ \sim Ba^{2+} > NH_4^+ > Ca^{2+} > Na^+ > Mg^{2+} \sim Cs^+ > Li^+$.

5.3. Biological relevance of G-quadruplexes

5. 3.1. G-Quadruplex binding proteins

One of the reasons of the biological relevance of the G-quadruplexes comes from the high number of proteins that have been shown to bind these DNA structures. Several research groups have identified proteins in diverse organisms that exhibit physical and functional interactions with DNA quadruplexes.

A compilation of proteins that have been shown to interact with G-quadruplexes have been reviewed by Fry in 2007 [45]. According to their function, G-quadruplex interacting proteins can be classified into five different groups:

- Proteins that bind preferentially and at high affinity to DNA quadruplex and in some cases increase its stability. Such are the cases of thrombin [15], the transcription factor MyOD [46], rat liver proteins named uqTBP25 [47] and qTBP42 [17], a *Tetrahymena* G-quadruplex binding protein [48], a bovine macrophage scavenger receptor [14] or some HIV-1 proteins [20,49].

- Proteins that promote the formation of quadruplexes. The earliest described protein within this group was the β subunit of the *Oxytricha* telomere-binding protein, which binds to the single-stranded form of telomeres and facilitate the association into G-quadruplex structures in a sodium dependent manner [50]. In a similar way RAP1, the telomere binding protein from *Saccharomyces cerevisiae*, selectively binds to and promotes the formation of G-quadruplexes in presence of potassium ions [51]. Other examples are yeast Hop1 protein [52] and the human DNA topoisomerase I [53].

- Proteins that destabilize quadruplex structures. Isolated from diverse species, proteins of this class disrupt different types of tetrahelical DNA. Interestingly, several of the destabilizing proteins are members of the heterogeneous nuclear ribonucleoprotein (hnRNP) family [54,55]. These are complexes of RNA and protein present in the cell nucleus during gene transcription and subsequent post-transcriptional modification of the newly synthesized RNA.

- DNA helicases that preferentially catalyze the unwinding of quadruplexes in ATP-hydrolysis dependent reaction. Helicases of such selectivity were identified in Simian virus 40 (SV40) [56], yeast [57] and human cells [58,59]. It is notable that three of the described enzymes are members of the RecQ family of helicases, which are important to ensure precise genetic recombination and chromosome segregation.

- Nucleases that specifically incise DNA at or next to quadruplex domains. As DNA recombination requires cleavage of strands in the involved chromosomes, identification of several nucleases that incise DNA within or close to tetraplex DNA domains strengthens the relevant role of quadruplex structures in this process [60-62].

5. 3.2. G-Quadruplex in aptamers

G-quadruplexes are part of the bioactive structure of some protein-binding aptamers. DNA aptamers are oligonucleotides that have been created through repeated round of in vitro selection [63] to bind biological targets (e.g. proteins) and that posses molecular recognition properties that rival antibodies [64,65].

The most well-known case is the thrombing binding aptamer (TBA). Crystallographic [66] and NMR [67] spectroscopic studies have shown that TBA forms a unimolecular G-quadruplex with two G-quartets and three loops (Figure 5.9). The structure and biological activity of this aptamer is K^+-dependent. Other

examples of DNA aptamers are inhibitors of human HIV integrase [68-69b] and adopt a unimolecular G-quadruplex similar to TBA.
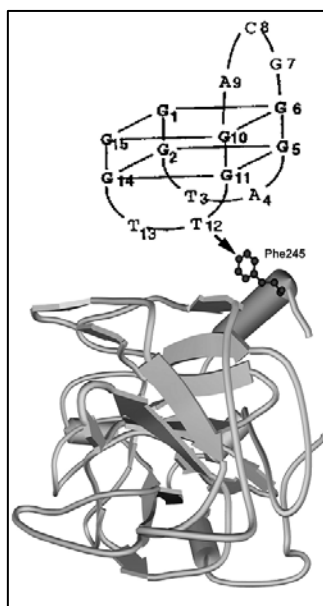
Figure 5.9. Schematic representation of the G-quadruplex TBA and its interaction with thrombin.

Studies where crystal structures are available reveal few direct interactions between the protein and the G-quadruplex core. Instead, the G-quadruplex seems to function as a scaffold on which loops are displayed for molecular recognition. However, more structural information is required to know if this preference to bind loops is a general trend in G-quadruplex-protein interactions.

5.3.3. G-quadruplexes in telomeres

Telomeres are non-coding DNA sequences that together with associated proteins are located at the ends of the chromosomes in eukaryotes. Telomeres are essential for chromosomal stability and genomic integrity, provide sites for recombination events and transcriptional silencing and appear to play a critical role in cellular aging and cancer [70-74]. These functions are mediated by tandem repeats of short guanine rich sequences that can form structures based on the G-quadruplex, typified by the hexanucleotide repeat d(TTAGGG)n in vertebrates.

In normal cells gradual loss of these telomeric sequences occurs with each successive round of cell division. After 20-30 cell replications a critical level of telomere shortening is reached and cells enter in replicative senescence, they cease to divide and might be directed to apoptotic death. This is why telomere shortening has been considered to be a 'molecular clock' of the aging process [75,76]. In contrast, telomeres of cancer cells do not shorten on replication but remains constant in length in succeeding generations. The explanation lies in the activation of telomerase, an enzyme which is overexpressed in 80-85% of tumour cells and

that adds TTAGGG repeats to the 3' end of telomere regions, causing the cells become immortal.

It has been proposed that the single stranded overhang of 5'-TTAGGG-3' repeats in the human telomere can fold into an intramolecular G-quadruplex, and stabilization of this structure has been shown to inhibit telomerase activity [77] because whereas single-stranded linear DNA is a telomerase substrate, G-quadruplex is not. Thus, an interesting pharmacological approach consists in inhibiting telomerase activity by stabilization of quadruplex with suitable drugs [78-82]. *In vivo* anticancer activity has been reported for a few telomeric quadruplex ligands [83-85].

5.3.4. G-quadruplexes in gene promoters

Sequences which can form G-quadruplexes have also been found in gen promoters, suggesting a function that may relate to gene regulation at the level of transcription. This has led to extensive investigations of the role of promoter G-quadruplex in regulation of the proto-oncogenes including *c-myc* [4-7], VEGF [8], KRAS [86,87], *bcl*-2 [10], HIF-1α [9] and *c-kit* [11,12].

These quadruplex structures may act as topological switches that are coupled to the initiation of transcription (Figure 5.10).
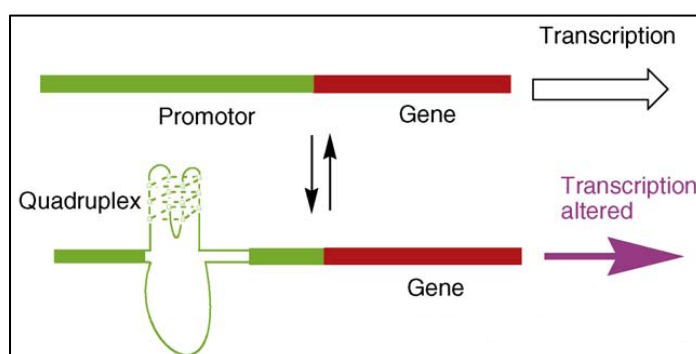
Figure 5.10. General scheme of G-quadruplex involvement in gene regulation. The formation of G-quadruplex, rather than duplex, in promoter regions is associated with an alteration in the transcription process.

There are a growing number of examples of G-quadruplex interactive small molecules that are able to modulate gene expression [5,88]. It has been proposed that small ligands can inhibit transcription by a stabilization of G-quadruplex with a consequential reduction in gene expression.

As an example, the group of Balasubramanian has reported the use of an isoalloxazine that binds G-quadruplex to reduce the levels of *c-kit* mRNA in *c-kit* expressing cell line [89].

5.4. Application of G-quadruplex structures in nanotechnology

5.4.1. G-wires

Formation of ordered structures by molecular self-assembly is an effective strategy for development of nanomaterials. Superstructures formed by G-rich DNAs had been observed in the early 90s in the presence of K^+ [90,91]. In 1994 Marsh and Henderson [22] first reported the spontaneously self-assembly of the telomeric DNA oligonucleotide 5'-GGGGTTGGGG-3' into long linear superstructures which they termed G-wires (Figure 5.11).
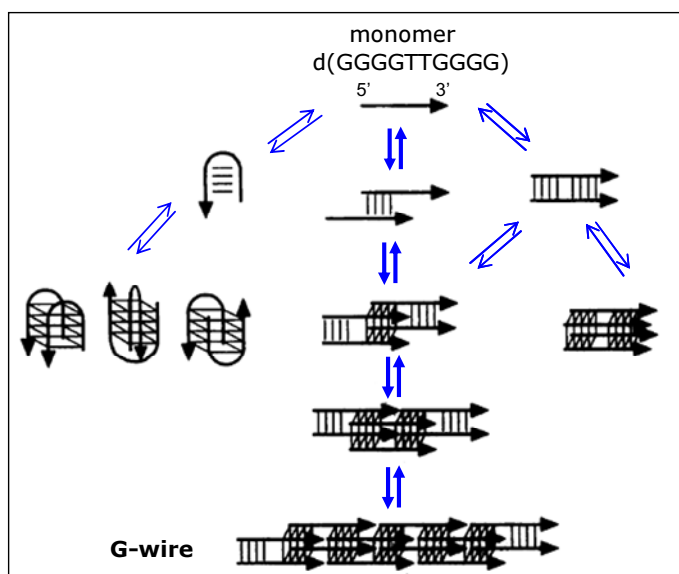
Figure 5.11. Scheme showing the main path for G-wire formation and the competing structures. The equilibrium between these structures is modulated by temperature, ionic species and concentrations.

The ability of this sequence to form self-assemble into long polymers clearly demonstrates its potential as scaffold structures for nanotechnology applications. In addition G-wires are more robust than duplex DNA when imaged by AFM [23].

The chemical modification of these guanine-rich DNA structures with functional moieties could increase their potential for nanostructure design and construction. Recently, Sugimoto and collaborators designed a DNA sequence that allows the switching and control of G-wire formation [92,93]. By incorporating a linker that rotates upon coordination with metal ions, they managed to control structural transition from antiparallel G-quadruplex to G-wire with Ni^{2+} and EDTA.

In addition to the scaffold role, some physical properties of G-wires, such as the central canal within which cations reside and an electron-rich external surface, suggest that they may be useful as functional components of nanoscale electronic devices [94].

5.4.2. Biosensors based on G-quadruplex DNA

G-quadruplex based aptamers have also applications in bioanalytical chemistry as they are used in biosensors development.

One of the most illustrating example are biosensors directed against thrombin, constructed by attaching a thrombin binding DNA aptamer labelled with methylene blue to a gold electrode. In the absence of target the immobilized aptamer remains relatively unfolded, thereby allowing the electron transfer. Upon thrombin binding, the equilibrium is displaced towards the folded G-quadruplex conformation and electron transfer is inhibited (Figure 5.12).
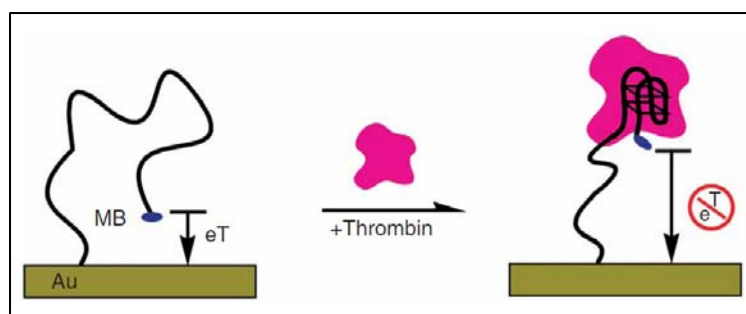
Figure 5.12. Scheme of an aptamer-based biosensor for thrombin detection.

5.5. Techniques employed in G-quadruplex structural studies

In this section an overview of the techniques commonly used for quadruplex conformational analysis will be briefly exposed.

The highest resolution structures (at atomic level) are obtained by **X-ray diffraction**, which has to date provided more than 50 structures including those with bound ligands (the 3D single crystal structures are available at the Nucleic Acids Data Bank in the http://ndbserver.rutgers.edu/). High resolution solution state nuclear magnetic resonance (**NMR**) has also provided quadruplex structures, although with significantly poorer definition. However NMR has also extensively used to assess quadruplex formation simply by measuring the exchangeable protons in the 10-12 p.p.m range [95,96].

UV spectroscopy and circular dichroism (**CD**) have long been used to characterize quadruplex structures as well as provide a convenient sensitive signal for monitoring transition between different conformations or ligand binding [49, 97]. This latter technique has been used in this work to study quadruplex stability and it will be explained in more detail in other sections in this chapter.

Fluorescent properties have also been used to monitor quadruplexes unfolding. If a donor and acceptor pair can be introduced at different positions of a

quadruplex, the fluorescence resonance energy transfer (**FRET**) can be easily monitored as a function of temperature to probe thermodynamic and kinetic stability of the structure [98,99].

5.6. Aim of the work

Previous work carried out by our group had analyzed the effect of 8-aminoguanine substitutions in the tetramolecular [d(TG$_4$T)]$_4$ parallel quadruplex formation [100]. Thermal stability studies showed that 8-aminoguanine replacement is not equally favourable at all positions but it could accelerate parallel quadruplex formation when inserted in the internal region. However replacement of a guanine in each quadruplex constituent d(TG$_4$T) sequence means that the four guanines relating to the same tetrad are modified. This can lead to the formation of multiple structures (for example by strands slipping to avoid an all-modified guanines tetrad if the resultant quartet is unstable) which makes difficult the kinetic and structural analysis. In addition theorical calculations are also complex when a modification is introduced in several guanines simultaneously.

The aim of this work is construct a molecule composed of four ODN strands whose 5'-ends are attached through a tetra-end-linker (trebler) and that is able to form a monomolecular parallel G-quadruplex, as proposed in the scheme of figure 5.13.
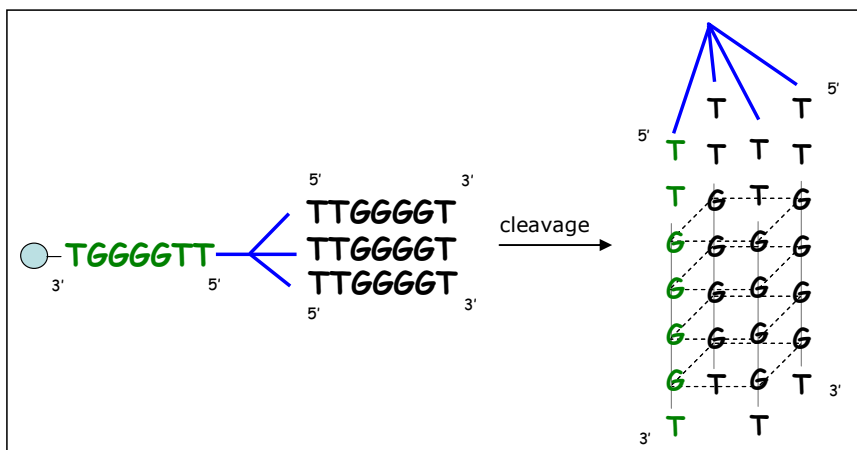
Figure 5.13. Scheme of the structure of ODNs designed for this work.

This system enables to modify just one single guanine (in the green strand) without having to replace the four nucleobases of the tetrad. In addition the use of this architecture will allow the interactions to be better characterized and provides a more reliable system to study effects of guanine substitutions than its tetramolecular counterpart. It is proposed that the fact the four quadruplex forming strands are covalently linked make the quadruplex structure more stable than when is formed by four separated strands. This can be useful for structural studies of alternative, less stable quartets such as tetrads formed by modified nucleosides.

In this chapter the use of this system to study the effect of 8-amino-guanine substitutions in quadruplex structure and stability will be adressed. NMR and CD analysis were performed for structural characterization and thermal denaturation studies.

5.7. Design and synthesis of the quadruplex forming oligonucleotides

The synthesis of a new modified ODN capable of forming a monomolecular parallel G-quadruplex (Scheme in Figure 5.13) has been carried out in an automatic synthesizer. The main structural feature of this ODN is the attachment of four strands through the 5'-ends by a tetra-end-linker. This branched structure was incorporated into the molecule with a commercially available phosphoramidite called "trebler" (figure 5.14). Commonly the presence of three adjacent DMT-bearing arms leads to lower coupling efficiency and increase the coupling time is needed.
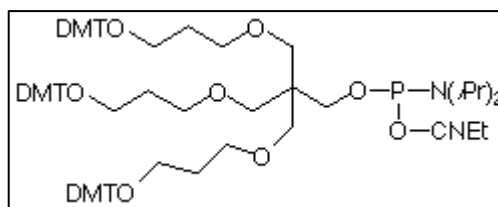
Figure 5.14. Branching unit used for the attachment of the four oligonucleotide strands that will form the parallel quadruplex.

Insertion of 8-amino-guanines was performed with the 8-amino-dG phosphoramidite shown in figure 5.15. In this molecule the amino groups of the nucleobase are protected with the dimethylaminomethylidine group. The use of 8-amino-dG in automatic oligonucleotide synthesis is straightforward and requires no changes from regular procedures, with the exception of the addition of 2-mercaptoethanol to the cleavage and deprotection solutions to avoid further oxidative damage [101].
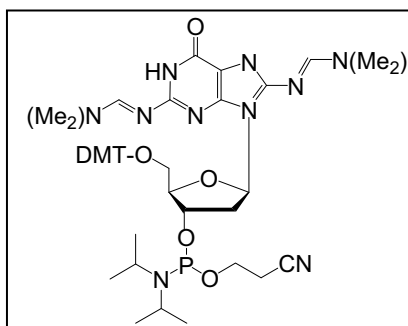
Figure 5.15. Phosphoramidite used for the introduction of 8-aminoguanines in the first chain of the quadruplex studied in this work.

The sequence of the chains was chosen mainly because the single strand d(TG$_4$T) is known to form a stable parallel tetramolecular quadruplex that has been well characterized in previous studies [32,33,102,103]. In this work an additional T is inserted to avoid steric hindrance of trebler with the nearest G-quartet.

The first part of the quadruplex (green chain in figure 5.13) was synthesized with the appropriate T and G 3'-phosphoramidites. The 8-amino-G phosphoramidite indicated above was used to introduce a modified guanine in the desired position. Secondly, the trebler phosphoramidite was coupled. After introduction of this branching unit the synthesis was carried on using T and G reversed phosphoramidite with a concentration higher than the one employed in standard synthesis because from there onward three bases need to be coupled in each cycle (as trebler provides three elongation points).

The different synthesized oligonucleotides were named **QO**, **Q1**, **Q2**, **Q3** and **Q4** depending on the position were 8-amino-G was inserted. Sequences corresponding to each quadruplex are listed in table 5.16.

Quadruplex	Sequence
Q0	$^{3'}$TGGGGTT$^{5'}$-trebler-$^{5'}$-[TTGGGGT]$_3$-$^{3'}$
Q1	$^{3'}$T**G**GGGTT$^{5'}$-trebler-$^{5'}$-[TTGGGGT]$_3$-$^{3'}$
Q2	$^{3'}$TG**G**GGTT$^{5'}$-trebler-$^{5'}$-[TTGGGGT]$_3$-$^{3'}$
Q3	$^{3'}$TGG**G**GTT$^{5'}$-trebler-$^{5'}$-[TTGGGGT]$_3$-$^{3'}$
Q4	$^{3'}$TGGG**G**TT$^{5'}$-trebler-$^{5'}$-[TTGGGGT]$_3$-$^{3'}$

Table 5.16. Oligonucleotide sequences used in this study. Bold case letters **G** correspond to 8-amino-G nucleotides.

Oligonucleotides were synthesized without performing final detritylation to facilitate reverse-phase HPLC purification. Upon completion of the chain assembly, the oligonucleotides were deprotected and cleaved from the support by a 0.1 M mercaptoethanol solution in aqueous concentrated ammonia for 24 hours at 55ºC to avoid oxidation of guanines.

ODNs were purified with the "*DMT ON*" protocol and peak corresponding to the DMT-protected product was collected. The figure 5.17 shows the HPLC profile of **Q0** (crudes of **Q1-Q4** presented a similar profile).
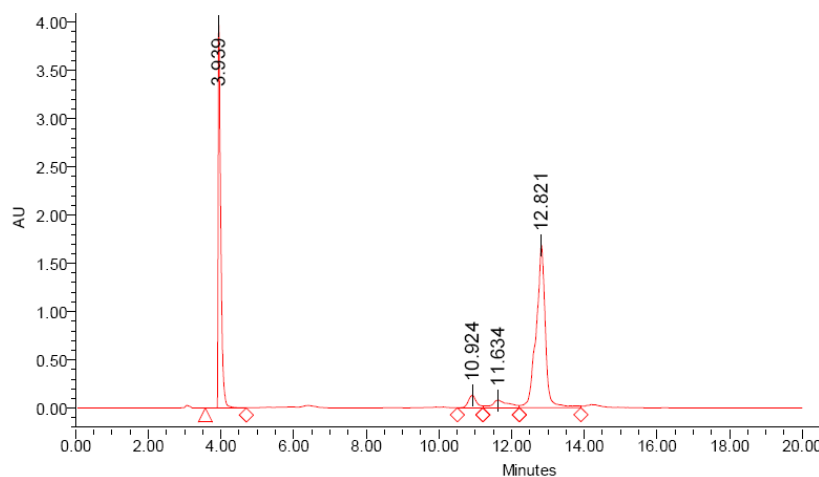
Figure 5.17. HPLC profile of the **Q0** sequence. Gradient: 15→ 80% B in 20 min (A: 5% ACN in 0.1 M TEAAc pH 6.5; B: 70% ACN in 0.1 M TEAAc pH 6.5)

As it can be seen the peak corresponding to truncated sequences (t_R=4 minutes, molecules without DMT) is much larger than the one corresponding to the desired product (t_R=12.8 minutes; molecules with DMT). Although the coupling time of 'trebler' was extended to 15 minutes the yield decreased to 40-50 % after the coupling of this phosphoramidite (according to the detritylation conductivity signal recorded by the automatic synthesizer detector). In addition coupling of reversed phosphoramidites is slightly lower than the 3'-standard phosphoramidites, specially the first ones coupled after the 'trebler' due to steric hindrance. This makes the overall yield to be quite low, as reflected in the HPLC profile of the figure 5.17. The yield was around 30-50% (depending of the sequence) according to the relative peak areas.

The purified oligonucleotides were detritylated, desalted by NAP-10, and analyzed by MALDI-TOF. As the MALDI spectra presented a multitude of poorly resolved peaks (figure 5.18.A) the samples were also analyzed by denaturing PAGE. For this purpose, electrophoresis was run in 20% polyacrylamide gel containing 8 M urea in TBE buffer. In figure 5.18.B the stained gel obtained after PAGE of purified and detritylated **Q0** is shown. Denaturing PAGE analysis revealed that the length of the purified **Q0** product corresponds to the desired quadruplex (4x7=28 bases).
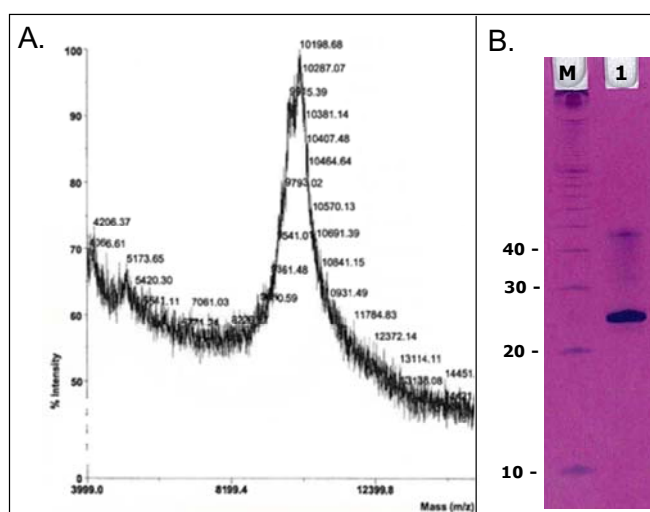
Figure 5.18. A) MALDI spectrum of the purified **Q0** product. The absence of a single well-defined peak suggests the possibility of the sample may contain different products. B) denaturing gel (20% polyacrylamide, 8M urea, TBE buffer) analysis of the purified **Q0** sequence. **M**: Marker (10-100 nt); **1**: purified and detritylated **Q0**.

As DMT groups attached to secondary hydroxyl groups (in the reversed phosphoramidites the DMT is protecting the 3'-OH) are known to detritylate slower than primary hydroxyl groups [104], the possibility of an incomplete deprotection was considered. This would explain the multitude of peaks in the MALDI spectra (quadruplexes with different number of DMT groups and consequently different MW) and the presence of just one single band in the denaturing gel (quadruplexes with different number of DMT groups but the same number of nucleotides).

To test this hypothesis the purified products were analyzed after the detritylation process by HPLC with the '*DMT ON*' protocol. The resulting HPLC profiles showed several peaks, which means that oligonucleotides of different hidrophobicity are obtained after the detritylation step suggesting that removal of DMT groups has not been completed. Figure 5.19 shows the HPLC profile obtained with **Q0** after the detritylation process (the rest of sequences showed a similar profile).

153
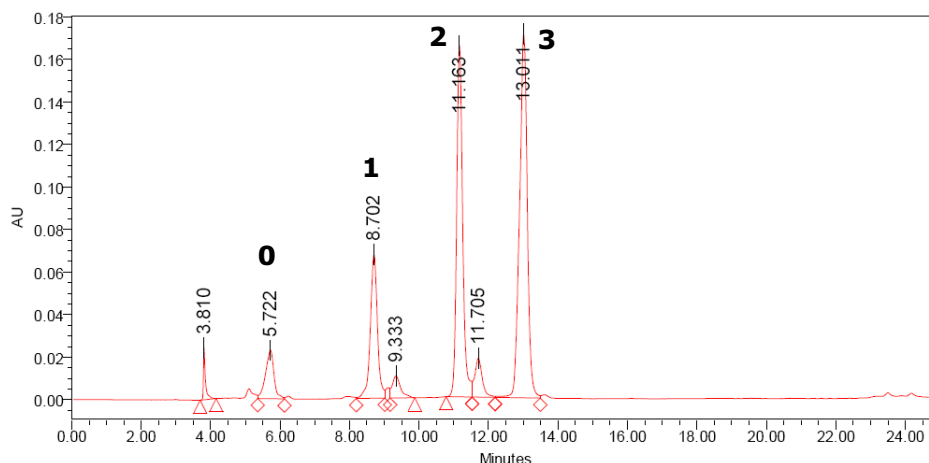
Figure 5.19. HPLC analysis of **Q0** after the detritylation process. Gradient: 15→ 80% B in 20 min (A: 5% ACN in 0.1 M TEAAc pH 6.5; B: 70% ACN in 0.1 M TEAAc pH 6.5)

All peaks were collected and analyzed by MALDI-TOF and denaturing PAGE. The table 5.20 summarizes the obtained MW values, including the main fragmentations observed for each of the products. The four collected products proved to correspond to the fully deprotected quadruplex (peak 0) and to quadruplex with one, two and three DMT groups respectively (peaks 1-3).

Sample	Obtained MW	Product and calculated MW
peak 0	n.d.[a]	Q0 → 9227.5
peak 1	9522/9221[b]	Q0+1DMT → 9530.8
peak 2	9821/9520[b]	Q0+2DMT → 9834.2
peak 3	10141/9823[b]/9521[b]	Q0+3DMT → 10137.6

Table 5.20. MW of the oligonucleotides analyzed in this study obtained by MALDI-TOF and their calculated MW values.

[a] Not appreciable signal. High MW ODNs that do not posses any hydrophobic group usually "fly" poorly in a MALDI-TOF instrument and an insufficient number of ionized particles reach the detector.

[b] Fragmentations originated by the loss of one or more DMT groups caused by the laser ionization of the mass spectrometry technique.

MW values obtained by MALDI-TOF confirmed the presence of quadruplexes with different number of DMT groups. Consequently, a second acidic treatment was required to completely remove the still-remaining protecting groups. Samples were subjected to a second detritylation step with acetic acid (80%) during 30 minutes at 55 ºC. HPLC showed a single peak eluting as quadruplex without DMT groups and confirmed the obtention of the fully deprotected sequences (Figure 5.21). However MALDI analysis did not provide good signals, which frequently occur when analysing large ODNs without hydrophobic groups (as in the case of the peak 0, Table 5.20).

154
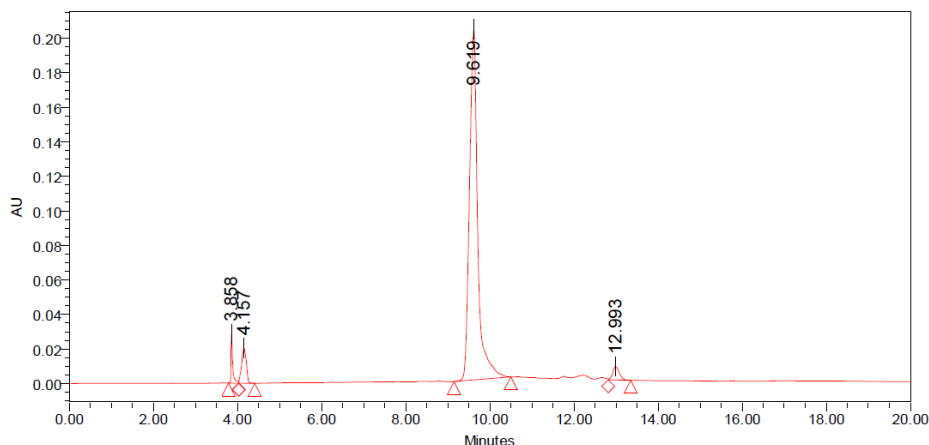
Figure 5.21. HPLC analysis of **Q0** after the second detritylation process, in which treatment with acetic acid (80%) at 55ºC during 30 minutes was performed. Gradient: 15→ 80% B in 20 min (A: 5% ACN in 0.1 M TEAAc pH 6.5; B: 70% ACN in 0.1 M TEAAc pH 6.5)

The structure and stability of the final detritylated, purified and desalted products **Q0**-**Q4** were studied by CD and NMR, as detailed in the next sections.

5.8. Thermal denaturation studies by circular dichroism

Circular dichroism (CD) is a spectroscopic technique which measures the differences between the absorbance of right and left-handed circularly polarized light and can be used to investigate the structure and topology of DNA quadruplexes by comparing their spectra with those of known structure. Different CD spectral signatures have been described for quadruplex and their distinct conformations [97,105]. Figure 5.22 shows the CD spectra of a reference set of DNAs of known quadruplex structure.
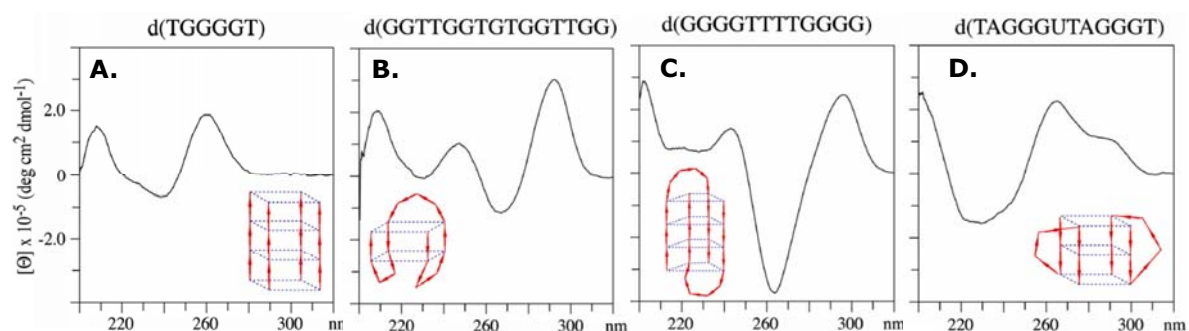
Figure 5.22. CD spectra of four reference quadruplex-forming sequences. Depiction of each structure is also shown. Extracted from reference [97].

A reference spectrum for a four stranded parallel quadruplex structure is that of d(TGGGGT) [102,103]. Its CD spectra has a positive band around 265 nm (Figure 5.22.A) that can be assigned to parallel strand quadruplex structures [106-

155

108]. The thrombin binding aptamer, d(GGTTGGTGTGGTTGG), adopts a chair type anti-parallel structure in solution [15,109,110] whose CD spectrum has a positive maximum near 295 nm and a negative band near 260 nm (Figure 5.22.B) that are characteristic of an anti-parallel structure [97,111,112]. Other molecule that presents a CD spectrum characteristic of an anti-parallel structure is the symmetric basket type formed by dimers of $d[G_4T_4G_4]$, although with a more pronounced negative band at 260 nm (Figure 5.22.C). Other sequences present CD spectra different from that of the typical parallel or anti-parallel structures as the example presented in figure 5.22.D. This CD spectrum contains two positive bands at both 260 and 290 nm that have been assigned to the parallel strand quartets and to the external loop residues respectively.

Since quadruplex DNA structures have distinctive circular dichroism spectra, temperature dependent changes in CD have often been used to determine quadruplex stability [113-115] by monitoring CD signal at appropriate wavelengths (260 nm for parallel quadruplexes and 295 nm for anti-parallel structures). CD has also been used to study ligand binding to quadruplexes [116] as well as the effects of cation [106-108,117] or chemical modifications on quadruplex structure [118-120].

In this work CD studies and CD thermal denaturation experiments were performed to demonstrate that the ODNs **Q0-Q4** can adopt a parallel G-quadruplex structure and to determine how substitution of a single G for 8-amino-G in different positions of these quadruplexes affects to their stability.

Since quadruplexes can adopt distinct conformations oligonucleotides were properly annealed by heating the samples to 95 ºC and slowly cooling to room temperature before recording CD spectra and melting profiles.

Firstly, CD spectra of 5 μM solutions of **Q0**-**Q4** in milliQ H_2O were registered at 20ºC. All samples had been purified by HPLC and desalted with a NAP column, which means that the only cations present in quadruplexes solutions are the triethylammonium coming from the HPLC buffers.

A positive band with a maximum around 260 nm and a negative band at 240 nm indicate the presence of a G-quadruplex structure involving four parallel strands. This CD spectral signature matches with that one obtained by other authors with the tetramolecular $[d(TG_4T)]_4$ in saline buffers [121], as it can be seen in figure 5.23. In this figure the CD spectra corresponding to the sequence **Q0** can be compared with the spectra registered in other works with samples of $[d(TG_4T)]_4$.
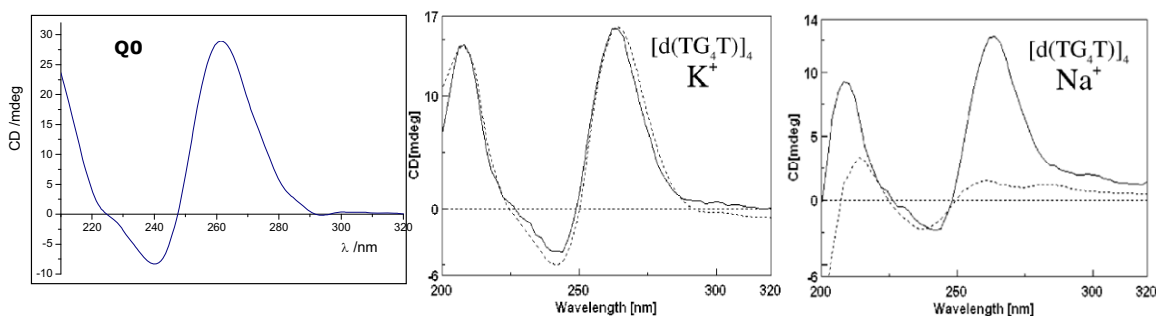
Figure 5.23. CD spectrum of **Q0** in non saline conditions at 20ºC (left column) registered in this work. CD spectra of d[(TG$_4$T)]$_4$ in 90 mM K$^+$ buffer (middle column) and in 90 mM Na$^+$ buffer (right column) at 25 °C (solid line) and 90 °C (dotted line); both extracted from reference [121].

All ODNs studied in this work adopted quadruplex structure in non saline conditions which indicates that these architectures can be formed even in absence of stabilizing cations such as K$^+$ or Na$^+$.

CD thermal denaturation experiments were performed monitoring the CD values (mdeg) at 260 nm in the range 10-90 ºC using a heating rate of 0.5 ºC/min. This low rate is selected to avoid hysteresis between melting and annealing curves (commonly observed in quadruplex studies due to slow kinetics of association-dissociation process), which is recommended for most melting experiments [112]. The melting profiles obtained with each sequence are shown in figure 5.24. In addition CD spectra were registered between 210-320 nm every 10 ºC.
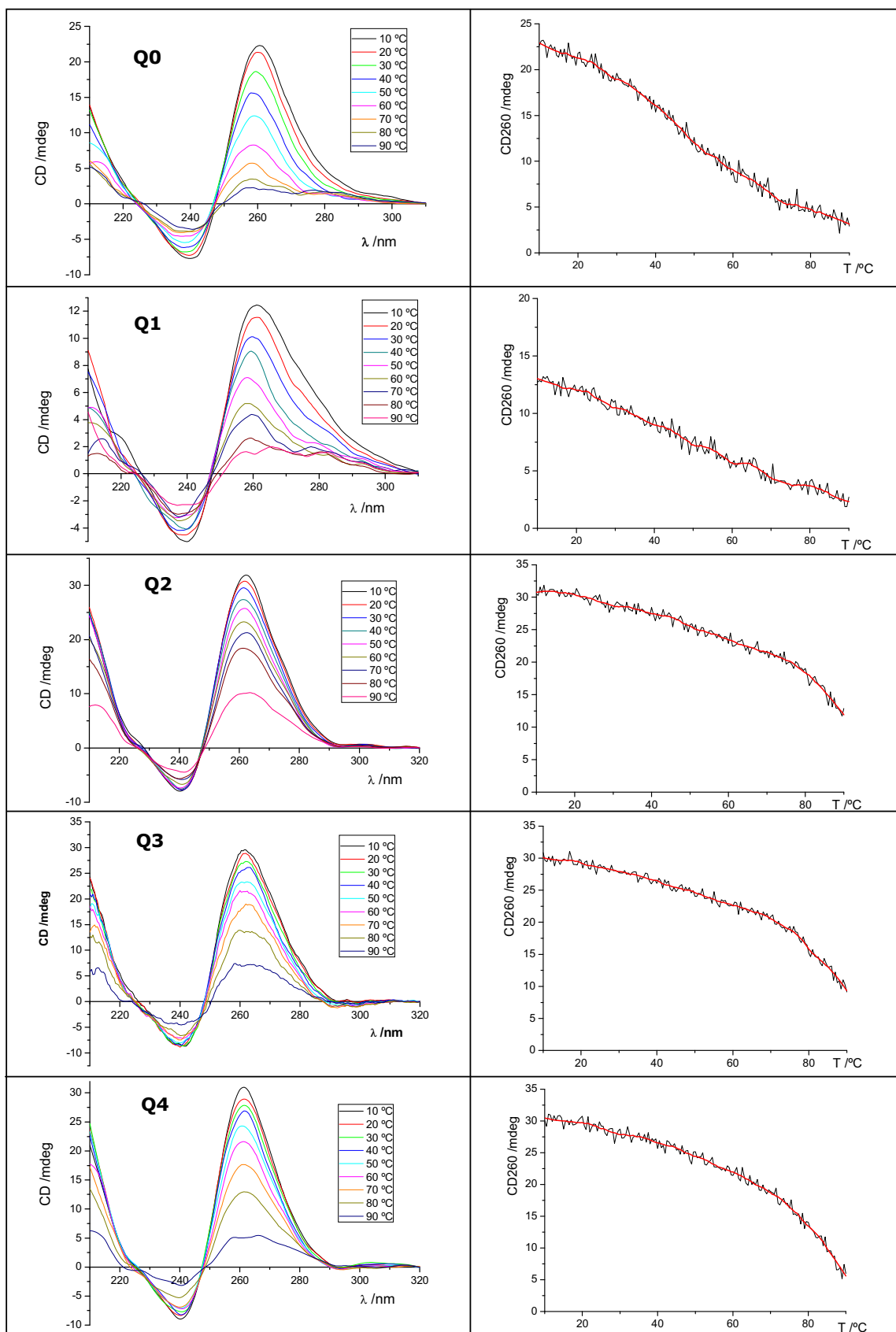
Figure 5.24. CD spectra of sequences **Q0-Q4** registered at different temperatures (left column). Melting profile of sequences **Q0-Q4** obtained by

monitoring the CD values (mdeg) at 260 nm in the range 10-90 ºC using a heating rate of 0.5 ºC/min (right column).

Typical descendant sigmoidal curves are obtained with **Q0** and **Q1** oligonucleotide sequences. However, melting profiles of **Q2-Q4** indicate that only partial fusion occurs. In these cases CD_{260} signal decreases when temperature raises but complete unfolding of quadruplex structure is not achieved. According with this, even when the **Q2-Q4** CD spectra are registered at 90 ºC, the 240 and 260 nm bands are still present, as seen in the graphics above.

CD thermal denaturation studies were also performed with diluted samples of some of the quadruplex solutions (1.25 μM of **Q3**). The melting curve profiles were found to be concentration independent which seems to indicate that quadruplexes are mainly present as monomolecular species.

Finally, the sigmoidal and exponential fitted curves corresponding to normalized melting profiles of all sequences studied in this work are summarized in the graphic of figure 5.25.
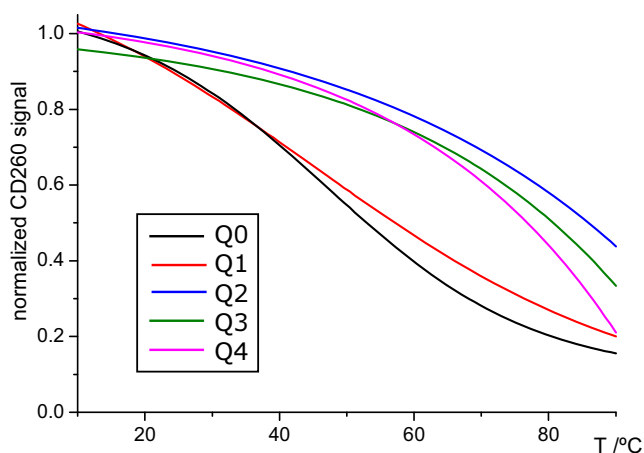
Figure 5.25. Sigmoidal (black and red line) and exponential (blue, green and pink line) fitted curves corresponding to normalized melting profiles of **Q0**-**Q4** in non saline conditions.

Comparison of the melting profiles of the different sequences enables a simple evaluation of their relative stabilities. From figure 5.25 it can be concluded that sequences with an 8-amino-guanine substitution in the internal region (**Q2-Q4**) form much more stable quadruplexes than the non-modified sequence (**Q0**). When the replacement is carried out in the first position (**Q1**) stability of the quadruplex is slightly increased.

Table 5.26 shows a list with an approximated melting temperature (Tm) value for each structure.

Sequence	Tm / ºC
Q0	50
Q1	52
Q2	>80 [a]
Q3	>80 [b]
Q4	>80 [c]

Table 5.26. Tm of the different quadruplex-forming sequences.
[a,b,c] As only partial fusion occurs Tm can not be calculated above this value.

5.9. Structural studies of the quadruplexes by ^{1}H-NMR

Nuclear magnetic resonance (NMR) spectroscopy is one of the principal techniques used to obtain structural information of molecules by exploiting the properties of their magnetic nuclei have in a magnetic field and applied electromagnetic (EM) pulse or pulses, which cause the nuclei to absorb energy from the EM pulse and radiate this energy back out at a specific resonance frequency.

NMR has been extensively used in the study of nucleic acids for determination of high resolution structures, insights into their dynamics and stability or study of ligand-binding. Although full structure determination of a ODN sequence requires registration of multidimensional spectra that allow complete assignment of resonances, monodimensional ^{1}H-NMR provides simple detection of quadruplex structures by assignment of exchangeable guanine imino protons in the 10-12 ppm range. These guanine imino protons have a characteristic shift when hydrogen bonded. In addition, they exchange relatively slowly with the deuterated solvent when compared to non-hydrogen-bonded protons.

The amount of sample typically used in solution NMR studies ranges between 1 and 3 mM. The little amount of samples obtained in this work did not allow studying all the sequences with this technique (as the preparation of solutions in such high concentration was not possible).

^{1}H-NMR studies were performed only with the **Q0** and the **Q4** sequence. Spectra of a 25 μM **Q0** solution and 75 μM **Q4** solution in 9:1 H_2O/D_2O (with and without K^+) were recorded at 5, 25 and 45 ºC using pulse field gradient WATERGATE for water suppression. Figure 5.27 shows the registered spectra of **Q0** and **Q4** solutions with 5 mM K^+, which were consistent with quadruplex formation.
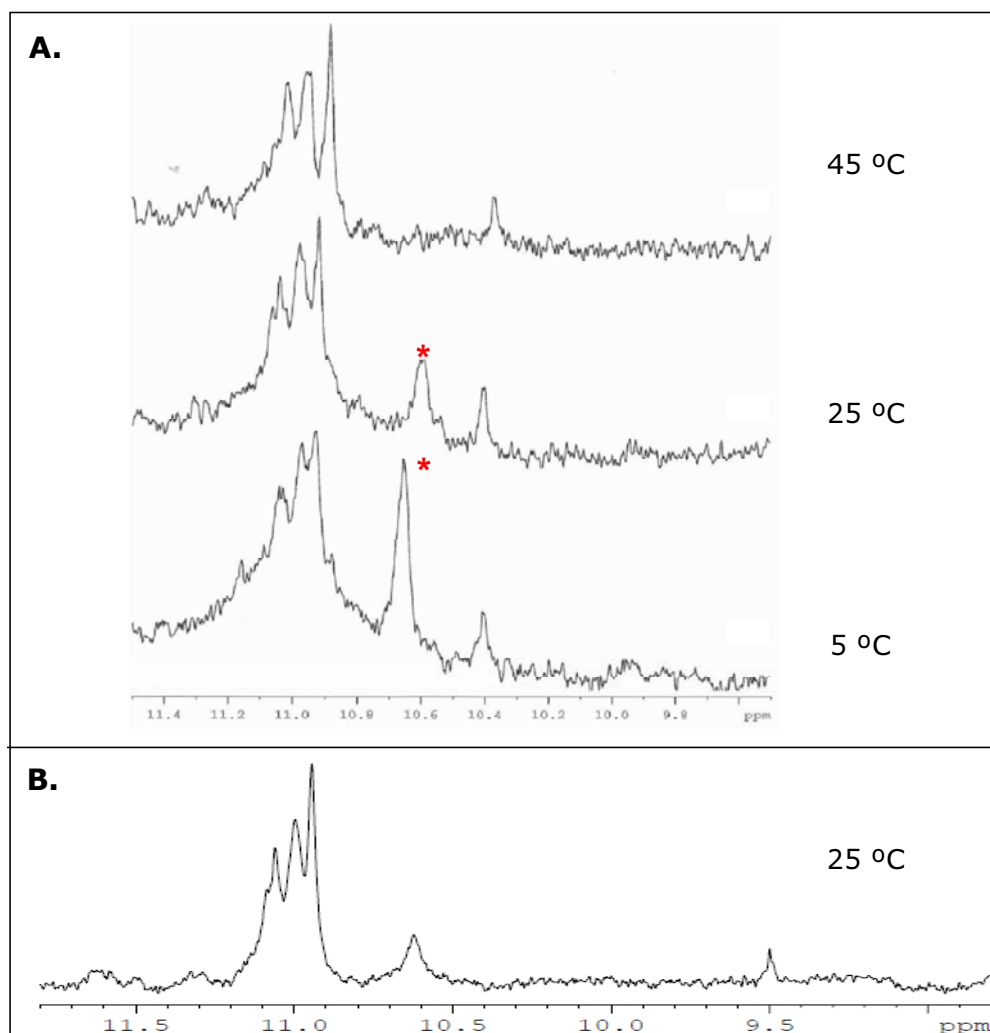
Figure 5.27. Imino proton region of the ^{1}H-NMR (600 MHz) spectra of the A) **Q4** and B) **Q0** sequences. The spectra were registered in H_2O/D_2O (9:1) solution at 75 and 25 μM, respectively. **Q4** spectra were recorded at 5, 25 and 45 ºC to study the effect of temperature in the quadruplex stability.

As it can be seen in the graphics the signal-to-noise ratio of these experiments is quite low. As it can be deduced looking at the low signal-to-noise ratio in the graphics above, sensitivity achieved with this ODN concentration is not enough to confidently assign all the obtained signals. However, on the basis of the comparison with the corresponding region of the spectrum of $[d(TG_4T)]_4$ obtained by other authors which displays a similar peak profile, singlets in the range 10.4-11.5 ppm are suggested to correspond to exchange imino protons involved in Hoogsteen N(1)H/O(6) hydrogen bonds of G-quartets, although in this work a partial overlapping of some signals is observed.

As in previously studied structures containing 8-amino guanines, the signals of the amino protons at position 8 were not observed in the NMR spectra [100].

In the case of **Q4**, at higher temperature, the spectra exhibited narrower signals (figure 5.27). This is commonly due to a shorter correlation time caused by the faster mobility of the molecules. At 45ºC the singlets are still present which means the quadruplex is still structured at this temperature (as observed also in CD spectra). However, the raise of the temperature led to the disappearance of the 10.7 ppm signal (denoted by a red asterisk in figure 5.27). This may be due to dissociation of multimeric species. To find out the oligomerization state of the samples at the concentration used in the NMR experiments a native gel electrophoreses was run on a non-denaturing polyacrylamide gel, as detailed in the next section.

5.10. Assessment of the quadruplex oligomerization state by native PAGE.

While in denaturing PAGE the electrophoretic mobility of biomolecules depends primarily on their molecular mass, in native PAGE separations are run in non-denaturing conditions which implies that the mobility depends on both the molecule's charge and its hydrodynamic size. Thus native gels are useful tools to study any process that alters either the charge or the conformation of a molecule and so has been widely used to detect oligomers and aggregates. In this work native PAGE was performed to asses the oligomerization state of the quadruplexes studied by NMR (**Q0** and **Q4**).

Native gel electrophoresis was run on 15 % non denaturing polyacrylamide gel in TAE buffer (1x). ODN solutions were prepared in a similar concentration to the one employed in NMR experiments and with 5 mM K^+. Electrophoretic analysis was carried out using the tetramolecular quadruplex $[d(TG_4T)]_4$ as reference. In both cases, **Q0** and **Q4** sequences resulted in two major bands (figure 5.28), suggesting that at this concentration they form not only monomeric species but also dimeric structures.
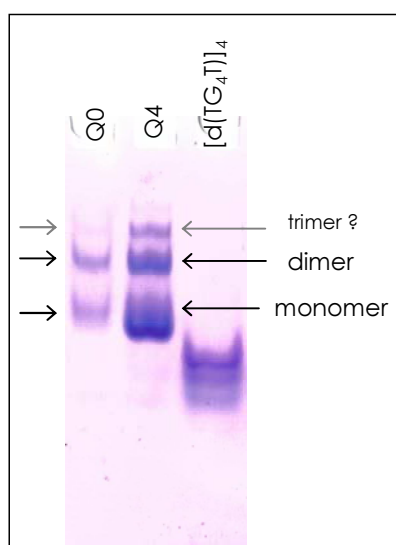
Figure 5.28. Native PAGE analysis to investigate the molecularity of the **Q0** and **Q4** sequences. $[d(TG_4T)]_4$ is loaded for comparison of relative migrations.

In figure 5.29 two hypothetical dimeric structures are proposed.
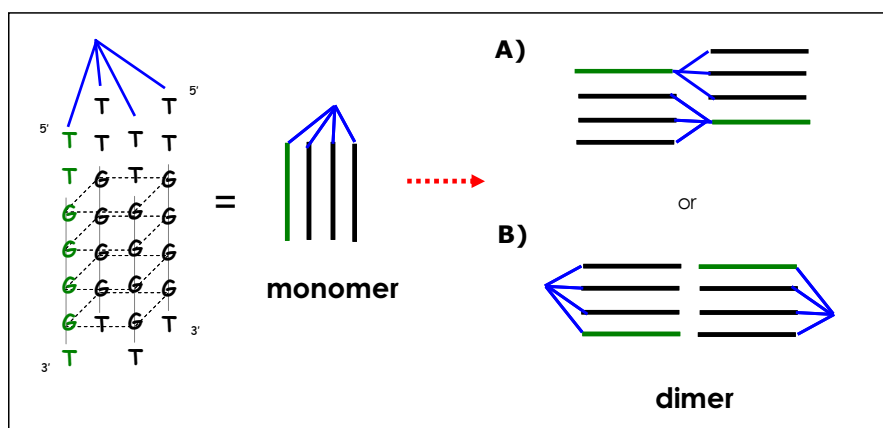
Figure 5.29. Scheme of two hypothetical dimerizations of the quadruplex-forming structures studied in this work.

It is proposed that the association of two molecules as represented in figure 5.29.A enables the formation of two parallel quadruplexes, each of them containing one strand belonging to the adjacent molecule (green line in the scheme above). A mixture of these forms could exist if 'trebler' linker was not flexible enough to allow organization of the four strands into a monomolecular quadruplex or might be favoured when using high DNA concentrations.

The model depicted in figure 5.29.B is proposed based on previous observations reported in literature. Crystallographic studies of d(TGGGGT) quadruplexes performed by Cáceres *et al*. [123] revealed stacking of thymine tetrads between neighbour quadruplexes packed in a head-to-head fashion.

5.11. Conclusions

The use of a branching unit has allowed the synthesis of a molecule containing four G-rich DNA strands whose 5'-ends are covalently attached and that has been shown to form a very stable parallel G-quadruplex, even in absence of stabilizing cations. This system has allowed the synthesis of quadruplexes with single modifications in just one of the strands.

Oligonucleotides with 8-amino-guanine substitutions provide more stable structures than non-modified sequences, especially when replacement is carried out in the internal region of the quadruplex. Evidences of higher-order structures have been observed when working with relatively concentrated samples but further study is needed to gain more conclusive information about this issue.

5.12. References

[1]. Thiele, D., and Guschlbauer, W. (1973) The Structures of Polyinosinic Acid. *Radiat. Environ. Biophys. 9*, 261-277.

[2]. Zimmerman, S.B., Cohen, G.H., and Davies, D.R. (1975) X-Ray Fiber Diffraction And Model-Building Study Of Polyguanylic Acid And Polyinosinic Acid. *J. Mol. Biol.* 92, 181-192.

[3]. Williamson, J.R., Raghuraman, M.K., and Cech, T.R. (1989). Monovalent Cation Induced Structure Of Telomeric DNA: The G-Quartet Model. *Cell* 59, 871-680.

[4]. Simonsson, T., Pecinka, P., and Kubista, M. (1998). DNA Tetraplex Formation In The Control Region Of *c-myc*. *Nucleic Acids Res.* 26, 1167-1172.

[5]. Siddiqui-Jain., A., Grand, C.L., Bearss, D.J., and Hurley, L.H. (2002) Direct Evidence For A G-Quadruplex In A Promoter Region And Its Targeting With A Small Molecule To Repress *c-myc* Transcription. *Proc Natl Acad Sci U S A* 99, 11593-11598.

[6]. Phan, A.T., Modi, Y.S., and Patel, D.J. (2004). Propeller-Type Parallel-Stranded G-Quadruplexes In The Human C-Myc Promoter. *J. Am. Chem. Soc.* 126, 8710-8716.

[7]. Ambrus, A., Chen, D., Dai, J., Jones, R.A., and Yang, D. (2005) Solution Structure Of The Biologically Relevant G-Quadruplex Element In The Human c-myc Promoter. Implications For G-Quadruplex Stabilization. *Biochemistry* 44, 2048-2058.

[8]. Sun,D., Guo,K., Rusche,J.J. and Hurley,L.H. (2005) Facilitation Of A Structural Transition In The Polypurine/Polypyrimidine Tract Within The Proximal Promoter Region Of The Human VEGF Gene By The Presence Of Potassium And G-Quadruplex-Interactive Agents. *Nucleic Acids Res*., 33, 6070–6080.

[9]. De Armond, R., Wood, S., Sun, D., Hurley, L.H. and Ebbinghaus, S.W. (2005) Evidence For The Presence Of A Guanine Quadruplex Forming Region Within A Polypurine Tract Of The Hypoxia Inducible Factor 1alpha Promoter. *Biochemistry*, 44, 16341–16350.

[10]. Dexheimer,T.S., Sun,D. and Hurley,L.H. (2006) Deconvoluting The Structural And Drug-Recognition Complexity Of The G-Quadruplex-Forming Region Upstream Of The *bcl*-2 P1 Promoter. *J. Am. Chem. Soc*., 128, 5404–5415.

[11]. Rankin, S., Reszka, A.P., Huppert, J., Zloh, M., Parkinson, G.N., Todd, A.K., Ladame, S., Balasubramanian, S. and Neidle, S. (2005) Putative DNA Quadruplex Formation Within The Human c-*Kit* Oncogene. *J. Am. Chem. Soc*., 127, 10584–10589.

[12]. Fernando, H., Reszka, A.P., Huppert, J., Ladame, S., Rankin, S., Venkitaraman, A.R., Neidle, S. and Balasubramanian, S. (2006) A Conserved Quadruplex Motif Located In A Transcription Activation Site Of The Human c-*Kit* Oncogene. *Biochemistry*, 45, 7854–7860.

[13]. Kumari, S., Bugaut, A., Huppert, J.L. and Balasubramanian, S. (2007) An RNA G-Quadruplex In The 5' UTR Of The *N-RAS* Proto-Oncogene Modulates Translation. *Nat. Chem. Biol.,* 3, 218–221.

[14]. Pearson, A. M., Rich, A. and Krieger, M. (1993) Polynucleotide Binding To Macrophage Scavenger Receptors Depends On The Formation Of Base-Quartet-Stabilized Four-Stranded Helices. *J. Biol. Chem*. 268, 3546-3554.

[15]. Macaya, R. F., Schultze, P., Smith, F. W., Roe, J. A. and Feigon, J. (1993) Thrombin-Binding DNA Aptamer Forms A Unimolecular Quadruplex Structure In Solution. *Proc Natl. Acad. Sci. U. S. A* 90, 3745-3749.

[16]. Weisman-Shomer, P. and Fry, M. (1994) Stabilization Of Tetrahelical DNA By The Quadruplex DNA Binding Protein QUAD. *Biochem. Biophys. Res. Commun*. 205, 305-311.

[17]. Sarig, G., Weisman-Shomer, P., Erlitzki, R. and Fry, M. (1997) Purification And Characterization Of qTBP42, A New Single Stranded And Quadruplex Telomeric DNA-Binding Protein From Rat Hepatocytes. *J. Biol. Chem.* 272, 4474-4482.

[18]. Oliver, A. W., Bogdarina, I., Schroeder, E., Taylor, I. A. and Kneale, G. G. (2000). Preferential Binding Of fd Gene 5 Protein To Tetraplex Nucleic Acid Structures. *J. Mol. Biol.*, 301, 575-584.

[19]. Kang, S. G. and Henderson, E. (2002) Identification Of Nontelomeric G4-DNA Binding Proteins In Human, *E. Coli*, Yeast, And *Arabidopsis*. *Mol Cells*, 14, 404-10.

[20]. Lyonnais, S., Gorelick, R. J., Mergny, J. L., Le Cam, E. and Mirambeau, G. (2003) G-Quartets Direct Assembly Of HIV-1 Nucleocapsid Protein Along Single-Stranded DNA. *Nucleic Acids Res* 31, 5754-5763.

[21]. Van Dyke, M. W., Nelson, L. D., Weilbaecher, R. G. and Mehta, D. V. (2004). Stm1p, A G4 Quadruplex And Purine Motif Triplex Nucleic Acid-Binding Protein, Interacts With Ribosomes And Subtelomeric Y' DNA In *Saccharomyces Cerevisiae. J. Biol. Chem.*, 279, 24323-24333.

[22]. Marsh, T. C., and Henderson, E. (1994) G-Wires: Self-Assembly of a Telomeric Oligonucleotide, d(GGGGTTGGGG), into Large Superstructures. *Biochemistry 33*, 10718-10724.

[23]. Marsh, T. C., Vesenka, J., and Henderson, E. (1995) A New DNA Nanostructure, the G-Wire, Imaged by Scanning Probe Microscopy. *Nucl. Acids Res. 23*, 696-700.

[24]. Alberti, P., Bourdoncle, A., Saccà, B., Lacroix, L., and Mergny, J. L. (2006) DNA Nanomachines and Nanostructures Involving Quadruplexes. *Organic biomolecular chemistry. 4*, 3383.

[25]. Xiao, Y., Lubin, A.A., Heeger, A. J., and Plaxco, K.W (2005) Label-Free Electronic Detection of Thrombin in Blood Serum using an Aptamer-Based Sensor. *Angew. Chem. Int. Ed. 117*, 5592-5595.

[26]. Kang, C., Zhang, X., Ratliff, R., Moyzis, R., and Rich, A. (1992). Crystal Structure Of Four-Stranded *Oxytricha* Telomeric DNA. *Nature* 356, 126-131.

[27]. Smith, F.W., and Feigon, J. (1992) Quadruplex Structure Of Telomeric DNA Oligonucleotides *Nature* 356, 164-168.

[28]. Schultze, P., Smith, F.W., and Feigon, J. (1994). Refined Solution Structure Of The Dimeric Quadruplex Formed From The *Oxytricha* Telomeric Oligonucleotide d(GGGGTTTTGGGG). *Structure* 2, 221-233.

[29]. Webba da Silva, M. (2007) Geometric Formalism for DNA Quadruplex Folding. *Chem. Eur. J.,* 13, 9738-9745.

[30]. Webba da Silva, M., Trajkovski, M., Sannohe, Y., Hessari, N.M., Sugiyama, H., and Plavec, J. (2009) Design of a G-Quadruplex Topology through Glycosidic Bond Angles. *Angew. Chem. Int. Ed. 48*, 9167-9170.

[31]. Wang, Y., and Patel, D. J. (1994) Solution Structure of the Tetrahymena Telomeric Repeat d(T2G4)4 G-Tetraplex. *Structure. 2*, 1141-1156.

[32]. Laughlan, G., Murchie, A.I.H., Norman, D.G., Moore, M.H., Moody, P.C.E., Lilley, D.M.J., and Luisi, B. (1994). The High-Resolution Crystal Structure of a Parallel-Stranded Guanine Tetraplex. *Science* 265, 520-524.

[33]. Phillips, K, Dauter, Z., Murchie, A.I.H., Lilley, D.M.J., and Luisi, B. (1997). The Crystal Structure of Parallel-stranded Guanine Tetraplex at 0.95 Å Resolution. *J. Mol. Biol.*, 273, 171-182.

[34]. Smith, F. W., Lau, F. W., and Feigon, J. (1994) d(G3T4G3) Forms an Asymmetric Diagonally Looped Dimeric Quadruplex with Guanosine 5'-Syn-Syn-Anti and 5'-Syn-Anti-Anti N-Glycosidic Conformations. *Proc Natl Acad Sci U S A. 91*, 10546-10550.

[35]. Töhl, J., and Eimer, W. (1997) Interaction of a G-DNA Quadruplex with Mono- and Divalent Cations A Force Field Calculation. *Biophys. Chem. 67*, 177-186.

[36]. Lane, A. N., Chaires, J. B., Gray, R. D., and Trent, J. O. (2008) Stability and Kinetics of G-Quadruplex Structures. *Nucl. Acids Res.* 36, 5482–5515.

[37]. Sen, D., and Gilbert, W. (1990) A Sodium-Potassium Switch In The Formation Of Four-Stranded G4-DNA. *Nature* 344, 410-414.

[38]. Miyoshi, D., Nakao, A., and Sugimoto, N. (2003) Structural Transition From Antiparallel To Parallel Gquadruplex Of d(G4T4G4) Induced By Ca2+. *Nucleic Acids Res.*, 31, 1156-1163.

[39]. Hud, N. V., Smith, F. W., Anet, F. A. L., and Feigon, J. (1996) The Selectivity for K+ Versus Na+ in DNA Quadruplexes is Dominated by Relative Free Energies of Hydration: A Thermodynamic Analysis by 1H NMR . *Biochemistry 35*, 15383-15390.

[40]. Nagesh, N., and Chatterji, D. (1995) Ammonium Ion At Low Concentration Stabilizes The Gquadruplex Formation By Telomeric Sequence. *J. Biochem. Biophys. Meth*. 30, 1-8.

[41]. Hud, N.V., Schultze, P., Sklenar, V., and Feigon, J. (1999). Binding Sites And Dynamics Of Ammonium Ions In A Telomere Repeat DNA Quadruplex. *J. Mol. Biol.* 285, 233-243.

[42]. Creze, C., Rinaldi, B., Haser, R., Bouvet, P., and Gouet, P. (2007) Structure of a d(TGGGGT) Quadruplex Crystallized in the Presence of Li+ Ions. *Acta Cryst. 63*, 682-688

[43]. Chen, F.M. (1992). Sr2+ Facilitates Intermolecular G-Quadruplex Formation Of Telomeric Sequences. *Biochemistry* 31, 3769 – 3776.

[44]. Kankia, B., Marky, L.A. (2001) Folding of the Thrombin Aptamer into a G-Quadruplex with Sr2+ Stability, Heat and Hydration. *J. Am. Chem. Soc.*, 123, 10799-10804.

[45]. Fry, M. (2007) Tetraplex DNA and its Interacting Proteins. *Frontiers in bioscience*. 12, 4336-4351.

[46]. Walsh, K. and Gualberto, A. (1992). MyoD Binds To The Guanine Tetrad Nucleic Acid Structure. *J. Biol. Chem*. 267, 13714 – 13718.

[47]. Erlitzki, R. and Fry, M. (1997). Sequence-Specific Binding Protein Of Single-Stranded And Unimolecular Quadruplex Telomeric DNA From Rat Hepatocytes. *J. Biol. Chem*. 272, 15881 – 15890.

[48]. Schierer, T. and Henderson, E. (1994). A Protein From *Tetrahymena thermophila* That Specifically Binds Parallel- Stranded G4-DNA. *Biochemistry* 33, 2240 – 2246.

[49]. D'Onofrio, J., Petraccone, L., Martino, L., Di Fabio, G., Iadonisi, A., Balzarini, J., Giancola, C. and Montesarchio, D. (2008) Synthesis, Biophysical Characterization, and Anti-HIV Activity of Glyco-Conjugated G-Quadruplex-Forming Oligonucleotides. *Bioconjugate Chem*. 19, 607–616.

[50]. Fang, G. and Cech, T.R. (1993). The Beta Subunit Of *Oxytricha* Telomere-Binding Protein Promotes G-Quartet Formation By Telomeric DNA. *Cell* 74, 875 – 885.

[51]. Giraldo, R. and Rhodes, D. (1994). The Yeast Telomere-Binding Protein RAP1 Binds To And Promotes The Formation Of DNA Quadruplexes In Telomeric DNA. *EMBO J.* 13, 2411 – 2420.

[52]. Muniyappa, K., Anuradha, S. and Byers, B. (2000) Yeast Meiosis-Specific Protein Hop1 Binds To G4 DNA And Promotes Its Formation. *Mol Cell Biol*, 20, 1361-1369.

[53]. Arimondo, P.B., Riou, J.F., Mergny, J.L., Tazi, J., Sun, J.S., Garestier, T. and Helene, C. (2000). Interaction Of Human DNA Topoisomerase I With G-Quartet Structures. *Nucleic Acids Res*. 28, 4832 – 4838.

[54]. Eversole, A. and Maizels, N. (2000). In Vitro Properties Of The Conserved Mammalian Protein hnRNP D Suggest A Role In Telomere Maintenance. *Mol Cell Biol*, 20, 5425-5432.

[55]. Khateb, S., Weisman-Shomer, P., Hershco, I., Loeb L.A., and Fry, M. (2004) Destabilization of tetraplex structures of the fragile X repeat sequence (CGG)n is mediated by homolog-conserved domains in three members of the hnRNP family. *Nucleic Acids Res*, 32, 4145-4154

[56]. Baran, N., Pucshansky, L., Marco, Y., Benjamin, S. and Manor, H. (1997). The SV40 Large T-Antigen Helicase Can Unwind Four Stranded Dna Structures Linked By G-Quartets. *Nucleic Acids Res*. 25, 297 – 303.

[57]. Huber, M. D., Lee, D. C. and Maizels, N. (2002) G4 Dna Unwinding By BLM And Sgs1p: Substrate Specificity And Substrate-Specific Inhibition. *Nucleic Acids Res*, 30, 3954- 3961.

[58]. Sun, H., Karow, J. K. Hickson I. D. and Maizels, N. (1998) The Bloom's syndrome helicase unwinds G4 DNA. *J Biol Chem*, 273, 27587-27592.

[59]. Fry, M. and Loeb, L. A. (1999) Human Werner syndrome DNA helicase unwinds tetrahelical structures of the fragile X syndrome repeat sequence d (CGG)n. *J Biol Chem*, 274, 12797-12802.

[60]. Liu, Z., Frantz, J. D., Gilbert, W. and Tye, B. K. (1993) Identification And Characterization Of A Nuclease Activity Specific For G4 Tetrastranded DNA. *Proc Natl Acad Sci U S A*, 90, 3157-3161.

[61]. Liu, Z. and Gilbert, W. (1994) The Yeast KEM1 Gene Encodes A Nuclease Specific For G4 Tetraplex DNA: Implication Of In Vivo Functions For This Novel DNA Structure. Cell, 77, 1083-1092.

[62]. Sun, H., Yabuki, A. and Maizels, N. (2001) A Human Nuclease Specific For G4 DNA. *Proc Natl Acad Sci U S A*, 98, 12444-12449.

[63]. Sampson, T. (2003) Aptamers and SELEX: The Technology. *World Patent Information. 25*, 123-129.

[64]. Jayasena, S. D. (1999) Aptamers: An Emerging Class of Molecules that Rival Antibodies in Diagnostics. *Clin. Chem. 45*, 1628-1650.

[65]. Brody, E. N., and Gold, L. (2000) Aptamers as Therapeutic and Diagnostic Agents. *Reviews in Molecular Biotechnology. 74*, 5-13.

[66]. Padmanabhan, K., and Tulinsky, A. (1996) An Ambiguous Structure of a DNA 15-mer Thrombin Complex. *Acta Crystallogr. Sect. D*, 52, 272 – 282.

[67]. Kelly, J. A., Feigon, J., and Yeates, T. O. (1996) Reconciliation of the X-Ray and NMR Structures of the Thrombin-Binding Aptamer d(GGTTGGTGTGGTTGG). *J. Mol. Biol. 256*, 417-422.

[68]. Wyatt, J.R., Vickers, T.A., Roberson, J.L., Buckheit, R.W., Klimkait, T., DeBaets, E., Davis, P.W., Rayner, B., Imbach, J.L., Ecker, D.J. (1994) Combinatorially Selected Guanosine-Quartet Structure Is A Potent Inhibitor Of Human Immunodeficiency Virus Envelope-Mediated Cell Fusion. *Proc. Natl. Acad. Sci. USA*, 91, 1356-1360

[69]. Jing, N., Rando, R.F., Pommier, Y. and Hogan, M.E. (1997). Ion Selective Folding of Loop Domains in a Potent anti-HIV Oligonucleotide. *Biochemistry* 36, 12498-12505.

[69b]. Montesarchio, D. (2008) G-Quadruplex Forming Oligonucleotides As Finely Tunable Aptamers: Towards Better DNA Mimics. *Nucleic Acids Symp. Ser.*, 52, 9–10.

[70]. Greider, C.W. (1994) Mammalian Telomere Dynamics: Healing, Fragmentation Shortening And Stabilization. *Curr. Opin. Genet. Dev*. 4, 203–211.

[71]. Blackburn, E.H. (1994) Telomeres: No end in sight. *Cell* 77, 621–623.

[72]. Rhodes, D. and Giraldo, R. (1995) Telomere Structure And Function. *Curr. Opin. Struct. Biol.* 5, 311–322.

[73]. Oganesian, L. and Bryan, T.M. (2007) Physiological Relevance Of Telomeric G-Quadruplex Formation: A Potential Drug Target. *Bioessays* 29, 155–165.

[74]. Verdun, R.E. and Karlseder, J. (2007) Replication and protection of telomeres. *Nature*, 447: 924–931.

[75]. Bodnar, A.G., Ouellette, M., Frolkis, M., Holt, S.E., Chiu, C.P., Morin, G.B., Harley, C.B., Shay, J.W., Lichtsteiner, S., and Wright, W.E. (1998) Extension of Life-Span by Introduction of Telomerase into Normal Human Cells. *Science* 279, 349-352.

[76]. Vogel, G. (2000) In Contrast to Dolly, Cloning Resets Telomere Clock in Cattle. *Science* 288, 586-587.

[77]. Zahler, A.M., Williamson, J.R., Cech, T.R., and Prescott, D.M. (1991) Inhibition Of Telomerase By G-Quartet DNA Structures. *Nature* 350, 718-720.

[78]. Sun, D., Thompson, B., Cathers, B. E., Salazar, M., Kerwin, S. M., Trent, J. O., Jenkins, T. C., Neidle, S., and Hurley, L. H. (1997) Inhibition of Human Telomerase by a G-Quadruplex-interactive Compound. *J. Med. Chem*., 40, 2113-2116.

[79]. Perry, P. J., Gowan, S. M., Reszka, A. P., Polucci, P., Jenkins, T. C., Kelland, L. R., Neidle, S. (1998) 1,4- and 2,6-Disubstituted Amidoanthracene-9,10-dione Derivatives as Inhibitors of Human Telomerase. *J. Med. Chem*., 41, 3253-3260.

[80]. Perry, P. J., Read, M. A., Davies, R. T., Gowan, S. M., Reszka, A. P., Wood, A. A., Kelland, L. R., Neidle, S. (1999) 2,7-Disubstituted Amidofluorenone derivatives as Inhibitors of Human Telomerase. *J. Med. Chem*., 42, 2679-2684.

[81]. Harrison, R. J., Gowan, S. M., Kelland, L. R., Neidle, S. (1999) Human Telomerase Inhibition by Substituted Acridine Derivatives. *Bioorg. Med. Chem. Lett*., 9, 2463-2468.

[82]. Alberti, P., Schmitt, P., Nguyen, C., Rivalle, C., Hoarau, M., S. Grierson, D., and Mergny, J. (2002) Benzoindoloquinolines Interact with DNA Tetraplexes and Inhibit Telomerase. *Bioorg. Med. Chem. Lett. 12*, 1071-1074.

[83]. Burger, A.M., Dai, F., Schultes, C.M., Reszka, A.P., Moore, M.J., Double, J.A., and Neidle, S. (2005) The G-Quadruplex-Interactive Molecule BRACO-19 Inhibits Tumour Growth, Consistent With Telomere Targeting And Interference With Telomerase Function. *Cancer Res* 65, 1489-1496.

[84]. Tauchi, T., Shin-Ya, K., Sashida, G., Sumi, M., Okabe, S., Ohyashiki, J.H., Ohyashiki. K. (2006) Telomerase Inhibition With A Novel G-Quadruplexinteractive Agent, Telomestatin: In Vitro And In Vivo Studies In Acute Leukemia. *Oncogene* 25, 5719-5725.

[85]. Phatak, P., Cookson, J.C., Dai, F., Smith, V., Gartenhaus, R.B., Stevens, M.F., and Burger, A.M. (2007) Telomere Uncapping By The G-Quadruplex Ligand RHPS4 Inhibits Clonogenic Tumour Cell Growth In Vitro And In Vivo Consistent With A Cancer Stem Cell Targeting Mechanism. *Br. J. Cancer* 96, 1223-1233.

[86]. Cogoi, S., Xodo, L.E. (2006) G-Quadruplex Formation Within The Promoter Of The KRAS Proto-Oncogene And Its Effect On Transcription. *Nucleic Acids Res.* 34, 2536-2549.

[87]. Cogoi, S., Paramasivam, M., Spolaore, B., Xodo, L.E., (2008) Structural Polymorphism Within A Regulatory Element Of The Human KRAS Promoter: Formation Of G4-DNA Recognized By Nuclear Proteins. *Nucleic Acids Res.* 36, 3765-3780.

[88]. Gomez, D., Lemarteleur, T., Lacroix, L., Mailliet, P., Mergny, J., and Riou, J. (2004) Telomerase Downregulation Induced By The G-Quadruplex Ligand 12459 In A549 Cells Is Mediated By hTERT RNA Alternative Splicing. *Nucl. Acids Res. 32*, 371-379.

[89]. Bejugam, M., Sewitz, S., Shirude, P.S., Rodriguez, R., Shahid, R., and Balasubramanian, S. (2007) Tri-Substituted Isoalloxazines As A New Class Of G-Quadruplex Binding Ligands: Small Molecule Regulation of c-kit oncogene expression. *J. Am. Chem. Soc.* 129, 12926-12927.

[90]. Sen, D., and Gilbert, W. (1992) Novel DNA Superstructures Formed By Telomere-Like Oligomers. *Biochemistry* 31, 65-70.

[91]. Lu, M., Guo, Q., and Kallenbach, N. R. (1992) Structure And Stability Of Sodium And Potassium Complexes Of dT4G4 And dT4G4T. *Biochemistry* 31, 2455-2459.

[92]. Miyoshi, D., Karimata, H., Wang, Z., Koumoto, K., and Sugimoto, N. (2007) Artificial G-Wire Switch with 2,2'-Bipyridine Units Responsive to Divalent Metal Ions. *J. Am. Chem. Soc. 129*, 5919-5925.

[93]. Karimata, H., Miyoshi, D., Fujimoto, T., Koumoto, K., Wang, Z., and Sugimoto, N. (2007) Conformational Switch of a Functional Nanowire Based on the DNA G-Quadruplex. *Nucleic Acids Symp Ser 51*, 251-252.

[94]. Calzolari, A., Di Felice, R., and Molinari, E. (2004) Electronic Properties of Guanine-Based Nanowires. *Solid State Commun. 131*, 557-564.

[95]. Feigon, J., Koshlap, K. M., and Smith, F. W. (1995) ^{1}H NMR spectroscopy of DNA triplexes and quadruplexes. *Methods Enzymol*. 261, 225-255.

[96]. Majumdar, A., and Patel, D. J. (2002) Identifying Hydrogen Bond Alignments in Multistranded DNA Architectures by NMR. *Acc. Chem. Res. 35*, 1-11.

[97]. Paramasivan, S., Rujan, I., and Bolton, P. H. (2007) Circular Dichroism of Quadruplex DNAs: Applications to Structure, Cation Effects and Ligand Binding. *Methods. 43*, 324-331.

[98]. Ying, L., Green, J. J., Li, H., Klenerman, D., and Balasubramanian, S. (2003) Studies on the Structure and Dynamics of the Human Telomeric G Quadruplex by Single-Molecule Fluorescence Resonance Energy Transfer. *Proc. Natl. Acad. Sci. USA 100*, 14629-14634.

[99]. Fegan, A., Shirude, P. S., Ying, L., and Balasubramanian, S. (2010) Ensemble and Single Molecule FRET Analysis of the Structure and Unfolding Kinetics of the c-Kit Promoter Quadruplexes. *Chem Commun. 46*, 946-948

[100]. Gros, J., Avino, A., Osa, J. L. d. l., Gonzalez, C., Lacroix, L., Perez, A., Orozco, M., Eritja, R., and Mergny, J. (2008) 8-Amino Guanine Accelerates Tetramolecular G-Quadruplex Formation. *Chem Commun. 25*, 2926-2928.

[101]. Rieger, R. A., Iden, C. R., Gonikberg, E., and Johnson, F. (1999) 8-Amino-2'-Deoxyguanosine Incorporation into Oligomeric DNA. *Nucleos. Nucleot. 18*, 73-88.

[102]. Aboul-ela, F., Murchie, A. I. H., and Lilley, D. M. J. (1992) NMR Study of Parallel-Stranded Tetraplex Formation by the Hexadeoxynucleotide d(TG4T). *Nature. 360*, 280-282.

[103]. Aboul-ela, F., Murchie, A. I. H., Norman, D. G., and Lilley, D. M. J. (1994) Solution Structure of a Parallel-Stranded Tetraplex Formed by d(TG4T) in the Presence of Sodium Ions by Nuclear Magnetic Resonance Spectroscopy. *J. Mol. Biol. 243*, 458-471.

[104]. Kumar, R.K., and Ravikumar, V. T. (2005) 4,4'-Dimethoxytrityl Group Derived from Secondary Alcohols: Are they Removed Slowly Under Acidic Conditions? *Bioorg. Med. Chem. Lett. 15*, 3426-3429.

[105]. Dapic, V., Abdomerovic, V., Marrington, R., Peberdy, J., Rodger, A., Trent, J. O., and Bates, P. J. (2003) Biophysical and Biological Properties of Quadruplex Oligodeoxyribonucleotides. *Nucl. Acids Res. 31*, 2097-2107.

[106]. Hardin, C.C., Henderson, E., Watson, T. and Prosser, J.K. (1991). Monovalent Cation Induced Structural Transitions In Telomeric Dnas: G-DNA Folding Intermediates. *Biochemistry* 30, 4460 – 4472.

[107]. Hardin, C. C., Watson, T., Corregan, M., and Bailey, C. (1992) Cation-Dependent Transition between the Quadruplex and Watson-Crick Hairpin Forms of d(CGCG3GCG). *Biochemistry 31*, 833-841.

[108]. Giraldo, R., Suzuki, M., Chapman, L. and Rhodes, D. (1994). Promotion Of Parallel DNA Quadruplexes By A Yeast Telomere Binding Protein: A Circular Dichroism Study. *Proc. Natl. Acad. Sci. USA* 91, 7658 – 7662.

[109]. Wang, K. Y., Krawczyk, S. H., Bischofberger, N., Swaminathan, S., and Bolton, P. H. (1993) The Tertiary Structure of a DNA Aptamer which Binds to and Inhibits Thrombin Determines Activity. *Biochemistry 32*, 11285-11292.

[110]. Schultze, P., Macaya, R. F., and Feigon, J. (1994) Three-Dimensional Solution Structure of the Thrombin-Binding DNA Aptamer d(GGTTGGTGTGGTTGG). *J. Mol. Biol. 235*, 1532-1547.

[111]. Smirnov, I., and Shafer, R.H. (2000) Effect of Loop Sequence and Size on DNA Aptamer Stability. *Biochemistry*, 39, 1462–1468.

[112]. Chang, C., Chu, J., Kao, F., Chiu, Y., Lou, P., Chen, H., and Chang, T. (2006) Verification of Antiparallel G-Quadruplex Structure in Human Telomeres by using Two-Photon Excitation Fluorescence Lifetime Imaging Microscopy of the 3,6-Bis(1-Methyl-4-Vinylpyridinium)Carbazole Diiodide Molecule. *Anal. Chem. 78*, 2810-2815.

[113]. Petraccone, L., Erra, E., Esposito, V., Randazzo, A., Mayol, L., Nasti, L., Barone, G., and Giancola, C. (2004) Stability and Structure of Telomeric DNA Sequences Forming Quadruplexes Containing Four G-Tetrads with Different Topological Arrangements. *Biochemistry 43*, 4877-4884.

[114]. Risitano, A., and Fox, K. R. (2004) Influence of Loop Size on the Stability of Intramolecular DNA Quadruplexes. *Nucl. Acids Res. 32*, 2598-2606.

[115]. Bugaut, A., and Balasubramanian, S. (2008) A Sequence-Independent Study of the Influence of Short Loop Lengths on the Stability and Topology of Intramolecular DNA G-Quadruplexes. *Biochemistry 47*, 689-697.

[116]. Garner, T. P., Williams, H. E. L., Gluszyk, K. I., Roe, S., Oldham, N. J., Stevens, M. F. G., Moses, J. E., and Searle, M. S. (2009) Selectivity of Small Molecule Ligands for Parallel and Anti-Parallel DNA G-Quadruplex Structures. *Org. Biomol. Chem. 7*, 4194–4200.

[117]. Rujan, I. N., Meleney, J. C., and Bolton, P. H. (2005) Vertebrate Telomere Repeat DNAs Favor External Loop Propeller Quadruplex Structures in the Presence of High Concentrations of Potassium. *Nucl. Acids Res. 33*, 2022-2031.

[118]. Esposito, V., Randazzo, A., Piccialli, G., Petraccone, L., Giancola, C. and Mayol, L. (2004) Effects of an 8-bromodeoxyguanosine incorporation on the parallel quadruplex structure [d(TGGGT)]4. *Org. Biomol. Chem*. 2, 313–318.

[119]. Uddin, M. K., Kato, Y., Takagi, Y., Mikuma, T., and Taira, K. (2004) Phosphorylation at 5' End of Guanosine Stretches Inhibits Dimerization of G-Quadruplexes and Formation of a G-Quadruplex Interferes with the Enzymatic Activities of DNA Enzymes. *Nucl. Acids Res. 32*, 4618-4629.

[120]. Virgilio, A., Esposito, V., Randazzo, A., Mayol, L., and Galeone, A. (2005) 8-Methyl-2'-Deoxyguanosine Incorporation into Parallel DNA Quadruplex Structures. *Nucl. Acids Res. 33*, 6188-6195.

[121]. Oliviero, G., Amato, J., Borbone, N., Galeone, A., Petraccone, L., Varra, M., Piccialli, G., and Mayol, L. (2006) Synthesis and Characterization of Monomolecular DNA G-Quadruplexes Formed by Tetra-End-Linked Oligonucleotides. *Bioconjug. Chem. 17*, 889-898.

[122]. Rachwal, P. A., and Fox, K. R. (2007) Quadruplex Melting. *Methods. 43*, 291-301.

[123]. Cáceres, C., Wright, G., Gouyette, C., Parkinson, G., and Subirana, J. A. (2004) A Thymine Tetrad in d(TGGGGT) Quadruplexes Stabilized with Tl+/Na+ Ions. *Nucl. Acids Res. 32*, 1097-1102.

CHAPTER 6

Experimental Section

6.1. Reagents

Phosphoramidites and ancillary reagents used during oligonucleotide synthesis were from Applied Biosystems (PE Biosystems Hispania S.A., Spain), Link Technologies (Link Technologies Ltd, Scotland) and Glen Research (Glen Research Inc., USA). The remaining chemicals were purchased from Panreac, Aldrich, Sigma or Fluka (Sigma-Aldrich Química S.A.,Spain). All reagents and solvents were of analysis or synthesis grade.

6.2. General methods

6.2.1. Flash column chromatography

Flash column chromatography was performed on wet packed Merk Silica Gel 60 (0.04 – 0.06 mm, 230-400 mesh ASTM).

6.2.2. Thin layer chromatography

TLC was performed on Merck Silica Gel 60 F254 aluminium sheets. Reagents used for revealing plates include $KMnO_4$ (1 g $KMnO_4$, 6.7 g K_2CO_3, 1.7 ml 5% aq. NaOH, 100 ml H_2O), ethanolic ninhydrin (3 % w/v) and detection by UV light was used when applicable.

6.2.3. NMR spectrometry

^1H (300 MHz), ^{13}C NMR (75 MHz) and ^{31}P NMR (121 MHz) spectra were carried out at the Instituto de Investigaciones Químicas y Ambientales-CSIC with a Unity-300 spectrometer from Varian (Palo Alto, California, USA) and at the Medicinal Chemistry Department of Göteborg University with a JEOL JNM-EX 400-MHz spectrometer. Chemical shifts are reported in parts per million (ppm) related to TMS as internal reference for ^1H and ^{13}C spectra and 85% phosphoric acid as external reference for ^{31}P spectra. Signals are described as s (singlet), d (doublet), t (triplet), or m (multiplet).

6.2.4. Infrared spectroscopy

IR spectra were obtained on a Perkin-Elmer 16 PC spectrometer at the Medicinal Chemistry Department of Göteborg University. A nujol mull of each product was obtained by grinding up the solid and mixing it with mineral oil to form a suspension, which placed in between KBr plates.

6.2.5. UV spectrophotometry

UV absorbance spectra were recorded with a Jasco V-650 Elmer spectrophotometer equipped with a Peltier temperature controller and 1 cm path length quartz cuvettes.

6.2.6. CD spectroscopy

CD spectroscopy experiments were performed in Instituto de Química Física Rocasolano (CSIC, Madrid) with the kind supporting of Dr. Douglas V. Laurents. CD spectra were recorded with a Jasco-810 spectropolarimeter using 1 cm pathlength quartz cuvettes in a volume of 350 µL.

6.2.7. Oligonucleotide synthesis

Oligonucleotide sequences were prepared according to the solid-phase methodology described in section 2.6 of this thesis using 2-cyanoethyl phosphoramidites as monomers. The syntheses were performed on an Applied Biosystems model 3400 DNA synthesizer using 0.2 and 1 µmol scales (polystyrene and CPG support, respectively).

The reagents used in the automatic synthesizer are indicated in Table 6.1.

Step	Solution
Coupling	2-cyanoethyl phosphoramidite 0,1 M in ACN
	1H-tetrazol 0,45 M in ACN
Capping	Ac_2O/lutidine/THF 1:1:8
	1-metilimidazol 6,5% in THF
Oxidation	I_2 0,02 M in THF/H_2O/pyridine
Detritylation	TCA 3% in DCM

Table 6.1. Reagent used in the different steps of automatic DNA synthesis cycle.

6.2.8. Oligonucleotides detritylation

-automatic procedure

Detritylation step can be performed by the automatic synthesizer if desired. In this case a solution of 3% TCA/DCM is flushed automatically through the column until DMT cation signal is undetectable.

-manual procedure (after HPLC purification using the "DMT ON" gradient)

The collected DMT containing fractions were evaporated using a Speed-Vac concentrator. Samples were then treated with 1 ml of 80 % aqueous acetic acid for 30 minutes at room temperature. 1 ml of water was added and DMT-OH was extracted twice with 6 ml of diethyl ether. Finally, the sample was reconcentrated *in vacuo* to dryness and oligonucleotides were desalted with a NAP column.

6.2.9. Deprotection and cleavage of oligonucleotides from the resin

After oligonucleotide synthesis the solid support was placed on a screwcap vial with 1-1.5 ml of concentrated aqueous ammonia. The vial was placed in a thermo block at 55°C for a minimum of 6 h (usually left overnight) or 1 h for cases in which guanines are protected with dmf group. Then, the vial was allowed to cool at room temperature and the solid support was removed by filtration using a glass pipette with a cotton plug. Ammonia solution was concentrated in a rotoevaporator. The residue was dissolved in water and filtered with HPLC filters (Nylon Acrodisc, 0.2 µm) previously to reversed-phase HPLC purification.

6.2.10. Analysis and purification by reverse phase HPLC

Oligodeoxynucleotides were purified on a Waters reverse-phase HPLC system using a Nucleosil 120 C18 column (10 µm, 200 x 10 mm) and the following solvents:
Solvent A: 5% acetonitrile in 0.1 M triethylammonium acetate (pH 6.5).
Solvent B: 70% acetonitrile in 0.1 M triethylammonium acetate (pH 6.5).
One of the three following programs was used:
A. 20 min linear gradient from 0 to 50% B with a flow rate of 3 mL/min (DMT OFF).
B. 20 min linear gradient from 15 to 80% B with a flow rate of 3 mL/min(DMT ON).
C. 20 min linear gradient from 5 to 35% B with a flow rate of 3 mL/min.

6.2.11. Analysis by ion exchange chromatography

Oligodeoxynucleotides were analyzed on a Waters HPLC system using an ion-exchange 1 ml Resource Q column from GE Healthcare (15 µm, 6.4 x 30 mm) and the following solvents:
Solvent A: 20 mM tris·HCl (pH 8.0)
Solvent B: 20 mM tris·HCl (pH 8.0), 2M NaCl
or
Solvent A': 20 mM tris·HCl (pH 8.0), 50% formamide
Solvent B': 20 mM tris·HCl (pH 8.0), 50% formamide, 1M NaCl
for denaturing conditions.
A 20 min linear gradient from 0 to 50 % B with a flow rate of 1 mL/min for the first system and from 0 to 100 % B' for the second one (denaturing) was used. In both cases saline gradient ranges from 0 to 1M NaCl.

6.2.12. Oligonucleotides desalting by gel filtration

Oligonucleotides coming from HPLC were desalted before used. NAP™ columns prepacked with Sephadex™ G-25 DNA Grade (GE Healthcare) were used. For samples containing ≤ 5 O.D, NAP-5 columns were employed while NAP-10 were used for samples containing higher oligonucleotide quantities.

First, the column was equilibrated with 3 complete refills of water. ODN samples were dissolved in 0.5 ml (for NAP-5) or 1 ml (for NAP-10), loaded onto the

column and allowed to enter the gel bed completely. Elution with water was performed and the first 1 ml (for NAP-5) or 1.5 ml (for NAP-10) fractions were collected which correspond to the purified and desalted oligonucleotides.

6.2.13. Preparation of oligonucleotides in the sodium salt form

Oligonucleotides coming from reversed-phase HPLC purification contain triethylammonium salts and counterions of the phosphates. In the cases in which $5'$-amino-oligonucleotides are desired to be conjugated to a N-hydrosuccinimide ester (section 3.5.3 of this thesis) these triethylammonium counterions should be exchanged by sodium ions. For this purpose sodium form of Dowex 50X4 (100-200 mesh) was used as ion-exchange resin. 1 g of this resin per μmol of oligonucleotide was weighted, soaked with water and poured in a column. The resin was washed with water until clear and transparent drops were eluted. Oligonucleotide samples were dissolved in 1 ml of water, loaded to the column and eluted with water. 1ml-fractions were collected and the UV-absorbing fractions were combined and concentrated in a Speed-Vac concentrator.

6.2.14. Oligonucleotides quantification

Optical absorbance at 260 nm is routinely used to measure the concentration of nucleic acids present in a solution.

The molar extinction coefficient (ε_{260}) is a physical constant that is unique for each sequence and describes the amount of absorbance at 260nm (A_{260}) of 1 mol·L^{-1} DNA solution measured in 1 cm path-length cuvette. This definition is derived from the Beer-Lambert law,

$$A = log(I_O / I) = \varepsilon \cdot c \cdot l$$

where **A** is the absorbance, **I_O** and **I** are, respectively, the intensities of incident and transmitted light, **c** is the molar concentration of an oligonucleotide (mol·L^{-1}), **l** is the length of the light path through the sample (cm), and ε is the molar extinction coefficient (L·mol^{-1}·cm^{-1}).

As interactions between adjacent bases alter absorbance, the neighbour effect must be taken into account to calculate the extinction coefficient. Thus, this coefficient is ultimately determined both by base composition and base order within an oligonucleotide.

The ε_{260} value of an oligonucleotide with sequence $5'$DpEp...KpL$^{3'}$ is calculated from the following equation:

ε_{260} (DpEpFpGp....KpL) = [2· (εDpE + εEpF + εFpG + ...+ εKpL) – εE – εF – εG - ....- εK]

where the coefficients for each individual base as well as for each pair of bases are indicated in the table below:

	ε_{260} (mM^{-1}·cm^{-1})		ε_{260} (mM^{-1}·cm^{-1})
pdA	15.4	dCpdG	9.0
pdC	7.4	dCpT	7.6
pdG	11.5	dGpdA	12.6
pT	8.7	dGpdC	8.8
dApdA	13.7	dGpdG	10.8
dApdC	10.6	dGpT	10.0
dApdG	12.5	TpdA	11.7
dApT	11.4	TpdC	8.1
dCpdA	10.6	TpdG	9.5
dCpdC	7.3	TpT	8.4

Table 6.2. ε_{260} (mM^{-1}·cm^{-1}) values of mono- and dinucleotides.

6.2.15. MALDI-TOF spectrometry

Matrix-assisted laser desorption ionization time-of-flight (MALDI-TOF) mass spectrometric analysis was carried out at the Mass Spectrometry Service at the University of Barcelona using a Voyager-DERP (Applied Biosystems) instrument equipped with N_2 laser at 337 nm, using a 3-ns pulse in negative mode.

Matrices used for MALDI-TOF analysis were prepared as follows:

• Diammonium hydrogen citrate (CA): 50 mg/ml in H_2O
• 3-Hydroxypicolinic acid (HPA): 50 mg/ml in ACN/H_2O 1:1 (v/v)
• 2,4,6-trihydroxyacetophenone monohydride (THAP): 50 mg/ml in ACN/H_2O 1:1 (v/v)

0.1 - 0.3 OD of oligonucleotides to be analyzed were dissolved in 10-20 μl of milliQ water and 1 μl of this solution was mixed with CA matrix and diluted 1:2 with HPA or THAP matrix. 1 μl of this sample was dropped on the plate and dried at room temperature.

6.2.16. Ionization mass spectrometry

Mass spectra by fast atom bombardment (FAB) and electrospray ionization (ESI) have been obtained by Dra. Irene Fernández in Mass Spectrometry Service of University of Barcelona with a VG-Quattro (Fison Instruments) equip using a capilar voltage of 10 kV and 3.5 kV respectively.

6.2.17. Denaturing Polyacrylamide Gel Electrophoresis

Oligonucleotide samples (0.1 – 0.3 O.D.) were dissolved in 20 μl of denaturing dye buffer (0.1% bromophenol blue dye in 90% formamide with 1mM EDTA, 10mM NaOH) and preheated to 90 ºC for 5 min before loading. Denaturing gels contained 20 % acrylamide (19:1 acrylamide:bisacrylamide) and 8.3 M urea in TBE buffer (89mM Tris-HCl, 89mM boric acid, 2mM EDTA, pH 8.0). Gels were run at 55ºC for 5h at 400 V in a Hoefer SE 600 electrophoresis unit using TBE as running buffer. After the electrophoresis, oligodeoxynucleotides were stained by STAINS-ALL (Sigma) using a solution of 0.01 % of the dye in water/formamide 55/45. After 15 min, the dye solution was removed, and the gel was washed with H_2O. After the background was bleached with light, the remaining blue stains were photographed.

6.2.18. Native Polyacrylamide Gel Electrophoresis

Oligonucleotide samples (0.1 – 0.3 O.D.) were dissolved in 20 μl of non-denaturing loading buffer containing 50% glycerol and 0.02% of bromophenol blue in TAE-Mg^{2+} (40 mM Tris, 2mM EDTA, 20 mM AcOH, and 12.5 mM magnesium acetate) and subsequently loaded on the native 15 % polyacrylamide gel (acrylamide/bisacrylamide 19 : 1) termostabilized at 4ºC. The electrophoresis was run at this temperature at 200 V in a SE-600 Hoefer Scientific apparatus using TAE-Mg^{2+} as running buffer. After the electrophoresis, oligodeoxynucleotides were stained by STAINS-ALL (Sigma) and revealed as indicated above.

6.2.19. Enzymatic degradation studies

0.5 OD of the oligonucleotide to be analyzed were incubated in 50 mM tris.HCl pH 8.0 and 10 mM magnesium chloride with snake venom phosphodiesterase (0.4 μg) and bacterial phosphatase (0.4 μg) in a total volume of 100 μL at 37°C overnight. The resulting mixture was diluted and analyzed by HPLC using the program "DMT OFF" on a Shimadzu instrument with a polystyrene column, Hamilton PRP-1 (250 x 10 mm) and flow rate of 3 mL/min.

6.3. Experimental section (Chapter 2)

6.3.1. Oligonucleotide synthesis

The oligonucleotides used in this chapter were prepared on 0.2 μmol scale in the automatic synthesizer using phosphoramidite chemistry on polystyrene solid support (LV200). For the first part of the clamp the appropriate C, T, LNA-T, and LNA-5'-methyl-C phosphoramidites were employed while reversed G and A phosphoramidite monomers were used for the second fragment of the clamp. Longer oxidizing and coupling times were used with LNA monomers, as indicated by the manufacturer. The phosphoramidite of 5'-methyl-C-LNA was dissolved in ACN/THF 3:1.

Oligonucleotides were deprotected and cleaved from the support with concentrated aq. NH_3 at 55ºC overnight. Oligonucleotides were synthesized without performing final detritylation to facilitate reversed-phase HPLC purification with the "DMT ON" protocol. All chromatograms presented a major peak, which was collected. Finally oligonucleotide clamps were detritylated, desalted by NAP-10, and quantified by measuring the absorbance at 260 nm. Their molar absorptivities were calculated assuming identical absorptivities for LNA and DNA monomeric nucleotides.

Determined masses of the oligonucleotides by MALDI-TOF ($[M-H]^-$) and their calculated theorical values (between parentheses) are as follows:

WC 11mer: 3194.0 (3194.2); WC 11mer/2'-O-Me: 3453.0 (3454.1); B22: 7949.6 (7952.1); B22-T: 8027.9 (8036.1); B22-C: 8072.2 (8078.1); B22-CT: 8122.9 (8134.1).

6.3.2. Thermal denaturation studies

Solutions of equimolar amounts of hairpins with or without the target WC pyrimidine strand were mixed in 0.1 M sodium phosphate/citric acid buffer (pH ranging from 5.0 to 7.0) containing 1 M NaCl, with a final duplex concentration of 2 μm. The solutions were heated to 90 ºC, allowed to cool slowly to r.t., and stored at 4 ºC until UV was recorded. Thermal melting curves were recorded at 260 and 295 nm at a heating rate of 1 ºC/min. The T_m values were determined at the maximum of the first derivative of the melting curve using OriginLab v7.0 software. T_m values are averages of at least two independent measurements within $\pm$ 1.0 ºC.

6.4. Experimental section (Chapter 3)

6.4.1. Synthesis of succinimidyl N-propargyl glutariamidate

Glutaric anhydride (2.61 g, 23 mmol), propargylamine (1.5 ml, 23 mmol), and triethylamine (3.21 ml, 23 mmol) were dissolved in DCM (50 ml) and stirred for 12 h at room temperature. After the DCM solvent was evaporated, the residue was acidified by adding 1 M HCl solution (5 ml). The solvent was removed under vacuum, and the crude mixture was purified by silica gel chromatography (CHCl$_3$/CH$_3$OH 5/1, *R*f=0.45) which despite yielded 4.3 g of *N*-propargyl glutariamidic acid impurified with triethylamine (62% yield). To a solution of *N*-propargyl glutariamidic acid (0.74 g impurified product, 2.4 mmol desired product) in DCM (25ml) was added *N*-hydroxysuccinimide (NHS) (0.28 g, 2.4 mmol), followed by the addition of 1-(3-dimethylaminopropyl)-3-ethylcarbodiimide hydrochloride (EDC; 0.48 g, 2.5 mmol) at room temperature. After stirring for 8 h, the mixture was washed with H$_2$O (2x20 ml) and the aqueous layer was extracted with DCM (30 ml). The combined organic layers were washed with brine, dried over Na$_2$SO$_4$, and concentrated *in vacuo* to yield 0.39 g of succinimidyl *N*-propargyl glutariamidate as a yellow solid (63% yield).
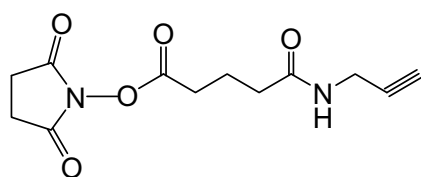
¹H NMR (CDCl$_3$) δ 4.05 (dd, 1H, J$_1$ = 3.9 Hz, J$_2$ = 2.7), 2.86 (s, 4H), 2.69 (t, 2H, J=6.9 Hz), 2.34 (t, 2H, J=7.2 Hz), 2.22 (t, 1H, J=2.7), 2.08-2.18 (m, 1H); **¹³C NMR** (CDCl$_3$) δ 171.3, 169.3, 168.3, 79.5, 71.4, 34.1, 29.9, 29.1, 25.6. HRMS (FAB+) *m/z*: calcd for C$_{12}$H$_{15}$O$_5$N$_2$ (M + H$^+$), 267.1; found, 267.6.20.8.

6.4.2. Synthesis of succinimidyl 5-azidovalerate

Firstly, methyl 5-bromopentanoate (143 μl, 1mmol) was reacted with NaN$_3$ (340 mg, 5 mmol) in DMF, and stirred for 12 h at room temperature. After the solvent was evaporated, the residue was dissolved in DCM and excess of NaN$_3$ was extracted with H$_2$O. The organic layer was evaporated and the residue was treated with LiOH (0.1 g, 4 mmol) in 6 ml of THF/H$_2$0 1:2. After hydrolysis, the solution was acidified with 1 M HCl solution, the THF removed by rotavaporation and the aqueous phase extracted with DCM. The combined organic layers were dried over Na$_2$SO$_4$ and concentrated *in vacuo* to yield 0.11 g of 5-azidovaleric acid (0.78 mmol, 78% yield).

Secondly, 1-(3-Dimethylaminopropyl)-3-ethylcarbodiimide hydrochloride (140 mg, 0.73 mmol) was added to a suspension of 100 mg (0.7 mmol) of 5-azidovaleric acid and 84 mg (0.73 mmol) of N-hydroxysuccinimide in DCM (5 mL) at room temperature and stirred overnight, followed by the addition of H$_2$O. The separated DCM phase was washed with H$_2$O and brine solution, dried over Na$_2$SO$_4$,

and evaporated to yield 104 mg (0.43 mmol, 62 % yield) of succinimidyl 5-azidovalerate as a pale yellow liquid.
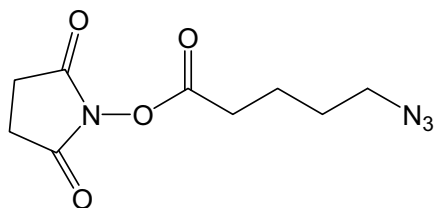
[1H NMR] (CDCl$_3$) δ 3.34 (t, 2H, J = 6.6 Hz), 2.84 (s, 4 H), 2.68 (t, 2H, J = 6.9 Hz), 1.88-1.72 (m, 4H); **[13C NMR]** (CDCl$_3$) δ 169.1, 168.2, 50.8, 30.4, 27.9, 25.6, 21.9.

6.4.3. Synthesis of 2-cyanoethyl hex-5-ynyl N,N-diisopropyl phosphoramidite

Hex-5-yn-1-ol (0.54 ml, 5 mmol) was dissolved in dry ACN (6 ml) under Ar, and DIPEA (2.6 ml, 15 mmol) was added with exclusion of moisture. The solution was cooled on ice, and chloro(2-cyanoethoxy)(diisopropylamino)phosphine (1.7 ml, 7.5 mmol) was added dropwise. The solution was stirred at r.t. for 2 h. The solvent was then removed *in vacuo*, and the residue was dissolved in DCM with 1% Et$_3$N. The solution was washed with H$_2$O and brine, dried (Na$_2$SO$_4$), and evaporated. The crude product was purified by silica gel column chromatography (AcOEt/hexane 1:9 with 4% Et$_3$N) to give the desired phosphoramidite (670 mg) as a pale yellow oil in 46% yield.
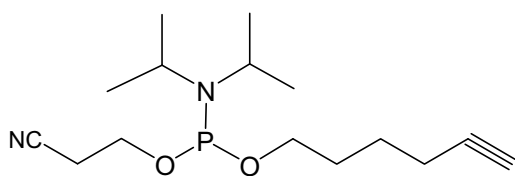
[1H-NMR] (CDCl$_3$): 3.90–3.55 (m, 6 H), 2.64 (t, J=5.4, 2 H), 2.23 (t, J=6.9, 2 H), 1.95 (t, J=2.7, 1 H), 1.78 –1.57 (m, 4H), 1.18 (d, J=6.9, 12 H). **[13C-NMR]** (CDCl$_3$; two diastereoisomers):117.6; 84.2; 68.5; 63.2, 63.0; 58.4, 58.2; 43.1, 42.9; 30.2, 30.1; 24.7, 24.6; 20.4, 20.3; 18.1. **[31P-NMR]** (CDCl$_3$):147.76. **ESI-MS**: 299.5 ([M+H$^+$]).

6.4.4. Synthesis of 6-bromohexyl 2-cyanoethyl N,N-diisopropyl phosphoramidite

6-Bromohexan-1-ol (0.26 ml, 2 mmol) was dissolved in dry ACN (4 ml) under Ar and DIPEA (1 ml, 6 mmol) was added with exclusion of moisture. The solution was cooled on ice and chloro(2-cyanoethoxy)(diisopropylamino)phosphine (0.7 ml, 3 mmol) was added dropwise. The solution was stirred at r.t. for 2.5 h. The solvent was then removed *in vacuo*, and the residue was dissolved in DCM with 1% Et$_3$N. The solution was washed with H$_2$O and brine, dried (Na$_2$SO$_4$), and evaporated. The crude product was purified by column chromatography (silica gel; AcOEt/hexane 1 : 9 with 4% Et$_3$N) to give the desired phosphoramidite (360 mg) as a pale yellow oil in 47% yield.
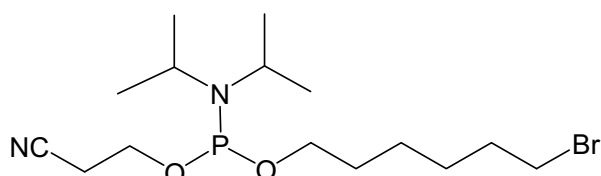
¹H-NMR (CDCl₃): 3.9 −3.76 (m, 2 H), 3.7−3.52 (m, 4 H), 3.41 (t, J=6.9, 2 H, CH2Br), 2.64 (t, J=6.6, 2 H), 1.92 − 1.82 (m, 2 H), 1.67 −1.59 (m, 2 H), 1.50−1.36 (m, 4 H), 2.35 (d, J=6.6, 12 H). **¹³C-NMR** (CDCl₃ ; two diastereoisomers): 117.6; 63.6, 63.4; 58.4, 58.2; 43.1, 42.9; 33.8; 32.7; 31.0, 30.9; 27.8; 25.2; 24.7, 24.6, 24.5 (4 Me); 20.4, 20.3. **³¹P-NMR** (CDCl₃): 147.73. **ESI-MS**: 381.3 ([M+ H⁺]).

6.4.5. Synthesis of oligonucleotides carrying a propargyl group at the 5'-end using 5'-amino-oligonucleotides

ODN 8 (8T-$^{5'}$aminohexyl, Table 3.10) was synthesized on 1 μmol scale. The phosphoramidite of 6-[(4-monomethoxytrityl)amino]hexan-1-ol (5'-Amino-Modifier C6, LinkTechnologies) was used for the introduction of the amino group at the 5'-end (coupling time = 300 s). After the removal of the MMT group the resulting amino-oligonucleotide–support was treated with 20 equivalents of succinimidyl N-propargyl glutariamidate in dioxane for 1 h at r.t. The resulting support was washed and treated with conc. NH₃ at r.t. for 2 h. **ODN 9** was purified by RP-HPLC (conditions A). The desired product eluted at 12.0 min (starting 8T-$^{5'}$aminohexyl suffered N-acetylation and eluted at 11.6 min). ESI-MS: 2760 [M+ 3 Na]⁺.

6.4.6. Synthesis of oligonucleotides carrying a propargyl group at the 5'-end using 5'-carboxy-oligonucleotides

ODN 10 (8T-$^{5'}$COONHS), **12** (8A-$^{5'}$COONHS), **14** (CT-$^{5'}$COONHS), **16** (pyr-CT-$^{5'}$COONHS) and **18** (CT$_{long}$-$^{5'}$COONHS) were synthesized either on 0.2 or 1 μmol scale. The phosphoramidite of 10-hydroxydecanoic acid N-hydroxysuccinimide ester (5'carboxy modifier C10, Glen Research) was used for the introduction of the N-hydroxysuccinimide ester group at the 5'-end (coupling time = 300 s). The resulting 5'-carboxy-oligonucleotide–supports were treated with 10 equivalents of propargylamine in DCM containing 10% Et₃N for 4 h at r.t. The resulting supports were washed and treated with conc. NH₃ at 55ºC for a minimum of 3 h or o.n in most cases. **ODN 11, 13, 15, 17** and **19** were purified by RP-HPLC using conditions A (for ODN 13) or C (for ODN 11,15,17,19). By-products corresponding to the 5'-carboxamide-ODNs (coming from nucleophilic substitution of NHS ester groups with NH₃) were eluted as small peaks before the desired products. These oligonucleotides were also isolated and analyzed. Retention times are indicated in the table 3.20 of this thesis. Determined masses of the oligonucleotides by MALDI-TOF ([M-H]⁻) and their calculated theorical values (between parentheses) are as follows: **8A-$^{5'}$COONHS**: 2691 (2692); **8A-$^{5'}$propargyl**: 2728 (2730); **CT-$^{5'}$COONHS:** 3441 (3442); **CT-$^{5'}$propargyl:** 3479 (3481); **pyr-CT-$^{5'}$COONHS:** 3837 (3839); **pyr-CT-$^{5'}$propargyl:** 3873 (3877); **CT$_{long}$-$^{5'}$COONHS:** 4961 (4965); **CT$_{long}$-$^{5'}$propargyl:** 4999 (5003).

6.4.7. Synthesis of oligonucleotides carrying an alkynyl group at the 5'-end using the phosphoramidite derivative of hex-5-yn-1-ol.

The hex-5-yn-1-ol phosphoramidite was used for the introduction of an alkynyl group at the 5'-end of oligonucleotides **20** (CT-$^{5'}$hexynyl) and **21** (GA-$^{5'}$hexynyl). Coupling was performed in the automatic synthesizer using a coupling time of 300 s. After ammonia deprotection (55ºC, o.n), the resulting oligonucleotides were purified by RP-HPLC. Oligonucleotide **20** eluted at 9.7 min (conditions C). MALDI-MS ([M-H]$^-$): 3351 (calc. 3353). Oligonucleotide **21** eluted at 10.3 min (conditions A). MALDI-MS ([M-H]$^-$): 3636.3 (calc. 3639).

6.4.8. Synthesis of oligonucleotides carrying an azido group at the 5'-end using 5'-amino-oligonucleotides.

ODN 8 (8T-$^{5'}$aminohexyl) was synthesized on 1 μmol scale as described above (section 6.4.5). After the removal of the MMT group the resulting amino-oligonucleotide–support was treated with 20 equivalents of succinimidyl 5-azidovalerate in dioxane for 1 h at r.t. The resulting support was washed and treated with conc. NH$_3$ at r.t. for 2 h. **ODN 22** was purified by RP-HPLC using conditions A. The desired product eluted at 13.2 min. ESI-MS: 2716 ([M + 2 Na]$^+$).

6.4.9. Synthesis of oligonucleotides carrying azido groups at the 5'-end using the iodination, followed by azide displacement.

Sequences **CT** and **GA** (ODN **3** and **4** respectively) were synthesized on 1 μmol scale and the last DMT group was removed. GA sequence was synthesized with dmf-protected guanines. The supports were treated with (triphenoxymethyl) phosphonium iodide (0.226 g, 0.5 mmol) in DMF (0.85 ml) to yield the 5'-iodo-oligonucleotides **23** and **25** (CT-$^{5'}$iodo and GA-$^{5'}$iodo). In this procedure the iodination solution was passed several times back and forth between two syringes fitted to the ends of the DNA synthesis column. The resulting supports were then washed with DMF and DCM and dried. Finally, resin carrying the 5'-iodo-oligonucleotide was treated with NaN$_3$ (68 mg, 1 mmol) in DMF (1 ml) overnight at r.t.

A small amount of resin was cleaved before undergoing each reaction to determine the yield of every step. Iodination was achieved with a yield of 85 % while azide displacement gave a final conversion of 70-73%, based on relative peak areas of HPLC chromatograms. Cleavage from the resin was performed with NH$_3$ for 3 h at r.t in the case of CT-$^{5'}$azido and for 1h at 55ºC in the case of GA-$^{5'}$azido.

ODN 24 and **26** were purified by RP-HPLC using conditions A (for ODN 24) or C (for ODN 26). Retention times of these products as well as of their intermediates are indicated in the table 3.29 of this thesis. Determined masses of the oligonucleotides by MALDI-TOF ([M-H]$^-$) and their calculated theorical values (between parentheses) are as follows: **CT**: 3194 (3194); **CT-$^{5'}$iodo**: 3302 (3304);

CT-$^{5'}$azido: 3217 (3219); **GA:** 3476 (3479); **GA-$^{5'}$iodo:** 3586 (3589); **GA-$^{5'}$azido:** 3502 (3504).

6.4.10. Synthesis of oligonucleotides carrying azido groups at the 5'-end using the phosphoramidite derivative of 6-bromohexan-1-ol.

The phosphoramidite of 6-bromohexan-1-ol was introduced in the DNA synthesizer and incorporated into the **CT** and **GA** sequence (coupling time = 300 s).

A small amount of CPG beads carrying the 5'-bromohexyl oligonucleotides were treated with concentrated ammonia at 55ºC o.n which resulted in nucleophilic substitution of bromine atom to give 5'-aminohexyl oligonucleotides as the major product (85 % yield), as concluded from analysis by RP-HPLC (figure 3.33) and MALDI-TOF. MALDI-MS ([M-H]$^-$): CT-$^{5'}$aminohexyl**:** 3373 (calc. 3372) and GA-$^{5'}$aminohexyl: 3657 (calc. 3658).

The rest of the support carrying the $^{5'}$-Br-oligonucleotide (CT-$^{5'}$bromohexyl and GA-$^{5'}$bromohexyl; **ODN 28** and **30**) was treated with NaN$_3$ (68 mg, 1 mmol) in DMF (1 ml) o.n at r.t to yield the desired $^{5'}$-N$_3$-oligonucleotides (**ODN 29** and **31)**. CT-$^{5'}$azidohexyl and GA-$^{5'}$azidohexyl were cleavaged from the support and purified by RP-HPLC (conditions C) eluting at 11.7 and 12.8 min respectively in 75-94% yield. Determined masses of the oligonucleotides by MALDI-TOF ([M-H]$^-$) and their calculated theorical values (between parentheses) are as follows: **CT-$^{5'}$azidohexyl**: 3397 (3398); **GA-$^{5'}$azidohexyl**: 3683 (3684).

6.4.11. CuAAC reactions to ligate two oligonucleotide strands in solution

To find the optimal conditions for the coupling reaction a small excess of 8T-$^{5'}$propargylglutaryl (**ODN 9,** 19.5 nmol) was mixed with 8T-$^{5'}$azidobutyryl (**ODN 22,** 15 nmol) in the presence of either CuSO$_4$/ascorbic acid or CuI. Three conditions were tested:

1) 0.1 equiv. of CuSO$_4$ and 0.5 equiv. of ascorbic acid in 0.07 ml of H$_2$O/t-BuOH (2:1), r.t. under Ar, 72 h.
2) 10 equiv. of CuSO$_4$ and 50 equiv. of ascorbic acid in 0.075 ml of H$_2$O/ t-BuOH (2:1), r.t. under Ar, 72 h with stirring.
3) 300 equiv. of CuI and 400 equiv. of DIPEA in 0.06 ml of H$_2$O/ACN (1:1), r.t. under Ar, 40 h with stirring.

Best results were obtained in trials 2 and 3 (75% yield) where an excess of the copper source was used. When copper catalyst was only 0.1 equiv. yield was between 10–15%. The presence of the product of cycloaddition was confirmed by gel electrophoresis. Mass spectrometry gave a mass value higher than expected (found 6157, calc. 5378) probably due to the presence of copper ions that were not completely eliminated from the reaction.

6.4.12. CuAAC reactions to ligate two oligonucleotide strands in solid phase

General protocol for click reaction on the resin:

A few milligrams of CGP resin functionalized with the 5'-azido-sequences (0.05 – 0.15 µmol) were placed in a 1 mL screw cap septum vial. In an Eppendorf tube, CuI (1-5 mg) was dissolved in 10 µl H_2O and 40 µl of ACN containing 3-7 µl of DIPEA, and then TBTA (0.5-2 mg) dissolved in 10 µl of DCM was added. This mixture was vortexed and added to a separate vial containing the 5'-alkyn-sequence in 40 µl of H_2O. The final solution was added to the vial containing the solid-supported DNA. This vial was filled with argon and gently rotated over two days. The solution was filtrated and the resin was washed thoroughly with ACN, a solution of ascorbic acid (0.02 g/ml) in H_2O, H_2O, 0.1 M EDTA, H_2O, and DCM/MeOH (1:1).

Variations of these protocols were performed in several experiments:

- when using homopyrimidine sequences: 2-4 mg of ascorbic acid in H_2O was added instead of TBTA/DCM
- use of ChemMatrix: in some experiments CM was used instead of CPG as solid support
- reactants inversely immobilized: in this case 5'-alkyne-sequence was on the resin and the 5'-azido-sequence in solution

The conditions used in all experiments are collected in the table below (table 6.3). In the last column, the methods employed for the characterization of the ligation products are indicated.

Azido-ODN (nmol)	Alkyn-ODN (equiv)	CuI/DIPEA (equiv)	Ascorbic (equiv)	TBTA (equiv)	Characterization
100 nmol **ODN 22**	2 eq. **ODN 13**	150/170	--	--	RP-HPLC (t_R=14.4 min), UV, enzymatic digestion
120 nmol **ODN 24**	4 eq. **ODN 21**	200/240	--	--	n.d
120 nmol **ODN 29**	4 eq. **ODN 21**	200/240	--	--	n.d
100 nmol **ODN 24**	9 eq. **ODN 11**	200/240	100	--	RP-HPLC (conditions C , t_R=11.2 min, 35%), PAGE ; MALDI-MS: 5870 (calc.5877)
100 nmol **ODN 29**	5 eq. **ODN 11**	200/240	100	--	RP-HPLC (conditions C , t_R=12.0 min, 40%);PAGE ; MALDI-MS:6051 (calc.6056)
100 nmol **ODN 29**	5 eq. **ODN 11**	200/240	100	75	RP-HPLC (conditions C, t_R=13.0 min, 40%)
500 nmol **ODN 27** [a]	1.5 eq. **ODN 11**	200/240	100	--	RP-HPLC (t_R=14.0 min with program C, 70%) ; MALDI-MS: 5990 (calc.5992)

150 nmol ODN 31 [b]	2.5 eq. ODN 15	160/190	160	--	n.d
140 nmol ODN 31	3 eq. ODN 15	70/135	--	--	PAGE
97 nmol ODN 31	1.9 eq. ODN 15	80/440	--	--	PAGE, enzymatic digestion
60 nmol ODN 31	1.6 eq. ODN 19	113/622	--	22	PAGE, enzymatic digestion
64 nmol ODN 31	1.6 eq. ODN 17	122/672	--	30	PAGE, enzymatic digestion, fluorescence (345 nm)
45 nmol ODN 26	2.6 eq. ODN 15	105/577	--	21	PAGE, enzymatic digestion
48 nmol ODN 26	2 eq. ODN 19	109/598	--	20	PAGE, enzymatic digestion
58 nmol ODN 26	1.8 eq. ODN 17	118/648	--	23	PAGE, enzymatic digestion
150 nmol ODN 24	1.3 eq. ODN 17	70/380	--	54	PAGE, fluorescence (345 nm)
2 eq. ODN 31 [c]	70 nmol ODN 15 [c]	75/410	--	88	AEC, PAGE

Table 6.3. Conditions used in different click reaction between two ODN strands.

[a] 5'-azido-ODN is supported in ChemMatrix

[b] No product was isolated, nor on CPG or CM

[c] In this case, the 5'-alkyne-ODN was immobilized on CPG and the 5'-azido-ODN was added in solution

6.4.13. Reaction of CT-$^{5'}$hexynyl and 8T-$^{5'}$propargyl with benzylazide

The solid support carrying oligonucleotide sequence CT-$^{5'}$hexynyl (**ODN 20**; 1.6 mg, 50 nmols) was treated with benzylazide (2 μl) in the presence of 4 mg of CuI, 4 μl of DIPEA , and 2 mg of ascorbic acid at r.t., in 0.15 ml of H_2O/ACN (1 : 1), stirring for 17 h. After the reaction, the support was extensively washed as described above and oligonucleotide was cleaved from the support. The desired compound eluted at 12.7 min (conditions C) as a major product. MALDI-MS: 3489 (calc. 3484).

A similar protocol was used to react 8T-$^{5'}$propargyl (**ODN 11**; 3 mg, 90 nmols) with benzylazide (2 μl) adding 3 mg of CuI, 4 μl of DIPEA , and 4 mg of ascorbic acid at r.t., in 0.14 ml of H_2O/ACN (1 : 1). The desired compound eluted at 17.6 min (conditions C) as a major product. MALDI-MS: 2792 (calc. 2792).

6.4. 14. Synthesis of novel unnatural amino acids by click chemistry

All the different synthetic steps to obtain the (S)-Nα-t-Boc-propargylglycine, the Nα-t-Boc-β-amino-L-alanine and the subsequent click reactions are described in the sections below:

### 6.4.15. Synthesis of (3R)-3,6-Dihydro-2,5-diethoxy-3-isopropyl-pyrazine

A mixture of 3(R)-isopropylpiperazine-2,5-dione (4.67 g, 30 mmol) and Et$_3$O·BF$_4$ (37.9 g, 197.8 mmol) in DCM (250 ml) was stirred at room temperature under nitrogen for 6 days. The solution was added in portions to a vigorously stirred mixture of saturated aqueous NaHCO$_3$ (300 ml) and DCM (200 ml) at 4ºC, while maintaining the pH between 8 and 9 by the addition of 3 M NaOH as required. The phases were separated and the aqueous phase was extracted with DCM (2 x 150 ml). The combined organic phases were washed with brine (200 ml), dried with MgSO$_4$ and concentrated under vacuum to give the crude as a yellow oil. Flash chromatography using hexane/ethyl acetate (9:1) as eluent yielded the pure product in 49 % yield (3.15 g, 14.7 mmol) as a colourless oil. R$_f$=0.32.
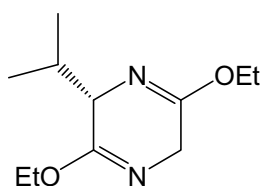
¹H-NMR (400MHz, CDCl$_3$): δ 0.75 (d, 3H), 1.0 (d, 3H), 1.24-1.28 (m, 6H), 2.15-2.27 (m, 1H), 3.91-3.97 (m, 3H), 4.0-4.21 (m, 4H). **¹³C-NMR** (400 MHz, CDCl$_3$) δ 14.4, 17.1, 19.1, 32.6, 46.9, 60.8, 61.1, 161.9, 164.4

6.4.16. Synthesis of (3R)-3,6-Dihydro-2,5-diethoxy-3-isopropyl-(6S)-propargyl-pyrazine

1.359 g of (3R)-3,6-Dihydro-2,5-diethoxy-3-isopropyl-pyrazine (6.36 mmol) were dissolved in 25 ml of dry THF under nitrogen atmosphere and allowed to cool to -78ºC. A solution of 2.5 M butillithium in n-hexane (2.8 ml, 7 mmol) was added dropwise and the mixture was stirred 45 minutes. A precooled solution (-78ºC) of propargylbromide (0.99 g, 8 mmol) in 10 ml of dry THF was added slowly and the reaction mixture was stirred overnight. The solvent was removed in vacuo and the residue was treated with 100 ml of 0,1 M potassium phosphate buffer (pH=7). The suspension was extracted with diethylether (3 x 100ml) and the combined organic phases were dried over MgSO$_4$ and concentrated under reduced pressure. The crude product was purified by flash chromatography on silica eluting with dichlorometane/ethylacetate (99:1) obtaining the pure product in a 67% yield (1.07 g, 4.24 mmol). R$_f$ = 0.33.
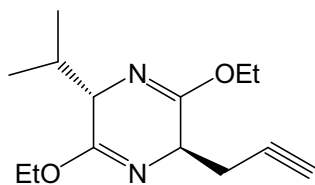
¹H-NMR (400 MHz, CDCl$_3$): δ 0.64 (d, 3H), 0.98 (d, 3H), 1.22 (t, 6H), 1.83 (t, 1H), 2.19-2.27 (m, 1H), 2.57-2.71 (m, 2H), 3.93 (t, 1H), 4.0-4.2 (m, 5H). **¹³C-NMR** (400 MHz, CDCl$_3$): δ 14.3, 16.6, 19.1, 25.1, 31.7, 54.4, 60.7, 60.9, 69.9, 80.7, 161.3, 164.3.

6.4.17.Synthesis of (S)-ethyl-2-(*tert*-butoxycarbonylamino)-pent-4-ynoate

1.07 g of (3R)-3,6-Dihydro-2,5-diethoxy-3-isopropyl-(6S)-propargyl-pyrazine (4.24 mmol) were dissolved in 16 ml of water/acetonitrile (1:1) and 0.96 ml of 99% TFA were added (12.73 mmol, 3 eq). The solution was stirred 5 minutes in the microwave oven at 60 ºC. The solution was concentrated to about 10 ml and 20 ml of DCM were added. The two phases were separated and the pH of the aqueous phase was brought to 10 by addition of 25% aqueous NH_3. The mixture was extracted with DCM (3 x 15 ml) and the organic solution was dried over Na_2SO_4 and evaporated. Crude product from the hydrolysis was dissolved in 40 ml of dry THF and 2 eq. of tert-butyldicarbonate were added. The mixture was stirred under reflux overnight. The solvent was evaporated and the residue was purified by flash chromatography on silica using hexane/diethylether (8:3) as eluent. Pure product was obtained in 73 % yield (0.75g, 3.11 mmol). Rf = 0.47.
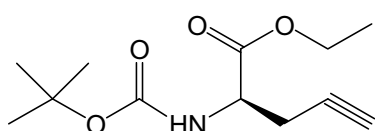
¹H-NMR (400 MHz, CDCl$_3$): δ 1.28 (t, 3H), 1.44 (s, 9H), 2.02-2.03 (t, 1H), 2.72- 2.73 (m, 2H), 4.18-4.29 (m, 2H), 4.41-4.46 (m, 1H). **¹³C-NMR** (400 MHz, CDCl$_3$): δ 14.3, 23.0, 28.4, 52.0, 61.9, 71.6, 78.8, 80.2, 155.2, 170.7.

6.4.18. Synthesis of (S)-Nα-t-Boc-propargylglycine

0.75 g of (S)-ethyl-2-(*tert*-butoxycarbonylamino)-pent-4-ynoate (3.11 mmol) were dissolved in 22 ml of water/THF (1:1) and 261 mg of LiOH·H$_2$O (6.22 mmol, 2 eq) were added. The mixture was heated for 20 minutes at 60ºC in a microwave oven. The solution was concentrated to about 2 ml and DCM (2 x 25 ml) was added. The phases were separated and the pH of the aqueous phase was brought to 3 by addition of 10 ml of 10% aqueous citric acid. The organic phase was dried over Na_2SO_4 and the solvent was removed under vacuum obtaining the desired product in 76 % yield as a yellow oil (0.44 g, 2.07 mmol).
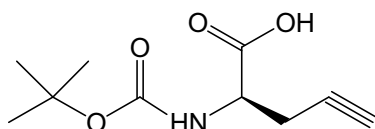
¹H-NMR (400 MHz, CDCl$_3$): δ 1.44 (s, 9H), 2.07 (s, 1H), 2.73-2.83 (m, 2H), 4.50-4.52 (m, 1H). **¹³C-NMR** (400 MHz, CDCl$_3$): δ 22.6, 28.4, 51.8, 72.0, 78.4, 80.8, 155.5, 175.3. **IR** υ$_{max}$ (KBr; cm^{-1}): 3431, 3308, 2980, 1717, 1508, 1394, 1368, 1160, 1063.

6.4.19. Synthesis of Nα-t-Boc-β-amino-L-alanine

A slurry of Nα-t-Boc-L-asparagine (0.51 g, 2.18 mmol), ethyl acetate (2.4 mL), acetonitrile (2.4 mL), water (1.2 mL), and PIDA (0.832 g, 2.58 mmol) was cooled and stirred at 16 °C for 30 min. The temperature was allowed to reach 20 °C, and the reaction was stirred until completion (4 h). The mixture was cooled to 0

°C and filtered. The filter cake was washed with 2 mL of ethyl acetate and dried in vacuo at 65 °C to give the desired product (2.70 g, 60 % yield). R_f=0.11 (EtOAc:MeOH 6:4).
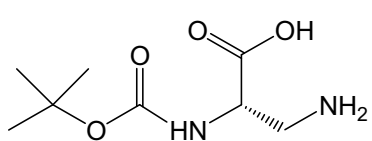
^{1}H-NMR (400 MHz, DMSO-D$_6$): δ 1.39 (s, 9H), 2.73-2.78 (m, 1H), 3.00-3.04 (m, 1H), 3.63-3.65 (m, 1H). **^{13}C-NMR** (400 MHz, DMSO-D$_6$): δ 28.7, 40.7, 51.6, 78.7, 155.5, 171.8.

6.4.20. General Procedure for sequential one-pot process for diazo transfer and azide-alkyne cycloaddition using CuSO$_4$ and sodium ascorbate.

Triflyl azide (TfN$_3$) was freshly prepared prior to each reaction. NaN$_3$ (6 eq per substrate amine) was dissolved in a minimum volume of water (solubility of NaN$_3$ in water is approximately 0.4 g/ml). At 0 °C an equal volume of dichloromethane was added and triflic anhydride (Tf$_2$O) (3 eq) was added dropwise to the vigorously stirred solution. After stirring for 2 h at 0 °C the aqueous phase was once extracted with the same volume of dichloromethane. The combined organic phases were washed with sat. NaHCO$_3$ solution and used without further purification.

The substrate amine, CuSO$_4$ (4 mol%) and NaHCO$_3$ (2 eq) were dissolved/suspended in the same volume of water as the volume of the TfN$_3$ solution to be employed. The TfN$_3$ solution was added, followed by addition of methanol to get a homogeneous solution with a proportion of 3:10:3 of H$_2$O/MeOH/DCM. The reaction was stirred at room temperature (1.5 - 2h) until TLC showed complete conversion of the starting amine. IR of the azide product showed a peak at 2110 cm^{-1}, as expected for azide compounds.

Then the acetylene component (1.1 eq), TBTA (5 mol %) and sodium ascorbate (30 mol % per substrate amine) were added and the reaction was heated to 70 °C in sealed vials under microwave irradiation (Biotage Initiator Instrument) until TLC showed complete conversion of the azide intermediate (about 30 min). In addition, as the click product and the starting azide showed similar Rf, reaction was let stirring at room temperature overnight to be sure that reaction is finished.

The reaction mixture was diluted with water and the organic solvents were removed under reduced pressure. The water was removed under reduced pressure by co-evaporation with toluene/ethanol (1:1). The crude product was purified by flash chromatography.

6.4.21. Synthesis of *(S)*-2-(*tert*-butoxycarbonylamino)-3-(4-phenyl-1H-1,2,3-triazol-1-yl)propanoic acid

Nα-t-Boc-β-amino-L-alanine (268 mg, 1.3 mmol) was reacted to phenylacetylene (143 μL, 1.3 mmol) according to general procedure detailed above. After flash chromatography (DCM/MeOH 8/3) the product was isolated as a yellow solid with 97 % yield. (419 mg, 1.26 mmol). Rf = 0.26.
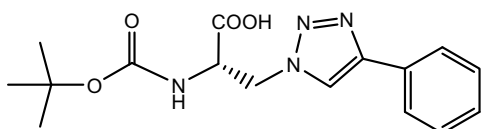
^{1}H-NMR (400 MHz, DMSO-D$_6$): δ 1.29 (s, 9H), 4.12 (m, 1H), 4.47-4.60 (m, 1H), 4.83-4.86 (m, 1H), 7.30 (t, 1H), 7.42 (t, 2H), 7.80 (d, 2H), 8.33 (s, 1H). **^{13}C -NMR** (400 MHz, DMSO-D$_6$): δ 28.6, 50.4, 54.2, 79.1, 122.6, 125.6, 128.4, 129.5, 131.3, 146.7, 155.8, 171.5. **IR** υ$_{max}$ (KBr; cm^{-1}): 3407, 2978, 1700, 1608, 1419, 1365, 1250, 1166, 1060, 763, 693.
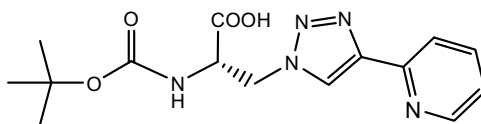
6.4.22. Synthesis of *(S)*-2-(*tert*-butoxycarbonylamino)-3-(4-(pyridin-2-yl)-1H-1,2,3-triazol-1-yl)propanoic acid

Nα-t-Boc-β-amino-L-alanine (108 mg, 0.53 mmol) was reacted to 2-ethynylpyridine (56 μL, 0.55 mmol) according to the general procedure. After flash chromatography (DCM/MeOH 7/3) the product was isolated as a yellow solid with a 86 % yield. (152 mg, 0.45 mmol). Rf = 0.21.

^{1}H-NMR (400 MHz, DMSO-D$_6$): δ 1.28 (s, 9H), 4.12 (s, 1H), 4.60-4.65 (m, 1H), 4.88-4.91 (m, 1H), 7.31 (t, 1H), 7.87 (t, 1H), 8.00 (d, 1H), 8.39 (s, 1H), 8.56 (d, 1H). **^{13}C -NMR** (400 MHz, DMSO-D$_6$): δ 28.6, 52.5, 56.2, 78.5, 119.8, 123.3, 124.2, 137.6, 147.4, 150.8, 155.4, 172.1. **IR** υ$_{max}$ (KBr; cm^{-1}): 3409, 2978, 1693, 1615, 1417, 1366, 1249, 1165, 1058, 784.

6.4.23. Synthesis of *(S)*-2-(*tert*-butoxycarbonylamino)-3-(4-(prop-1-en-2-yl)-1H-1,2,3-triazol-1-yl)propanoic acid

Nα-t-Boc-β-amino-L-alanine (108 mg, 0.53 mmol) was reacted to 2-methyl-1-buten-3-yne (53 μL, 0.55 mmol) according to the general procedure. After flash chromatography (DCM/MeOH 7/3) the product was isolated as a yellow solid with a 86 % yield. (135 mg, 0.45 mmol). Rf = 0.44.
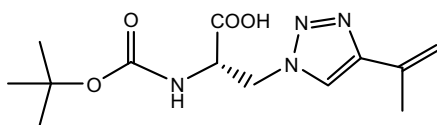
^{1}H-NMR (400 MHz, DMSO-D$_6$): δ 1.30 (s, 9H), 2.01 (s, 3H), 4.13-4.14 (m, 1H), 4.47-4.53 (m, 1H), 4.78-4.82 (m, 1H), 5.00 (s, 1H), 5.56 (s, 1H), 7.96 (s, 1H). **^{13}C -NMR** (400 MHz, DMSO-

D$_6$): δ 20.9, 28.6, 52.0, 56.1, 78.5, 111.6, 122.2, 134.4, 147.5, 155.3, 172.6. **IR** υ$_{max}$ (KBr / cm^{-1}). 3410, 2979, 2106, 1699, 1599, 1418, 1367, 1248, 1167, 1062, 1026.

6.4.24. Synthesis of (*S*)-2-(*tert*-butoxycarbonylamino)-3-(4-(1-hydroxy cyclohexyl)-1H-1,2,3-triazol-1-yl)propanoic acid

Nα-t-Boc-β-amino-L-alanine (108 mg, 0.53 mmol) was reacted to 1-ethynyl-1-cyclohexanol (68 mg, 0.55 mmol) according to the general procedure. After flash chromatography (DCM/MeOH 7/3) the product was isolated as a white solid with a quantitative yield. (188 mg, 0.53 mmol). Rf = 0.41.

¹H-NMR (400 MHz, DMSO-D$_6$): δ 1.31 (s, 9H), 1.39-1.47 (m, 4H), 1.64-1.67 (m, 4H), 1.79-1.86 (m, 2H), 4.10-4.11 (m, 1H), 4.44-4.50 (m, 1H) , 4.74-4.79 (m, 1H), 7.71 (s, 1H). **¹³C -NMR** (400 MHz, DMSO-D$_6$): δ 22.2, 25.9, 28.7, 38.4, 38.5, 51.8, 56.2, 68.5, 78.4, 121.8, 155.4, 155.8, 172.6. **IR** υ$_{max}$ (KBr / cm^{-1}): 3410, 2934, 2860, 1699, 1599, 1506, 1418, 1366, 1253, 1167, 1060, 965, 850, 757.

6.4.25. Synthesis of (*S*)-2-(*tert*-butoxycarbonylamino)-3-(4-p-tolyl-1H-1,2,3- triazol-1-yl)propanoic acid
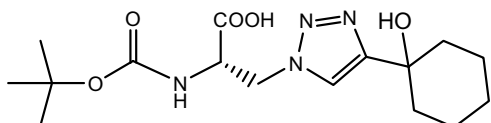
Nα-t-Boc-β-amino-L-alanine (108 mg, 0.53 mmol) was reacted to 4-ethynyltoluene (70 μL, 0.55 mmol) according to the general procedure. After flash chromatography (DCM/MeOH 7/3) the product was isolated as a yellow solid with a quantitative yield (211 mg, 0.61 mmol). Rf = 0.43.

¹H-NMR (400 MHz, DMSO-D$_6$): δ 1.27 (s, 9H), 2.30 (s, 3H), 4.19-4.28 (m, 1H), 4.57-4.62 (m, 1H), 4.86-4.88 (m, 1H), 7.21 (d, J=8 Hz, 2H), 7.68 (d, J=7.7 Hz, 2H), 8.28 (s, 1H). **¹³C -NMR** (400 MHz, DMSO-D$_6$): δ 21.4, 28.6, 52.2, 56.2, 78.6, 121.9, 125.6, 128.8, 129.9, 137.4, 146.6, 155.4, 172.9. **IR** υ$_{max}$ (KBr; cm^{-1}): 3420, 2978, 1699, 1596, 1424, 1366, 1250, 1166, 1062.

6.4.26. Synthesis of (*S*)-2-(*tert*-butoxycarbonylamino)-3-(4-(4-(trifluoro methyl) phenyl)-1H-1,2,3-triazol-1-yl)propanoic acid
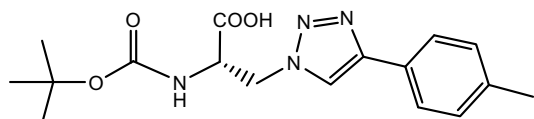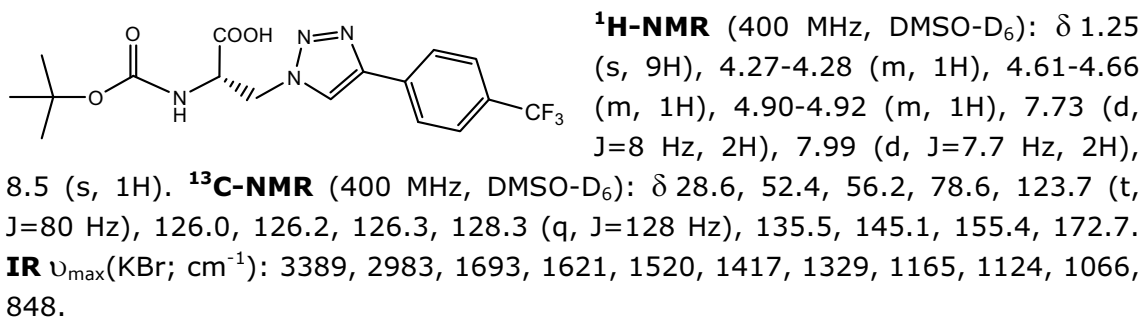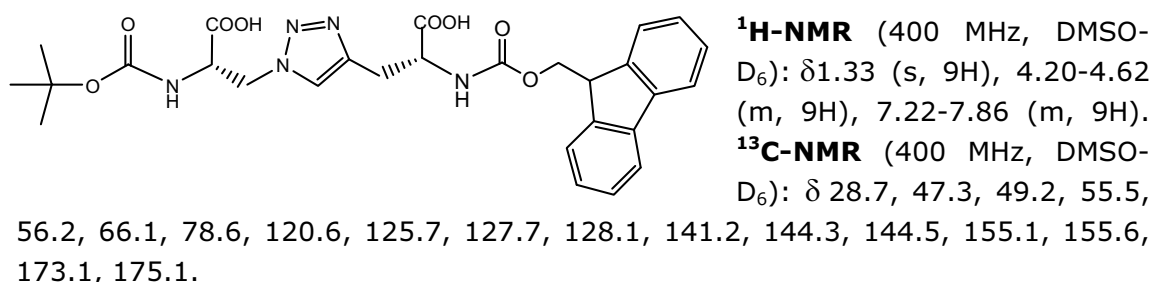
Nα-t-Boc-β-amino-L-alanine (108 mg, 0.53 mmol) was reacted to 4-ethynyl-α,α,α-trifluorotoluene (90 μL, 0.55 mmol) according to the general procedure. After flash chromatography (DCM/MeOH 8/2) the product was isolated as a white solid with a quantitative yield (217 mg, 0.54 mmol). Rf = 0.34.

¹H-NMR (400 MHz, DMSO-D₆): δ 1.25 (s, 9H), 4.27-4.28 (m, 1H), 4.61-4.66 (m, 1H), 4.90-4.92 (m, 1H), 7.73 (d, J=8 Hz, 2H), 7.99 (d, J=7.7 Hz, 2H), 8.5 (s, 1H). **¹³C-NMR** (400 MHz, DMSO-D₆): δ 28.6, 52.4, 56.2, 78.6, 123.7 (t, J=80 Hz), 126.0, 126.2, 126.3, 128.3 (q, J=128 Hz), 135.5, 145.1, 155.4, 172.7. **IR** υ$_{max}$(KBr; cm^{-1}): 3389, 2983, 1693, 1621, 1520, 1417, 1329, 1165, 1124, 1066, 848.

6.4.27. Synthesis of (*S*)-2-(*tert*-butoxycarbonylamino)-3- (4-((S)-2-(((9H-fluoren-9-yl)methoxy)carbonylamino)propyl)-1H-1,2,3-triazol-1-yl) propa noic acid

Nα-t-Boc-β-amino-L-alanine (200 mg, 0.98 mmol) was reacted to Fmoc-propargyl glycine (401 mg, 1.2 mmol) according to the general procedure. After flash chromatography (gradient of increasing polatity from DCM/MeOH 8/2 to DCM/MeOH 6/4) the product was isolated as a yellow solid with a 95% yield. (523 mg, 0.93 mmol).

¹H-NMR (400 MHz, DMSO-D₆): δ1.33 (s, 9H), 4.20-4.62 (m, 9H), 7.22-7.86 (m, 9H). **¹³C-NMR** (400 MHz, DMSO-D₆): δ 28.7, 47.3, 49.2, 55.5, 56.2, 66.1, 78.6, 120.6, 125.7, 127.7, 128.1, 141.2, 144.3, 144.5, 155.1, 155.6, 173.1, 175.1.

6.5. Experimental section (Chapter 4)

6.5.1. Conjugation of oligonucleotides to 1,4,8,11-tetraazacyclotetradecane

The 6-bromohexyl-(2-cyanoethyl)-(N,N-diisopropyl)-phosphoramidite was introduced in the DNA synthesizer and incorporated into the oligonucleotide sequences **15C** and **³′-disulfide-15C.** After oligonucleotide synthesis, each ⁵′Br-(CH₂)₆-ODN-support was placed on a screw cap vial and incubated with 1 ml of DCM/DIPEA (95:5) containing 100 equivalents of cyclam at 55ºC for 24 hours. The resulting oligonucleotide **15C-⁵′-crown1** and **³′-disulfide-15C-⁵′-crown1** were cleavaged from the support and purified by RP-HPLC (conditions C) eluting at 11 and 12.3 min respectively. Determined masses of the oligonucleotides by MALDI-TOF ([M-H]⁻) and their calculated theorical values (between parentheses) are as follows: **15C-⁵′-crown1**: 4929.7 (4927.9); **³′-disulfide-15C-⁵′-crown1**: 5168.8 (5171.9).

6.5.2. Conjugation of oligonucleotides to 1,5-diaza-9,13-dithiacyclohexadecane

The 6-bromohexyl-(2-cyanoethyl)-(N,N-diisopropyl)-phosphoramidite was introduced in the DNA synthesizer and incorporated into the oligonucleotide sequences **15C** and **3'-disulfide-15C**. After oligonucleotide synthesis, each $^{5'}$Br-$(CH_2)_6$-ODN-support was placed on a screw cap vial and incubated with 1 ml of DMSO/DIPEA (95:5) containing 100 equivalents of 1,5-diaza-9,13-dithiacyclohexadecane at 55 ºC for 24 hours. The resulting oligonucleotide **15C-5'-crown2** and **3'-disulfide-15C-5'-crown2** were cleavaged from the support and purified by RP-HPLC (conditions C) eluting at 11.9 and 13.2 min respectively. Determined masses of the oligonucleotides by MALDI-TOF ([M-H]⁻) and their calculated theorical values (between parentheses) are as follows: **15C-5'-crown2**: 4988.5 (4991.9); **3'-disulfide-15C-5'-crown2**: 5228.1 (5235.9).

6.5.3. Copper chelation studies with the 5'-crown-oligonucleotides

1 O.D of each 5'-crown-ODN was incubated overnight with 10 equivalents of $CuCl_2$ in 0.5 ml of milliQ water at 4 ºC. The excess of copper was removed by passing the solution through a NAP-5 (Sephadex G-25) column. Desalted samples were analyzed by MALDI-TOF and the found MW was compared with those calculated for ODNs complexated with one Cu^{2+} atom per strand. Determined masses of the oligonucleotides by MALDI-TOF ([M-H]⁻) and their calculated theorical values (between parentheses) are as follows: **15C-5'-crown1 /Cu²⁺**: 4996.5 (4991.4); **3'-disulfide-15C-5'-crown1 /Cu²⁺**: 5243.4 (5235.4). **15C-5'-crown2 /Cu²⁺**: 5000.2 (5055.4); **3'-disulfide-15C-5'-crown2 /Cu²⁺**: 5243.1 (5299.4). As deduced from this values, only oligonucleotides derivatized with crown **1** appeared to chelate Cu (II) strong enough to remain bound after passing through the desalting cartridge.

6.5.4. Gold Electrode Preparation

Polycrystalline gold disk electrodes (0.5 cm in diameter, 0.196 cm^2) were polished with a microcloth coated with a suspension of 1 μm alumina powder (Buehler GmbH, Germany), rinsed, and sonicated for 15 min in Milli-Q water to remove any remaining polishing agent. The electrodes were then dipped in 0.1 M H_2SO_4 and activated by holding the potential at +2.0 V for 5 s and then at -0.35 V for 10 s, followed by potential cycling from -0.35 to +1.5 V at 4 V/s for 100 scans. Finally, the CV characteristic of a clean polycrystalline gold surface was recorded in 0.1 M H_2SO_4 at 0.1 V/s. The microscopic area was calculated by integration of the cathodic peak associated with the reduction of the gold oxide using a value of 400 μC·cm^{-2} for a monolayer of chemisorbed oxide on polycrystalline gold. The electrodes were subsequently washed with Milli-Q water.

In the experiments in which gold surfaces were modified with thiolated SAMs, reductive desorption with KOH solution was performed at the end of electrochemical measurements, as detailed in section 6.5.10.

6.5.5. Electrochemical measurements

Voltammetric experiments were performed with a potentiostat PGSTAT10 from Autolab, using GPES 4.9 software for electrochemical measurements (Eco Chemie BV, The Netherlands). A conventional three-electrode cell with a polycrystalline gold working electrode, a platinum gauze wire as the counter electrode and a saturated calomel reference electrode (SCE) were used. Other electrode references such as Ag/AgCl, NaCl (3M in H_2O) and Hg/Hg_2SO_4, K_2SO_4 (saturated in H_2O) were used when indicated. All solutions were deoxygenated by bubbling nitrogen or argon for 30 min before the measurements, and all experiments were carried out at room temperature.

6.5.6. Formation of alkanethiol self assembled monolayers

To form alkanethiol monolayers, gold electrodes were immersed into solutions with thiol-containing molecules for different time periods.

Thioctic SAMs were obtained by dipping of the gold electrode in a 1 mM solution of thioctic acid in EtOH during 24 hours. After the self-assembly step the electrode was thoroughly rinsed with EtOH to remove physisorbed molecules.

Mixed monolayer surfaces containing ssDNA and MCH or MCE were prepared by immersing the clean gold substrate in a solution of R-S-S-ssDNA or HS-ssDNA (see 6.5.7 section below), followed by a 2 h exposure of the sample to either an aqueous solution of 2.0 mM MCH or MCE. Before electrochemical analysis, electrodes were rinsed thoroughly with milliQ water.

6.5.7. DNA immobilization on gold electrodes

Two procedures for DNA immobilization were performed. In first instance, ODNs were directly attached without performing reduction of disulfide groups. In this protocol ODN solutions were prepared either at 30 or 300 μM in phosphate buffered saline (PBS; 0.1 M phosphate, pH 7.4). KCl and $MgCl_2$ were added in some cases to achieve 1M and 4 mM final concentrations respectively, according to the table 4.33 of chapter 4. Then, 10 μl of each ODN solution was placed on the gold surfaces. The electrodes were covered with a plastic chamber to avoid evaporation of the solution and left at room temperature during 20 hours.

The second protocol for DNA SAM formation consisted in reduction of the disulfide bridges before oligonucleotide immobilization on gold electrodes and higher functionalization density was achieved. In this case 1 μl of 300 μM disulfide-modified DNA sequences was mixed with 2 μl of 10 mM TCEP and incubated at r.t. for 2.5 hours to reduce the disulfide bond. Then, samples were diluted to a total volume of 20 or 200 μl with PBS (pH=7.2; 10 mM KH_2PO_4 with 1M KCl and 1 mM $MgCl_2$). Gold electrodes were treated with 20 μl of each ODN solution at room temperature overnight.

Nonspecifically adsorbed DNA was displaced with an alkanethiol SAM as detailed in the previous section. Modified electrodes were rinsed thoroughly with milliQ water before the electrochemical measurements.

6.5.8. DNA hybridization and electrochemical characterization

Hybridization was carried out with a 30 μM solution of the complementary oligonucleotide in PBS (pH=7.2; 10 mM KH_2PO_4 with 1M KCl and 1 mM Mg^{2+}). ssDNA/Au electrodes were incubated at room temperature with 10 μl of this solution during a minimum of 4 hours and overnight in some cases. Both ssDNA/Au and the resulting dsDNA/Au electrodes were treated with PBS containing 1 mM methylene blue for 1.5 h, subsequently rinsed and transferred to 0.1 M KH_2PO_4 solution of pH 7.4 for DPV measurements. Differential pulse (DP) voltammograms were registered in the potential interval 0 to −0.5 V versus Ag/AgCl, and the DP conditions were as follows: step potential, 1 mV; pulse amplitude, 20 mV; modulation time, 0.02 s; interval time, 0.1 s.

6.5.9. Electrochemical study of copper–dsDNA–gold electrodes

Gold electrodes functionalized with oligonucleotides (ssDNA and dsDNA) were incubated with a 10 mM solution of $CuSO_4$ in H_2O during 4 hours at room temperature and rinsed with water. Cyclic voltammograms were registered at different scan rates between 0.5 to -0.5 V (vs Ag/AgCl, 3M NaCl) in 0.1 M KH_2PO_4 at pH 7.4.

6.5.10. Reductive desorption of thiolated SAMs from gold electrodes

Electrochemical desorption experiments were performed by immersing thiolated SAMs into thoroughly degassed 0.50 M KOH. Unless indicated, the initial potential (respect to Ag/AgCl, NaCl, 3M in H_2O) was 0 V, the switching potential was -1.5 V, and the scan rate was 100 mV·s^{-1}. Potential was cycled until constant voltammograms were obtained.

6.6. Experimental section (Chapter 5)

6.6.1. Synthesis of the quadruplex forming sequences

The oligonucleotides used in this chapter were prepared on 0.2 μmol scale in the automatic synthesizer using phosphoramidite chemistry on polystyrene solid support (LV200).

The first part of the quadruplex was synthesized with the appropriate T and G standard 3'-phosphoramidites. 8-amino-dG-3'-CE phosphoramidite was used to introduce a modified guanine in desired positions. The trebler phosphoramidite was then coupled and synthesis was carried on using T and G 5'-phosphoramidites. As

trebler provides three elongation points. reversed phosphoramidites were used in 0.3 M concentration, instead of 0.1 M. Coupling times for trebler, 8-Amino-dG and 5'-phosphoramidites are indicated in the table below.

phosphoramidite	coupling time (s)
8-amino-dG-3'-CE	300
trebler	900
dT-5'-CE	180
dmf-dG-5'-CE	180

Table 6.4. Coupling times for non standard phosphoramidites used in this work.

Oligonucleotides were synthesized without performing final detritylation to facilitate reverse-phase HPLC purification. Deprotection and cleavage from the support was performed by a 0.1 M mercaptoethanol solution in aqueous concentrated ammonia for 24 hours at 55 ºC.

ODNs were purified with the "*DMT ON*" protocol and peak corresponding to the DMT-protected product was collected. (t_R= 12.82 min). The purified oligonucleotides were detritylated with 1 ml of 80 % aqueous acetic acid (45 minutes at room temperature + 30 minutes at 55 ºC), desalted by NAP-10, and analyzed by MALDI-TOF and denaturing PAGE, following the protocols described in "General Methods".

6.6.2. CD experiments

All samples were heated to 95 ºC and slowly cooled to room temperature prior to measurements. CD spectra of the quadruplexes were registered every 10 ºC (in the interval 10-90 ºC) at 5 μM quadruplex concentrations. The wavelength was varied from 210 to 320 nm at 50 nm·min^{-1}. The spectra were recorded with a response of 4 s, at 1.0 nm bandwidth and normalized by subtraction of the background scan with milliQ water. CD thermal denaturation experiments were performed monitoring the CD value (mdeg) at 260 nm in the range 10-90 °C with 0.5 °C/min heating rate.

6.6.3. ^{1}H-NMR of quadruplex structures

^{1}H-NMR studies were performed in the Instituto de Química Física Rocasolano (CSIC), with the kind supporting of Dr. Carlos González and Dra. Irene Pinto, using a Bruker spectrometer operating at 600 MHz and equipped with cryoprobes.

Experiments were performed with a 25 μM **Q0** solution and 75 μM **Q4** solution in 9:1 H_2O/D_2O containing 5 mM of KCl. ^{1}H NMR spectra were acquired at

different temperatures, ranging from 5 to 45 ºC. Water suppression was achieved by including a WATERGATE [1] module in the pulse sequence prior to acquisition.

[1] Piotto, M., Saudek, V., and Sklenar, V. (1992). Gradient-tailored excitation for single-quantum NMR spectroscopy of aqueous solutions. *Journal of Biomolecular NMR* 2, 661-665.

6.6.4. Study of quadruplex oligomerization state by native PAGE

0.16 OD of **Q0** and 0.3 OD of **Q4** sequence dissolved in 25 and 15 μl of milliQ water respectively was mixed with 2 μl of non denaturing buffer and samples were loaded onto 15% native polyacrylamide gel according to the protocol described in "General Methods". 0.25 OD of the sequence TG_4T in 20 μl of cacodylate buffer containing 100 mM K^+ was mixed with 2 μl of non denaturing buffer and used as a reference for monomeric quadruplex.

CHAPTER 7

Conclusions

7. Conclusions

The synthesis of parallel-stranded hairpins or clamps carrying LNA residues at the Hoogsteen strand has been described and the stability of the triplex formed with their DNA and RNA target sequences were analyzed by melting experiments.

The presence of LNA residues in the polypyrimidine strand enhances the stability of parallel duplexes, and therefore the stability of Hoogsteen base pairs, especially at pH 5.0.

Regarding triple helix-formation, LNA-modified parallel clamps bind to their polypyrimidine target strands with greater affinity than hairpins containing only natural bases, with an increase in Tm between 8 and 12 ºC respect to the unmodified triplexes. Triplex stabilization by LNA residues is even stronger when the polypyrimidine target strand is an RNA sequence, in which case an increase in Tm of 15-20 ºC relative to unmodified triplexes was observed.

A novel strategy to obtain parallel clamps using the non-templated chemical ligation of two oligonucleotides by 5'-5' linkages has been reported. Efficient protocols for introducing azido and alkyne functionalities at the 5' end of oligonucleotides have been developed. The chemical ligation of such structures by Cu(I)-catalyzed cycloaddition reaction has been performed and the following remarks have been noted:

- An excess of copper ions (and not a catalytic amount) is required, likely due to the retention of this cation by phosphate groups of DNA, and exclusion of atmospheric oxygen is essential to avoid oxidation of Cu(I). Moreover, adding ascorbic to CuI gave very good results for ligation of homopyrimidine sequences but partial degradation was observed when using this reducing agent in the presence of guanine rich DNA sequences so TBTA was employed as the only Cu(I) stabilizer when working with homopurine strands.

- Alkyne groups activated by a neighbouring electrowithdrawing amide moiety gave better yields than hex-5-ynyl group.

- Direct attachment of the azido group to the C5 of ribose ring (from 5'-iodinated precursor) gave lower CuAAC yields than those cases in which a hexyl chain is the linker between azido group and C5. This effect is more pronounced for purine terminated oligonucleotides.

- The use of ChemMatrix support for the synthesis of oligonucleotides and subsequent click reaction gave higher yields than CPG in the case of linking two polypyrimidine sequences, probably due to the hydrophilic nature of this support.

Synthesis of parallel hairpins has been achieved but moderate yields (less than 20%) were observed in some CuAAC reactions carried out in this thesis, which

might be explained because of the lacking of proximity between azido and alkynyl groups, according to several studies reporting the distance dependence of the reaction.

Cu(I)-catalyzed azide-alkyne cycloaddition reaction has been also used to synthesize novel unnatural aminoacids. A small library of compounds was synthesized from different alkynes by click chemistry with Nα-t-Boc-α-azido-L-alanine and the triazole products were isolated in very good yields.

The synthesis of ODNs carrying Cu(II) complexes was described. Several sequences were functionalized with a bromohexyl group and conjugated to two different copper tatradentate ligands by nucleophilic substitution.

These modified DNA strands were immobilized to gold electrodes either directly, by covalent attachment though sulfur-gold bonds or indirectly, through hybridization with a complementary strand linked to the electrode surface. Electrochemical studies were performed with both systems.

Cyclic voltammetry studies, although still preliminary, showed electrochemical signals corresponding to redox processes of copper ions chelated to *cyclam* linked to the hybridized strand, probably due to a better electron transfer through this system.

A novel system to construct stable monomolecular parallel G-quadruplexes was developed. The use of a branching unit has enabled the synthesis of a molecule containing four G-rich DNA strands whose 5'-ends are covalently attached and this system allows introduction of single modifications in just one of the strands.

This novel structure was shown to form a very stable parallel G-quadruplex, even in absence of stabilizing cations.

The effect of 8-amino-guanine substitutions in quadruplex stability was studied by NMR and CD thermal denaturation studies. We have reported that oligonucleotides with 8-amino-guanine substitutions provide more stable structures than non-modified sequences, especially when replacement is carried out in the internal region of the quadruplex.

Appendix

8. Appendix

8.1. Scientific publications:

The work developed during this thesis lead to the publication of the following articles:

· Alvira, M., Eritja, R. (2010) "**Triplex-stabilizing properties of parallel clamps carrying LNA derivatives at the Hoogsteen strand**" *Chem Biodivers*. 7(2):376-82.

· Alvira, M., Quinn, S.J., Aviñó, A., Fitzmaurice, D., Eritja, R. (2008) "**Synthesis of oligonucleotide conjugates carrying viologen and fluorescent compounds**". *The Open Org. Chem. J.*, 2, 41-45.

· Mazzini, S., García-Martín, Alvira, M., Aviñó, A., Manning, B., Albericio, F., Eritja, R. (2008) "**Synthesis of oligonucleotide derivatives using ChemMatrix supports**". *Chem Biodivers*., 5, 209-218.

· Alvira, M., Eritja, R. (2007) "**Synthesis of oligonucleotides carrying 5'-5' linkages using copper-catalyzed cycloaddition reactions**" *Chem. Biodivers*., 4, 2798-2809.

8.2. Oral communications and posters:

The work developed during the PhD has also been presented in several communications and posters in different congresses:

<u>Oral talks:</u>

· "1,3-dipolar cycloaddition reactions for promising modifications of therapeutic oligonucleotides". Perspectives on Nucleic Acid Chemistry for Therapy. Sesimbra, Portugal. June 2008.

· "Synthesis of oligonucleotides carrying azido and alkynyl groups at the 5'- ends and their use in Huisgen's 1,3-dipolar cycloaddition reactions". 3rd Nucleic Acid Chemistry and Biology (NACB) PhD Summer School, Odense, Denmark. 24-28 June 2007.

· "Synthesis of oligonucleotides carrying azido and alkynyl groups at the 5'-end and their use in Huisgen's 1,3-dipolar cycloaddition reactions." 6ª Reunión de Ácidos Nucleicos y Nucleótidos (RANN-VI), Valencia, Spain. 22-23 November 2007.

<u>Poster presentations:</u>

· "Synthesis and applications of modified oligonucleotides for triplex and quadruplex formation" Alvira, M., Aviñó, A., Fàbrega, C., Tintoré, M., Ferreira, R., Mazzini, S., Eritja, R. IRT 2010 - XIX International Round Table on Nucleosides, Nucleotides and Nucleic Acids. Lyon, France 29th August-3rd September 2010.

· "Triplex and quadruplex DNA: Chemical synthesis of modified DNA structures and study of their stability" Alvira, M. Eritja, R. First IRB Barcelona PhD Student Symposium: "The Architecture of Life". Barcelona, November 2009

· "Use of synthetic DNA for the assembly of nanostructures" Eritja, R., Garibotti, A., Manning, B., Ramos, R., Aviñó, A., Alvira, M., Leigh, S., Preece, J. IBEC Bioengineering and Nanomedicine Symposium '07, Barcelona, 7 November 2007.

· "Synthesis of oligonucleotides and oligonucleotide-peptide conjugates using ChemMatrix supports". Mazzini, S., García-Martin, F., Aviñó, A., Alvira, M., Albericio, F., Eritja, R. 3rd Nucleic Acid Chemistry and Biology (NACB) Symposium, Odense, Denmark. 27-28 June 2007.

"Triplex formation using oligonucleotide clamps carrying 8-aminopurines". Aviñó, A., Grimau, M.G., Alvira, M., Eritja, R., Gargallo, R., Orozco, M., González, C. XVII IRT on Nucleosides, Nucleotides and Nucleic Acids, Bern, Switzerland. September 2006.